

https://dspace.org/

Characterization of mycobacterial peptidoglycan remodelling enzymes

Mashilo, Poppy

2018
https://hdl.handle.net/10539/25367

Downloaded from a DSpace repository. https://dspace.org/

Characterization of Mycobacterial peptidoglycan remodelling enzymes

Poppy Mashilo (607878)



A dissertation submitted to the Faculty of Health Science, University of the Witwatersrand, Johannesburg, in fulfillment of the requirements for the degree of Master of Science in Medicine.

May 2018

Declaration

I, Poppy Mashilo declare that this dissertation is my own work. It is being submitted for the degree of Master of Science in Medicine at the University of the Witwatersrand, Johannesburg. It has not been submitted before for any degree or examination at this or any other university.

_____

Poppy Mashilo

_____ Day of _____ 2018

This dissertation is dedicated to my amazing parents,

for their endless love, support, encouragement and sacrifices. Your desire for your children to achieve more than you were granted by life is the rock upon which my life is built. I am truly grateful for all that you have done for me and this humble work is a sign of my love to you!

Presentations arising from this study

Conference: Biennial Research Day and Postgraduate Expo

Presentation: Poster

Venue and year: University of the Witwatersrand, 2016

Conference: Molecular Biosciences Research Thrust (MBRT)

Presentation: Poster

Venue and year: University of the Witwatersrand, 2016

Conference: Molecular Biosciences Research Thrust (MBRT)

Presentation: Poster

Venue and year: University of the Witwatersrand, 2017

Achievement: **1st prize for best poster presentation**

Abstract

Mycobacterium tuberculosis (TB), the causative agent of tuberculosis, is responsible for over one million deaths per annum, a substantive proportion of these due to multidrug resistant or extensively drug resistant strains. The available antibiotics are rapidly becoming ineffective due to the development of resistance mechanisms by the pathogen. Considering this, there is an urgent need for novel and highly effective new TB drugs, with novel modes of action. The peptidogycan (PG) layer in the cell wall has emerged as a rich area for drug discovery. It undergoes constant reconstruction by penicillin binding proteins (PBPs) and other enzymes to allow for cell growth and division, while preventing lysis. In this study, we characterize the function of two Low Molecular Mass PBPs, known as D,D-carboxypeptidases (D,D-CPases, MSMEG_6113 and MSMEG_2433) in *Mycobacterium smegmatis*, a model organism for TB research. Using a bacterial two hybrid system, we demonstrate that MSMEG_2433 interacts with PonA1 (A High Molecular Mass PBP involved in PG synthesis) and FtsH (An AAA family protease and a member of the divisome complex). We also demonstrate that MSMEG_6113 forms a complex with FtsI (A High Molecular mass PBP and also part of the divisome complex) and a cell division control protein, Cdc48. We demonstrate that the two D,D-CPases associate with their partnering proteins via their C-terminal transpeptidase domain. The importance of these identified interactions for cell division and growth was tested through deletion of partnering proteins from the mycobacterial genome, particularly FtsI and Cdc48. FtsI is essential for mycobacterial growth *in vitro* as demonstrated by the inability to recover mutants through allelic exchange by homologous recombination, while Cdc48 is dispensable for growth. We noted morphological and cell division defects in the Cdc48 deletion mutant strain. The absence of Cdc48 results in bulging, kinking and chaining phenotypes, in addition to misplacement of the FtsZ ring. Collectively, our observations describe the presence of novel PG hydrolysing protein complexes that may mediate essential steps in PG synthesis and bacterial proliferation. Targeting these complexes may provide an attractive avenue for the development of novel TB therapeutics.

Acknowledgements

First and foremost, I would like to thank the ALMIGHTY who has allowed me the opportunity to engage in this project and provided me the strength to do justice to my work and contribute my best to it. **Proverbs 3:5**

I would also like to thank all my financial sponsors, the National Research Foundation (NRF), the University of the Witwatersrand and the DST/NRF Centre of Excellence for Biomedical TB Research (CBTBR).

To my supervisor **Professor Bavesh Kana**, thank you for your guidance, great support and kind advice throughout the entire course of this research study. It was a real privilege for me to share of your exceptional scientific knowledge and your extraordinary human qualities.

A special thank you to Miranda Waldron at the University of Cape Town Centre of Imaging and Analysis, for doing all SEM imaging and the DNA Sequencing Facility of Stellenbosch University for sequencing all constructs generated in this study.

To my colleagues at the CBRTR, thank you for your companionship and for providing a so pleasurable and friendly working atmosphere. The moments of leisure shared together helped to overcome some more difficult moments. I am also truly thankful for your always prompt help, whenever I needed it. To Nombeko and Moagi, I would like to express my greatest gratitude for your guidance that helped me a lot in designing this dissertation work.

To my parents, my sister and my family at large, thank you for your prayers, constant support, encouragement and love, and without which I would not have come this far. You all gave me the strength to reach for the stars and chase my dreams and for that, I am very grateful.

Last but not least, I would like to express my deepest gratitude to my closest friends for their unconditional friendship, support and patience. Thank you for your understanding and encouragement in my many, many moments of crisis.

Table of Contents

Declaration…….....ii

Dedication…….....iii

Presentations arising from this study……iv

Abstract……v

Acknowledgements……vi

List of figures……..xii

List of tables……xvi

Nomenclature…….xvii

1. Introduction……...1

1.1. Tuberculosis……...1

1.2. TB infection and TB disease……..2

1.3. TB treatment and drug resistance……...3

1.4. The mycobacterial cell envelope……4

1.5. Mycobacterial cell growth and division…….6

1.6. PG biosynthesis……..8

1.7. PG remodelling……..9

1.8. Penicillin binding proteins……11

1.8.1. Penicillin binding (PB) domain and enzymatic activity of PBPs…….11

1.8.2. High molecular mass PBPs (HMM PBPs)……...13

1.8.3. Low molecular mass PBPs (LMM PBPs)……15

1.8.3.1. Endopeptidases……...16

1.8.3.2. D,D-carboxypeptidases (D,D-CPases)……....17

1.9. Hypothesis and research motivation…….19

1.10. Aims and objectives……...19

1.10.1. Aim……....19

1.10.2. Specific objectives…….19

2. Materials and methods……..….20
2.1. Databases and Bioinformatics tools used……...20
2.2. Chemicals and reagents used……..…22
2.3. Bacterial strains and plasmids constructed and/or used……..22
2.4. Bacterial strains culture conditions…….28
2.4.1. Growth conditions of *E. coli* DH5α and derivative strains…….28
2.4.2. Growth conditions for *Msm* and derivative strains……..29
2.5. Nucleic acid extraction……29
2.5.1. *E. coli* plasmid DNA extractions……...29
2.5.1.1. Small scale plasmid DNA extraction……....29
2.5.1.2. Large scale plasmid DNA extraction……....29
2.5.2. Mycobacterial chromosomal DNA extractions……....30
2.5.2.1. Small scale chromosomal DNA extraction……30
2.5.2.2. Large scale chromosomal DNA extraction……30
2.6. DNA manipulations…….31
2.6.1. DNA amplification by Polymerase chain reaction (PCR)……...31
2.6.1.1. Roche FastStart Taq PCR…….31
2.6.1.2. Q5 high fidelity PCR…….32
2.6.2. Restriction enzyme digestions…….32
2.6.3. Nucleic acid quantification……..…32
2.6.4. DNA visualization and purification……...…..32
2.6.4.1. Agarose gel electrophoresis……...…32
2.6.4.2. DNA fragment purification……..…33
2.6.5. DNA ends modifications…….....33
2.6.5.1. Dephosphorylation of DNA…….....33
2.6.5.2. Phosphorylation of DNA…….…...33
2.6.6. DNA ligation…….…....….34

2.6.7. DNA sequencing……34
2.7. Bacterial transformations……..34
2.7.1. Preparation and transformation of *E. coli* chemically competent cells…….34
2.7.2. Preparation and transformation of *Msm* electro-competent cells……..34
2.8. Confirmation of D,D-CPase interacting partners and determination of D,D-CPase domains responsible for interaction……...…36
2.8.1. Confirmation of D,D,-CPase interacting partners…….....36
2.8.2. Determination of D,D-CPase domains responsible for interaction……...…38
2.9. Knockout mutant generation and phenotypic characterization……38
2.9.1. Generation of *Msm* mutant strains……...….39
2.9.2. Generation of MSMEG_0858 and MSMEG_4233 knockout mutants…….40
2.9.3. Genotypic confirmation of the parental and mutant strains by Southern blot analysis…….....41
2.9.3.1. Electro-blotting……..…42
2.9.3.2. DNA probe labeling……..43
2.9.3.3. Hybridization…….43
2.9.3.4. Immunological detection……...…43
2.10. Generation of Mms complemented strains……44
2.11. Generation of MSMEG_4233 SCO recombinant (merodiploid) strain…….44
2.12. Generation of MSMEG_4233 mutant in the merodiploid strain……...45
2.13. Phenotypic analysis of *Msm* knockout mutant strains…….…..46
2.13.1. Growth kinetic analysis……..….…46
2.13.2. Minimum inhibitory concentration (MIC) determination…….…..46
2.13.3. Ethidium bromide diffusion assay……...…46
2.13.4. Microscopy……..47
2.13.4.1. Copper click reaction with D-alanine analogue (click chemistry)……...47
2.13.4.2. DMN-Trehalose staining……..…47

2.12.4.3. Scanning electron microscopy……48
2.14. FtsZ localization……..…...48
3. Results……..…...49
3.1. Protein interaction……....49
3.1.1. Confirmation of MSMEG_2433 and MSMEG_6113 interacting partners using the M-PFC assay……49
3.1.2. STRING analysis of MSMEG_2433 and MSMEG_6113 interacting partners ..…52
3.1.3. Cloning of genes encoding D,D-CPases and their selected partners into M-PFC bait and prey vectors……..……54
3.1.4. Confirmation of MSMEG_2433 and MSMEG_6113 interacting partners by M-PFC assay using full length clones……..…55
3.1.5. Cloning of genes encoding functional domains of the two D,D-CPases into M-PFC bait vector……...57
3.1.5.1. Cloning of genes encoding signal peptide and transpeptidase domain of MSMEG_6113 into pUAB400……...57
3.1.5.2. Cloning of genes encoding signal peptide, transpeptidase domain and C-terminal region of MSMEG_2433 into pUAB400……..58
3.1.6. Determination of MSMEG_6113 and MSMEG_2433 interacting partners…….61
3.1.7. Bioinformatics analysis of selected MSMEG_6113 and MSMEG_2433 partnering proteins (Cdc48, FtsI, FtsH and PonA1)……63
3.1.7.1. Sequence alignment of Cdc48, FtsI, PonA1 and FtsH in various rod shaped bacteria……...……63
3.1.7.2. Domain organization of Cdc48, FtsI, PonA1 and FtsH…….....68
3.2. Generation of *Msm* deletion mutants defective in *cdc48* and *ftsI* genes……..70
3.2.1. Construction of *cdc48* and *ftsI* gene deletion constructs……..71
3.2.2. Generation of *cdc48* and *ftsI* deletion mutant strains in *Msm*……..73
3.2.2.1. Generation of *Msm* Δ*cdc48* strain……..73

3.2.2.2. Generation of *Msm* Δ*ftsI* strain……...75

3.2.3. Genetic complementation of Δ*cdc48* strain……..77

3.2.3.1. Construction of the *cdc48* complementation vector……...…77

3.2.3.2. Generation of Δ*cdc48* complemented strain……...…78

3.2.4. Generation of *ftsI* deletion mutant in the merodiploid strain…….....79

3.2.4.1. Construction of *ftsI* complementation vector……...…..79

3.2.4.2. Generation of Δ*ftsI* mutant strain in the merodiploid background……...…..80

3.2.5. Phenotypic characterization of Δ*cdc48* mutant……...……81

3.2.5.1. The role of Cdc48 in regulating *Msm* growth kinetics……...……82

3.2.5.2. Cdc48 plays a role in antibiotic sensitivity and cell wall permeability..……83

3.2.5.3. Microscopic analyses…….……85

3.2.5.4. Localization of FtsZ in the Δ*cdc48* mutant……90

4. Discussion……...……92

5. Conclusion and future studies……..….100

5.1. Conclusion…….….100

5.2. Future studies…….….100

6. Appendices……101

7. References…….…116

List of figures

Figure 1.1. Global estimated TB incidence rates……...2

Figure 1.2. Diagrammatic representation of mycobacterial cell envelope composition……5

Figure 1.3. Models of mycobacterial polar growth and cell division……....7

Figure 1.4. Schematic representation of stages of PG biosynthesis……..9

Figure 1.5. Schematic representation of the PG structure……10

Figure 1.6. Illustration of the active site of penicillin-binding (PB) domain……...12

Figure 1.7. Schematic representation of domain organization of HMM PBPs……14

Figure 1.8. Schematic representation of domain organization of LMM PBPs……16

Figure 2.1. Diagrammatic representation of experimental layout of interaction work done in this study…….36

Figure 2.2. Schematic diagram demonstrating the M-PFC assay principle…….37

Figure 2.3. Flowchart summarizing the steps involved in generation of knockout mutants…39

Figure 2.4. Schematic representation of the two step allelic exchange by homologous recombination procedure…….40

Figure 2.5. Diagrammatic representation of the steps involved in Southern blot analysis…….....42

Figure 2.6. Schematic representation of integration of pMV306H*ftsI* into the *attb* site in the genome of MSMEG_4233 SCO…….45

Figure 3.1. MSMEG_6113 interacting protein partners revealed by STRING analysis……..53

Figure 3.2. MSMEG_2433 interacting protein partners revealed by STRING analysis……..54

Figure 3.3. Protein interaction between MSMEG_6113, MSMEG_2433 and their selected partners in *Msm* using M-PFC assay……...56

Figure 3.4. Restriction profile of pUAB400+6113SP……..57

Figure 3.5. Restriction profile of pUAB400+6113TP…….58

Figure 3.6. Restriction profile of pUAB400+2433SP……..59

Figure 3.7. Restriction profile of pUAB400+2433TP…….60

Figure 3.8. Restriction profile of pUAB400+2433Cter……...61

Figure 3.9. Protein interaction between MSMEG_6113, MSMEG_2433 domains and their selected partners in *Msm* using the M-PFC assay……...63

Figure 3.10A. Comparison of the conserved *Msm* Cdc48 sequence with other Cdc48 homologues…….64

Figure 3.10B. Comparison of the conserved *Msm* FtsI sequence with other FtsI homologues…….65

Figure 3.10C. Comparison of *Msm* PonA1 sequence with other PonA1 homologues……66

Figure 3.10D. Comparison of the conserved *Msm* FtsH sequence with other FtsH homologues…….67

Figure 3.11A. Schematic representation of domain organization of *Msm* Cdc48 protein…...68

Figure 3.11B. Schematic representation of domain organization of *Msm* FtsI protein…….69

Figure 3.11C. Schematic representation of domain organization of *Msm* PonA1 protein…...69

Figure 3.11D. Schematic representation of domain organization of *Msm* FtsH protein……..70

Figure 3.12. Schematic diagram illustrating the general strategy of suicide vector construction using Cdc48 as an example…….71

Figure 3.13. Restriction profile of p2NIL*cdc48*_Pac knockout construct……...72

Figure 3.14. Restriction profile of p2NIL*ftsI*_Pac knockout construct……73

Figure 3.15. PCR screening of Δ*cdc48* deletion mutants…….74

Figure 3.16. Southern blot analysis of *Msm* Δ*cdc48* strain……..75

Figure 3.17. PCR screening of Δ*ftsI* deletion mutants……76

Figure 3.18. Restriction profile of pMV306H*cdc48* construct……77

Figure 3.19. PCR confirmation of site-specific integration of pMV306H*cdc48* into Δ*cdc48* mutant……..78

Figure 3.20. Restriction profile of pMV306H*ftsI* constructs……...80

Figure 3.21. PCR confirmation of site-specific integration of pMV306H*ftsI* into *ftsI* SCOstrain……81

Figure 3.22. Growth kinetics of Δ*cdc48* strain in comparison to the wildtype and complemented strains……..82

Figure 3.23. Minimum inhibitory concentrations (MICs) of Δ*cdc48* strain in comparison to the wildtype and complemented strains……..84

Figure 3.24. Δ*cdc48* cell wall permeability assessment……...85

Figure 3.25. SEM micrographs of wildtype mc^2155 and Δ*cdc48* strains……86

Figure 3.26. Quantification of the Δ*cdc48* morphological defects revealed by SEM in comparison to wildtype……...87

Figure 3.27. Microscopic analysis of Δ*cdc48* strain phenotypes in comparison to the wildtype and Δ*cdc48*:: *cdc48* strains…….....88

Figure 3.28. Quantification of the observed staining patterns revealed under the microscope... ……..89

Figure 3.29. Cell length Quantification in the Δ*cdc48* mutant…….89

Figure 3.30. Microscopic analysis of Δ*cdc48* strain phenotypes in comparison to the wildtype and Δ*cdc48*:: *cdc48* strain after DMN-Trehalose staining……..90

Figure 3.31. Localization of FtsZ_GFP in the Δ*cdc48* mutant in comparison to the wildtype… ……..91

Figure 3.32. Quantification of FtsZ_GFP *in vivo* localization patterns……...91

Figure 4.1. Proposed model of Cdc48 function in mycobacterial physiology……....98

Figure C1. Restriction profile of pUAB300……...105

Figure C2. Restriction profile of pUAB400……...106

Figure C3. Restriction profile of pUAB400:: 2433……106

Figure C4. Restriction profile of pUAB300:: 6900……107

Figure C5. Restriction profile of pUAB300:: 4227……107

Figure C6. Restriction profile of pUAB300:: 0031……108

Figure C7. Restriction profile of pUAB300:: 6105……108

Figure C8. Restriction profile of pUAB400:: 6113……109

Figure C9. Restriction profile of pUAB300:: 4233……109

Figure C10. Restriction profile of pUAB300:: 0858……..110

Figure C11. Restriction profile of pUAB300:: 5637……..110

Figure C12. Restriction profile of pUAB300:: 0365……..111

Figure C13. Restriction profile of pUAB300:: 6112……..111

Figure C14. Restriction profile of p2NIL……...112

Figure C15. Restriction profile of p2NIL*cdc48*……112

Figure C16. Restriction profile of p2NIL*ftsI*……113

Figure C17. Restriction profile of pGOAL17……113

Figure C18. Restriction profile of pMV306H……114

Figure C90. Δ*cdc48* cell wall permeability assessment……115

Figure D1: DNA molecular weight markers used in this study……115

List of tables

Table 2.1. Databases and bioinformatics tools used……20

Table 2.2. Plasmids constructed and/or in this study……...22

Table 2.3. Bacterial strains generated and/or used in this study……..25

Table 2.4. Parameters used for primer design……..31

Table 3.1. Confirmation MSMEG_6113 interaction with its putative interacting partners including appropriate controls using M-PFC assay…….50

Table 3.2. Confirmation MSMEG_2433 interaction with its putative interacting partners including appropriate controls using M-PFC assay……51

Table 3.3. Interaction of MSMEG_6113, MSMEG_2433 and their selected putative partnering proteins……...56

Table 3.4. Interaction MSMEG_6113 SP and TP domain with Cdc48 and FtsI as well as that of MSMEG_2433 SP,TP and Cter region with FtsH and PonA1……62

Table 3.5. MICs (μg/ml) of wildtype, Δ*cdc48* and Δ*cdc48*::*cdc48* strains……..83

Table A1. Media and supplements……101

Table A2. Solutions used for *E. coli* plasmid DNA extractions……101

Table A3. Solutions used for *Msm* plasmid DNA extractions……...101

Table A4. Solutions used for DNA precipitation……...101

Table A5. Solutions used for DNA electrophoresis……...102

Table A6. Agarose gel recipes……...102

Table A7. Solutions used for preparations of *E. coli* competent cells……...102

Table A8. Southern blot solutions……..102

Table B1. Primers used for generation of full length partners for M-PFC assay……...103

Table B2. Primers used for domain truncation……..103

Table B3. Primers used for amplification of genes for mutant generation……104

Table B4. Primers used for amplification of genes for mutant complementation……104

Table B5. Primers used confirmation of site-specific integration of complementing vector……105

Nomenclature

µ	Micro
AAA	ATPases associated with various cellular activities
Amp	Ampicillin
AG	Arabinogalactan
ATP	Adenosine triphosphate
attB	$tRNA^{Gly}$ attachment site
BSA	Bovine serum albumin
bp	base pairs
$CaCl_2$	Calcium chloride
CFUs	Colony forming units
CTAB	Cetyltrimethylammonium bromide
D-ala	D-alanine
DCO	Double cross-over
D-gln	D-glutamine
D,D-CPases	D,D-carboxypeptidases
DNA	Deoxyribonucleic acid
dNTPs	Deoxynucleotide triphosphate
E. coli	*Escherichia coli*
EMB	Ethambutol
EtBr	Ethidium bromide
g	grams
GFP	Green fluorescent protein
HIV	Human Immunodeficiency virus
HMM	High molecular mass
HP	Hypothetical protein
Hyg	Hygromycin

INH	Isoniazid
Kan	Kanamycin
Kbp	kilo base pairs
L-ala	L-alanine
LA	Luria-Bertani agar
LB	Lysogeny broth
LMM	Low molecular mass
LTBI	Latent TB infection
m	Milli
M	Molar
MA	Mycolic acid
*m*DAP	*Meso*- diaminopimelic acid
MDR-TB	Multi-drug resistant TB
mDHFR	Murine dihydrofolate reductase
MIC	Minimum inhibitory concentration
M-PFC	Mycobacterial protein fragment complementation
Msm	*Mycobacterium smegmatis*
Mtb	*Mycobacterium tuberculosis*
min	minutes
n	nano
NaCl	Sodium chloride
NAG	*N*-acetylglucoseamine
NAM	*N*-acetylmuramic acid
NEB	New England Biolabs
OD_{600}	Optical density at 600 nanometer wavelength
ORF	Open reading frame
PBPs	Penicillin binding proteins

PBS	Phosphate buffered saline
PCR	Polymerase chain reaction
PG	Peptidoglycan
PZA	Pyrazinamide
RIF	Rifapicin
Rpfs	Resuscitation promoting factors
rpm	Revolutions per minute
Sec	seconds
SCO	Single cross-over
SDS	Sodium dodecyl sulphate
SEM	Scanning electron microscope
SP	Signal peptide
TB	Tuberculosis
TBE	Tris borate EDTA
trim	Trimethoprim
UDP	Uridine diphosphate
WHO	World Health Organization
X-gal	5-bromo-4chloro-3-indolyl-D-thiogalactopyranoside
XDR-TB	Extensively-drug resistant TB

1. Introduction

1.1. Tuberculosis

Tuberculosis (TB) is an airborne infectious disease caused by the human pathogen *Mycobacterium tuberculosis* (*Mtb*) discovered in 1882 by Robert Koch. The disease has been around for millennia, being recorded as early in history as the Egyptian and Greco-Roman civilizations (De Backer et al., 2006). Presently, TB still remains a foremost public health burden worldwide and the ninth leading cause of death due to bacterial infection, primarily in middle and low income countries (WHO, 2017). In 2016 alone, approximately 10.4 million new TB cases were reported, with 1.7 million deaths resulting from TB infections (of which 374 000 and 1.3 million were from HIV positive and HIV negative patients, respectively), ranking TB as one of the top 10 causes of death worldwide above HIV and malaria, as reported by the World Health Organization (WHO, 2017). TB infection is prevalent in developing countries, particularly the Sub-Saharan African countries and the burden is heterogeneously distributed in the world (Figure 1.1.). For example, in South Africa TB incidence is more than 250 fold greater (>500 cases per 100 000 population per year) than the United States (<10 cases per 100 000 population per year) (WHO, 2017). It has also been reported that TB incidence is nearly 10% higher in men than women (Dye, 2006) and in all new cases worldwide, approximately 10% occur in children (Swaminathan and Rekha, 2010).

South Africa also ranks fourth among the 10 highest drug-resistant TB burdened countries in the world, after China, India and Russia (WHO, 2017). The global burden of TB disease in these countries is exacerbated by a number of factors that severely compromise current TB interventions. These factors include a decline in health care systems, high population density, poor socio-economic conditions, co-infection with TB-HIV and the emergence of drug resistant TB. Other risk factors that are responsible for driving the TB epidemic include malnutrition, which is attributed to nearly 27% of TB cases worldwide, air pollution, excessive alcohol, type II diabetes and smoking (Lonnroth *et al*., 2010). Among the TB risk factors, HIV infection is the strongest, with 12% of all new cases of active TB disease and 25% of all TB-related deaths occurring in HIV-positive individuals (Getahun *et al*., 2015). The majority (75%) of HIV-associated active TB disease cases and deaths occur in Africa (Getahun *et al*., 2015), making TB a particular source of concern in the continent.

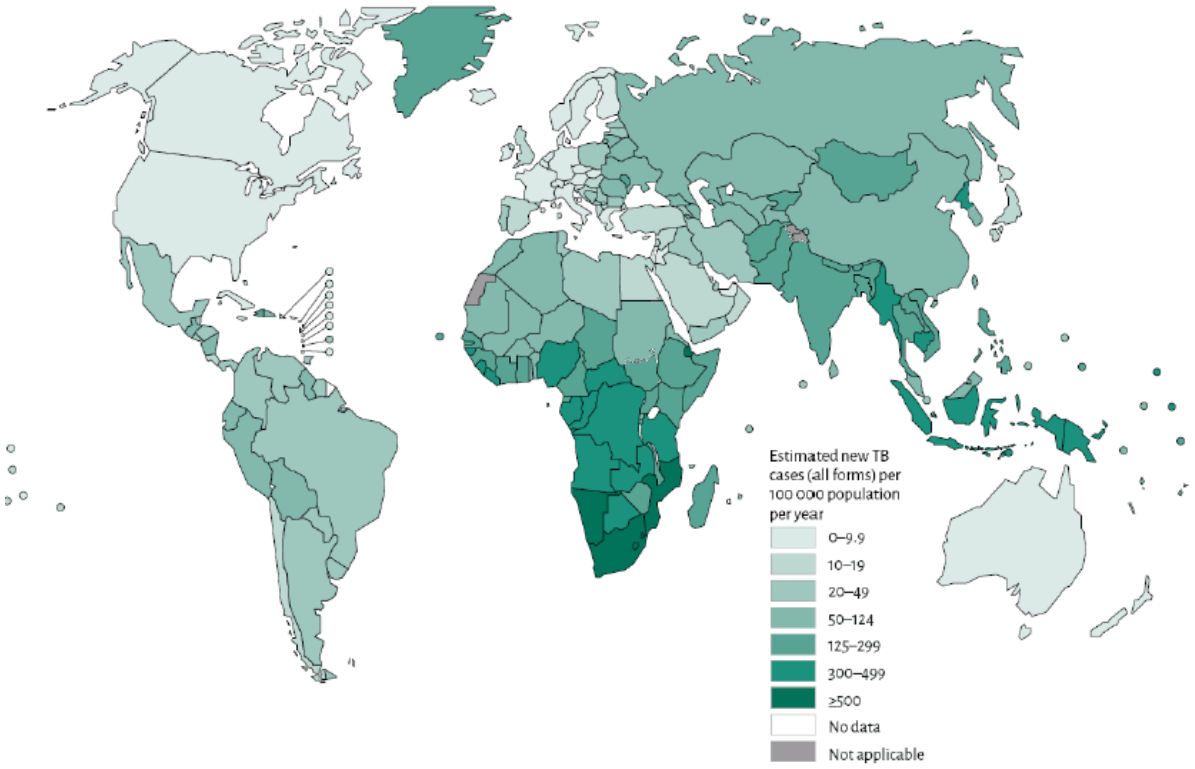


Figure 1.1: Global estimated TB incidence rates. TB burden is heterogeneously distributed and is prevalent in developing countries, particularly the Sub-Saharan African region. Reproduced from Global Tuberculosis Report 2017, WHO (2017).

1.2. TB infection and TB disease

Mtb is an extremely well adapted human pathogen. On average, an infectious individual might infect 3-10 individuals per year (van Leth *et al*., 2008), of whom only a minority will progress to active TB disease. Infection with *Mtb* can lead to two broad outcomes: elimination or persistence of the pathogen and therefore, TB can present as a dynamic spectrum, from asymptomatic infection to active TB disease (Esmail *et al*., 2014). The infectious life cycle of *Mtb* starts with the transmission of the bacilli from a patient with active pulmonary TB through the respiratory route, placing their contacts at risk of infection (Zumla *et al*., 2013a). Infection begins when aerosolized *Mtb* enters the lungs via inhalation, where it reaches the alveolar space and encounters the resident alveolar macrophages (Gonzalo-Asensio *et al*., 2017). These alveolar macrophages internalize the bacilli by receptor-mediated phagocytosis and produce pro-inflammatory components, which lead to the recruitment of a large number of immune cells (including B cells and T cells) to the infection site, thus inducing granuloma formation (Lin et al., 2014; Gonzalo-Asensio *et al*., 2017).

The granuloma is an organized structure consisting of the infected macrophages surrounded by highly differentiated cells such as epithelioid cells, multinucleated giant cells and foamy cells, all surrounded by a ring of T lymphocytes (Miranda *et al*., 2012; Marakalala *et al*., 2016). The granuloma creates an immune microenvironment that acts to constrain the infection. If the infection is contained by the granuloma without any substantial tissue damage or further progression of disease, the person is said to have latent TB infection (LTBI). Individuals with LTBI are asymptomatic and nearly 2 billion people (approximately one third of the world's population) are estimated to harbor LTBI (Gonzalo-Asensio *et al*., 2017). It is estimated that 5% to 15% of these individuals have a defined risk of progressing to active TB disease throughout their lifetime (Andrews *et al*., 2012). In a case where the granuloma fails to control bacteria, the infection progress to active TB disease. Individuals with active TB disease display symptoms such as fever, weight loss, persistent cough and fatigue. In the absence of treatment, TB can be frequently fatal and nearly 50% of the people who suffer with the disease will die from it (Tiemersma *et al*., 2011).

1.3. TB treatment and drug resistance

Of all the individuals diagnosed with active TB disease annually, 80% of them are infected with *Mtb* strains that are completely susceptible to the available antimicrobials used for TB treatment while the remaining proportion (20%) are infected with drug-resistant strains (WHO, 2015; Onozaki *et al*., 2015). Treatment options differ for LTBI, drug-resistant and drug-sensitive active TB disease, and it is estimated that nearly 44 million lives were saved by TB treatment between the year 2000 and 2016 (WHO, 2017). The recommended treatment regimens for LTBI include the use of Isoniazid (INH) for 6-9 months, a combination of INH and Rifapentine for 3 months, followed by 3-4 months of INH and Rifampicin (RIF) or 3-4 months of RIF alone (WHO, 2014). The standard treatment for drug-sensitive TB includes chemotherapy for a period of 6 months, using a composition of first line drugs and second line drugs. The treatment is made up of a combination of Pyrazinamide (PZA), INH, Ethambutol (EMB) and RIF for the initial two months (intensive treatment phase), followed by RIF and INH for the next four months (continuation phase) (WHO, 2010; Nahid *et al*., 2016). Although the success rate of the 6 months regimen is high, there are several limitations to it. A certain fraction of patients develop toxicity symptoms, which when combined with the long duration of treatment undermines patient compliance (Pai *et al*., 2016). Failure to complete treatment can result in relapse and emergence of drug resistance.

The emergence of drug resistance is a major concern. Globally, 3.5% of new active TB disease cases and 20.5% of previously treated cases have multi drug- resistant TB (MDR-TB). MDR-TB is defined as resistance to the 2 most effective first line drugs, RIF and INH. A small proportion (9.7%) of MDR-TB cases progress to extensively drug-resistant TB (XDR-TB), defined as resistance to 3 or more of the 6 classes of second line drugs (Pai *et al*., 2016). Therapeutic options for drug resistant TB are expensive, lengthy, and use highly toxic drugs with uncertain efficacy (Koul *et al*., 2011). In mycobacteria, the emergence of resistance to first line drugs is essentially attributed to genetic mutations in various drug target-encoding genes. This highlights a crucial demand for identification of novel drug targets and the development of highly effective drugs that have the potential to reduce duration of TB treatment. The mycobacterial cell envelope discussed below, particularly the peptidoglycan layer of the cell wall has emerged as a rich area for drug discovery.

1.4. The mycobacterial cell envelope

The mycobacterial cell envelope is made of complex, multiple layers including a capsule-like layer, the envelope core/ cell wall and the plasma membrane (Figure 1.2) (Hett and Rubin, 2008). The outer layer of the cell envelope is a polymer of polysaccharides (mannan, glucan and arabinomannan), lipids (lipopolysaccharides, lipooligosaccharides, phospholipids and several other lipids) and proteins (Mishra *et al*., 2011; Lee *et al*., 2012). The envelope core, herein referred to as the cell wall, is required for bacterial growth, cell shape, virulence and it plays a significant role in mediating the intrinsic resistance to antibiotics (Bansal-Mutalik and Nikaido, 2014). The cell wall consists of a mycolic acids (MAs) layer esterified to the arabinogalactan (AG) layer, which is connected to the muramic residue of the peptidoglycan (PG) layer through a linker disaccharide (Kaur *et al*., 2009). MAs have been associated with reduction of *Mtb*-induced host inflammatory response (Hett and Rubin, 2008) and they play a principal role in the inherent decreased permeability to small molecules. The AG layer plays part in retaining the integrity of the cell envelope and also plays an essential role in regulating permeability of the cell by functioning as an anchor for MA layer which is impermeable (Hett and Rubin, 2008). PG layer provides the bacterium with strength to withstand the difference in pressure between the environment and the interior of the cell and as a result, it is essential for bacterial survival. It is also important in maintaining the specific shape of bacterial cells (Hett and Rubin, 2008).

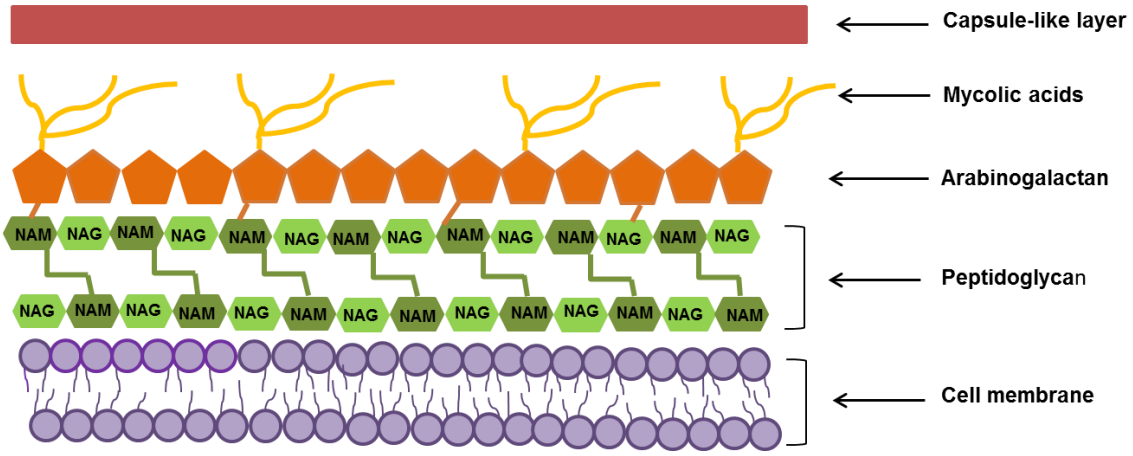


Figure 1.2: Diagrammatic representation of mycobacterial cell envelope composition. The envelope consists of the outer most capsule-like layer (red rectangle), the envelope core (cell wall) which is made up of the mycolic acid layer (yellow threads), arabinogalactan layer (orange pentagons) and PG layer represented by the green hexagons cross-linked by the stem peptides (dark green lines). The lipid bilayer represented by purple circles. Figure drawn by student, adapted from Hett and Rubin (2008).

One target of TB antimicrobials is the cell wall and many drug compounds that are under development or in clinical use target each layer of the cell wall and enzymes associated with its synthesis (Zumla *et al*., 2013b). For example, EMB inhibits the synthesis of AG and lipoarabinomannan and INH inhibits MA synthesis. Many antibiotics that are used widely, such as D-cycloserine, β-lactams and glycopeptides target various stages of PG synthesis and are routinely used to treat many bacterial infections (Zumla *et al*., 2013b). However, despite their widespread use, bacteria have established strategies to deal with the stress created by these antibiotics. For example, they mediate β-lactam resistance by expressing penicillin-insensitive L,D-transpeptidases to form L,D-cross links instead of D,D-cross-links (Magnet *et al*., 2007). They can also confer vancomycin (a glycopeptide that binds the terminal D-Ala-D-Ala of the stem peptide) resistance by replacing the D-Ala-D-Ala with D-Ala-D-Serine or D-Ala-D-Lactate (Mainardi *et al*., 2008). In addition, bacteria activate their cell-wall stress stimulon when exposed to antibiotics, leading to overexpression of PG biosynthesis-associated genes (Steidl *et al*., 2008). Regardless of all these resistance mechanisms, PG still remains an attractive antibacterial target and in order to combat MDR and develop new TB drugs, it is essential to have an indepth understanding on how PG is synthesized and modified.

1.5. Mycobacterial cell growth and division

One of the many reasons why *Mtb* remains an extraordinary successful human pathogen is that during cell growth and division, mycobacteria produce heterogeneous daughter cells (Santi *et al*., 2013), which further undergo cell wall remodeling during infection, thus allowing the bacterium to withstand the stresses encountered during infection (Aldridge *et al*., 2012). This facilitates adaptation of the bacteria to the host and could possibly have a major role in clinical latency. The bacterial cell proliferation process is divided into two stages, where the parental cell first undergoes elongation, then followed by division of the elongated cell into two daughter cells. In numerous bacteria, the cell division process is symmetric resulting in production of equally sized daughter cells that equally share the contents of the mother cell (Typas *et al*., 2012). However, in mycobacteria, cell growth and division occur in an asymmetric manner, producing unequally sized daughter cells (Santi *et al*., 2013). Mycobacteria grow by inserting newly synthesized cell wall subunits at their sub-polar regions, and all cells consist of one pole which is inherited from the previous cell division (old pole) and one which is synthesized during division, termed new pole (Figure 1.3A and 1.3B) (Aldridge *et al*., 2012). In Firmicutes like *E. coli*, an actin like filament, MreB, spatially directs lateral cell wall synthesis. Mycobacteria lack MreB homologues and thus elongate by polar growth rather than lateral wall extension (Hett and Rubin, 2008). The polar growth in mycobacteria is explained by two models. In the first model, cytokinesis is used to explain the asymmetry in the cell division process (Santi *et al*., 2013). This model proposes that both cell poles grow in a symmetric manner until cytokinesis, and from thereon, growth starts to occur predominately at the old pole until cell separation, resulting in generation of two unequally sized daughter cells (Figure 1.3A) (Santi *et al*., 2013; Kieser and Rubin, 2014). The second model proposes that elongation of the poles occur at different rates throughout the cell cycle, with the old pole always elongating faster than the new pole at all stages of the process (Aldridge *et al*., 2012; Santi *et al*., 2013). Cell division is also asymmetric, generating daughter cells of unequal sizes (Figure 1.3B) (Aldridge *et al*., 2012; Santi *et al*., 2013; Kieser and Rubin, 2014).

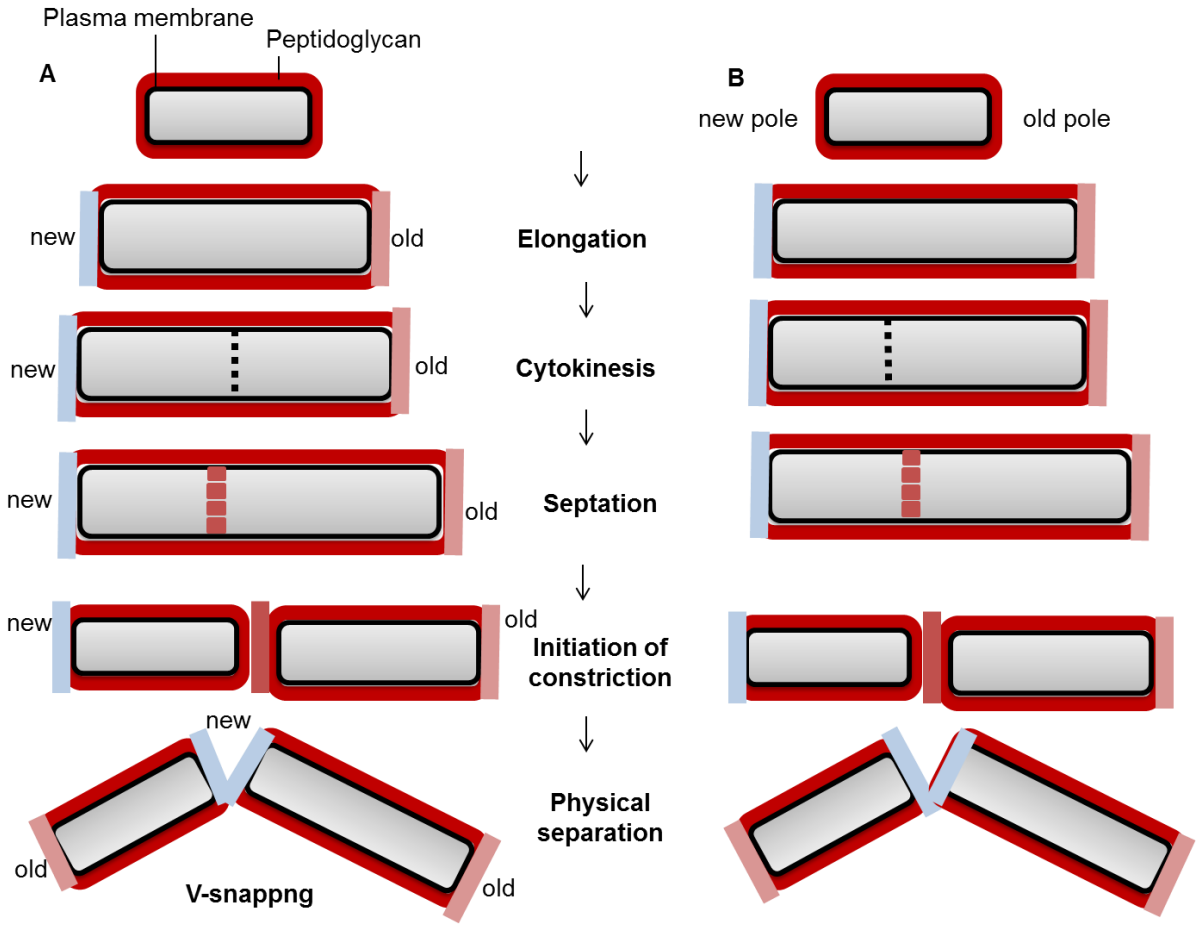


Figure 1.3: Models of mycobacterial polar growth and cell division. In mycobacteria, cells elongate by growing from the tips of their cell poles, and the parent cells consist of an old pole (light pink) and new pole (light blue). Cell growth and division result in generation of unequally sized daughter cells. (A) The cell grows in a symmetric manner, however, after cytokinesis, growth predominantly takes place at the old pole. Constriction of the septum generates two daughter cells that vary in size. (B) Cell elongation occurs at different rates throughout the cell cycle, and elongation is much faster at the old pole compared to new pole. In mycobacteria, the final stage of division where the cells physically separate is characterized by what is termed as V-snapping, which in turn generates two daughter cells that differ in size. Figure drawn by student, adapted from (Kieser and Rubin, 2014).

The cell division process can be divided into several stages: following elongation, the plasma membrane is synthesized roughly at mid-cell during cytokinesis, this is then followed by septation, where PG septum is synthesized at mid-cell. The cell wall then constricts and the septum is hydrolyzed as the daughter cells physically separate. In mycobacterial, cell separation is characterized by what is termed the 'v-snapping' phenotype (Figure 1.3 A and B). A large multiprotein complex termed the divisome is responsible for cell division, and it consists of a number of proteins coordinating septal PG synthesis and septum splitting during cell division (Kieser and Rubin, 2014). Proteins making up the divisome complex include:

cytoskeletal-like proteins (FtsZ), structural proteins (SepF, FhaB, CwsA, FtsW, CrgA, FtsQ), PG synthases (PonA1, PBPB, PBPA) and PG hydrolases (RipA, RipC, RpfB) (Hett and Rubin, 2008; Typas *et al*., 2012). Septation is initiated by polymerization of FtsZ into a Z-ring at mid-cell, with several regulatory factors serving to regulate subcellular placement of this Z-ring. Once the Z-ring is formed, it facilitates recruitment of structural elements to form the divisome. PG synthases synthesize the septal PG, which is then cleaved by the hydrolases to physically separate the daughter cells (Kieser and Rubin, 2014). The unique mode of elongation and division in mycobacteria generates a population of daughter cells that differ in growth rate, cell size, as well as cell wall composition (Singh *et al*., 2013) and therefore contribute to the ability of the pathogen to persist in the host.

1.6. PG biosynthesis

PG is made of linear glycan strands that are cross-linked by short stem peptide chains, forming a 3D net-like structure that surrounds the bacterial cell. These glycan strands consist of alternating *N*-acetylglucosamine (Glc*N*Ac or NAG) and *N*-acetylmuramic acid (Mur*N*Ac or NAM) residues that are connected by β-1,4-glycosydic bonds (Hett and Rubin, 2008; Vollmer *et al*., 2008). The oligopeptide that serve to cross-link the glycan strands is usually a pentapeptide made of L-alaline-D-glutamine-*meso*-diaminopimalate-D-alanine-D-alanine or a tretrapeptide in which the terminal D-alanine is removed. The biosynthesis of the PG layer is a multistep-process, which is mediated by an array of periplasmic and cytoplasmic enzymes (Figure 1.4). The initial stage of PG synthesis occurs in the cytoplasm, with the synthesis of UDP-Mur*N*ac through a series of steps. The first step involves UDP-Glc*N*ac synthesis from fructose-6-phosphate by GlmSMU enzymes and thereafter, UDP-Mur*N*ac is synthesized from UDP-Glc*N*ac by MurAB enzyme activity (Figure 1.4) (White *et al*., 2010). Subsequently, the aminoligases MurC, MurD, MurE and MurF catalyze the sequential addition of L-Ala, D-Glu, *m*-DAP, and D-Ala-D-Ala dipeptide to UDP-Mur*N*ac, respectively, resulting in the formation of UDP-Mur*N*ac pentapeptide molecule (Figure 1.4) (White *et al*., 2010; Jankute *et al*., 2015). The subsequent step involves the formation of lipid linked PG intermediates. The membrane step starts with the transfer of phosphor-Mur*N*ac-pentapeptide of UDP-Mur*N*ac pentapeptide to decaprenyl-phosphate (a membrane-bound lipid carrier) by the integral membrane protein MraY, leading to the formation of lipid I (Figure 1.4). This is followed by coupling of Glc*N*ac moiety from UDP-Glc*N*ac to lipid I by the activity of the peripherally associated membrane protein MurG, yielding lipid II. Lipid II is then flipped across the inner membrane by either RodA or FtsW (Figure 1.4) (Bouhss *et al*., 2008; Jankute *et al*., 2015).

The final steps of PG synthesis occur in the periplasm, where the newly formed lipid II is incorporated into the existing PG by penicillin binding proteins (PBPs) to form a mature PG sacculus (Bouhss *et al.*, 2008).

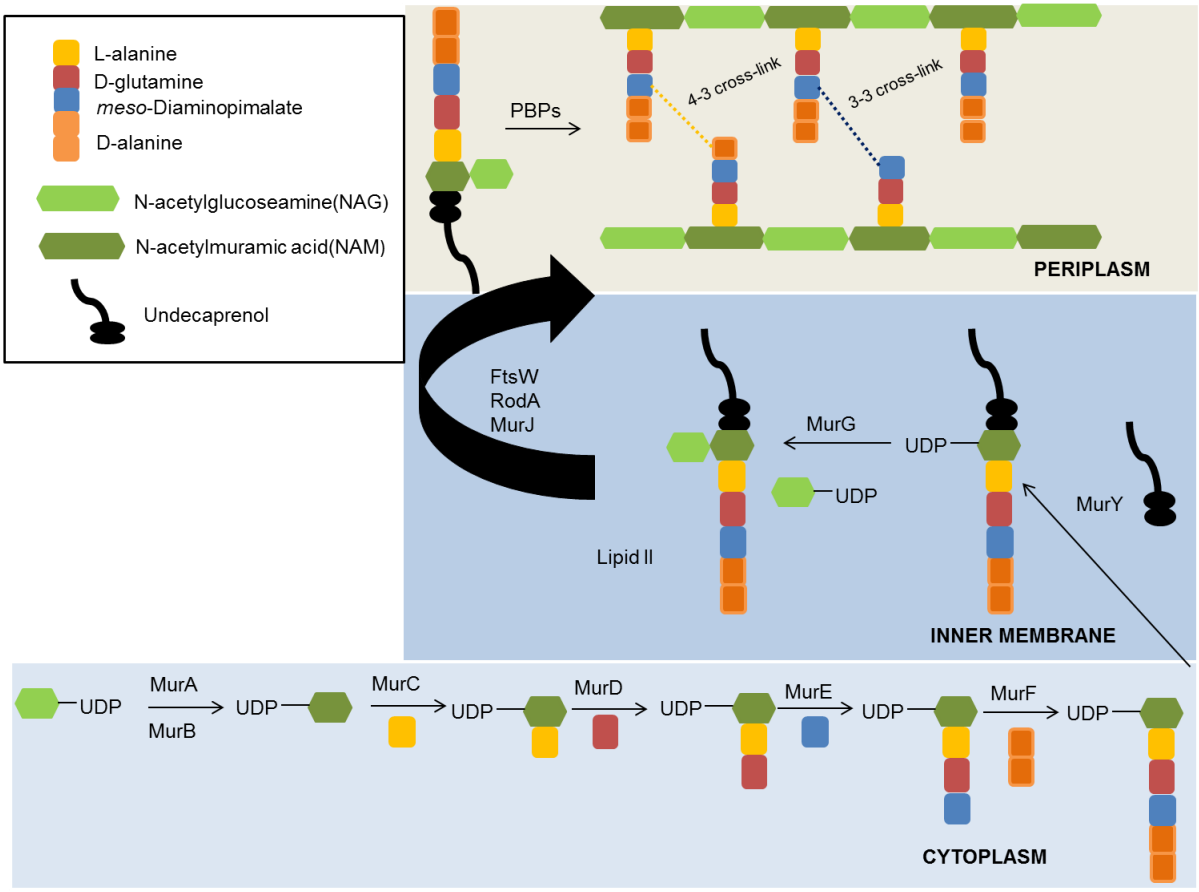


Figure 1.4: Schematic representation of stages of PG biosynthesis. Lipid II production begins in the cytoplasm where NAG (light green hexagon) is converted to NAM (dark green hexagon) by MurA and MurB, followed by addition of the stem pentapeptide through the enzymatic activities of aminoligases (MurC-MurF). In the inner membrane, MurY and MurG catalyze formation of lipid I and Lipid II, respectively. Once lipid II is formed, it is flipped to the periplasmic space by the action of a flippase (FtsW/RodA/MurJ), where it gets incorporated into the pre-existing PG through the action of PBPs. Figure drawn by student, adapted from (White *et al.*, 2010).

1.7. PG remodelling

The constant growth and division of the bacterial cell requires continuous remodelling of the PG layer to allow for a range of functions including the insertion of new PG units, secretion apparatus and pili (Vollmer *et al.*, 2008). The process of PG remodelling is facilitated by a set of enzymes termed PG hydrolases. These enzymes play significant roles such as regulating cell wall growth, PG turnover during growth, as well as regulating daughter cell separation during cell division and autolysis (Lee and Huang, 2013). PG hydrolases have the ability to

degrade bacterial PG at different sites (as shown in Figure 1.5). They act on existing amide (amidases), glycosidic (glycosidases) and peptide (peptidases) bonds in the PG sacculus (Figure 1.5) (Hett and Rubin, 2008).

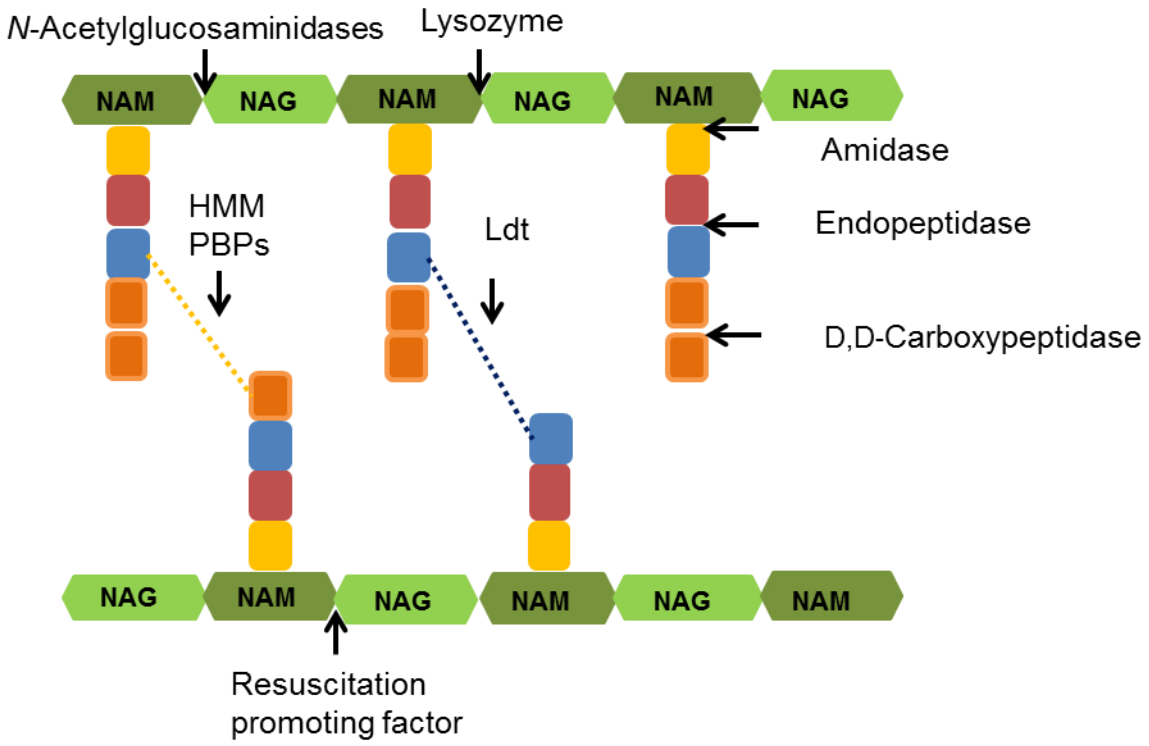


Figure 1.5: Schematic representation of the PG structure. The diagram displays the site of action (as indicated by black arrows) of selected PG hydrolases acting on the amide, glycosidic and peptide bonds. The 4,3 cross-links are indicated by the yellow dotted line and the 3,3 cross-links are indicated by the blue dotted line. PG constituents are indicated as follows: light green hexagon (Glc*N*Ac), dark green hexagon (Mur*N*Ac), yellow square (L-alanine), red square (D-glutamine), blue square (*meso*- Diaminopimalate) and orange square (D-alanine). Figure drawn by student, adapted from (Vollmer *et al*., 2008).

N-Acetylmuramyl-L-alanine amidases (amidases) cleave the amide bond between NAM and L-alanine of the pentapeptide resulting in separation of the entire stem peptide chain from the glycan strand (Uehara and Park, 2007) and are involved in septum cleavage and daughter cell separation during the last stages of cell division (Heidrich *et al*., 2002). Glycosidases are involved in cleavage of the glycan backbone and are further divided into three classes: lytic transglycosylases, lysozymes and *N*-Acetylglucosaminidases. The β-1,4 glycosidic bond between Glc*N*ac and Mur*N*ac can be cleaved differentially by lytic transglycosylases or lysozymes, with lysozyme cleavage yielding a product with a terminal reducing Mur*N*ac residue. Lytic transglycosylase activity results in the formation of 1,6-anhydro ring on the Mur*N*ac residue due to modification of the Mur*N*ac residue during catalysis, permitting

glycan bone expansion and insertion of new PG subunits (Vollmer *et al*., 2008). These enzymes are also involved in β-lactam resistance due to the role of the 1,6-anhydro product in β-lactamase induction (Tayler *et al*., 2010). Another group of PG hydrolases are the resuscitation promoting factors (Rpfs). Rpfs are functionally and structurally similar to lytic transglycosylases and have been shown to play a significant role in reactivation of dormant bacteria *in vitro* (Mukamolova *et al*., 1998; Kana *et al*., 2008; Machowski *et al*., 2014). *N*-Acetylglucosaminidases are a class of glycosidases that cleave the glycosidic bonds between NAG and NAM residues. This group of enzymes have not been extensively studied however, they have been postulated to have a role in cell wall turnover (Vollmer *et al*., 2008). Further, a number of enzymes act on the stem peptide, these are known as peptidases. Peptidases cleave within the stem peptide and this includes carboxy- and endopeptidases that hydrolyze various D,D- and L,D- bonds in the stem peptide, respectively (Machowski *et al*., 2014). PG hydrolases have the potential to destroy the bacterial cell wall completely if their activity is not carefully regulated, hence they are considered potential targets for anti-TB drug development (Kumar *et al*., 2013).

1.8. Penicillin binding proteins

Penicillin binding proteins (PBPs) are a large group of cell wall associated enzymes that bind β-lactam antibiotics (Sauvage *et al*., 2008). These periplasmic enzymes are responsible for PG synthesis and remodelling by facilitating polymerization of glycan strands and subsequent incorporation of the newly synthesized material into the existing wall (Derouaux *et al*., 2013; Ghosh *et al*., 2008). Based on their mobility during sodium dodecyl sulfate polyacrylamide (SDS-PAGE), and their amino acid sequences, these proteins can be divided into 2 broad categories: high molecular mass (HMM) PBPs, which are multidimodular PBPs with molecular weight of more than 50 kDa and low molecular mass (LMM) PBPs, which have molecular mass of less than 50kDa (Sauvage *et al*., 2008).

1.8.1. Penicillin-binding (PB) domain and enzymatic activity of PBPs

PBPs are acyl-serine transferases, the action of which is catalyzed by an active-serine moiety (Scheffers and Pinho, 2005; Rossi *et al*., 2016). The interaction between the PBPs and their substrate is mediated by functional motifs that are specific to these enzymes. These motifs make up the active site encompassing residues that are broadly conserved in PBPs, including a SXXK tetrad which contains the active serine followed by a lysine (1st motif), a SXN triad (2nd motif), and a KTG (T/S) triad which makes the 3rd motif (Figure 1.6) (Sauvage *et al*.,

2008; Laddomada *et al*., 2016). It has been hypothesized that these conserved motifs asume roughly the same spacing and order along polypeptide chains in different species (Scheffers and Pinho, 2005), as they have been identified in various bacterial PBPs including *Streptomyces* K15, PBP4 of *Pseudomonas aeruginosa* (*P. aeruginosa*), *Bacillus subtilis* (*B. subtilis*) PBP4a and *Escherichia coli* (*E. coli*) PBP4 (Rossi *et al*., 2016).The correct orientation of these sites is crucial for acetylation and deacetylation reactions to occur.

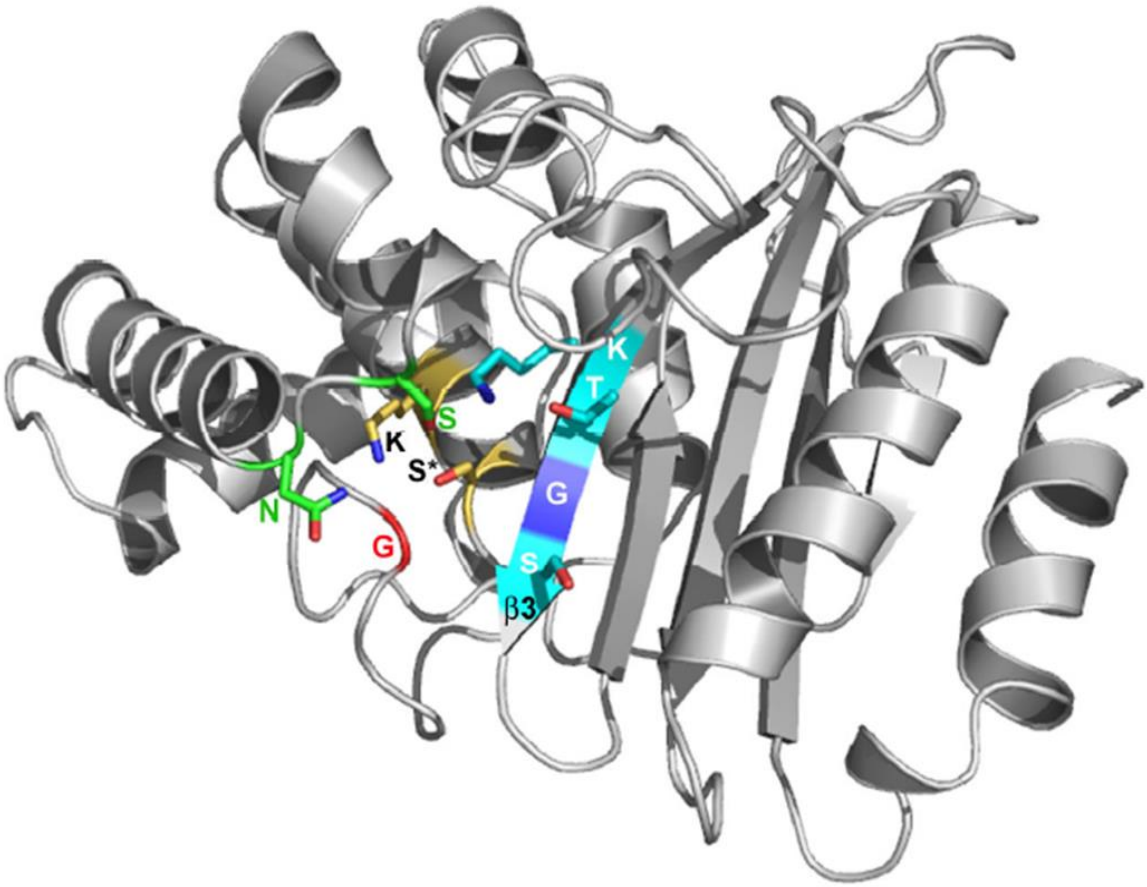


Figure1.6: Illustration of the active site of penicillin binding (PB) domain. The ribbon structure shows the PB domain and conserved motifs of the active site. Highlighted in yellow with black letters is the SxxK motif. The SxN motif is highlighted in green with green letters, and the last motif KTS (T/S) is highlighted in cyan with white letters. The red letter represents the glycine found in the active site. The active serine residue is shown by (*). Reproduced from (Sauvage *et al*., 2008).

The reaction catalyzed by PBPs follows a three-step mechanism. In the first step, the enzyme and the stem pentapeptide of the PG form a non-covalent Hendri-Michaelis acyl-enzyme complex via a tetrahedral intermediate. This is followed by the nucleophilic attack of the serine present in the active site of the enzyme on the D-alanyl carbonyl of the terminal D-Ala-D-Ala peptide bond, resulting in the formation of an acyl-enzyme intermediate and release of

the terminal D-Ala (acetylation). The last step which is the deacetylation, consist of either hydrolysis reaction called carboxypeptidation, with the release of shortened peptide, or endopeptidation reaction, resulting in formation of cross-link with the neighbouring stem peptide in PG known as the acceptor strand (Sauvage et al., 2008; Rossi *et al*., 2016). B lactams that target PBPs mimic the PG D-Ala-D-Ala C-terminus, hence PBPs recognize them as substrates and form the acyl-enzyme complex with them. The formation of this stable acyl-enzyme complex is essentially irreversible. Thus, β-lactams are mechanism-based, covalent PBPs inhibitors (Tipper and Strominger, 1965). Alteration in the copy number of PBPs as well as their β-lactams affinity can confer β-lactam resistance in a bacterial cell (Henry *et al*., 2010).

1.8.2. High molecular mass PBPs (HMM PBPs)

HMM PBPs are responsible for PG polymerization and insertion of newly synthesized PG subunits into the pre-existing wall and they have also been shown to play a role in cell elongation and septation (Ghosh et al., 2008). HMM PBPs are further divided into subclass A and B, depending on the structure of their N-terminal domain and its catalytic activity. Class A HMM PBPs are bifunctional enzymes consisting of both the transglycosylase and transpeptidase activities, whereas Class B HMM PBPs are monofunctional with only transpeptidase activity (Goffin and Ghuysen, 2002). The general topology of HMM PBPs consists of a cytoplasmic tail, a transmembrane anchor and two domains connected by a β-rich linker, located in the periplasm (Figure 1.7) (Macheboeuf *et al*., 2006; Sauvage *et al*., 2008). In both classes, the C-terminal PB domain has a transpeptidase activity and is responsible for catalyzing cross-linking of stem peptides between adjacent glycan strands (Figure 1.7). In class A, the N-terminal domain has glycosyltransferase activity and is responsible for catalyzing the polymerization of glycan chains (Figure 1.7). The N-terminal domain of class B HMM PBPs has no catalytic activity and it is hypothesized to have a role in cell morphogenesis by interacting with various proteins involved in the cell cycle (Sauvage *et al*., 2008).

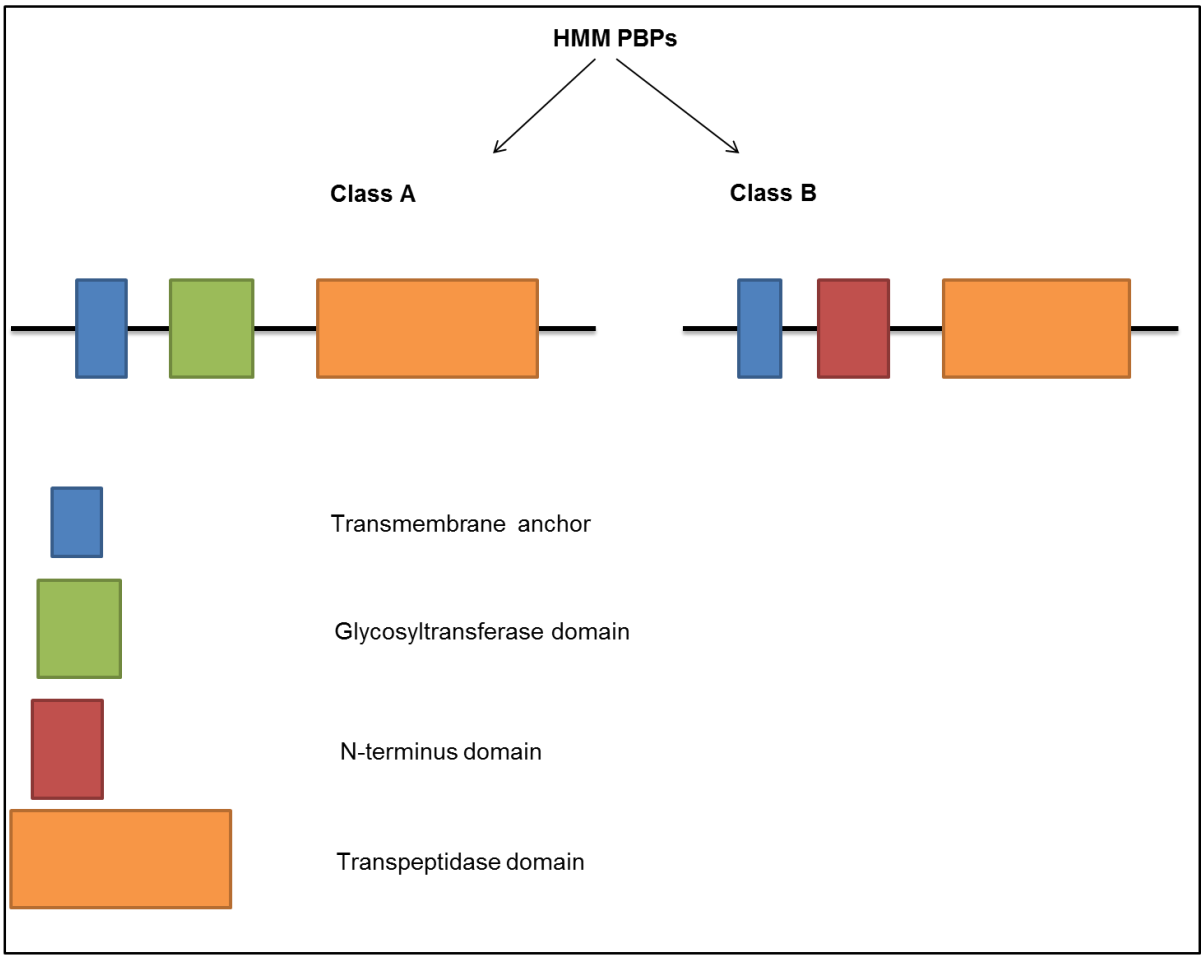


Figure 1.7: Schematic representation of domain organization of HMM PBPs. (A) Class A HMM PBPs are bifunctional, having both glycosyltransferase activity and transpeptidase activity. (B) Class B HMM PBPs are monofunctional and they only possess transpeptidase activity. The N-terminal domain of class B HMM PBPs has no catalytic activity. Both class A and B PBPs are associated with the membrane through a transmembrane anchor. Figure drawn by student.

Most organisms possess a number of HMM PBPs. *Streptococccus pneumoniae* (*S. pneumoniae*) possesses three bifunctional class A PBPs, which are dispensable for survival of the bacteria, and two essential class B PBPs designated PBP2b and PBP2x, that play a role in PG synthesis in the periplasm and formation of the septum, respectively (Sham *et al*., 2012). A low level β-lactam resistance in *S. pneumoniae* is attributed to mutations in the two class B PBPs, and additional mutations in class A PBP1a are required for high level β-lactam resistance (Zapun *et al*., 2008). In *B. subtilis*, PBP1 is amongst the four class A PBPs and it is required for efficient asymmetric septum formation during sporulation (Scheffers and Errington, 2004). In addition, *B. subtilis* has six class B PBPs, with PBP2 playing a role in cell division (Daniel *et al*., 2000). The activities of HMM PBPs have been well defined in *E. coli*, and two of the five (PBP3 and PBP2, both class B PBPs) are essential for cell division,

cell elongation and maintenance of the rod shape, respectively (Sauvage *et al*., 2008). Among the three bifunctional class A PBPs (PBP1a, PBP1b and PBP1c) in *E. coli*, PBP1a and PBP1b have the highest synthetic activity, of which at least one of them is required for cell survival as they are individually dispensable but simultaneous disruption of the two is lethal for the cell (Dörr et al., 2014). Mycobacteria possesses 2 class A PBPs, PBP1 (*ponA1*) and PBP1a (*ponA2*) and both these genes are present in *Mtb* and *Mycobacterium smegmatis* (*Msm*). In addition, *Msm* possesses a third class A PBP-encoding gene, annotated as *ponA3*. Class B PBPs include PBPA, PBPB and PBP-lipoprotein (Machowski *et al*., 2014; Kieser *et al*., 2015a). PBPB (FtsI) is essential for cell survival and it is recruited to the cell division site (Datta *et al*., 2006).

1.8.3. Low molecular mass PBPs (LMM PBPs)

LMM PBPs are often termed "accessory cell division proteins" and are involved in cell separation, PG maturation and recycling (Eagan and Vollmer, 2013). LMM PBPs are generally termed class C PBPs (Sauvage *et al*., 2008). LMM PBPs are monofunctional, with either D,D-carboxypeptidase activity (D,D,-CPase), which cleave of the terminal D-Ala from the pentapeptide chain, or they have D,D-endopeptidase activity, which cleaves peptide cross bridges (Ghosh *et al*., 2008; van Heijenoort, 2011). The transpeptidase domain of D,D-CPases is located downstream of the signal peptide and they also consist of a C-terminal transmembrane or amphipathic helix that allows for membrane association (Figure 1.8) (Macheboeuf *et al*., 2006).

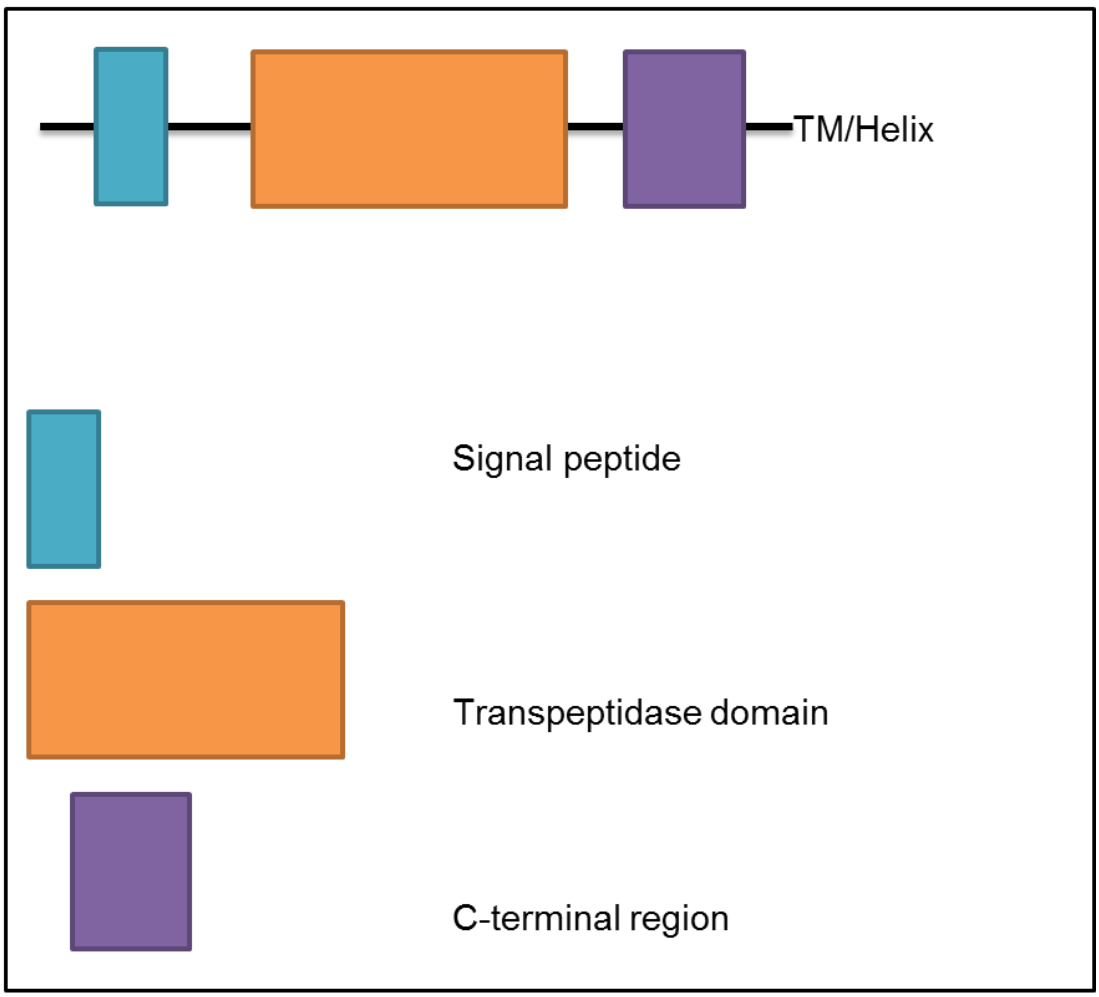


Figure 1.8: Schematic representation of domain organization of LMM PBPs. LMM PBPs are generally termed class C PBPs, and their structure is different from that of HMM PBPs in that their transpeptidase domain is encoded immediately downstream of the signal peptide found in the N-terminus. They are associated with the membrane through a transmembrane helix (TM) or an amphipathic helix. Figure drawn by student.

1.8.3.1. Endopeptidases

Endopeptidases are enzymes that cleave the peptide cross bridges in the PG (Ghosh *et al*., 2008), they cleave diverse D,D- and L,D- bonds within the stem peptide. In *B. subtilis*, PBP4a is the only LMM PBP that has been shown to have endopeptidase activity. PBP4 of *Staphylococcus aureus* (*S. aureus*) possesses transpeptidase activity that is needed for the high degree of cross-linking in the PG of this bacterium (Wyke *et al*., 1981). *E. coli* has two endopeptidases, PBP4 and PBP7 encoded by *dacB* and *pbpG*, respectively. PBP4 of *E. coli* is a bifunctional LMM PBP due to its minimal D,D-CPase activity in addition to its strong endopeptidase activity (Ghosh *et al*., 2008). This enzyme is dispensable for growth and the mutants display no growth defects or any detectable morphological changes. However, it has been shown that this enzyme has a primary role in repairing and/or regulating excessive

and/or inappropriate PG cross-links via its PG hydrolyzing activity (Thunnissen *et al*, 1995; Meberg *et al*, 2004). The *E. coli* PBP7 plays a role in septum cleavage and biofilm formation (Ghosh et al., 2008; Sauvage *et al*., 2008). PBP3 and PBP4 of *Neisseria gonorrhoeae* (*N. gonorrhoeae*) display sequence similarities to *E. coli* PBP4 and PBP7, respectively. In *Vibrio cholerae* (*V. cholerae*), VC0632 is more similar to *E. coli* PBP4, while VC0870 is more similar to PBP7 (Möll *et al*., 2015). Endopeptidases play a role in cell shape maintenance in a wide variety of bacteria. In mycobacteria, RipA is the most well characterized endopeptidase that is essential for growth *in vitro* (Hett *et al*., 2007) and it has been associated with resuscitation of dormant cells due to its interaction with RpfB and RpfE (Nikitushkin *et al*., 2015).

1.8.3.2. D,D-carboxypeptidases (D,D-CPases)

D,D-CPases are LMW PBPs that play a role in controlling the level of PG cross-links. This set of enzymes is involved in the last step of PG synthesis. They control the degree of PG cross-linking in the cell by cleaving off the terminal D-alanine from the side chain of the pentapeptide, generating a tetrapeptide stem, which is unable to act as a donor to form 4,3 PG cross-links (Egan and Vollmer, 2013). D,D-CPases are known to be important in maintaining bacterial cell shape. Although their biochemical activities are well known, their physiological roles still remain elusive due to their genetic redundancy. In *E. coli* the D,D-CPases include PBP5, PBP6 and PBP6b/DacD encoded by *dacA*, *dacC* and *dacD*, respectively (Ghosh *et al*., 2008). Individual deletion of these genes does not result in any drastic cell growth defects or altered cell morphology in *E. coli* (Denome *et al*., 1999). Among the three *E. coli* D,D-CPases, PBP5 is the most abundant and well characterized. PBP5 has been shown to have a role in cell shape maintenance and studies have also pointed out its accessory regulatory role in both bacterial cell division and elongation (Ghosh *et al*., 2008). Mutants lacking PBP5 display subtle changes in cell shape (Nelson and Young, 2000). In addition, deletion of other *E. coli* D,D-CPases in conjunction with PBP5 results in extensive morphological defects such as branches, kinks and bends, which can be restored when PBP5 expression is restored (Nelson and Young, 2001). The PBP5-mediated morphological restoration is dependent on both the C-terminal domain and the D,D-CPase activity of the enzyme (Nelson and Young, 2001). Overexpression of PBP5 is detrimental, resulting in conversion of normal rod-shaped *E. coli* cells into spherical form (Santos *et al*., 2002). All these observations suggest that PBP5 is important in stabilizing growth of the cell versus septal PG synthesis (Potluri *et al*., 2010). Both *E. coli* PBP6 and PBP6b share some degree of sequence homology with PBP5,

however, PBP6 displays weaker D,D-CPase activity towards other substrates when compared to PBP5. Although the three *E. coli* D,D-CPases share similar primary structures, they are likely to have distinct functions *in vivo* during the different growth phases (Ghosh *et al*., 2008).

N. gonorrhoeae has two D,D-CPases (PBP3 and PBP4), and PBP3 is involved in PG biosynthesis (Stefanova *et al*., 2003). Similar to the bifunctional *E. coli* PBP4, PBP3 of *N. gonorrhoeae* possesses weak endopeptidase activity in addition to its strong D,D-CPase activity (Stefanova *et al*., 2003). *V. cholerae* encodes two D,D-CPases (VC0947 encoded by *dacA-1* and VCA0270 encoded by *dacA-2*), which are highly similar to *E. coli* PBP5 as they share 60% sequence similarities with PBP5 at the protein level (Chowdhury and Ghosh, 2011). DacA-1 is believed to be the principal D,D-CPase in *V. cholera* and its deletion leads to altered cell morphology and severe growth impairment (Möll *et al*., 2015). In *B. subtilis*, PBP5 (*dacA*), PBP5* (*dacB*) and DacF display D,D-CPase activities. PBP5 is the major D,D-CPase in *B. subtilis* expressed during lag phase and promotes PG maturation (Ghosh et al., 2008). PBP5* is highly expressed during sporulation and it plays a role in the synthesis of spore cortex, whereas DacF is expressed within the forespore during the early stationary phase and it is believed to have a role in PG modification during sporulation (Popham *et al*., 1999). *S. pneumoniae* possesses a single D,D-CPase (PBP3), which plays a role in directing cell division proteins to the septum, with PBP3 mutants displaying cell division defects (Morlot *et al*., 2004). *Listeria monocytogenes* (*L. monocytogenes*) PBP5 regulates cell wall thickness and deletion of this enzyme results in altered cell morphology (Korsak *et al*., 2005).

In mycobacteria, the biological roles of D,D-CPases has not been well defined. *Mtb* has three D,D-CPase homologues: Rv3627c, Rv2911(encoded by *dacB2*) and Rv3330 (encoded by *dacB1*). In *Msm*, MSMEG_6113 is the equivalent of Rv3627c, MSMEG_1661 is the equivalent of Rv3330, MSMEG_2432 and MSMEG_2433 are Rv2911 duplicates (Machowski *et al*., 2014). In addition, *Msm* has a distinct D,D-CPase, annotated as MSMEG_1900. Studies conducted in our laboratory have shown that MSMEG_6113 is essential and that MSMEG_2433 is expressed at comparatively higher transcript abundance compared to other D,D-CPases in *Msm* (Ealand *et al*., unpublished).

Considering these collective findings, D,D-CPases are considered to be genetically redundant and highly conserved in a number of bacteria, implying that they have important but unrecognized physiological roles. The possible interaction of mycobacterial D,D-CPases with

other proteins in the cell, particularly HMW PBPs, may point to additional roles of these D,D-CPases in maintaining cell wall homeostasis. This MSc dissertation was aimed at addressing this knowledge gap.

1.9. Hypothesis and research motivation

Putative interacting partners of two *Msm* D,D-CPases designated MSMEG_6113 and MSMEG_2433 have been identified in a screen conducted in our laboratory using a bacterial two-hybrid system called the mycobacterial protein fragment complementation (M-PFC) assay. The M-PFC assay that was used to screen the *Msm* library identified 10 and 20 potential interacting partners for MSMEG_6113 and MSMEG_2433, respectively. Interestingly, a number of these partners were key regulators of cell division and elongation. It was therefore hypothesized that mycobacterial D,D-CPases play a significant role in cell growth, particularly in cell elongation and division, through interaction with various protein partners. To test this, we proposed to first confirm the putative D,D-CPase-interacting partners identified in the above-mentioned screen using full-length constructs. To test the importance of the interaction for cell division and growth, we propose to delete some of the interacting partners from the mycobacterial genome.

1.10. Aims and objectives

1.10.1. Aim

Considering the broad number of distinct proteins that were identified as interacting partners of the two D,D-CPases, combined with the predicted importance of these partners in PG synthesis and proliferation, the main aim of this study was to investigate the functional role of the two mycobacterial D,D-CPases through interaction and gene knockout studies.

1.10.2. Specific objectives

- To confirm interaction of MSMEG_6113 and MSMEG_2433 with their putative partnering proteins using M-PFC assay.
- To determine domains of the two D,D-CPases that are responsible for interaction with selected protein partners.
- To create *Msm* knockout mutant strains lacking selected protein partners.
- To perform phenotypic characterization of the resulting mutants using microscopy and microbiological assays.

2. Materials and methods

2.1. Databases and bioinformatics tools used

Various databases and bioinformatics tools were used throughout this study to obtain genomic DNA and amino acid sequences, and to analyze genes and proteins of interest. Table 2.1 illustrates databases and bioinformatics tools used in this study.

Table 2.1: Bioinformatics tools and databases used to obtain and analyze DNA and protein sequences. The table also provides online website addresses.

Database/bioinformatics tool	Use in the study	Address
SmegmaList	This database was used to interrogate *Msm* strain mc^2155 gene and protein sequences of interest.	ch/smegmalist.html
TubercuList	This database was used to interrogate *Mtb* strain H37RV gene and protein sequences of interest.	http://tuberculist.epfl.ch
BioCyc	This database was used to interrogate transcriptional units and operonic structures of genes of interest.	https://biocyc.org
pFam	This database was used to identify functional domains in protein sequences on interest.	http://pfam.xfam.org/
STRING	This database was used to investigate known and predicted physical (direct) and functional (indirect) protein-protein interaction	https://string-db.org

	of the D,D-CPases studied.	
NCBI BLAST	Basic Local Alignment Search Tool was used to identify genes that encode for selected partnering proteins in *Msm* genome and related organisms.	https://www.ncbi.nlm.nih.gov/BLAST
MUSCLE Clustal Omega	The two tools were used to identify regions of similarity among various amino acid sequences of selected D,D-CPases partnering proteins by aligning the multiple sequences. Also used for phylogenetic tree generation.	www.ebi.ac.uk/Tools/msa/muscle www.ebi.ac.uk/Tools/msa/ClustalO
I-TASSER	The Iterative Threading ASSEmbly Refinement server was used to predict three dimensional structure models and function of selected partnering proteins.	http://zhanglab.ccmb.med.umich.edu/I-TASSER/
SignalP 4.1	The server was used to identify signal peptides within amino acid sequences of interest, as well as predicting the signal peptide cleavage sites.	http://www.ebs.dtu.dk/services/signalP/

2.2 Chemicals and reagents used

Enzymes used throughout this study for DNA manipulation purposes were supplied by Roche, Fermentas and New England Biolabs (NEB), unless otherwise stated. Reagents for Media and solution preparation were obtained from Sigma Aldrich and Thermo Fischer Scientific (Appendix A). All primers were synthesized by the Inqaba Biotech group (Appendix B).

2.3 Bacterial strains and plasmids constructed and/or used

All plasmids and bacterial strains generated/used throughout this study are listed in Table 2.2 and Table 2.3., respectively. For all strains, glycerol freezer stocks were made using 66% glycerol (1:1 volume) and were stored in -80 °C.

Table 2.2. Plasmids constructed and/or used in this study

Plasmids	Description	Source/reference
p2NIL	*E. coli* cloning vector. Kan^R	Parish and Stoker, 2000
pGOAL17	Plasmid carrying *lacZ-bla-sacB* genes as *Pac*I cassette. Amp^R	Parish and Stoker, 2000
pMV306H	*E. coli-Mycobacterium* integrating shuttle vector, integrating at the L5 *attB* site in the genome of mycobacteria. Hyg^R	H. Boshoff
pUAB300	*E. coli- Mycobacterium* episomal shuttle vector carrying N-terminal mDHFR fragment 1 and 2, together with the glycine linker. Hyg^R	Singh *et al*., 2006
pUAB400	*E. coli- Mycobacterium* integrating shuttle vector carrying N-terminal mDHFR fragment 3. Kan^R	Singh *et al*., 2006
p2NIL*cdc48*	Derivative of p2NIL carrying the ΔMSMEG_0858 deletion allele. The deletion allele was generated by deleting 2040 bp (amino acid 34-679) from MSMEG_0858. Kan^R	This study
p2NIL*ftsI*	Derivative of p2NIL carrying the ΔMSMEG_4233 deletion allele. The deletion allele was generated by deleting 1749 bp (amino acid 34-582) from	This study

	MSMEG_4233. Kan^R	
p2NIL*cdc48*_Pac	Derivative of p2NIL*cdc48* carrying the *lacZ* and *sacB* genes from pGOAL17. Kan^R	This study
p2NIL*ftsI*_Pac	Derivative of p2NIL*ftsI* carrying the *lacZ* and *sacB* genes from pGOAL17. Kan^R	This study
pMV306H*cdc48*	Derivative of pMV306H carrying MSMEG_0858 wild type allele and the upstream native promoter region. Hyg^R	This study
pMV306H*ftsI*	Derivative of pMV306H carrying MSMEG_4233 wild type allele and the upstream native promoter region. Hyg^R	This study
pUAB300+6900	Derivative of pUAB300 carrying full length copy of MSMEG_6900. Hyg^R	This study
pUAB300+4227	Derivative of pUAB300 carrying full length copy of MSMEG_4227. Hyg^R	This study
pUAB300+0031	Derivative of pUAB300 carrying full length copy of MSMEG_0031. Hyg^R	This study
pUAB300+6105	Derivative of pUAB300 carrying full length copy of MSMEG_6105. Hyg^R	This study
pUAB300+4233	Derivative of pUAB300 carrying full length copy of MSMEG_4233. Hyg^R	This study
pUAB300+0858	Derivative of pUAB300 carrying full length copy of MSMEG_0858. Hyg^R	This study
pUAB300+5637	Derivative of pUAB300 carrying full length copy of MSMEG_5637. Hyg^R	This study
pUAB300+0365	Derivative of pUAB300 carrying full length copy of MSMEG_0365. Hyg^R	This study
pUAB300+6112	Derivative of pUAB300 carrying full length copy of MSMEG_6112. Hyg^R	This study
pUAB400+6113	Derivative of pUAB400 carrying full length copy of MSMEG_6113. Kan^R	This study
pUAB400+2433	Derivative of pUAB400 carrying full length copy of MSMEG_2433. Kan^R	This study

pUAB400+6900	Derivative of pUAB400 carrying full length copy of MSMEG_6900. Kan^R	This study
pUAB400+4227	Derivative of pUAB400 carrying full length copy of MSMEG_4227. Kan^R	This study
pUAB400+0031	Derivative of pUAB400 carrying full length copy of MSMEG_0031. Kan^R	This study
pUAB400+6105	Derivative of pUAB400 carrying full length copy of MSMEG_6105. Kan^R	This study
pUAB400+4233	Derivative of pUA400 carrying full length copy of MSMEG_4233. Kan^R	This study
pUAB400+0858	Derivative of pUAB400 carrying full length copy of MSMEG_0858. Kan^R	This study
pUAB400+5637	Derivative of pUAB400 carrying full length copy of MSMEG_5637. Kan^R	This study
pUAB400+0365	Derivative of pUAB400 carrying full length copy of MSMEG_0365. Kan^R	This study
pUAB400+6112	Derivative of pUAB400 carrying full length copy of MSMEG_6112. Kan^R	This study
pUAB300+6113	Derivative of pUAB300 carrying full length copy of MSMEG_6113. Hyg^R	This study
pUAB300+2433	Derivative of pUAB300 carrying full length copy of MSMEG_2433. Hyg^R	This study
pUAB400+6113SP	Derivative of pUAB400 carrying 147 bp sequence encoding the signal peptide of MSMEG_6113. Kan^R	This study
pUAB400+6113TP	Derivative of pUAB400 carrying 685 bp sequence encoding the transpeptidase domain of MSMEG_6113. Kan^R	This study
pUAB400+6113LR	Derivative of pUAB400 carrying 611 bp sequence encoding the linker region of MSMEG_6113. Kan^R	This study
pUAB400+2433SP	Derivative of pUAB400 carrying 90 bp sequence encoding the signal peptide of MSMEG_2433. Kan^R	This study

pUAB400+2433TP	Derivative of pUAB400 carrying 685 bp sequence encoding the transpeptidase domain of MSMEG_2433. Kan^R	This study
pUAB400+2433Cter	Derivative of pUAB400 carrying the 99 bp sequence encoding the C terminal region of MSMEG_2433. Kan^R	This study
pMV306H+GFP	Derivative of pMV306H carrying the green fluorescence protein (GFP). Hyg^R	CBTBR
pMV306H+FtsZGFP	Derivative of pMV306H carrying the full copy of *ftsZ* gene tagged with green fluorescence protein (GFP). Hyg^R	CBTBR

Amp^R: Ampicillin resistance, Hyg^R: Hygromycin resistance, Kan^R: Kanamycin resistance, GFP: Green fluorescence protein, *attB*: $tRNA^{GLY}$ attachment site.

Table 2.3. Bacterial strains generated and/or used in this study

Strain	**Description**	**Source/reference**
E. coli DH5α	*SupE44 Δlacu169 hsdR17 recA1 endA1 gyrA96 thi-1 relA1*	Promega, Madison, W1
mc^2155	Efficient *Msm* ATTCC 607 transformation mutant.	Snapper *et al*., 1990
mc^2155::pUAB400(pUAB300)	Derivative of mc^2155 carrying the pUAB400 plasmid integrated at the *attB* site, and the episomal pUAB300 plasmid, Kan^RHyg^R	D.B. Ralefeta (CBTBR)
mc^2155::pUAB5439(pUAB3145)	Derivative of mc^2155 carrying the pUAB400+5439 plasmid and the pUAB300+3145 plasmid. Kan^RHyg^R	D.B Ralefeta (CBTBR)
mc^2155::pUAB6113(pUAB4233)	Derivative of mc^2155 carrying the pUAB400+6113 plasmid and the pUAB300+4233 plasmid. Kan^RHyg^R	This study
mc^2155::pUAB6113(pUAB0858)	Derivative of mc^2155 carrying the	This study

	pUAB400+6113 plasmid and the pUAB300+0858 plasmid. $Kan^{R}Hyg^{R}$	
$mc^{2}155$::pUAB6113(pUAB5637)	Derivative of $mc^{2}155$ carrying the pUAB400+6113 plasmid and the pUAB300+5637 plasmid. $Kan^{R}Hyg^{R}$	This study
$mc^{2}155$::pUAB6113(pUAB0365)	Derivative of $mc^{2}155$ carrying the pUAB400+6113 plasmid and the pUAB300+0365 plasmid. $Kan^{R}Hyg^{R}$	This study
$mc^{2}155$::pUAB6113(pUAB6112)	Derivative of $mc^{2}155$ carrying the pUAB400+6113 plasmid and the pUAB300+6112 plasmid. $Kan^{R}Hyg^{R}$	This study
$mc^{2}155$::pUAB2433(pUAB6900)	Derivative of $mc^{2}155$ carrying the pUAB400+2433 plasmid and the pUAB300+6900 plasmid. $Kan^{R}Hyg^{R}$	This study
$mc^{2}155$::pUAB2433(pUAB4227)	Derivative of $mc^{2}155$ carrying the pUAB400+2433 plasmid and the pUAB300+4227 plasmid. $Kan^{R}Hyg^{R}$	This study
$mc^{2}155$::pUAB2433(pUAB0031)	Derivative of $mc^{2}155$ carrying the pUAB400+2433 plasmid and the pUAB300+0031 plasmid. $Kan^{R}Hyg^{R}$	This study
$mc^{2}155$::pUAB2433(pUAB6105)	Derivative of $mc^{2}155$ carrying the pUAB400+2433 plasmid and the pUAB300+6105 plasmid. $Kan^{R}Hyg^{R}$	This study
$mc^{2}155$::pUAB2433SP(pUAB4227)	Derivative of $mc^{2}155$ carrying the pUAB400+2433SP plasmid and	This study

	the pUAB300+4227 plasmid. $Kan^R Hyg^R$	
mc^2155::pUAB2433TP(pUAB4227)	Derivative of mc^2155 carrying the pUAB400+2433TP plasmid and the pUAB300+4227 plasmid. $Kan^R Hyg^R$	This study
mc^2155::pUAB2433Cter(pUAB4227)	Derivative of mc^2155 carrying the pUAB400+2433Cter plasmid and the pUAB300+4227 plasmid. $Kan^R Hyg^R$	This study
mc^2155::pUAB2433TP(pUAB6900)	Derivative of mc^2155 carrying the pUAB400+2433TP plasmid and the pUAB300+6900 plasmid. $Kan^R Hyg^R$	This study
mc^2155::pUAB2433Cter(pUAB6900)	Derivative of mc^2155 carrying the pUAB400+2433Cter plasmid and the pUAB300+6900 plasmid. $Kan^R Hyg^R$	This study
mc^2155::pUAB6113SP(pUAB0858)	Derivative of mc^2155 carrying the pUAB400+6113SP plasmid and the pUAB300+0858 plasmid. $Kan^R Hyg^R$	This study
mc^2155::pUAB6113TP(pUAB0858)	Derivative of mc^2155 carrying the pUAB400+6113TP plasmid and the pUAB300+0858 plasmid. $Kan^R Hyg^R$	This study
mc^2155::pUAB6113SP(pUAB4233)	Derivative of mc^2155 carrying the pUAB400+6113SP plasmid and the pUAB300+4233 plasmid. $Kan^R Hyg^R$	This study
mc^2155::pUAB6113TP(pUAB4233)	Derivative of mc^2155 carrying the pUAB400+6113TP plasmid and the pUAB300+4233 plasmid.	This study

	$Kan^R Hyg^R$	
Δ*cdc48*	Derivative of mc^2155 carrying an unmarked in frame deletion in *cdc48* (MSMEG_0858). Constructed by electroporation of the p2NIL*cd48*_Pac plasmid into mc^2155 strain.	This study
Δ*cdc48::cdc48*	Genetically complemented derivative of Δ*cdc48* carrying a full length copy of *cdc48* integrated at the *attB* site. Constructed by electroporation of pMV306*cdc48* into the Δ*cdc48* strain. Hyg^R	This study
mc^2155::FtsZ_GFP	Derivative of mc^2155 expressing FtsZ_GFP fusion protein. Constructed by electroporation of the pMV306H+FtsZ_GFP plasmid into mc^2155. Hyg^R	This study
Δ*cdc48*::FtsZ_GFP	Derivative of Δ*cdc48* expressing FtsZ_GFP fusion protein. Constructed by electroporation of the pMV306H+FtsZ_GFP plasmid into Δ*cdc48*. Hyg^R	This study

Hyg^R: Hygromycin resistance, Kan^R: Kanamycin resistance, GFP: Green fluorescence protein, *attB*: $tRNA^{GLY}$ attachment site.

2.4. Bacterial strains culture conditions

2.4.1 Growth conditions for *E. coli* DH5α and derivative strains

E. coli strains were grown on Luria-Bertani agar (LA) or in Luria- Bertani broth (LB) supplemented with appropriate antibiotics at the following concentrations: 100 µg/ml Ampicillin (Amp), 200 µg/ml Hygromycin (Hyg), and 50 µg/ml Kanamycin (Kan). Incubation at 37 °C was used for cultures carrying plasmids < 8 kbp and cultures carrying

plasmids > 8 kbp were incubated at 30 °C, with shaking at 250 rpm, to prevent plasmid rearrangement.

2.4.2 Growth conditions for *Msm* and derivative strains

Msm strains were grown on Middlebrook 7H10 solid media supplemented with 0.2 % glucose, 0.5 % glycerol, 0.085% NaCl (herein referred as 7H10 agar), and appropriate antibiotics at 37 °C or in Middlebrook 7H9 liquid media supplemented with 0.2% glucose, 0.085% NaCl, 0.5% glycerol, 0.05% Tween 80 (herein referred to as 7H9) and appropriate antibiotics at 37 °C with shaking at 100 rpm unless stated otherwise. The concentrations of antibiotics used were as follows: 50 µg/ml Hyg and 25 µg/ml Kan.

2.5 Nucleic acid extractions

2.5.1. *E. coli* plasmid DNA extractions

2.5.1.1. Small scale plasmid DNA extraction

The alkaline lysis mini-preparation method (Birnboim and Doly, 1979) was used for small scale plasmid DNA extraction from *E. coli* DH5α derivative strains carrying plasmids of interest. The strains were grown at 37 °C overnight in 2 ml LB media supplemented with appropriate antibiotics. Cells were then harvested by centrifugation at 12 470 x g and the pellets were re-suspended in 100 µl of solution I. Thereafter, 200 µl of solution II (Table A2) was added, mixed by inversion and incubated at room temperature for 5 min. This was followed by addition of 150 µl solution III to the mixture and incubation on ice for 5 min. The suspensions were then centrifuged for 10 min and the supernatant was transferred to a clean Eppendorf tube, followed by addition of 3 µl of RNAseA (10 mg/ml) and incubation for 15 min at 42 °C. Plasmid DNA was then precipitated by adding 600 µl of isopropanol to the mixture and centrifugation at 12 470 x g for 30 min. The isopropanol supernatant was then discarded and the pellet was washed with 70 % ethanol and dried using an Eppendorf concentrator 5301. The pellet was resuspended in nuclease free water and quantified using the Nanodrop spectrophotometer (NanoDrop technologies) and stored at 4 °C until further use.

2.5.1.2. Large scale plasmid DNA extraction

Bulk DNA extractions were done using the Macherey-Nagel Nucleobond plasmid DNA extraction Kit and following manufacturer's instructions. Briefly, the strains were grown at

37 °C overnight in 50-100 ml LB supplemented with appropriate antibiotics. Cells were then harvested by centrifugation at 4 500 x g for 15 min at 4 °C. The supernatant was discarded and the pellet was resuspended in 8 ml of cell lysis buffer to lyse the cells. The cell lysate was incubated at room temperature for 5 min. Thereafter, 8 ml of neutralization buffer was added to the sample, mixed thoroughly until the solution turned colorless. The column and the filter paper were first equilibrated with 12 ml of equilibration buffer. This was followed by addition of the clarified cell lysate, which passed through the column. Subsequently, the column was washed with 5 ml of equilibration buffer. The filter was then removed and the column was washed for the second time to remove impurities with 8 ml wash buffer. The plasmid DNA was eluted from the column by addition of 5 ml elution buffer and eluate was then collected into a clean tube. This was followed by precipitation of the plasmid DNA by addition of 3.5 ml isopropanol and centrifugation at 4 500 x g for 30 min at 4 °C. The DNA pellet was washed with 2 ml of 70 % ethanol and was dried using Eppendorf concentrator 5301. The pellet was resuspended in nuclease free water and quantified using the Nanodrop spectrophotometer (NanoDrop technologies) and stored at 4 °C until further use.

2.5.2. Mycobacterial chromosomal DNA extractions

2.5.2.1 Small scale chromosomal DNA extraction

The colony boil method (Tortoli *et al*., 2001) was used for extraction of chromosomal DNA from *Msm* mc^2 155 and derivative strains. Half a colony was scraped from solid media and resuspended in 50 µl of dsH_2O. Thereafter, 50 µl of chloroform was added to the suspension and mixed by vortexing. The mixture was then incubated at 95 °C for 5 min, followed by centrifugation at 12 470 x g for 5 min. The aqueous layer was then transferred into a clean tube and used as template for PCR.

2.5.2.2. Large scale chromosomal DNA extraction

The Cetyltrimethylammonium bromide (CTAB) method was used for bulk extraction of chromosomal DNA from *Msm* and derivative strains as previously decribed by Wilson (1997). The strains were first grown for two days at 37 °C on 7H10 agar. The cells were scraped off the plate and resuspended in 500 µl of TE buffer. The cells were then heat killed by incubation at 65 °C for 20 min, followed by addition of 70 µl lysozyme (10 mg/ml) and incubation at 37°C for an hour. Thereafter, 6 µl of proteinase K (10 mg/ml) and 70 µl of 10 % SDS were mixed into the suspension and the mixture was incubated for 2 hours at 65 °C.

This was followed by addition of 100 µl of NaCl (5M) with mixing, followed by addition of 80 µl of pre-warmed (65 °C) CTAB/NaCl. The suspension was then incubated at 65 °C for 10 min. An equal volume of chroroform: isoamyl alcohol (24:1 v/v) was added, mixed vigorously and centrifuged at 1 470 x g for 5 min at room temperature. The top aqueous layer was transferred into a fresh Eppendorf tube and the DNA was precipitated by addition of 600 µl isopropanol and centrifugation at 12 470 x g for 20 min. The pellet was then washed with 1 ml of 70 % ethanol by centrifugation at 12 470 x g for 3 min, dried using an Eppendorf concentrator 5301, resuspended in nuclease free water and quantified by the Nanodrop spectrophotometer (NanoDrop technologies) and stored at 4 °C until further use.

2.6 DNA manipulations

2.6.1 DNA amplification by Polymerase Chain Reaction (PCR)

Table 2.4 shows parameters used for primer design using the online Primer3 program (http://bioinfo.ut.ee/primer3).

Table 2.4: Parameters used for primer design

	Size (bp)	Tm (°C)	%GC
Minimum	18	55	55
Maximum	25	63	65
Optimum	23	60	62

2.6.1.1. Roche Faststart Taq PCR

The Roche Faststart Taq DNA polymerase protocol was used by following the manufacturer's instructions for PCR screening of clones and confirmation of gene deletion mutants. PCR reactions were set up using the following components: 5 µl of 10X recommended buffer, 10 µl 5x GC buffer, 2.5 µl of forward and reverse primer to a final concentration of 1 µM each, 8 µl of dNTPs to a final concentration of 0.2 µM, 2 U Taq polymerase, and 50- 100 ng of template DNA. The final reaction volume was made up to 50 µl with nuclease free water. The reactions were incubated in a thermocycler (Bio-Rad laboratories) using the following cycling conditions: 4 min of initial denaturation at 95 °C, 30 cycles of 30 sec of secondary denaturation at 95 °C, 45 sec of annealing at 65 °C, 1 min of extension at 72 °C and 10 min of final extension at 72 °C.

2.6.1.2 Q5 high-fidelity PCR

Q5 High-fidelity DNA polymerase (NEB) was used for high-fidelity PCR by following the manufacturer's instructions for amplification of DNA fragments used for cloning purposes. PCR reactions were set up using the following components: 10 µl of 5X Q5 reaction buffer, 10 µl 5X high GC enhancer, 2.5 µl of forward and reverse primer to a final concentration of 0.5 µM each, 1 µl of dNTPs to a final concentration of 200 µM, 0.5 µl Q5 High-Fidelity DNA polymerase, 50- 100 ng of template DNA, made up with nuclease free water to a final reaction volume of 50 µl. The reactions were incubated in a thermocycler (Bio-Rad laboratories) using the following cycling conditions: 30 sec of initial denaturation at 98 °C, 35 cycles of 10 sec of secondary denaturation at 98 °C, 30 sec of annealing at 70 °C, 30 sec of extension at 72 °C and 2 min of final extension at 72 °C.

2.6.2. Restriction enzyme digestions

Restriction enzymes used in this study for digestion of plasmid or PCR DNA were purchased either from Roche Applied Science (Roche), Fermentas or New England Biolabs (NEB). Restriction digestion reactions were performed as per manufacturer's instructions. Briefly, 1 µg of DNA was digested with 1 U restriction enzyme in 1X recommended buffer and addition of sdH_2O to a final reaction volume of 20 µl. Reactions were incubated for an hour at 37 °C, followed by heat inactivation at 65 °C for 10 min unless advised otherwise by the manufacturer.

2.6.3 Nucleic acid quantification

Quantification of all DNA was carried out using the Nanodrop ND-1000 spectrophotometer (Nanodrop Technologies), which quantifies DNA by measuring absorbance of the sample at a wavelength of 260 nm.

2.6.4 DNA visualization and purification

2.6.4.1. Agarose gel electrophoresis

Agarose gel electrophoresis was used for visualization of DNA. The percentage of agarose in gels depended on the molecular weight of the sample/s to be analyzed. Low molecular weight DNA was separated by using 2 % agarose gels made in 1X TAE buffer (1 mM EDTA and 40 mM Tris-acetate) and high molecular weight DNA was separated by using 0.8-1 % agarose gels. Electrophoresis was carried out in 1X TAE buffer at 80-90 V in electrophoresis tanks

(Bio-Rad laboratories). DNA molecular weight markers were also run on the same gel for molecular size estimation of the DNA sample analyzed. Visualization of the gels was achieved by the use of SYNGENE G-Box system.

2.6.4.2 DNA fragment purification

Fragment purification was performed for either the product of restriction digest of plasmids or PCR fragments using the NucleoSpin PCR clean-up and gel extraction kit (Macherey-Nagel), as per manufacturer's instructions. Briefly, DNA was run on an agarose gel and the fragment was then excised from the gel. The gel slice was solubilized by mixing with binding buffer and incubation at 50 °C for 5-10 min. For PCR fragment clean-up, 1 volume of the sample was directly mixed with 2 volumes of the binding buffer. Thereafter, the solubilized gel fragment or PCR DNA fragment was loaded into the NucleoSpin column which was placed in a collection tube. The sample was then centrifuged for 30 sec at 11 000 x g to allow binding of DNA to the column. The flow-through was then discarded and the column was washed twice with 700 µl of wash buffer and centrifuged at 11 000 x g for 30 sec. The flow-through was discarded and the column was dried by centrifugation at 12 470 x g for 1 min. This was followed by elution of DNA into a fresh Eppendorf tube by addition of 30 µl of elution buffer and centrifugation at 11 000 x g for 1 min. The DNA was stored at 4°C for subsequent DNA manipulation steps.

2.6.5. DNA ends modification

2.6.5.1. Dephosphorylation of DNA

Dephosphorylation of the 5'ends of linearized plasmid DNA was carried out using Antarctic Alkaline Phosphatase (NEB). The reaction contained 1 µg of plasmid DNA, 2 µl of Antarctic Alkaline Phosphatase buffer, 1 U of Antarctic Alkaline Phosphatase and sdH_2O to a final volume of 20 µl. The reaction was then incubated for an hour at 37 °C, followed by heat inactivation at 65 °C for 20 min.

2.6.5.2. Phosphorylation of DNA

Polynucleotide Kinase (NEB) was used for phosphorylation of PCR products. 1 U of Polynucleotide Kinase was added to 1 µg of PCR product, 2 µl of Polynucleotide Kinase buffer, 2 µl of 10 mM ATP and sdH_2O to a final reaction volume of 20 µl. This was then incubated for 1 hour at 37 °C and heat inactivation at 65 °C for 20 min.

2.6.6. DNA ligation

DNA fragments were ligated together using T4 DNA ligase (NEB). Ligation reactions contained a constant amount of plasmid DNA of 50 ng, desired volume of insert DNA, 1 U of enzyme, 2 µl of T4 DNA ligase reaction buffer and sdH_2O to a final reaction volume of 20 µl. This was then incubated at room temperature for 20 min, followed by heat inactivation of the enzyme at 65 °C for 10 min. The following equation was used to calculate the amount of insert DNA required for 1:1 (vector: insert) ligation reaction.

Amount of insert DNA (ng) = 50 ng x size of insert (bp) / size of vector (bp)

2.6.7. DNA sequencing

All constructs generated in this study by PCR based cloning techniques were sequenced in order to confirm that no mutations have been introduced into the gene/region of interest during the process. DNA sequencing was done by the DNA Sequencing Facility of Stellenbosch University and the sequencing data was analysed using the DNASTAR software (DNASTAR).

2.7. Bacterial transformations

2.7.1. Preparation and transformation of *E. coli* chemically competent cells

E. coli chemically competent DH5α cells were prepared and transformed following the protocol previously decribed by Sambrook *et al*., 1989. A single colony was picked and inoculated into 5 ml of LB and incubated at 37 °C overnight. Thereafter, 1 ml of the overnight culture was used to inoculate 100 ml of fresh LB and incubated at 37 °C for 3-5 hours. The sample was then put on ice for 20 min followed by harvesting the cells by centrifugation at 4 500 x g for 10 min at 4 °C. The pellet was then resuspended in 10 ml of ice cold $CaCl_2$ (0.1 M) and chilled on ice for 20 min. The cells were then harvested as before, resuspended in 5 ml of $CaCl_2$ and kept on ice or used immediately for transformation.

Transformation of the chemically competent cells was done by mixing 100 µl of cells with the desired volume of plasmid DNA, followed by incubation on ice for 15 min and transformation by heat shock at 42 °C for 90 sec. Subsequently, cells were chilled on ice for 2 min and recovered with 800 µl of warm LB. Following this, cells were incubated for an hour at 37 °C with 100 rpm shaking. Cells were then selected on LA media supplemented with

appropriate antibiotics and incubated overnight at 37 °C to allow for selection of positive transformants.

2.7.2. Preparation and transformation of *Msm* electro-competent cells

Msm competent cells were prepared as previously described by Larsen (2002). Briefly, 50-100 ml of fresh 7H9 media was inoculated with a starter culture, followed by growth to an OD_{600} of 0.5-0.8 at 37 °C. Cells were then harvested by centrifugation at 4500 x g for 10 min at 4 °C, followed by three washes with gentle resuspension in 30 ml ice cold 10 % glycerol and centrifugation as before. Following the washing steps, cells were resuspended in 3 ml 10% glycerol and kept on ice until used.

For electroporations, 400 µl of the cells was mixed with 1 µg of plasmid DNA and transferred into a pre-chilled 0.2 cm GenePulser cuvette (BioRad). The BioRad GenePulser X-Cell^{TM} system (BioRad) was used to perform electroporations under the following parameters: Voltage 2 500 V, Capacitance 25 µF, Resistance 1000 Ω and Distance 0.2 cm. Following pulsing, cells were rescued with 800 µl of LB, transferred into a fresh tube and incubated at 37 °C for 3-16 hours. This was followed by selection of the cells on 7H10 media supplemented with appropriate antibiotics for 3-7 days at 37 °C.

2.8. Confirmation of D,D-CPase interacting partners and determination of D,D-CPase domains responsible for interaction

Figure 2.1. gives a diagrammatic representation of the work done in this study.

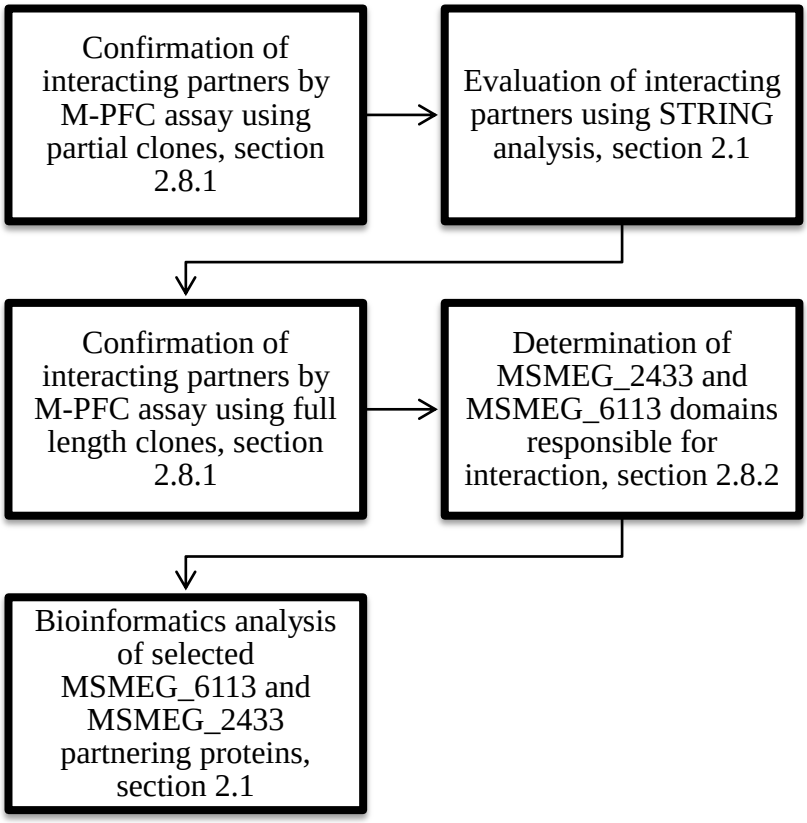


Figure 2.1: Diagrammatic representation of experimental layout of interaction work done in this study. Identified partnering proteins were first confirmed and evaluated by M-PFC assay and STRING analysis. Thereafter, few partners were selected and verified using full length clones, followed by identification of D,D-CPase interacting domains as well as functional analysis of the selected partners through bioinformatics. Sections refer to the relevant sections of the materials and methods.

2.8.1. Confirmation of D,D-CPase interacting partners

To confirm previously identified putative interacting partners of MSMEG_6113 and MSMEG_2433, the mycobacterial protein fragment complementation (M-PFC) two-hybrid system was used as previously described (Singh *et al*., 2006). This system is based on functional rearrangement of two murine dihydrofolate reductase (mDHFR) domains (an adenine binding domain (F[2]) and a discontinuous domain (f[1]& f[3]) which are autonomously tagged to two proteins to test interaction when co-transformed into mycobacteria. Where there is interaction between the two proteins, the mDHFR domains reassemble into a functional enzyme that hydrolyses trimethoprim (trim), thus allowing for

selection of positive interacting partners on trim supplemented media (Figure 2.2). Briefly, the ORFs of the genes of interest were cloned separately into pUAB400 and pUAB300 plasmids as described in section 2.6.6., and the resulting constructs were confirmed by sequencing before subsequent use. The plasmids were then co-transformed into wildtype mc^2155 following the protocol outlined in section 2.7.2. The resulting transformants were subsequently picked, resuspended in 1 ml fresh 7H9 broth and inoculated onto 7H10 agar supplemented with Hyg (50 µg/ml), Kan (25 µg/ml) and trim (7.5 µg/ml) and incubated at 37 °C for 7 days to allow for selection of positive interaction. To confirm the functionality and efficacy of the M-PFC system, the prey and the bait vectors carrying Rpf interacting protein A (RipA) and resuscitation promoting factor B (RpfB), respectively, were used as positive controls based on proven interaction (Hett *et al*., 2007; Hett *et al*, 2008). In addition to the wildtype mc^2155, the empty vector strains were used as negative controls.

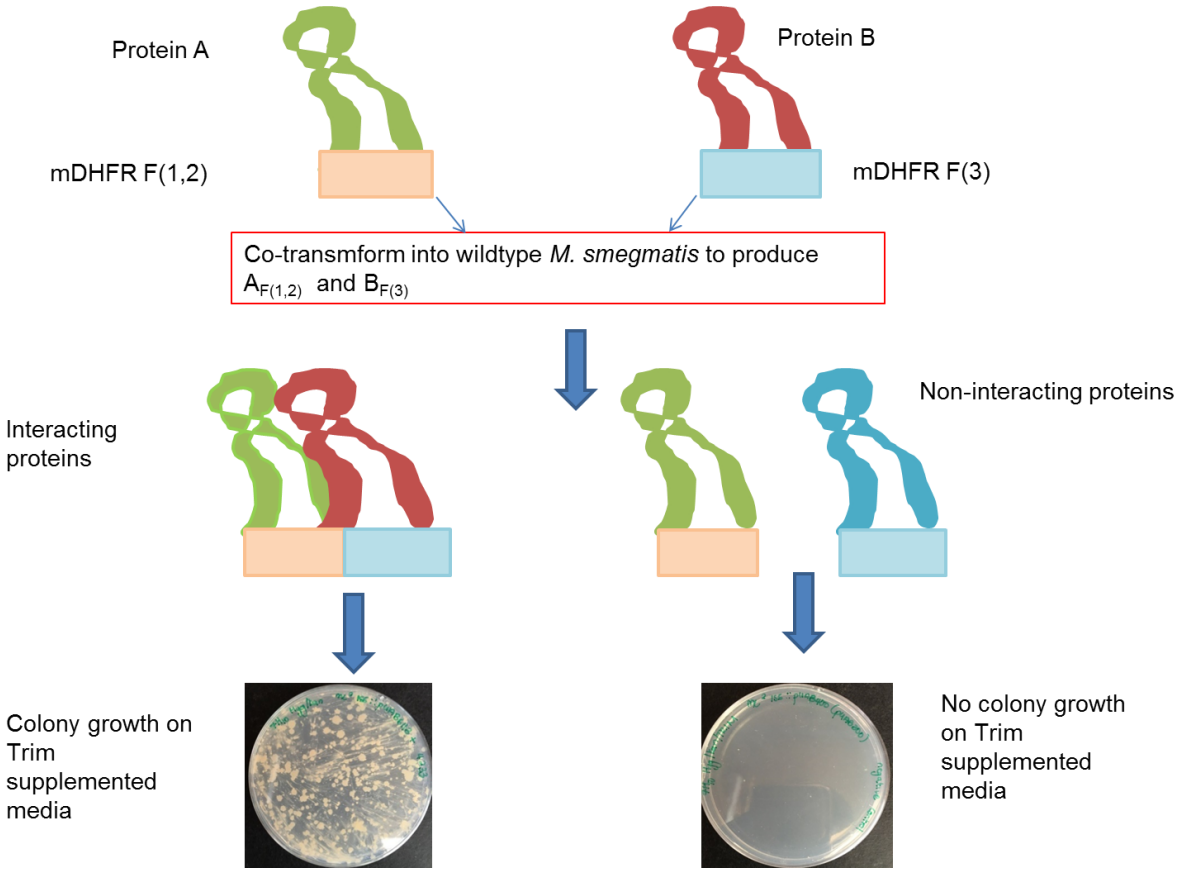


Figure 2.2: Schematic diagram demonstrating the M-PFC assay principle. When interacting proteins A and B are fused with mDHFR subunits (F1,2) and (F3) and co-transformed into mycobacterial cell, the subunits reassemble into a functional protein which hydrolyses trim, thus allowing for survival of the transformants on trim plates. In a case where the proteins do not interact, reconstitution of the mDHFR activity does not occur thus no growth is observed on the plates. Figure drawn by student, adapted from (Singh *et al*., 2006).

2.8.2. Determination of D,D-CPase domains responsible for interaction

To determine D,D-CPase domains that are responsible for interaction with the partnering proteins, sequences encoding functional domains found in D,D-CPases were cloned separately into pUAB400 plasmid and then co-transformed with pUAB300 prey constructs into wildtype mc^2155 and positive interactions were selected as previously described. For MSMEG_6113, the sequences encoding signal peptide (SP) and the transpeptidase domain (TP) were cloned separately into pUAB400. The resulting constructs (pUAB400+6113SP, pUAB6113+ 6113TP) were then co-transformed with the previously generated pUAB300 constructs carrying selected partnering proteins (FtsI [MSMEG_4233] and Cdc48 [MSMEG_0858]). The same procedure was followed with MSMEG_2433, where sequences encoding signal peptide, transpeptidase domain and the C-terminal region (Cter) were individually cloned into pUAB400, and then co-transformed with pUAB300 constructs carrying PonA1 (MSMEG_6900) and FtsH (MSMEG_6105). Positive interaction was scored as growth on 7H10 plates supplemented with Kan, Hyg and trim. The same controls that were used above, were also used for this assay.

2.9. Knockout mutant generation and phenotypic characterization

The flowchart in Figure 2.3 summarizes the steps involved in generation of knockout mutant strains, from suicide vector construction to characterization of these strains.

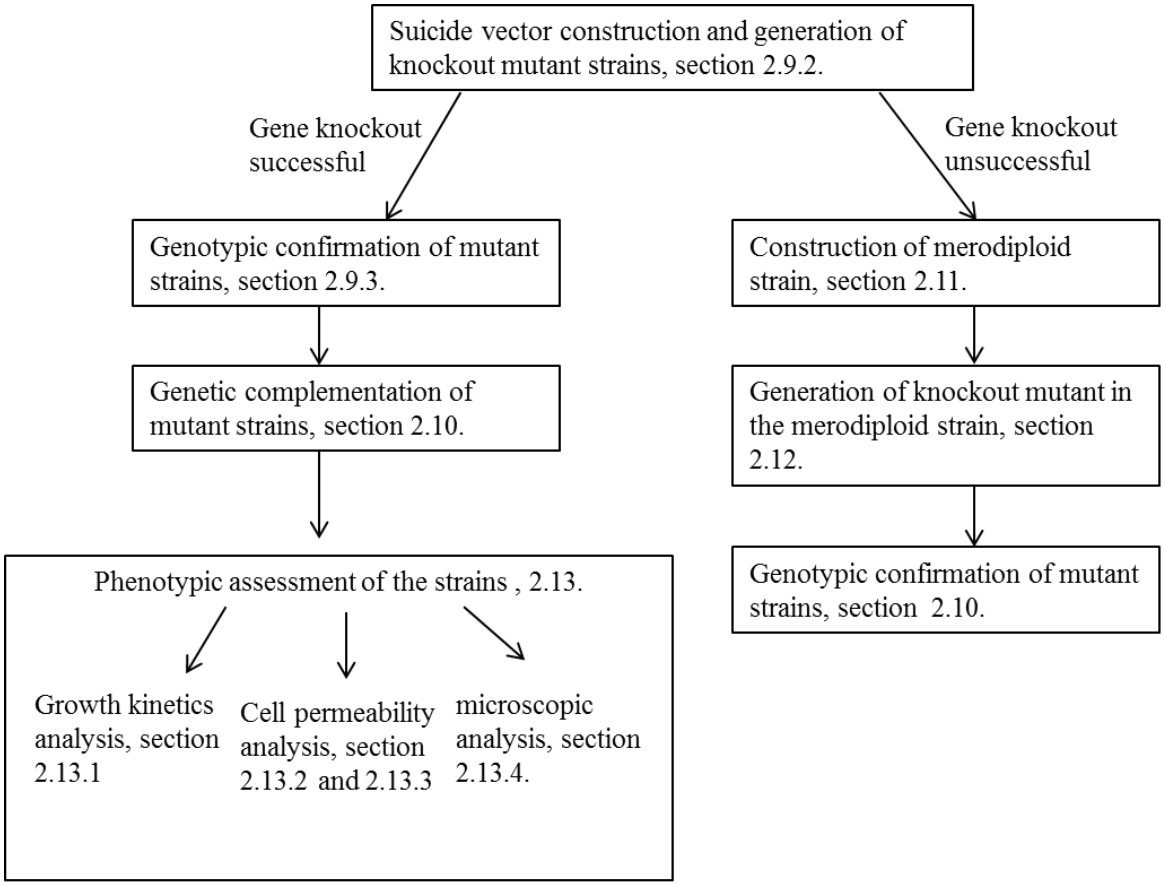


Figure 2.3: Flowchart summarizing the steps involved in generation of knockout mutant strains, from suicide vector construction to characterization of the strains. Sections refer to the relevant sections of the materials and methods.

2.9.1. Generation of *Msm* mutant strains

The two-step allelic exchange by homologous recombination (Gordhan and Parish, 2001) was used for generation of *Msm* knockout deletion mutants. A schematic representation of this approach is shown in Figure 2.4. This method involves suicide vector construction, where homologous sequences of the downstream and the upstream region and a small fragment of the 5' and 3' ends of the gene of interest are fused together and cloned into the vector. The vector also contains selectable markers (*aph* and *lacZ*) to allow for selection of single cross-over (SCO) recombinants and the *sacB* gene, which serves as a counter-selectable marker facilitating a second cross-over event. The vector is incorporated into the genome of *Msm* by homologous recombination with either the upstream or downstream region resulting in a SCO strain carrying both the wildtype and mutated copies of the gene (identified as blue colonies growing on 7H10 plates supplemented with Kan and X-gal). The second cross-over event can either occur in the same homologous region as the first cross-over, generating a wildtype

strain, or it can occur in the opposite homologous region resulting in the generation of the mutant strain carrying the inactive copy of the gene of interest (identified as white colonies growing in the presence of X-gal and sucrose).

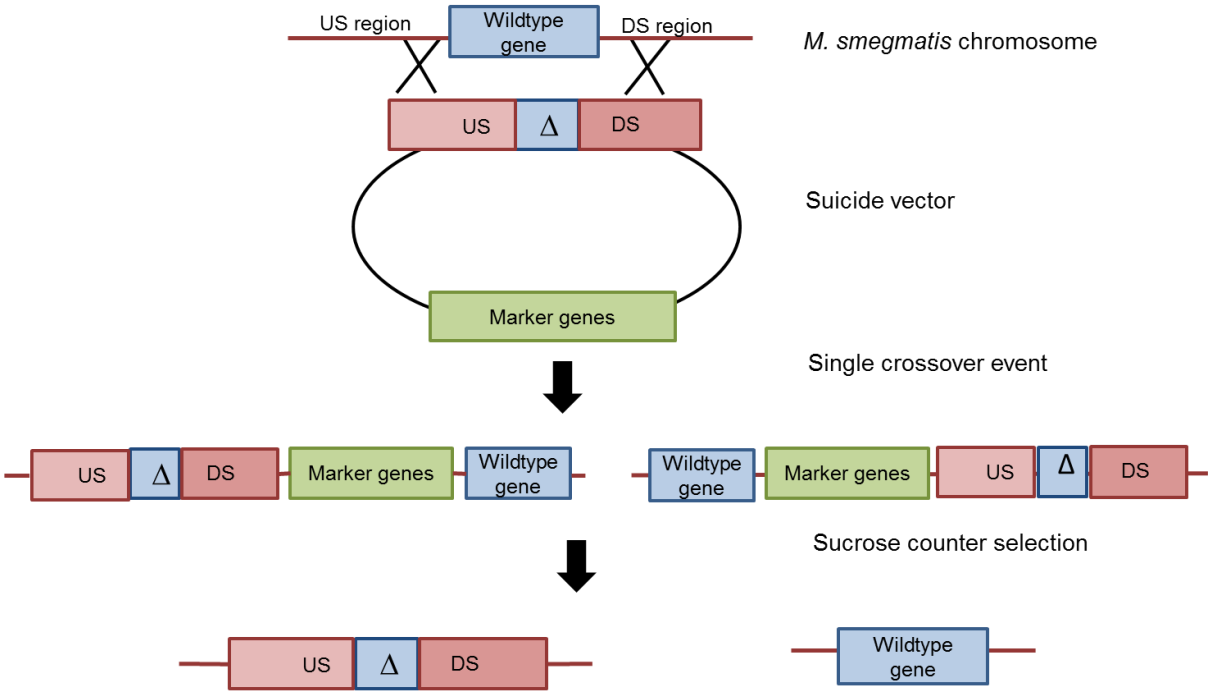


Figure 2.4: Schematic representation of the two step allelic exchange by homologous recombination procedure. The suicide vector carrying a truncated version of the gene of interest as well as marker genes is incorporated into wildtype mc^{2}155 strain by homologous recombination with either the upstream or downstream region resulting in a SCO strain carrying both the wildtype and mutated copy of the gene. A double crossover event results in generation of either a wildtype gene or a knockout mutant. US and DS represents the upstream and downstream regions, respectively. Δ indicates a mutant gene. Figure drawn by student, adapted from (Gordon and Parish, 2011).

2.9.2. Generation of MSMEG_0858 and MSMEG_4233 knockout mutants

Primers were designed to amplify the upstream (1500 bp) and the downstream (1500 bp) regions flanking the gene of interest along with 99 bp of the 5'end of the gene and 99 bp of the 3'end of the gene. The regions were amplified following the protocol outlined in section 2.6.1.2. and the resulting PCR fragments were cloned into the p2NIL plasmid as per protocol outlined in section 2.6.6. to generate suicide vector. In addition to this, the counter-selection marker gene, *sacB* (encoding levansucrase), and selectable marker gene *lacZ* (encoding β-galactosidase) were excised from pGOAL17 plasmid as a single linear fragment (termed the PAC cassette) and cloned into the *Pac*I site of the suicide vector. The resulting construct was electroporated into wildtype mc^{2}155 according to the protocol outlined in section 2.7.2. The

transformants were selected on 7H10 agar supplemented with Kan (25 µg/ml) and 2 % X-gal and incubated at 37 °C for 3-5 days. SCO strains were identified as blue colonies growing on Kan due to the presence of Kan marker (*aph*) and the *lacZ*, encoding β-galactosidase, which hydrolyses X-gal resulting in production of blue pigment. SCOs were then selected and grown overnight in 5 ml of 7H9 broth containing Kan (25 µg/ml) at 37 °C. This was then used to inoculate 5 ml of fresh 7H9 broth and grown at 37 °C overnight in the absence of antibiotics to allow for the second cross-over event to occur, resulting in loss of the suicide vector. Cells were harvested by centrifugation at 12 470 x g for 10 min and the pellet was resuspended in 500 µl of fresh 7H9, from which 100 µl was used to prepare a dilution series from 10^{-1}-10^{-7}. From this, 100 µl of each dilution were selected on two sets of 7H10 plates, 1 set containing only 2 % X-gal and another set containing 2 % X-gal and 5% sucrose. The *sacB* gene encodes the enzyme levansucrase which degrades sucrose, resulting in production of toxic levans that kills the cells retaining the suicide vector. Cells that have undergone a successful second cross-over event are able to grow in the presence of sucrose due to the loss of the *sacB* gene and emerge as white colonies growing on 7H10 agar supplemented with sucrose. These white colonies were then picked, resuspended in 50 µl of 7H9 broth and 10 µl of the suspension was spotted onto two sets of 7H10 plates, 1 set with 2 % X-gal only and the other set with 2% X-gal and Kan (25 µg/ml) to ensure that the vector backbone has been lost. White colonies that did not grow on Kan were picked and taken forward for PCR screening to confirm the genotype.

2.9.3. Genotypic confirmation of the parental and mutant strains by Southern blot analysis

Southern blot analysis was performed to confirm the genotype of the mutant strains generated in this study. Southern blot analysis can disclose details about DNA size, abundance and identity. This technique involves separation of DNA fragments based on size by gel electrophoresis, transferring and immobilization of the separated fragments onto a nitrocellulose membrane, followed by hybridization with a chemiluminescent labelled sequence-specific probe, extensive washing and chemiluminescent detection of labelled hybridized DNA bands using X-ray films. A brief description of the steps involved in this method are shown in Figure 2.5 and discussed in the sections below. For detailed solution recipes used for Southern blots see Appendix A, (Table A8).

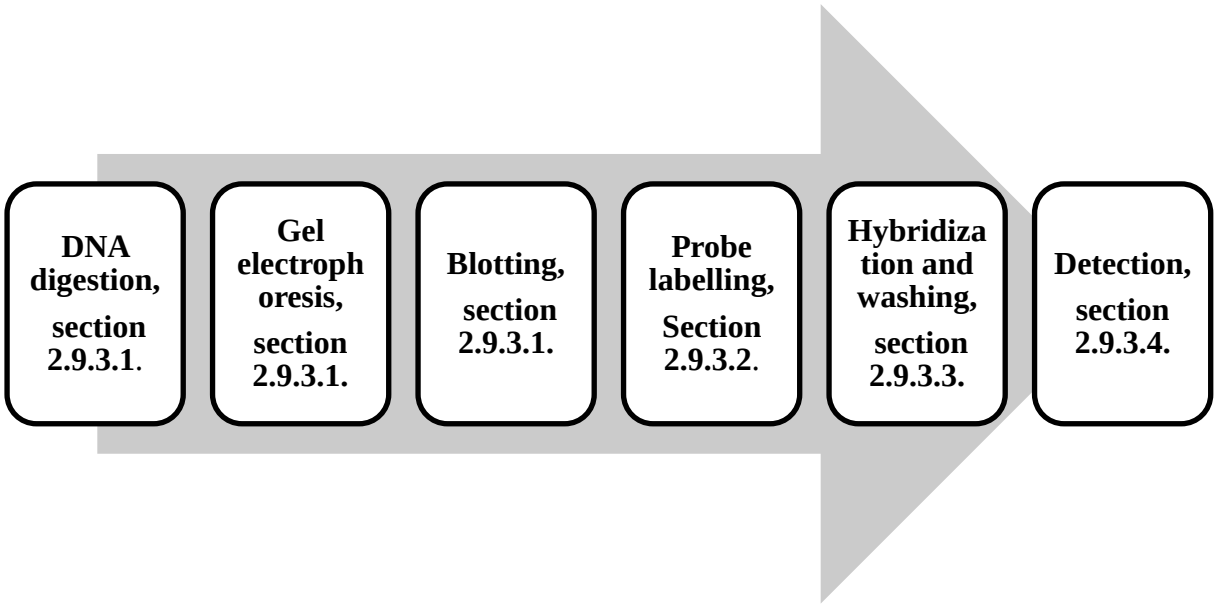


Figure 2.5: Diagrammatic representation of the steps involved in Southern blot analysis. The nitrocellulose membrane and the UVC 500 Crosslinker were from Amersham Biosciences, the probe labelling kit and all hybridizing solutions as well as the hybridizing bag were supplied by Roche. The hybridization oven and the X-ray films were supplied by Thermo scientific. Figure drawn by student.

2.9.3.1. Electro-blotting

Chromosomal DNA was extracted from derivative SCO strains, DCO mutant strains as well as the wildtype *Msm* following the protocol detailed in section 2.5.2.2. Subsequently, 2 µg of genomic DNA was digested with 1 U of appropriate restriction enzyme overnight at 37 °C. The fragments were separated on 0.8 % agarose gel at 80 V for 2-3 hours, and the gel was visualized alongside a ruler using SYNGENE G-BOX system. Following this, the gel was soaked in depurination solution for 15 min with shaking. The depurination solution was then discarded and the gel was washed twice with sdH_2O, soaked in denaturation solution at room temperature for 30 min with shaking. The gel was then neutralized by washing in 1X TBE buffer. A Hybond^{TM} N-nitrocellulose membrane (Amersham Biosciences) was then overlaid with the gel, sandwiched between 2 layers of Whitman filter papers and 2 layers of porous sponge, all of which were enclosed in a plastic cassette. This was then transferred into an electroblotting unit filled with 1X TBE buffer. The DNA was transferred onto the nitrocellulose membrane at 4 °C for 2 hours at 600 mA and 130 V. Following this, the DNA was cross-linked to the nitrocellulose membrane by ultra violet radiation using a UVC 500 Crosslinker (Amersham Biosciences) at 2500 mJ/cm^3 for 2 min.

2.9.3.2. DNA probe labelling

Probes used for Southern blots were synthesized using the PCR DIG Probe Synthesis Kit, following manufacturer's instructions (Roche). This kit allows for specific labelling of probes by incorporating alkali-labile digoxygenin-labelled dUTP (DIG-dUTP) in place of dTTP into the sequence of the probe during PCR reaction. The DIG-labelled and unlabelled PCR products were synthesized as indicated in section 2.6.1.1. Incorporation of DIG dUTP into the probe sequence was confirmed by running the PCR products on 1 % agarose gel. The DIG-labelled DNA fragment is expected to have higher molecular size compared to the unlabelled fragment. The probe was then stored at -20 °C until required.

2.9.3.3. Hybridization

Following crosslinking, the nitrocellulose membrane was pre-hybridized by placing the membrane into a Hybaid HB-OV-BM roller bottle (Thermo Scientific) containing 12 ml of DIG Easy hyb solution (Roche) and incubated at 60 °C for 30 min in a Hybaid Micro-4 hybridization oven (Thermo Scientific). The labelled probe was then denatured at 65 °C for 10 min, added to the membrane in the hybridization bottle and hybridized overnight at 60 °C. Following hybridization, the membrane was washed twice with solution 1 for 5 min at room temperature with shaking, followed by two washes with solution 2 for 15 min at 68 °C in the hybridization oven.

2.9.3.4. Immunological detection

Prior to immunological detection, the membrane was exposed to several wash steps at room temperature with shaking. The membrane was first rinsed in wash buffer for 5 min, followed by incubation in 1X blocking buffer for 30 min. The membrane was then incubated for 30 min in 20 ml of 1X antibody buffer and washed twice for 15 min in wash buffer. Following this, the membrane was placed in a hybridization bag (Roche) with the DNA side facing up, and 1 ml of chloro-5-substituted adamantyl-1,2-dioxetane phosphate (CSPD) substrate was spread evenly onto the membrane. Excess CSPD was removed from the hybridization bag followed by incubation for 10 min at 37 °C. The membrane was then exposed to X-ray films (CL-XposureTm Film, Thermo Scientific) for 30 min. Films were developed manually in the darkroom by 30 sec incubation in developing solution, followed by rinsing in sdH_2O for 30 sec, 30 sec incubation in fixing solution and final rinsing in sdH_2O for 30 sec. The film was then left to dry.

2.10. Generation of *Msm* complemented strains

To confirm that any phenotypic variation observed from the mutant strains was due to loss of functional copy of the gene of interest and not due to polar effects, complemented strains were generated where the gene of interest was reintroduced in the background of the mutant strain. This was achieved by amplifying the full length copy of the gene of interest together with the 200 bp upstream region of the gene to include its native promoter and cloning into an integrating vector (pMV306H), which allows for integration of the functional gene into the *attB* (phage attachment) site in the genome of mycobacteria. The resulting complementation constructs were then electroporated into mutant strains following the protocol in section 2.7.2. To confirm that integration of the complementing gene was successful, genomic DNA was extracted from the resultant complemented strains as indicated in section 2.5.2.1. and used for PCR screening as indicated in section 2.6.1.1.

2.11. Generation of MSMEG_4233 SCO recombinant (merodiploid) strain

Failure to generate MSMEG_4233 targeted gene knockout mutant by allelic exchange was taken as an indication of the essentiality of MSMEG_4233 gene function, hence a merodiploid strain was generated in order to prove the essentiality of this gene and to demonstrate that the wildtype copy of the gene can only be inactivated in the presence of a second copy of the gene located elsewhere in the genome. A merodiploid strain was generated by electroporating MSMEG_4233 complementation vector construct (described above in section 2.10.) into the genome of the MSMEG_4233 SCO recombinant strain as per protocol in section 2.7.2. A schematic representation of this approach is shown in Figure 2.6. This was then followed by extraction of genomic DNA from the resultant merodiploid strain as per protocol in section 2.5.2.1 and the DNA was then used for PCR screening as indicated in section 2.6.1.1. to confirm successful integration of complementation vector into the SCO recombinant strain.

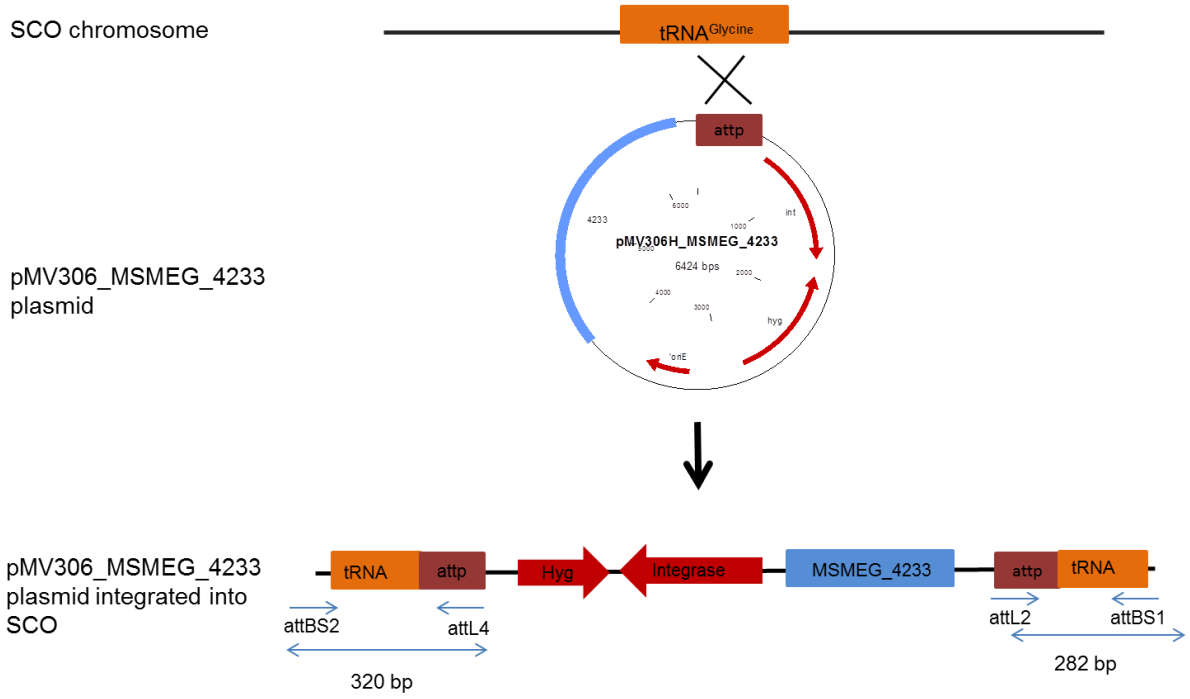


Figure 2.6: Schematic representation of integration of pMV306*ftsI* into the *attB* site in the genome of MSMEG_4233 SCO. The plasmid uses L5 based integration system, where the attachment site (red) integrates at the tRNA^{Glycine} (orange) locus on the SCO chromosome, resulting in the incorporation of the plasmid into the genome. Shown in blue arrows are the primers used to confirm site specific integration of the plasmid and expected amplicon sizes. Figure drawn by student.

2.12. Generation of MSMEG_4233 mutant in the merodiploid strain

To generate MSMEG_4233 mutant, the merodiploid strain was grown overnight in 5 ml of 7H9 broth containing Kan (25 µg/ml) and Hyg (50 µg/ml) at 37 °C. This was then used to inoculate 5 ml of fresh 7H9 broth, followed by growth at 37 °C overnight in the absence of antibiotics to allow for second cross-over event to occur. Cells were harvested by centrifugation at 4000 x g for 10 min and the pellet was resuspended in 500 µl of fresh 7H9, from which 100 µl was used to prepare a dilution series from 10^{-1}-10^{-7}. One hundred µl of each dilution was spread on two sets of 7H10 plates, 1 set containing only 2 % X-gal and another set containing 2 % X-gal and 5% sucrose and incubated 5-7 days at 37 °C. Colonies were subjected to sucrose selection as described in section 2.9.1 and PCR screening was performed to confirm the genotype.

2.13. Phenotypic analysis of *Msm* knockout mutant strains

2.13.1. Growth kinetics analysis

The growth rate of *Msm* derivative strains was analyzed in comparison to the wildtype strain by performing three independent growth curve experiments in standard 7H9 media. Briefly, a pre-culture of each strain was started from 1 ml of frozen culture in 5 ml 7H9 broth containing appropriate antibiotics when necessary and incubated at 37 °C overnight with shaking at 100 rpm. Each pre-culture was diluted to an OD_{600} = 0.01 in 50 ml 7H9 broth supplemented with appropriate antibiotics and incubated at 37 °C with shaking at 100 rpm. Growth rates were determined by recording OD_{600} at three hour intervals and the data was then used to generate scatter plots. In addition to this, colony forming units (CFU) counts were enumerated to confirm the number of bacteria. This was done by making 10-fold serial dilutions of each strain at each growth phase and plating the dilutions on 7H10 agar plates. The plates were then incubated at 37 °C for two days, following which, CFU/ml was determined.

2.13.2. Minimum inhibitory concentration (MIC) determination

To determine antibiotic MICs of the mutant strains in comparison to the wildtype, bacterial strains were grown in 5 ml of 7H9 supplemented with appropriate antibiotics when necessary at 37 °C with shaking at 100 rpm to an OD_{600}=0.2-0.3. Serial 2-fold dilutions of the antibiotics were added per well in a 96-well plate containing 7H9 broth. Per well, 100 fold diluted cultures were added. The plates were incubated for 5-7 days at 37 °C. The tested antibiotics and their starting concentrations were as follows: Amoxicilin (512 µg/ml), Cycloserine (100 µg/ml), Ethambutol (102.4 µg/ml), Imipenem (100 µg/ml), Isoniazid (250 µg/ml), Rifampicin (25.6 µg/ml), Teicoplanin (100 µg/ml) and Vancomycin (100 µg/ml). The experiment was done in three biological repeats.

2.13.3. Ethidium bromide diffusion assay

Ethidium bromide (EtBr) assay was used to determine cell permeability of mutant strains in comparison to the wildtype. This technique is based on accumulation of EtBr inside the cell, which is a result of the relationship between efflux activity of cell membrane proteins and permeability of the cell wall. Briefly, cells were grown in 7H9 with appropriate antibiotics when necessary at 37 °C overnight with shaking at 100 rpm to an OD_{600}=0.8. Cell cultures were then centrifuged at 4500 x g for 5 min, the supernatant was discarded and the pellet was

washed in PBS. Subsequently, the pellet was resuspended in PBS supplemented with 0.4 % glucose and the OD_{600} was adjusted to 0.4. From this, a 50 µl aliquot of cell suspension was added into a 96-well plate, followed by addition of EtBr at concentrations ranging from 10 – 0.07 µg/ml. Thereafter, fluorescence was measured every 60 sec using a plate reader (excitation: 530 nm, emission: 585 nm) for an hour at 37 °C. Measurements were done in triplicates.

2.13.4. Microscopy

2.13.4.1. Copper Click reaction with D-alanine analogue (click chemistry)

To investigate the spatial distribution of PG synthesis in growing cells, the click chemistry technique was used. This technique allows for labelling of sites of new PG synthesis by incorporating a D-alanine, PG-precursor analogue into the PG during synthesis of the cell wall. Briefly, bacterial strains were grown at 37 °C overnight with shaking at 100 rpm to an OD_{600}=0.5-0.6. Cells were then harvested by centrifugation at 12 470 x g and then resuspended in 1 ml 7H9 broth. Subsequently, 1 µl of 10 M D-alanine analogue stock solution was added to the cells, followed by 3 hours incubation at 37 °C with shaking at 100 rpm. Following incubation, the cells were harvested and washed 3 times in PBSTB buffer (1X PBS, 0.05 % BSA and 0.01 % tween20). For copper click reaction to occur, 500 µl of PBSTB, 500 µl of 1 M $CuSO_4$, 500 µl of 128 µM TBTA (tris- (benzyltriazolylmrthyl) amine), 10 µl of 1.2 mM Sodium ascorbate and 10 µl of 20 µM azido probe were added in the order listed and the reaction was allowed to proceed for 60 min at room temperature with shaking. Following this, cells were washed 3 times in PBS and 5 µl of the cells was spotted onto glass slide with 2 % agarose pad and visualized with the Zeiss Axio Observer Z1 inverted fluorescent microscope. Analysis of all images taken was done using the ZEN lite software.

2.13.4.2. DMN- Trehalose Staining

In addition to click chemistry, DMN (4-*N*,*N*-dimethylamino-1,8-naphthalimide) -Trehalose staining was also used for *in vivo* staining of the cell wall. This technique makes use of a trehalose derivative attached to a dye that yields green fluorescence once incorporated into the cell wall. Bacterial strains were grown overnight at 37 °C with shaking at 100 rpm to an OD_{600}=0.6. Cells were then harvested by centrifugation at 12 470 x g for 5 min followed by a single wash in 100 µl PBS. Thereafter, cells were resuspended in 100 µl fresh 7H9 broth, 10

µl of 100 µM DMN-Trehalose stain was added to the cells and incubated for an hour at 37 °C with shaking. Following incubation, cells were harvested by centrifugation at 12 470 x g for 5 min and then resuspended in 50 µl sdH_2O. Thereafter, 5 µl of the cells was spotted onto glass slide with 2 % agarose pad and visualized with the Zeiss Axio Observer Z1 inverted fluorescent microscope and analysis of all images taken was done using the ZEN lite software.

2.13.4.3. Scanning electron microscopy (SEM)

SEM was conducted in order to characterize the *Msm* strains based on their surface cell morphology. Cells were grown to an OD_{600} = 0.5-0.8 in 50 ml 7H9 broth supplemented with appropriate antibiotics at 37 °C with 100 rpm shaking overnight. Thereafter, cells were harvested by centrifugation at 4000 x g for 10 min, followed by washing in 0.01 M PBS twice. The cells were then resuspended and fixed in 500 µl of 2.5 % gluteraldehyde at 4 °C overnight. Thereafter, cells were harvested and washed 3 times in 1 ml PBS, followed by staining with 100 µl of 2 % osmium tetraoxide for an hour at room temperature. Cells were then washed twice in PBS and dehydrated by 2 min of resuspension in increasing concentrations of ethanol (30 %, 50 %, 70 %, and twice in 100 %). Dehydrated cells were stored at room temperature in 100 % ethanol until viewed under SEM. Before imaging, cells were spotted on a filter, coated twice with carbon and viewed using the FEI Nova NanoSEM 320. Preparation of cells for SEM was done by student but imaging was outsourced to Miranda Waldron at the Centre of Imaging and Analysis, University of Cape Town. The student then analysed the resulting images.

2.14. FtsZ localization

For localization of proteins of interest, a previously generated protein fusion (FtsZ_GFP) was electroporated into wildtype *Msm* and derivative mutant strains following the protocol outlined in section 2.7.2. The resultant transformants were then grown in 5 ml of 7H9 broth containing appropriate antibiotics to an OD_{600}=0.5-0.6 overnight at 37 °C. Subsequently, cells were harvested by centrifugation at 12 470 x g for 5 min and resuspended in 50 µl of fresh 7H9 broth. Following this, 5 µl of the cells was mounted onto a glass slide with 2 % agarose pad. The slides were then covered with cover slips and visualized with the Zeiss Axio Observer Z1 inverted fluorescent microscope and analysis of all images taken was done using the ZEN lite software.

3. Results

3.1. Protein interactions

The first part of this study was aimed at characterizing the *Msm* D,D-CPases designated MSMEG_2433 and MSMEG_6113, through interaction with their respective partnering proteins that were previously identified in screen conducted in our lab using bacterial two-hybrid system. In this regard, the approach involved confirming interaction between the two D,D-CPases with their full-length putative partnering proteins and further characterizing these partners through bioinformatics analyses as well as determining interaction domains of the two D,D-CPases.

3.1.1. Confirmation of MSMEG_2433 and MSMEG_6113 interacting partners using the M-PFC assay

The screen conducted in our lab identified 20 and 10 possible interacting partners for MSMEG_2433 and MSMEG_6113, respectively. Partial clones of these putative partners were obtained and first propagated on 7H10 Hyg/Kan solid media. Colonies that emerged were sub-cultured on 7H10 Hyg/Kan media supplemented with trim. Any growth on the plates was scored as positive interaction and all tested clones were confirmed as positive, Table 3.1. Interestingly, a number of these partners were key regulators of cell elongation and division. The assay revealed that MSMEG_6113 and MSMEG_2433 possibly interacts with HMM PBPs, which play a significant role in cross-linking PG during the last stages of PG synthesis. In addition, the assay also revealed other partners, including proteins of the transcriptional and translational machinery (DNA polymerase III subunit delta and RNA polymerase sigma factor E), metalloproteases and several hypothetical proteins as possible interacting partners of the two D,D-CPases. Table 3.1 and Table 3.2. summarize the results obtained using M-PFC assay including all controls used in the assay. Three independent assays were conducted to confirm these interactions. In the first assay, colony numbers were lower compared to the ones in the second and third assay and this was possibly due to experimental errors or variation in electroporation efficiency.

Table 3.1: Confirmation of MSMEG_6113 interaction with its putative interacting partners including appropriate controls using M-PFC assay.

	1st assay		2nd assay		3rd assay	
Test	Positive (+) negative (-)	number of colonies	Positive (+) negative (-)	number of colonies	Positive (+) negative (-)	number of colonies
mc^2 155	-	0	-	0	-	0
mc^2:: pUAB400 (pUAB300) (-ve control)	-	0	-	0	-	0
mc^2:: RipA +RpfB (+ve control)	+	287	+	600	+	lawn
mc^2::pUAB6113+penicillin binding protein B (MSMEG_4233)	+	610	+	lawn	+	lawn
mc^2::pUAB6113+hypothetical protein (MSMEG_6112)	+	221	+	lawn	+	lawn
mc^2::pUAB6113+cell division control protein (MSMEG_0858)	+	456	+	lawn	+	lawn
mc^2::pUAB6113+enoyl-CoA hydratase/isomerase (MSMEG_0259)	+	527	+	lawn	+	lawn
mc^2::pUAB6113+penicillin binding protein 4 (MSMEG_5637)	+	542	+	lawn	+	lawn
mc^2::pUAB6113+hypothetical protein (MSMEG_0610)	+	578	+	lawn	+	lawn
mc^2::pUAB6113+hypothetical protein (MSMEG_0365)	+	511	+	lawn	+	lawn
mc^2::pUAB6113+integral membrane protein (MSMEG_4287)	+	622	+	lawn	+	lawn

mc^2::pUAB6113+coniferyl aldehyde dehydrogenase (MSMEG_2242)	+	428	+	lawn	+	lawn

* The plus (+) sign indicates positive interaction and the minus (–) sign indicates negative or no interaction observed using M-PFC assay.

Table 3.2: Confirmation of MSMEG_2433 interaction with its putative interacting partners, including appropriate controls using M-PFC assay.

	1st assay		2nd assay		3rd assay	
Test	Positive (+) negative (-)	number of colonies	Positive (+) negative (-)	number of colonies	Positive (+) negative (-)	number of colonies
mc^2 155	-	0	-	0	-	0
mc^2::pUAB400 (pUAB300) (-ve control)	-	0	-	0	-	0
mc^2::RipA+RpfB (+ve control)	+	287	+	lawn	+	lawn
mc^2::pUAB2433+ UDP-diphospho- muramoypentapeptide beta-acetylglucoseamyl transferase (MSMEG_4227)	+	298	+	lawn	+	lawn
mc^2::pUAB2433+glutamine synthetase (MSMEG_3561)	+	lawn	+	lawn	+	lawn
mc^2::pUAB2433+RNA polymerase sigma factor RpDE (MSMEG_1914)	+	525	+	lawn	+	lawn
mc^2::pUAB2433+hypothetical protein (MSMEG_3858)	+	527	+	lawn	+	lawn
mc^2::pUAB2433+beta lactamase (MSMEG_4337)	+	596	+	lawn	+	lawn
mc^2::pUAB2433+conserved hypothetical protein (MSMEG_5691)	+	lawn	+	lawn	+	lawn

mc^2::pUAB2433+tRNA pseudouridine synthase A (MSMEG_1527)	+	lawn	+	lawn	+	lawn
mc^2::pUAB2433+penicillin binding protein transpeptidase domain protein (MSMEG_0031)	+	476	+	lawn	+	lawn
mc^2::pUAB2433+transglycosidase (MSMEG_6201)	+	387	+	lawn	+	lawn
mc^2::pUAB2433+penicillin binding protein 1(MSMEG_6900)	+	532	+	lawn	+	lawn
mc^2::pUAB2433+ATP-dependent zinc metalloprotease (MSMEG_6105)	+	566	+	lawn	+	lawn
mc^2::pUAB2433+glycosyl transferase (MSMEG_4947)	+	lawn	+	lawn	+	lawn
mc^2::pUAB2433+UDP-N-acetylenolpyrovoyl-glucosamine reductase (MSMEG_0928)	+	406	+	lawn	+	lawn
mc^2::pUAB2433+DNA polymerase III subunit delta (MSMEG_6153)	+	591	+	lawn	+	lawn

* The plus (+) sign indicates positive interaction and the minus (–) sign indicates negative or no interaction observed using M-PFC assay.

3.1.2. STRING analysis of MSMEG_6113 and MSMEG_2433 interacting partners.

In addition to M-PFC assay, MSMEG_6113 and MSMEG_2433 interacting partners were evaluated using STRING database (https://string-db.org). The associations in this database include direct (physical) interactions and indirect (functional) interactions. A number of proteins that were predicted by STRING as possible interacting partners of MSMEG_6113 and MSMEG_2433 were consistent with those revealed by M-PFC assay. These include penicillin binding protein 4 (MSMEG_5637), a hypothetical protein (MSMEG_6112) and penicillin binding protein B (MSMEG_4233) for MSMEG_6113 (Figure 3.1.). For MSMEG_2433, penicillin binding protein A (MSMEG_0031), penicillin binding protein 1

(MSMEG_6900) and UDP-diphospho- muramoylpentapeptide beta N-acetylglucosaminyltransferase (MSMEG_4227) were identified as interacting partners (Figure 3.2).

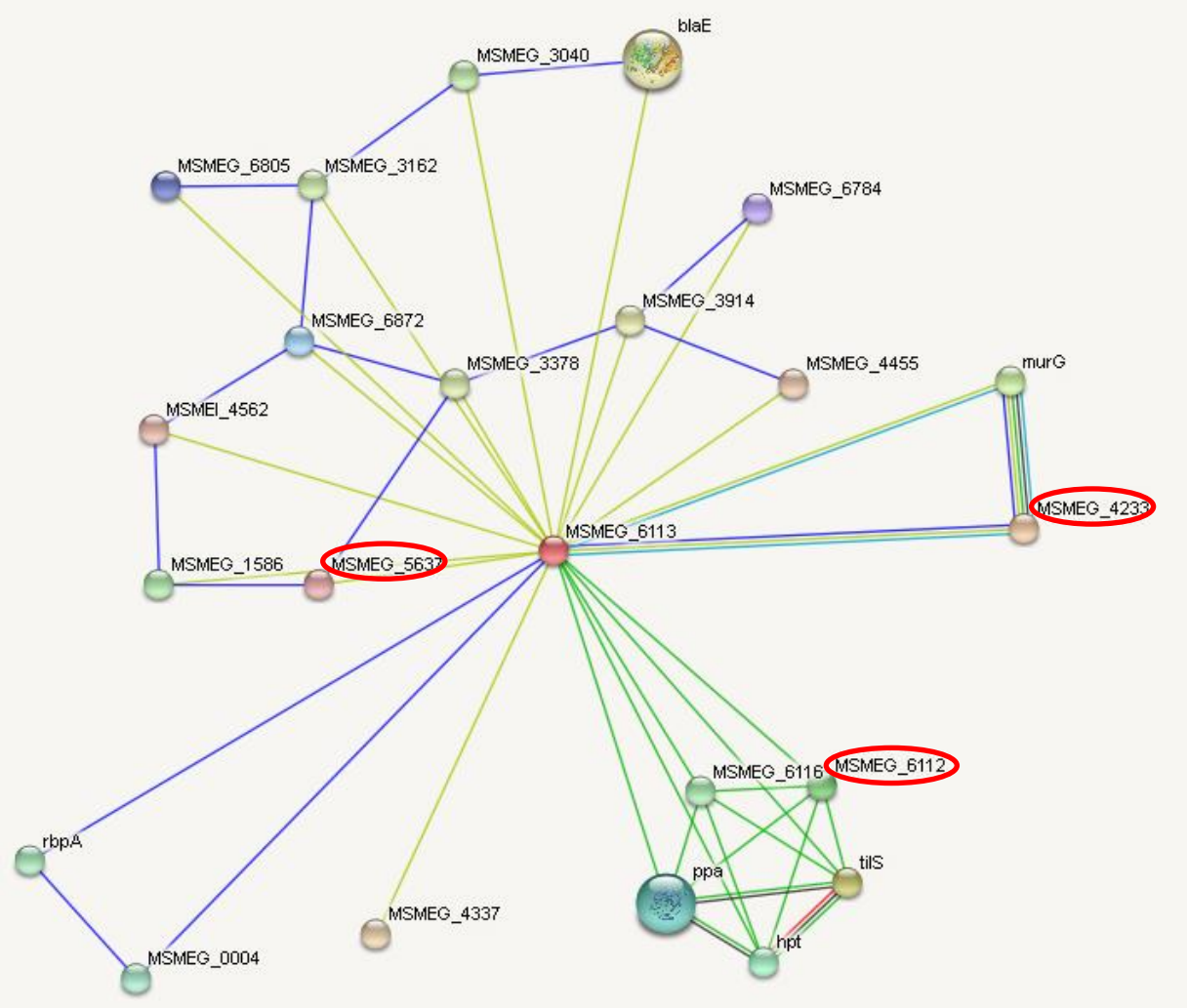


Figure 3.1: MSMEG_6113 interacting protein partners revealed by String analysis. The nodes represent proteins and the lines represent protein-protein associations, with known interactions represented by turquoise lines. Blue, green and red lines represent predicted interaction obtained by gene co-occurrence, gene neighbourhood and gene fusions respectively. The other associations are represented by black and yellow lines. https://string-db.org accessed on 1 June 2016.

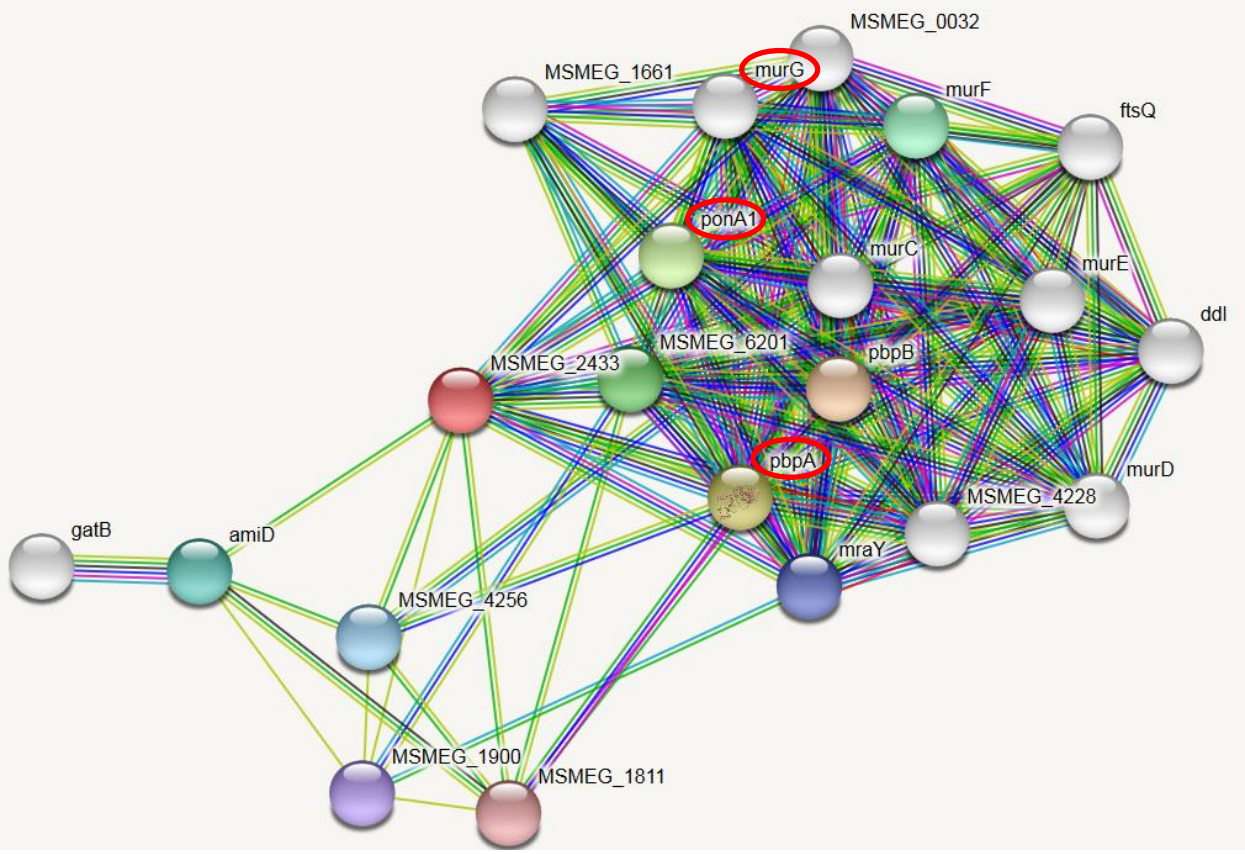


Figure 3.2: MSMEG_2433 interacting protein partners revealed by String analysis. The nodes represent proteins and the lines represent protein-protein associations, with known interactions illustrated by purple and turquoise lines. Blue, green and red lines represent predicted interaction obtained by gene co-occurrence, gene neighbourhood and gene fusions respectively. The other associations are represented by black and yellow lines. https://string-db.org accessed on1 June 2016.

3.1.3. Cloning of genes encoding D,D-CPases and their selected partners into M-PFC bait and prey vectors

The screen that identified these interactions made use of a DNA library consisting of genomic fragments. As such, fragments of the putative proteins were identified as possible interacting partners. To further confirm interactions, the genes encoding full length proteins were cloned for M-PFC analysis. For this component, five MSMEG_6113 interacting partners were selected including penicillin binding protein B (PBPB) also known as FtsI, cell division control protein 48 (Cdc48), penicillin binding protein 4 (PBP4), hypothetical proteins MSMEG_0365 and MSMEG_6112. In addition, four MSMEG_2433 partnering proteins were also selected including penicillin binding protein 1 (PonA1), penicillin binding protein A (PBPA), ATP-dependent zinc metalloprotease (FtsH) and UDP-diphospho-muramoylpentapeptide beta *N*-acetylglucosaminyltransferase (MurG). The rationale for

selecting these included a demonstrated role in cell wall biology or cell division/elongation. Two hypothetical proteins were chosen as exploratory objectives. The ORFs of the genes encoding the above selected proteins and the two D,D-CPases were cloned separately into pUAB300 (prey) and pUAB400 (bait) vectors respectively, following the protocol outlined in section 2.6.6. Prior to cloning, the genetic integrity of the vectors was confirmed by extensive restriction digest (results shown in Appendix C1, C2). The resulting constructs were analyzed by restriction profiling and further confirmed by sequencing. Restriction analysis of all constructs yielded the expected banding patterns (see appendix C4-C14). Sequencing revealed no mutations.

3.1.4. Confirmation of MSMEG_2433 and MSMEG_6113 interacting partners by M-PFC assay using full length clones

Electroporation of the *Msm* mc^2155 strain with the above generated constructs was performed following the protocol outlined in section 2.7.2. to generate mc^2155 strains carrying both tagged derivatives of D,D-CPases and their selected partners. The strains were then propagated on 7H10 media containing Kan/Hyg. All strains grew on 7H10 Kan/Hyg plates, indicating the presence of the constructs carrying the desired genes. To test for protein interactions, colonies were picked from the above plates and resuspended in 1 ml fresh 7H9 media, then sub-cultured on 7H10 Kan/Hyg media supplemented with trim and incubated for 4-5 days at 37°C. Colony growth on the plates was scored as positive interaction and all tested strains were positive. The mc^2155 cells only control (A in Figure 3.3) and the empty vector control mc^2 155::pUAB400(pUAB300) (C in Figure 3.3) tested negative as expected (Table 3.3. and Figure 3.3.). The mc^2155::RipA+RpfB positive control (B in Figure 3.3) showed strong interaction between the two proteins as indicated by the number of colonies and the time at which colonies emerged (two days post incubation) (Table 3.3. and Figure 3.3). Numerous studies have demonstrated interaction between RipA and RpfB and this interaction has been shown to play important role in various cell division processes (Hett *et al*., 2007; Hett *et al*., 2008). MSMEG_6113 was shown to interact strongly with MSMEG_6112 (E in Figure 3.3) (Table 3.3 and Figure 3.3). This strong interaction between MSMEG_6113 and MSMEG_6112 (HP) may be due to the fact that the genes encoding the two proteins are found next to each other in an operon. MSMEG_2433 was able to interact strongly with FtsH and PBPA (Table 3.3. and Figure 3.3.). Strong interaction is indicated by bacterial lawn while weak interaction is demonstrated by less number of colonies formed.

Table 3.3: Interaction of MSMEG_6113, MSMEG_2433 and their selected putative partnering proteins.

Test strains	Positive (+)/ negative (-)	Number of colonies*
(A) mc^2 155	-	0
(B) mc^2 155:: RipA+ RpfB	+	lawn
(C) mc^2 155:: pUAB400 + pUAB300	-	0
(D) mc^2 155:: pUAB6113 + PBPB/FtsI	+	414
(E) mc^2 155:: pUAB6113 + hypothetical protein (HP) (MSMEG_6112)	+	lawn
(F) mc^2 155:: pUAB6113 + Cdc48	+	420
(G) mc^2 155:: pUAB6113 + hypothetical protein (HP) (MSMEG_0365)	+	428
(H) mc^2 155:: pUAB6113 + PBP4	+	312
(I) mc^2 155:: pUAB2433 + FtsH	+	lawn
(J) mc^2 155:: pUAB2433 + MurG	+	368
(K) mc^2 155:: pUAB2433 + PonA1	+	392
(L) mc^2 155:: pUAB2433 + PBPA	+	lawn

*The table shows results observed using M-PFC assay including test strains and appropriate controls. Colony numbers indicate the strength of the observed interactions.

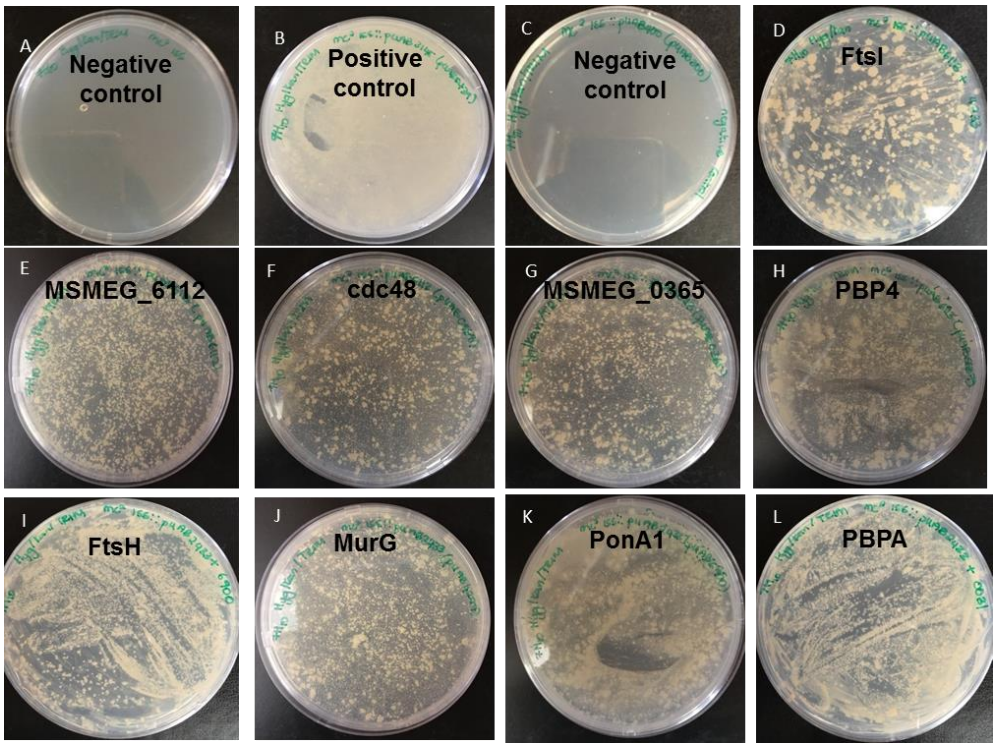
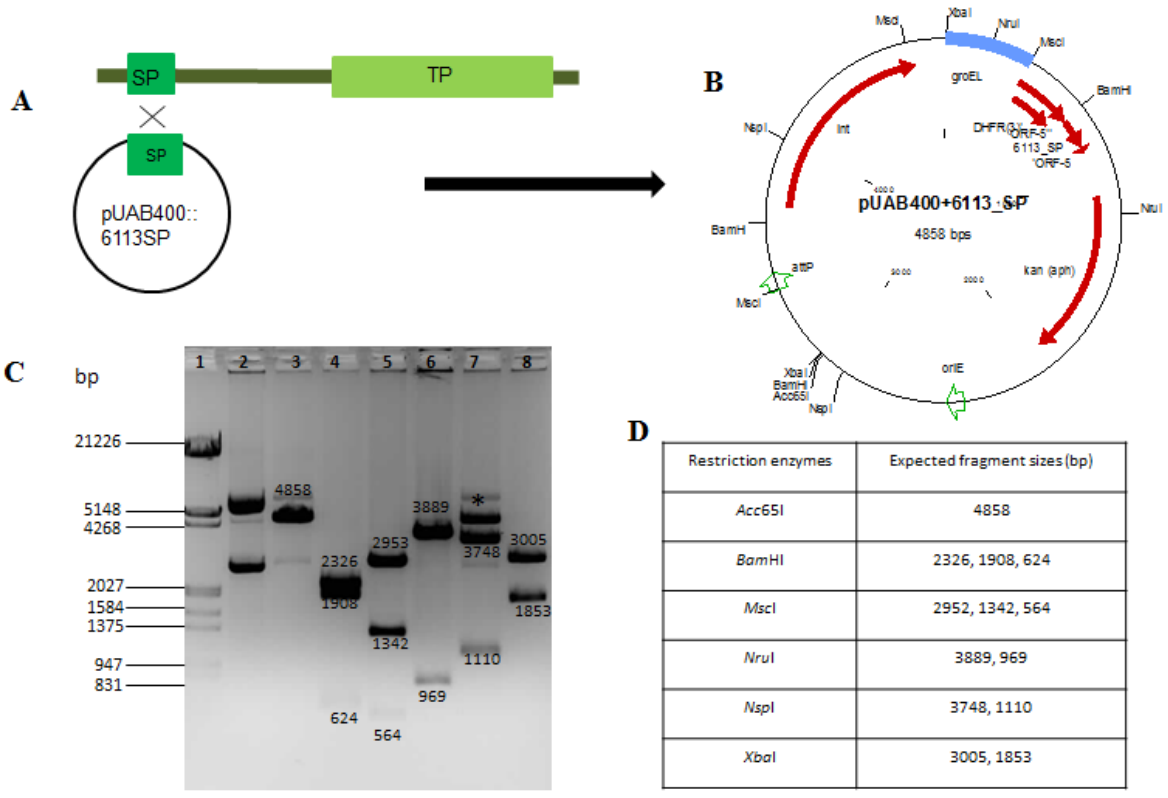


Figure 3.3: Protein interaction between MSMEG_6113, MSMEG_2433 and their selected partners in *Msm* using the M-PFC assay. *Msm* cells were transformed with M-PFC plasmids, transformants were selected on 7H10 plates supplemented with Kan/Hyg, and later sub-cultured onto 7H10 Hyg/Kan plates containing 7.5 µg/ml trim. (A) Wildtype $mc^2$155 cells only negative control, (B) RipA+ RpfB positive control, (C) empty vector negative control, (D-H) MSMEG_6113 positive interacting partners, (I-L) MSMEG_2433 positive interacting partners. The plates were incubated for 5 days.

3.1.5. Cloning of genes encoding functional domains of the two D,D-CPases into M-PFC bait vector

3.1.5.1. Cloning of genes encoding signal peptide and transpeptidase domain of MSMEG_6113 into pUAB400

After confirming the interactions, we next sought to determine which regions in the D,D-CPases interact with the partnering proteins. The ORFs of the genes encoding the signal peptide (SP) and the transpeptidase (TP) domain of MSMEG_6113 were cloned separately into the M-PFC bait vector pUAB400, following the protocol outlined in section 2.6.6. A selected clone per construct was verified by restriction profiling with at least 6 restriction enzymes (Figure 3.4. and 3.5.) and further confirmed by sequencing (results not shown). Restriction enzymes used for profiling pUAB400+6113SP construct yielded the expected banding patterns with the exception of *Nsp*I which had an extra band and this could be due to the star activity of the enzyme (Figure 3.4C). An unexpected cleavage pattern was observed with pUAB400+6113TP where digestion by *Aat*II yielded aberrant bands (Figure 3.5B) however, sequencing results of these constructs revealed no mutations (data not shown), this construct was used for further works.

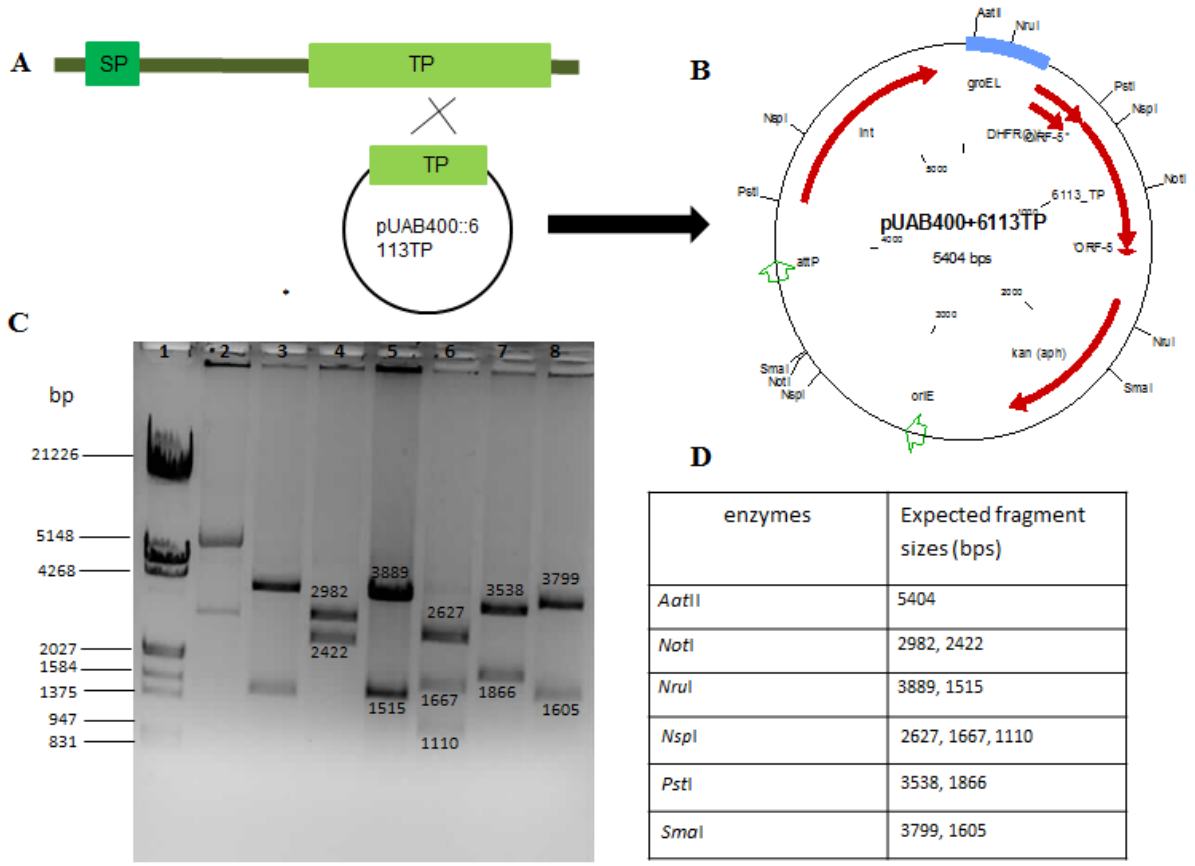


D

Restriction enzymes	Expected fragment sizes (bp)
Acc65I	4858
BamHI	2326, 1908, 624
MscI	2952, 1342, 564
NruI	3889, 969
NspI	3748, 1110
XbaI	3005, 1853

See figure legend on the next page

Figure 3.4: Restriction profile of pUAB400+6113SP. (A) Domain organization of MSMEG_6113 indicating the location of the signal peptide and cloning of the signal peptide into pUAB400. (B) Plasmid map of the final pUAB400+6113SP construct used for transformation. (C) 0.8 % agarose gel indicating expected DNA band sizes, lane (1) DNA marker III (Fermentas), lane (2) uncut construct control, lane (3) *Acc*65I, lane (4) *Bam*HI, lane(5) *Msc*I, lane (6) *Nru*I, lane (7) *Nsp*I, lane (8) *Xba*I. (D) Table showing restriction enzymes used for profiling and the expected fragment sizes.



D

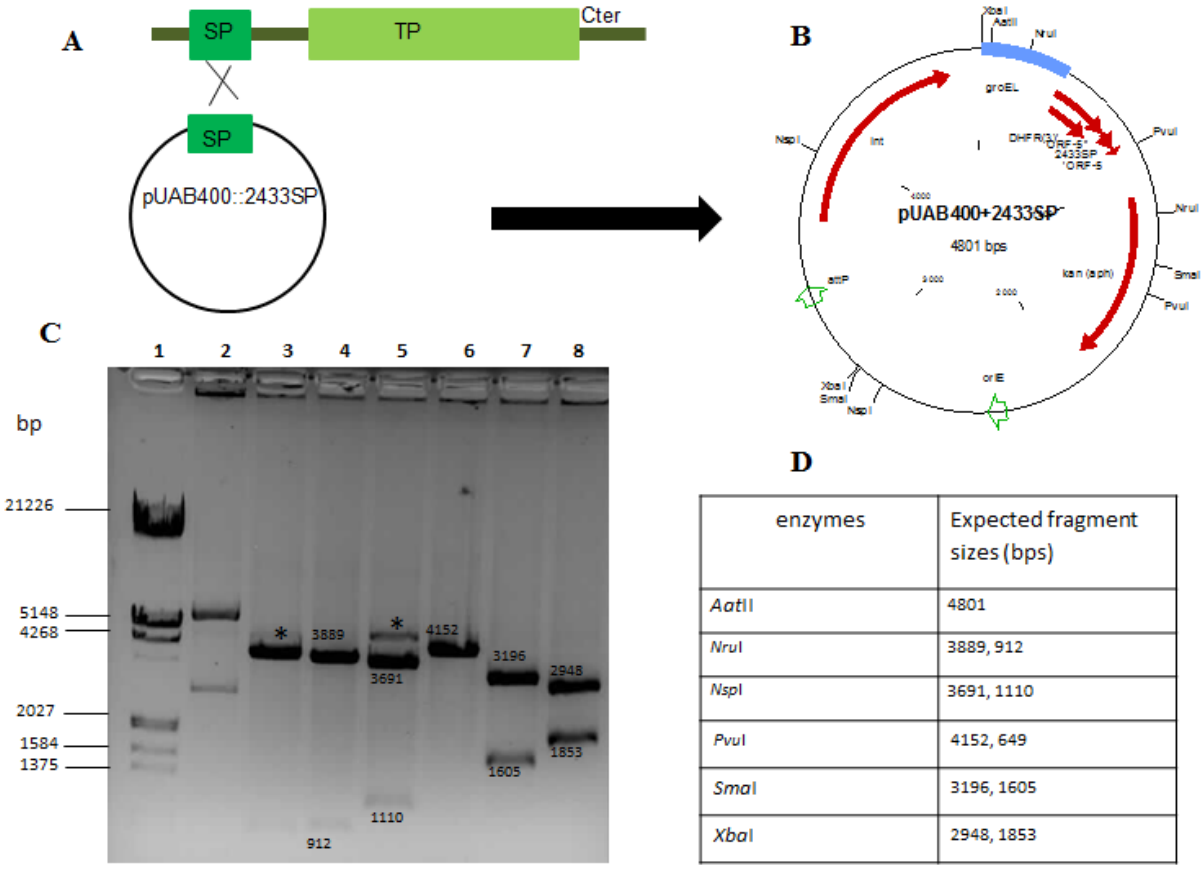
enzymes	Expected fragment sizes (bps)
*Aat*II	5404
*Not*I	2982, 2422
*Nru*I	3889, 1515
*Nsp*I	2627, 1667, 1110
*Pst*I	3538, 1866
*Sma*I	3799, 1605

Figure 3.5: Restriction profile of pUAB400+6113TP. (A) Domain organization of MSMEG_6113 indicating the location of the transpeptidase domain and cloning of the transpeptidase domain into pUAB400. (B) Plasmid map of the final pUAB400+6113TP construct used for transformation. (C) 0.8% agarose gel indicating expected DNA band sizes, lane (1) DNA marker III (Fermentas), lane (2) uncut construct control, lane (3) *Aat*II, lane (4) *Not*I, lane(5) *Nru*I, lane (6) *Nsp*I, lane (7) *Pst*I, lane (8) *Sma*I. (D) Table showing restriction enzymes used for profiling and the expected fragment sizes.

3.1.5.2. Cloning of genes encoding signal peptide, transpeptidase domain and C-terminal region of MSMEG_2433 into pUAB400

As with MSMEG_6113, the domains in MSMEG_2433 were investigated for their ability to interact with putative interacting partners. For this, the region encoding the signal peptide, transpeptidase domain and the C-terminal region of MSMEG_2433 were separately cloned into the M-PFC bait vector pUAB400 following the protocol outlined in section 2.6.6. A

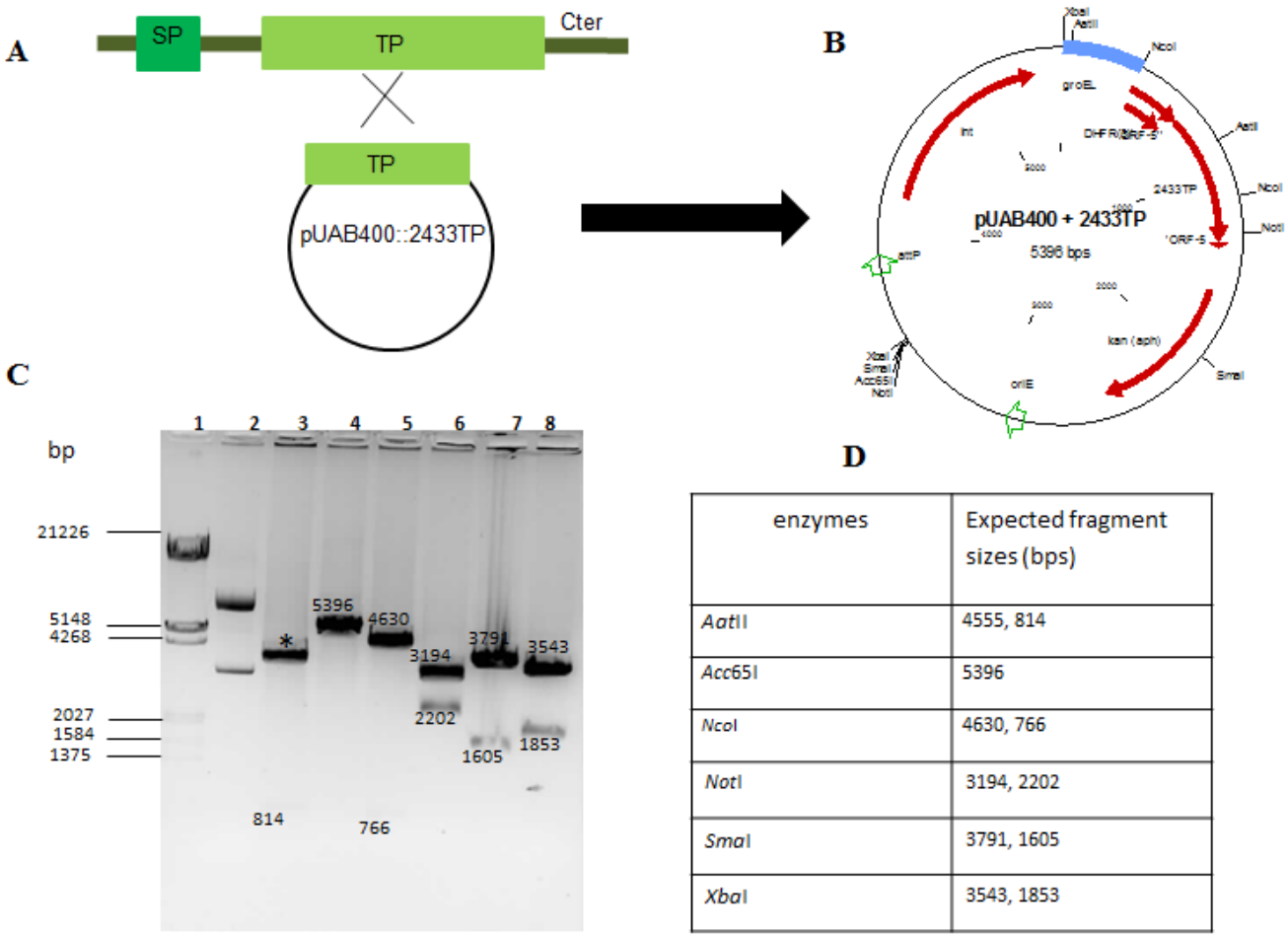
selected positive clone per construct was verified by restriction analysis following the protocol outlined in section 2.6.2. (Figure 3.6., 3.7. and 3.8.) and further confirmed by sequencing, which revealed that no mutations had occurred in the cloned regions during PCR (results not shown). Restriction enzymes used for profiling the constructs yielded the expected banding patterns with the exception of *Nsp*I which had an extra band in all cases and this again was attributed to star activity (Figure 3.6B and 3.8B). Digestion by *Aat*II yielded unexpected cleavage pattern (Figure 3.6B, 3.7B and 3.8B) whereby the aberrant *Aat*II site was mapped to the vector backbone and not the region of interest.



D

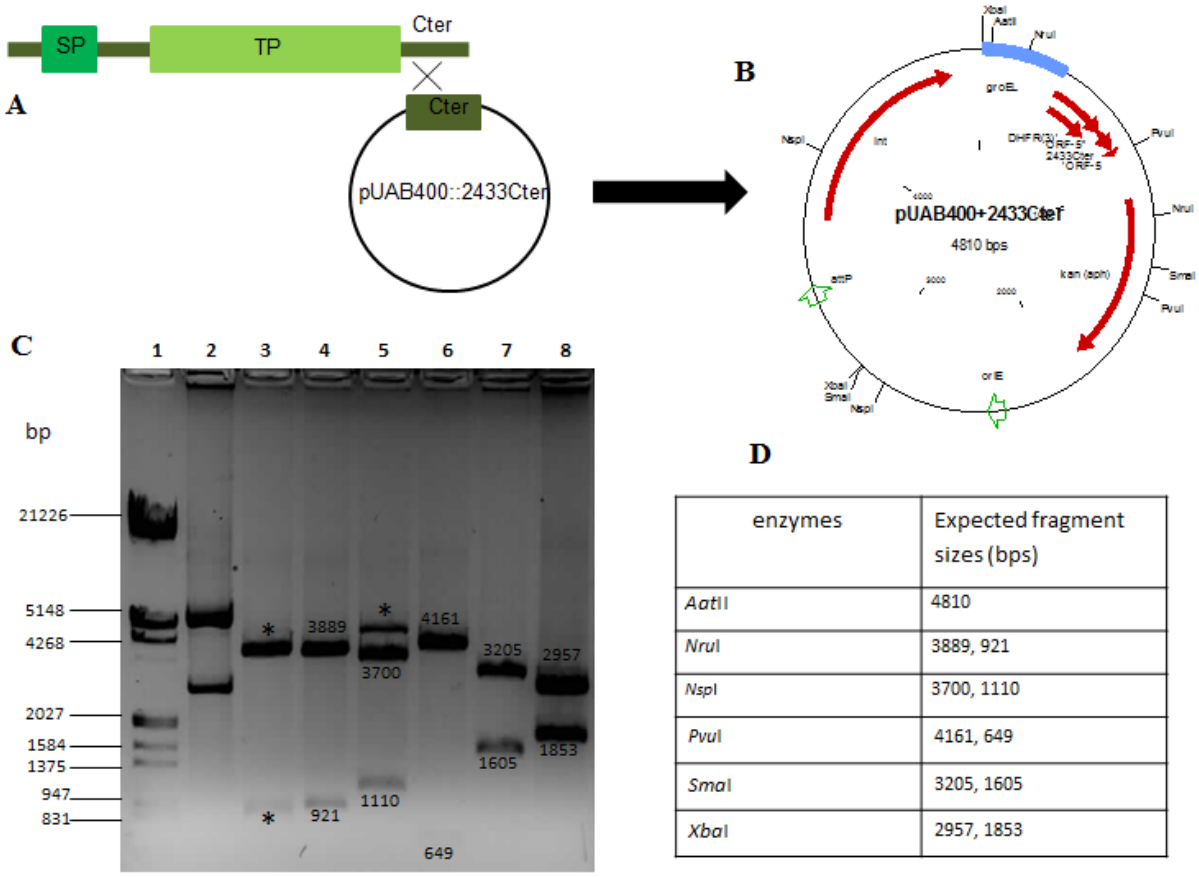
enzymes	Expected fragment sizes (bps)
*Aat*II	4801
*Nru*I	3889, 912
*Nsp*I	3691, 1110
*Pvu*I	4152, 649
*Sma*I	3196, 1605
*Xba*I	2948, 1853

Figure 3.6: Restriction profile of pUAB400+2433SP. (A) Domain organization of MSMEG_2433 indicating the location of the signal peptide and cloning of the signal peptide into pUAB400. (B) Plasmid map of the final pUAB400+2433SP construct used for transformation. (C) 0.8% agarose gel indicating expected DNA band sizes, lane (1) DNA marker III (Fermentas), lane (2) uncut construct control, lane (3) *Aat*II, lane (4) *Nru*I, lane(5) *Nsp*I, lane (6) *Pvu*I, lane (7) *Sma*I, lane (8) *Xba*I. (D) Table showing restriction enzymes used for profiling and the expected fragment sizes.



enzymes	Expected fragment sizes (bps)
*Aat*II	4555, 814
*Acc*65I	5396
*Nco*I	4630, 766
*Not*I	3194, 2202
*Sma*I	3791, 1605
*Xba*I	3543, 1853

Figure 3.7: Restriction profile of pUAB400+2433TP. (A) Domain organization of MSMEG_2433 indicating the location of the transpeptidase domain and cloning of transpeptidase domain into pUAB400. (B) Plasmid map of the final pUAB400+2433TP construct used for transformation. (C) 0.8% agarose gel indicating expected DNA band sizes, lane (1) DNA marker III (Fermentas), lane (2) uncut construct control, lane (3) *Aat*II, lane (4) *Acc*65I, lane(5) NcoI, lane (6) *Not*I, lane (7) *Sma*I, lane (8) *Xba*I. (D) Table showing restriction enzymes used for profiling and the expected fragment sizes.



enzymes	Expected fragment sizes (bps)
*Aat*II	4810
*Nru*I	3889, 921
*Nsp*I	3700, 1110
*Pvu*I	4161, 649
*Sma*I	3205, 1605
*Xba*I	2957, 1853

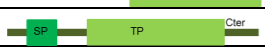
Figure 3.8: Restriction profile of pUAB400+2433Cter. (A) Domain organization of MSMEG_2433 indicating the location of the C-terminal region and cloning of C-terminal region into pUAB400. (B) Plasmid map of the final pUAB400+2433Cter construct used for transformation. (C) 0.8% agarose gel indicating expected DNA band sizes, lane (1) DNA marker III (Fermentas), lane (2) uncut construct control, lane (3) *Aat*II, lane (4) *Nru*I, lane(5) *Nsp*I, lane (6) *Pvu*I, lane (7) *Sma*I, lane (8) *Xba*I. (D) Table showing restriction enzymes used for profiling and the expected fragment sizes.

3.1.6. Determination of MSMEG_6113 and MSMEG-2433 interacting domains

To determine the interacting domains of MSMEG_6113 and MSMEG_2433, co-electroporation of mc^{2}155 with the above generated constructs was performed following the protocol outlined in section 2.7.2. These generated mc^{2}155 strains carrying both tagged derivatives of selected partnering proteins and functional domains of MSMEG_6113 and MSMEG_2433 were then propagated on 7H10 media containing Kan/Hyg. All strains grew on 7H10 Kan/Hyg plates, indicating the presence of the constructs carrying the desired genes. To test for protein interaction, colonies were picked from the above plates and resuspended in 1 ml fresh 7H9 media then sub-cultured on 7H10 Kan/Hyg media supplemented with trim and incubated for 4-5 days at 37°C. Positive interaction was scored as growth observed on the plates. The mc^{2}155 cells only control (A in Figure 3.9) and the empty vector control

mc^2 155::pUAB400(pUAB300) (B in Figure 3.9) tested negative as expected (Table 3.4. and Figure 3.9.). Of all the constructs tested for MSMEG_6113, the signal peptide and the transpeptidase domain were sufficient for interaction with Cdc48 and FtsI. However, signal peptide interaction was slightly weaker than that of the transpeptidase domain (Figure 3.9 D, E, F, and G). Of all the constructs tested for MSMEG_2433, only the constructs containing the transpeptidase domain were sufficient for interaction with FtsH and PonA1 (Figure 2.9 I and K), while constructs containing the C-terminal region failed to interact (Figure 3.9. J and L). These results revealed that the two D,D-CPases most likely interact with their partners at the transpeptidase domain responsible for cleaving PG crosslinks.

Table 3.4: Interaction of MSMEG_6113 SP and TP domain with Cdc48 and FtsI, as well as that of MSMEG_2433 SP, TP domain and C-ter region with FtsH and PonA1.

Test strains	Region tested	Positive (+)/ negative (-)	Number of colonies
(A) mc^2 155	-	-	0
(B) mc^2 155:: pUAB400 + pUAB300	-	-	0
(C) mc^2 155:: RipA + RpfB	-	+	lawn
Full-length MSMEG_6113		Not tested	Not tested
(D) mc^2 155:: pUAB6113SP + Cdc48		+	lawn
(E) mc^2 155:: pUAB6113TP + Cdc48		+	lawn
(F) mc^2 155:: pUAB6113SP + FtsI		+	lawn
(G) mc^2 155:: pUAB6113TP + FtsI		+	lawn
Full-length MSMEG_2433		Not tested	Not tested
(H) mc^2 155:: pUAB2433SP + FtsH		+	480
(I) mc^2 155:: pUAB2433TP + FtsH		+	lawn
(J) mc^2 155:: pUAB2433Cter + FtsH		-	0
(K) mc^2 155:: pUAB2433TP + PonA1		+	lawn
(L) mc^2 155:: pUAB2433Cter + PonA1		-	0

*The table shows results observed using M-PFC assay including appropriate controls. Colony numbers indicate the strength of the observed interactions.The D,D-CPase region tested for interaction is also shown, the plus (+) sign indicates positive interaction and the minus (–) sign indicates negative or no interaction observed using M-PFC assay. The full-length MSMEG_6113 and MSMEG_2433 were not tested and their domain organizations were only included in the table to show the spatial location of the regions tested.

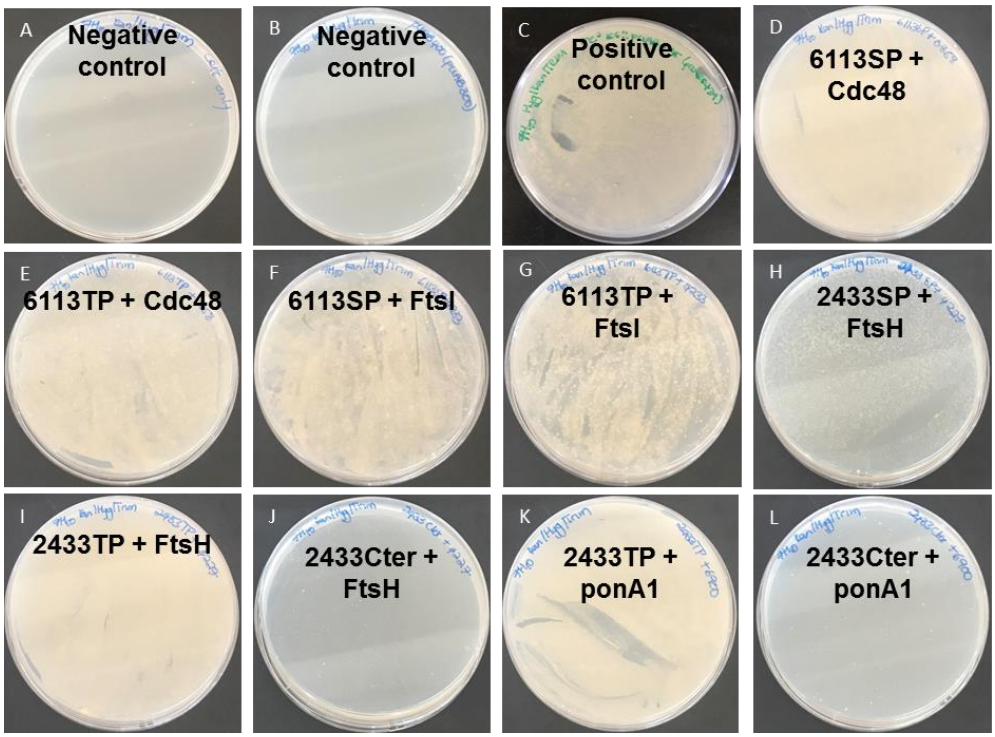


Figure 3.9: Protein interaction between MSMEG_6113, MSMEG_2433 domains and their selected partners in *Msm* using the M-PFC assay. *Msm* cells were transformed with M-PFC plasmids, transformants were selected on 7H10 plates supplemented with Kan/Hyg, and later sub-cultured onto 7H10 Hyg/Kan plates containing 7.5 µg/ml trim. (A) Wildtype mc^2155 cells only negative control, (B) empty vector negative control (C) RipA+ RpfB positive control, (E-L) Tested MSMEG_6113 and MSMEG_2433 domains with selected partners. The plates were incubated for 7 days.

3.1.7. Bioinformatics analyses of selected MSMEG_6113 and MSMEG_2433 partnering proteins (Cdc48, FtsI, FtsH and PonA1)

3.1.7.1. Sequence alignment of Cdc48, FtsI, PonA1 and FtsH in various rod shaped bacteria

Our analysis thus far confirmed various interacting partners for MSMEG_6113 and MSMEG_2433 and also highlighted what domains are required for interaction. We next turned our attention to detailed bioinformatics analysis of the putative interacting partners. To identify conserved catalytic residues within the selected protein partners, clustalO analysis (www.ebi.ac.uk/Tools/msa/ClustalO) was conducted using amino acid sequences from each protein. The sequences were compared with those of commonly studied rod-shaped bacteria including *Mtb*, *E. coli*, *B. subtilis*, *M. leprae*, *M. bovis* and *M. marinum* by conducting a clustalO alignment. Alignment of Cdc48 proteins revealed that the GxGK (T/S) motif (also known as the ATP-binding motif or A-box) is conserved throughout the different species (Figure 3.10 A). FtsI and PonA1 alignments confirmed the presence of all three conserved

catalytic motifs (SxxK, SxN and KTG (T/S) of PBPs (Figure 3.10 B and Figure 3.10 C) and these motifs occurred in the same position across the different organisms assessed. Alignment analysis of amino acid sequences of the FtsH protein revealed the presence of three conserved motifs including the two ATP-binding motifs (GPPGTGKT and IIFVDEID), the AAA family signature motif (GVILIAATNRPDILDPALLRPGR) and Zn^{2+}-binding motif (HEGGH). These motifs shared 100% identity at the amino acid level with *Mtb* FtsH protein (Figure 3.10 D). The alignments indicated that all residues responsible for the coordinated activities of these proteins are highly conserved across the different organisms particularly in mycobacteria, suggesting that they could have similar physiological roles in different mycobacterial species.

```
Ms          LDEWLRLSLDEPELLKTLGATPHLGVLVSGPAGVGKATMVRAVCASRRVVELDGPEVGAL
MMAR        LTEWLKLALDEPHLLQSLGAGTNLGVLVSGPAGVGKVTLVRAVCAGRRLVELDGPEVGAL
Mt          LTEWLKLALDEPHLLQTLGAGTNLGVLVSGPAGVGKATLVRAVCDGRRLVTLDGPEIGAL
Mb          LTEWLKLALDEPHLLQTLGAGTNLGVLVSGPAGVGKATLVRAVCDGRRLVTLDGPEIGAL
            * ***:*:****.**::***  :*************.*:***** .**:* *****:***

Ms          QVDERLRSVTSAVAAVTESGGVLFIADVDALLPAGNEMRPPEPVATLILAELRKAVATPG
MMAR        APENRLKAVASAVATVRDGGGVLLITDVDALLPAT-----AEPVAALILGELRTAVATDG
Mt          AAGDRVKAVASAVQAVRHEGGVLLITDADALLPAA-----AEPVASLILSELRTAVATAG
Mb          AAGDRVKAVASAVQAVRHEGGVLLITDADALLPAA-----AEPVASLILSELRTAVATAG
               :*:::*:*** :* . ****:*:*.******       ****:***.***.**** *

Ms          VAFIATSAVPENVDARLRAPEVCDRELGLSLPDATARRSLLEMLLRGVPSEDLDLGDIAD
MMAR        VVLIATTAAPDQLDARLRAPDLCDRELGLPLPDAATRKALLEALLRHVPTGDLDIDEIAS
Mt          VVLIATSARPDQLDARLRSPELCDRELGLPLPDAATRKSLLEALLNPVPTGDLNLDEIAS
Mb          VVLIATSARPDQLDARLRSPELCDRELGLPLPDAATRKSLLEALLNPVPTGDLNLDEIAS
            *.:***:* *:::*****:*::******* ****::*::*** **. **: **::.:**.

Ms          HTPGFVVADLAAVVREGALRAAARASSSDDDPVLRHADLEGALTVIRPLSRSASEEVSVG
MMAR        RTPGFVVADLAALLREAALRAASRASTDGQPPELNQEDLLGALTVIRPLSRSASSEVAVG
Mt          RTPGFVVADLAALVREAALRAASRASADGRPPMLHQDDLLGALTVIRPLSRSASDEVTVG
Mb          RTPGFVVADLAALVREAALRAASRASADGRPPMLHQDDLLGALTVIRPLSRSASDEVTVG
            :***********::**.*****:***:..  * *.: ** **************.**:**

Ms          SVTLDDVGDMVETKRALTEAVLWPLQHPDTFSRLGIDPPRGVLLYGPPGCGKTFVVRALA
MMAR        SITLDDVGDMAQAKQALTEAVLWPLQHPDTFARLGVEPPRGVLLYGPPGCGKTFVVRALA
Mt          DVTLDDVGDMAAAKQALTEAVLWPLQHPDTFARLGVEPPRGVLLYGPPGCGKTFVVRALA
Mb          DVTLDDVGDMAAAKQALTEAVLWPLQHPDTFARLGVEPPRGVLLYGPPGCGKTFVVRALA
            .:********. :*:*****************:***::**********************

Ms          SSGRLSVHAVKGSELMDKWVGSSEKAVRELFARARDSAPSLVFLDEIDALAPRRGQNFDS
MMAR        STGQLSVHAVKGSELMDKWVGSSEKAVRELFRRARDSAPSLVFLDEVDALAPRRGQSFDS
Mt          STGQLSVHAVKGSELMDKWVGSSEKAVRELFRRARDSAPSLVFLDELDALAPRRGQSFDS
Mb          STGQLSVHAVKGSELMDKWVGSSEKAVRELFRRARDSAPSLVFLDELDALAPRRGQSFDS
            *:*:*************************** **************:*********.***
```

Figure 3.10 A: Comparison of the conserved *Msm* Cdc48 sequence with other Cdc48 homologues. Shown is the amino acid sequence alignment of Ms (*Msm*), MMAR (*M. marinum*), Mt (*Mtb*) and Mb (*M. bovis*). Two conserved ATP-binding motifs A-box (first and second last row) and B-box (last raw) are highlighted in yellow shading. www.ebi.ac.uk/Tools/msa/ClustalO accessed on 20/06/2017.

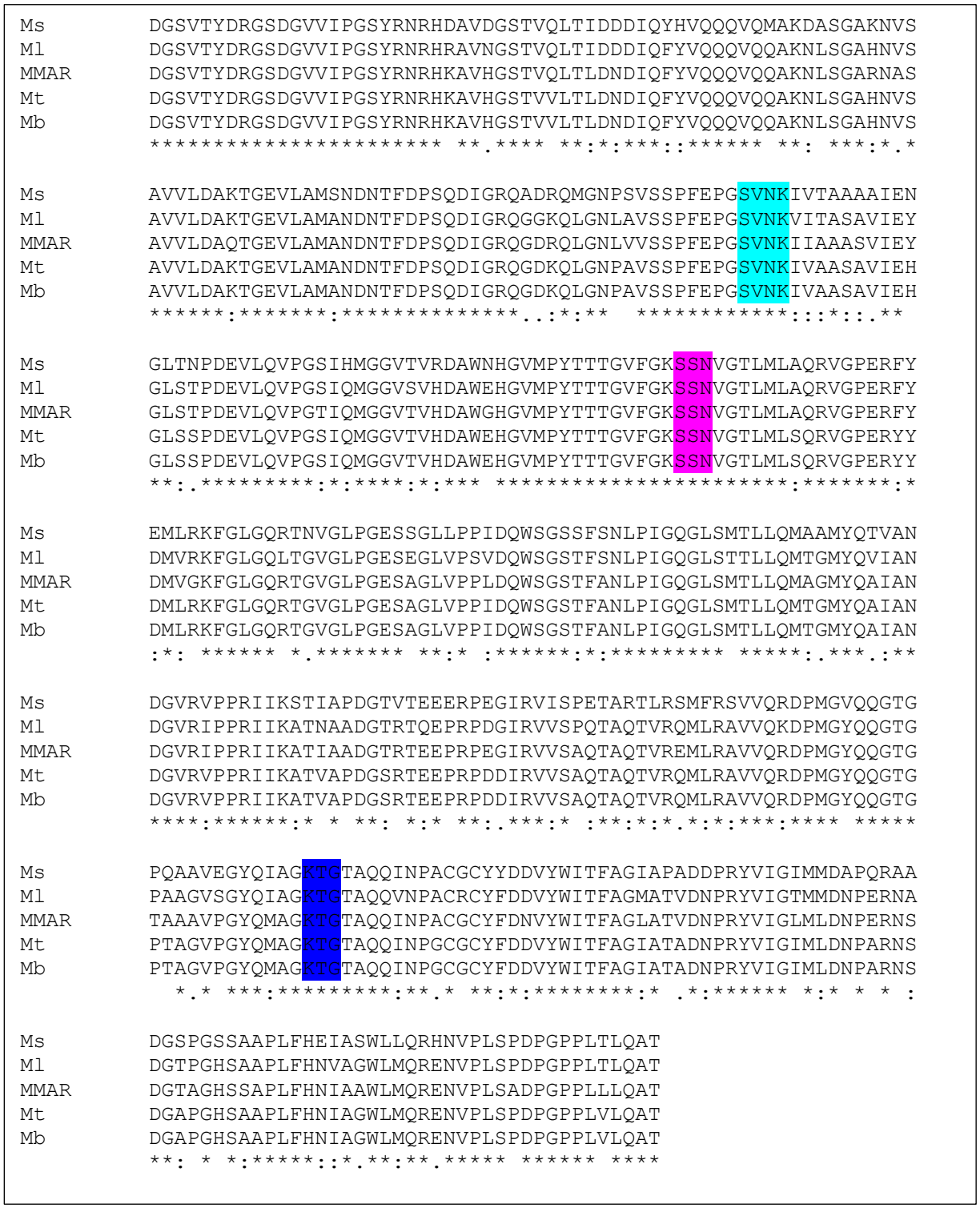


Figure 3.10 B: Comparison of the conserved *Msm* FtsI sequence with other FtsI homologues. Shown is the amino acid sequence alignment of Ms (*Msm*), Ml (*M. leprae*) MMAR (*M. marinum*), Mt (*Mtb*) and Mb (*M.bovis*). The three conserved motifs of PBPs are also shown. Highlighted in turquoise blue is the SxxK motif containing the active serine residue. The SxN motif is highlighted in purple shading and the KTG motif is shown in dark blue shading. www.ebi.ac.uk/Tools/msa/ClustalO accessed on 20/06/2017.

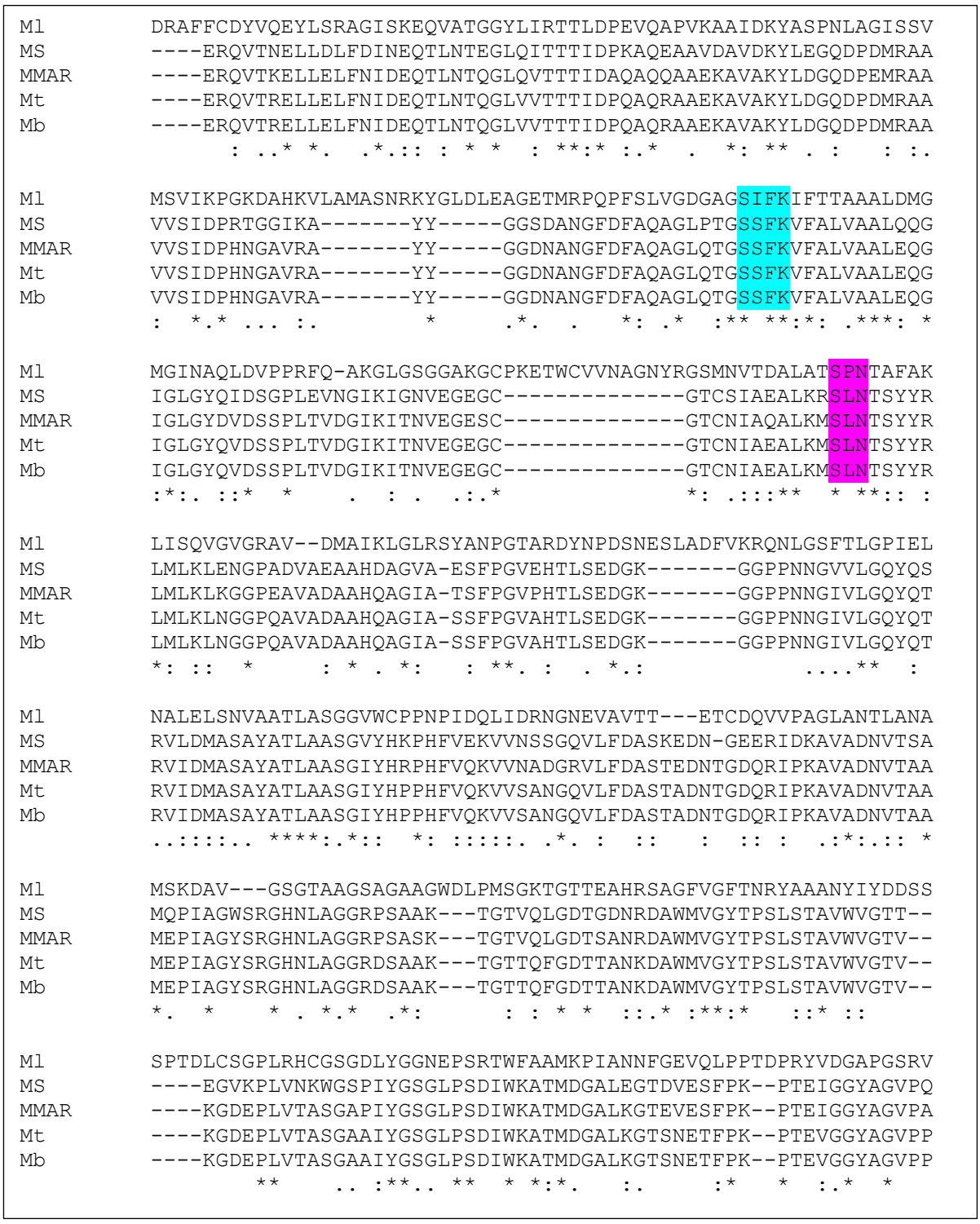


Figure 3.10 C: Comparison of *Msm* PonA1 sequence with other PonA1 homologues. Shown is the amino acid sequence alignment of Ms (*Msm*), Ml (*M. leprae*) MMAR (*M. marinum*), Mt (*Mtb*) and Mb (*M. bovis*). Conserved motifs of PBPs are also shown. Highlighted in turquoise blue is the SxxK motif containing the active serine residue and the SxN motif is highlighted in purple shading. www.ebi.ac.uk/Tools/msa/ClustalO accessed on 20/06/2017.

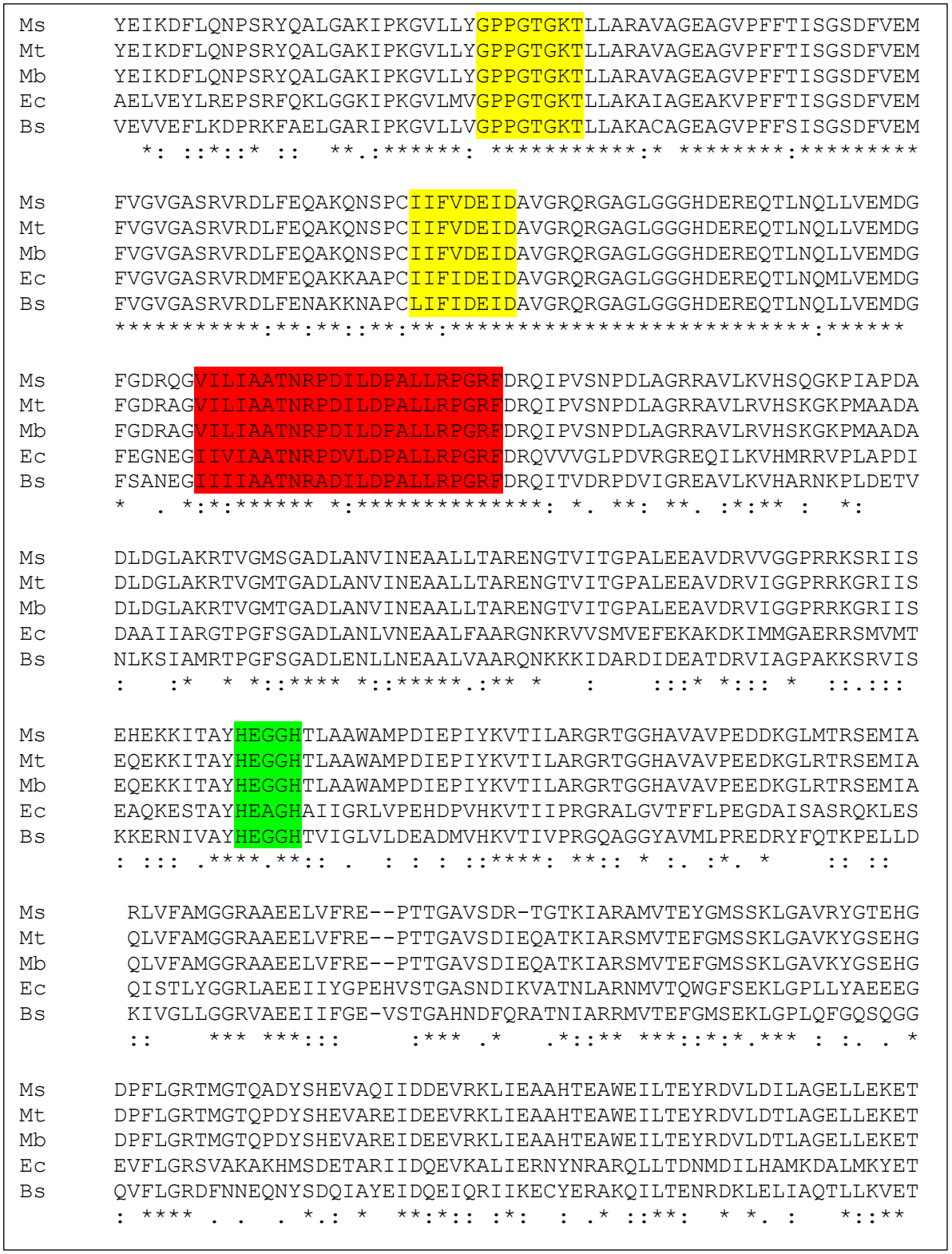


Figure 3.10 D: Comparison of the conserved *Msm* FtsH sequence with other FtsH homologues. Shown is the amino acid sequence alignment of Ms (*Msm*), Mt (*Mtb*), Mb (*M. bovis*), Ec (*E. coli*) and Bc (*B. subtilis*). The two conserved ATP-binding motifs are shown in yellow, highlighted in red shading is the AAA signature motif and in green shading is the Zn^{2+}-binding motif. www.ebi.ac.uk/Tools/msa/ClustalO accessed on 20/06/2017).

3.1.7.2. Domain organization of Cdc48, FtsI, PonA1 and FtsH

To examine domain organizations of the selected partnering proteins, Pfam analysis (http://pfam.xfam.org/) was conducted using amino acid sequences from each protein. The results revealed that Cdc48 is a member of the AAA (ATPases associated with various cellular activities) family of ATPases due to the presence of two AAA-type ATPase domains, D1 (aa 266-319) and D2 (aa 522-653) (Figure 3.11 A). This protein is a magnesium-dependent ATPase and the two AAA domains are capable of ATP hydrolysis. In addition, the Cdc48 protein also comprises of an N-terminal β-barrel domain (aa 24-107) (Figure 3.11 A). FtsI, also known as PBPB, is a monofunctional Class B HMM PBP with only transpeptidase activity. The FtsI structure comprises of an N-terminal PBP dimer (aa 91-266) and the C-terminal transpeptidase domain (aa 307-625) (Figure 3.11 B). The transpeptidase domain is responsible for catalysing stem peptide cross-links. PonA1 is a bifunctional class A HMM PBP. The N-terminus contains transglycosylase domain (aa 117-299) responsible for catalysing polymerization of glycan strands (Figure 3.11 C). The transpeptidase domain (aa 391-669) is also present in the C-terminal region of the protein (Figure 3.11 C). Both enzymatic activities of the two domains are required for normal cell growth. Analysis of amino acid sequence of FtsH revealed the presence of an N-terminal AAA domain (aa 199-332) and a C-terminal protease domain (aa 392-601) designated peptidase_M41 domain (Figure 3.11 D). Like Cdc48, FtsH also belongs to the AAA family of ATPases. FtsH protease activity is stimulated by metal ions such a Zn^{2+}, hence the protein is considered an ATP-dependent Zn^{2+} metalloprotease.

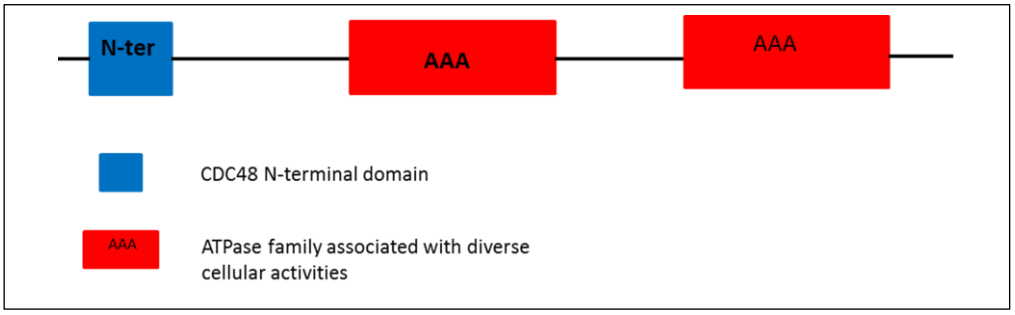


Figure 3.11 A: Schematic representation of domain organization of *Msm* Cdc48 protein. The functional domains are represented by different colours. Shown in blue is the N-terminal domain and in red are the two AAA domains (D1 and D2). The conserved AAA domains each contain the signature nucleotide binding and hydrolysis motifs. Both D1 and D2 domains are capable of ATP hydrolysis however, under physiological conditions D1 shows weak ATPase activity. http://pfam.xfam.org/ accessed on 15/05/2017.

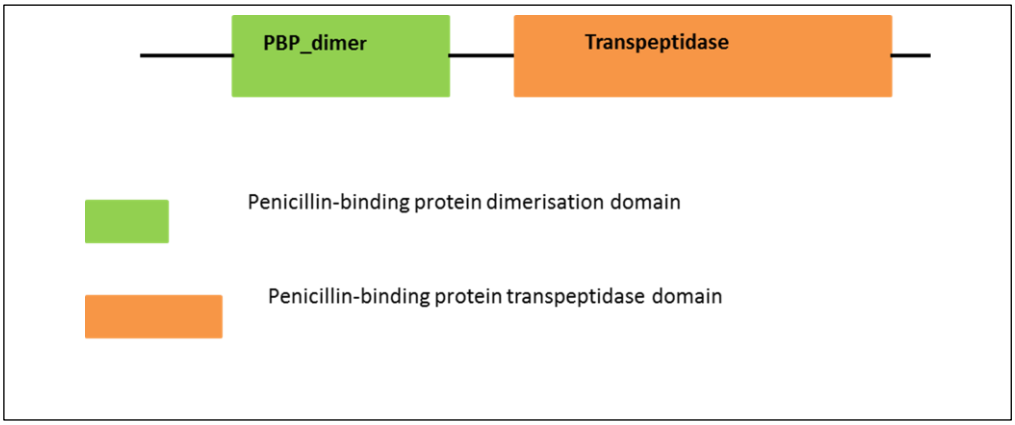


Figure 3.11 B: Schematic representation of domain organization of *Msm* FtsI protein. The functional domains of the protein are represented by different colours. Shown in green is the N-terminal PBP_dimer and in orange is the transpeptidase domain. The N-terminal dimerization domain is highly stable and is implicated in polymerization of PBP. The transpeptidase domain is needed for cross linking of septal PG. http://pfam.xfam.org/ accessed on 15/05/2017.

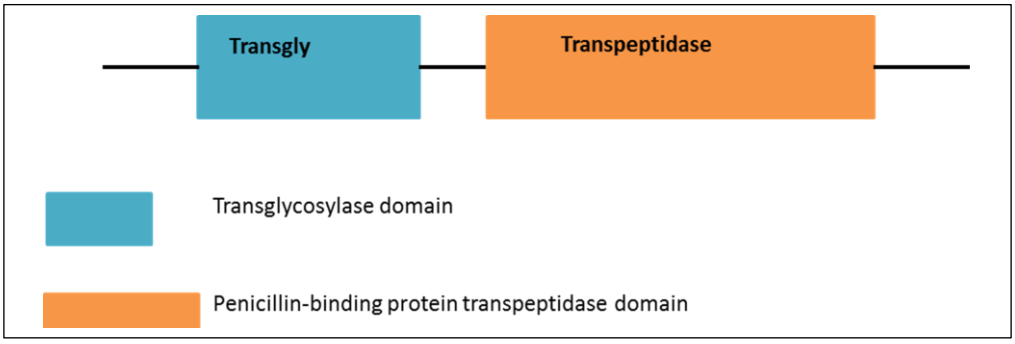


Figure 3.11 C: Schematic representation of domain organization of *Msm* PonA1 protein. The functional domains of the protein are represented by different colours. Shown in blue is the N-terminal transglycosylase domain and in orange is the transpeptidase domain found in the C-terminal region. Both the transglycosylase and the transpeptidase domains covalently incorporate the newly synthesized PG units into the pre-existing PG sacculus. Although the transpeptidase domain of PonA1 is dispensable for growth, loss of this protein affects antibiotic sensitivity in mycobacteria (Kieser et al., 2015a). http://pfam.xfam.org/ accessed on 15/05/2017.

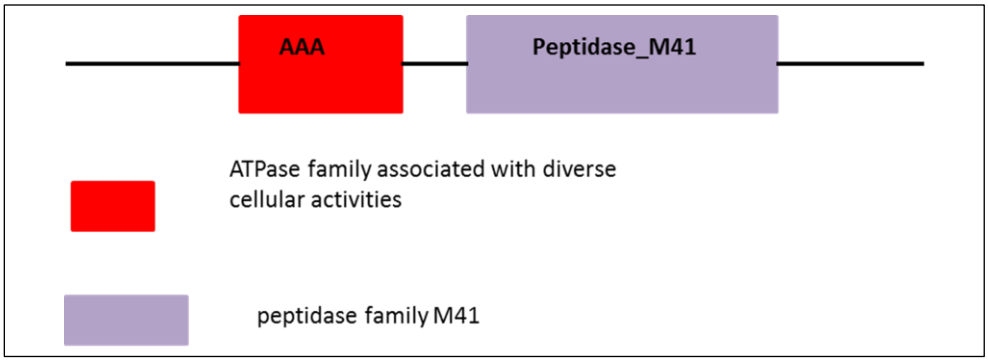


Figure 3.11 D: Schematic representation of domain organization of *Msm* FtsH protein. The functional domains of the protein are represented by different colours. Shown in red is the N-terminal AAA domain and in purple is the protease domain. Similar to AAA domain of Cdc48, the AAA domain of FtsH also has ADP bound active site and is capable of ATP hydrolysis. The FtsH peptidase domain is involved in efficient protein degradation, hence FtsH is involved in the proteolytic degradation of specific integral membrane and cytoplasmic proteins that participate in diverse cellular functions. http://pfam.xfam.org/ (15/05/2017).

3.2. Generation of *Msm* deletion mutants defective in *cdc48* and *ftsI* genes

The protein interaction and bioinformatics analysis identified several D,D-CPases interacting partners with potentially important roles in the mycobacterial physiology. To further probe this, the second part of this study was aimed at interrogating the functional roles of selected MSMEG_2433 and MSMEG_6113 partnering proteins by generating *Msm* mutant strains lacking genes encoding selected partners through two step allelic exchange by homologous recombination. This method involves the construction of a suicide plasmid carrying the inactive copy of the gene of interest (Figure 3.12). Initially, this method was planned for use to delete all four selected partners, two of MSMEG_2433 (FtsH and ponA1) and two of MSMEG_6113 (Cdc48 and FtsI) however, due to time constraints only MSMEG_6113 partners were taken forward for evaluation.

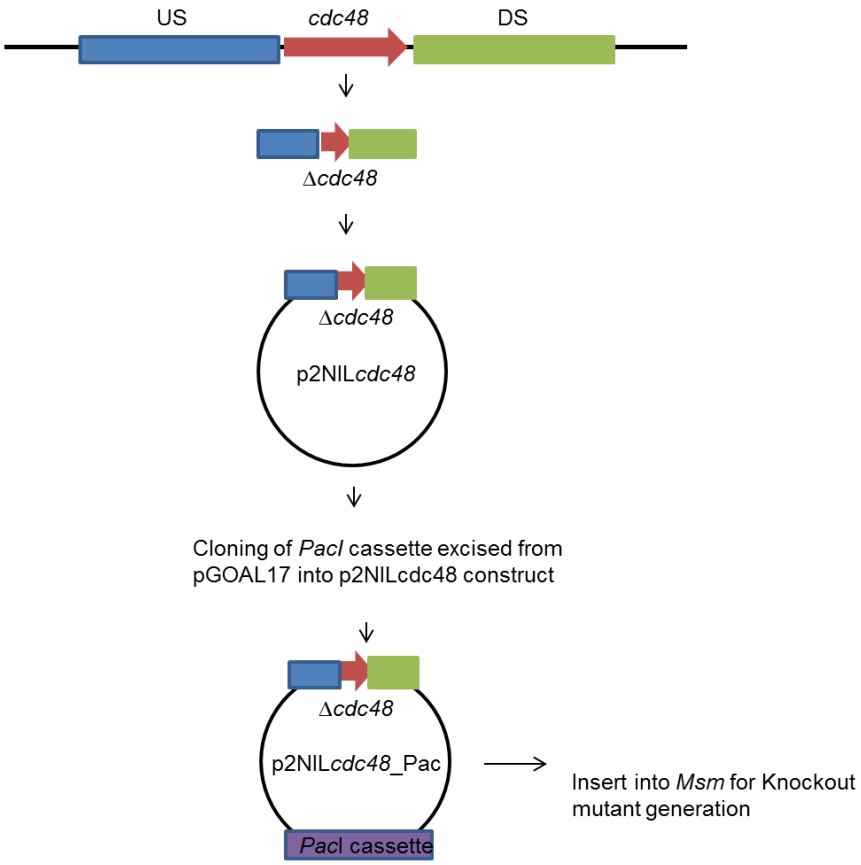
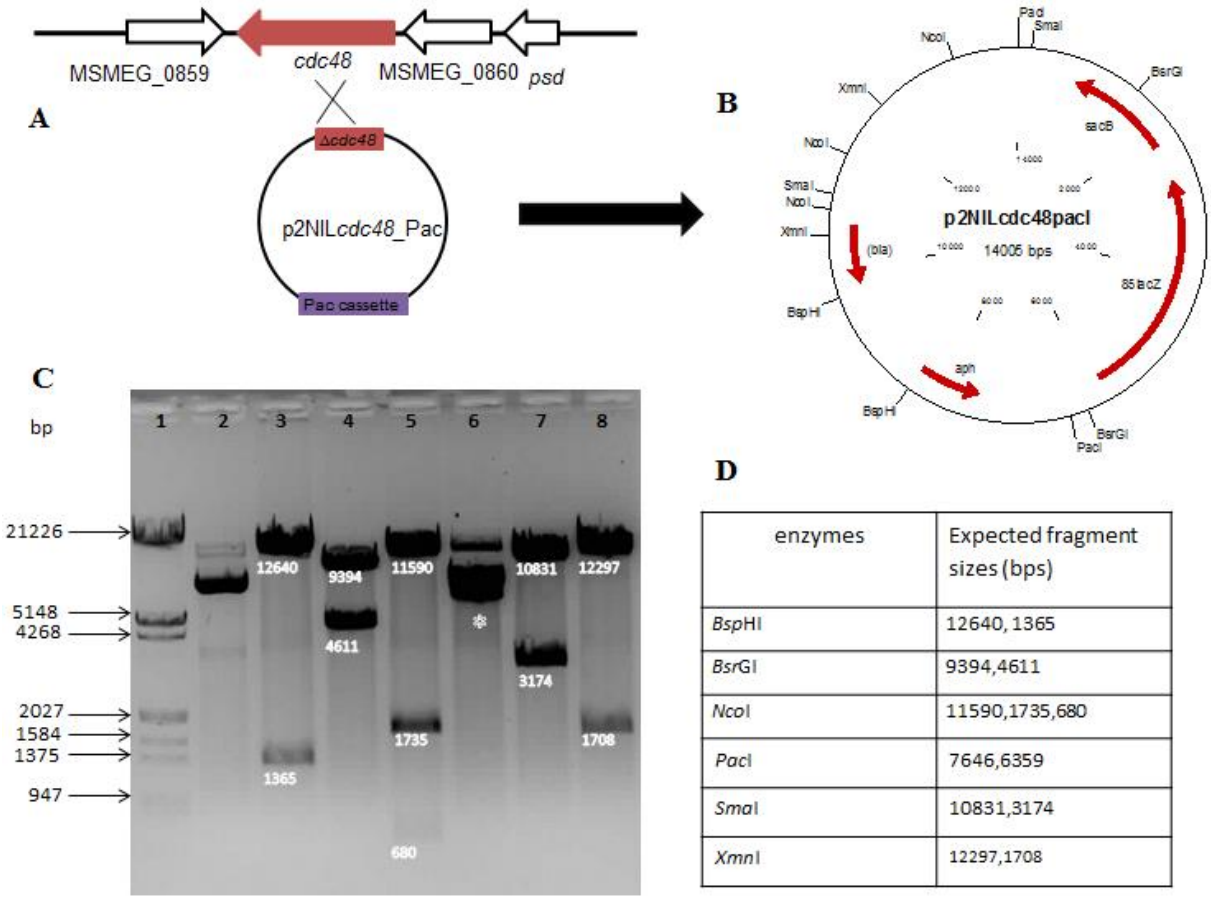


Figure 3.12: Schematic diagram illustrating the general strategy of suicide vector construction using *cdc48* as an example. Homologous sequences of the downstream and the upstream region and a small fragment of the 5' and 3' ends of the gene of interest are fused together and cloned into the p2NIL plasmid generating p2NIL*cdc48* construct. Subsequently, the Pac cassette from pGOAL17 is ligated into the p2NIL*cdc48* construct generating the final p2NIL*cdc48*_Pac suicide vector construct.

3.2.1. Construction of *cdc48* and *ftsI* gene deletion constructs

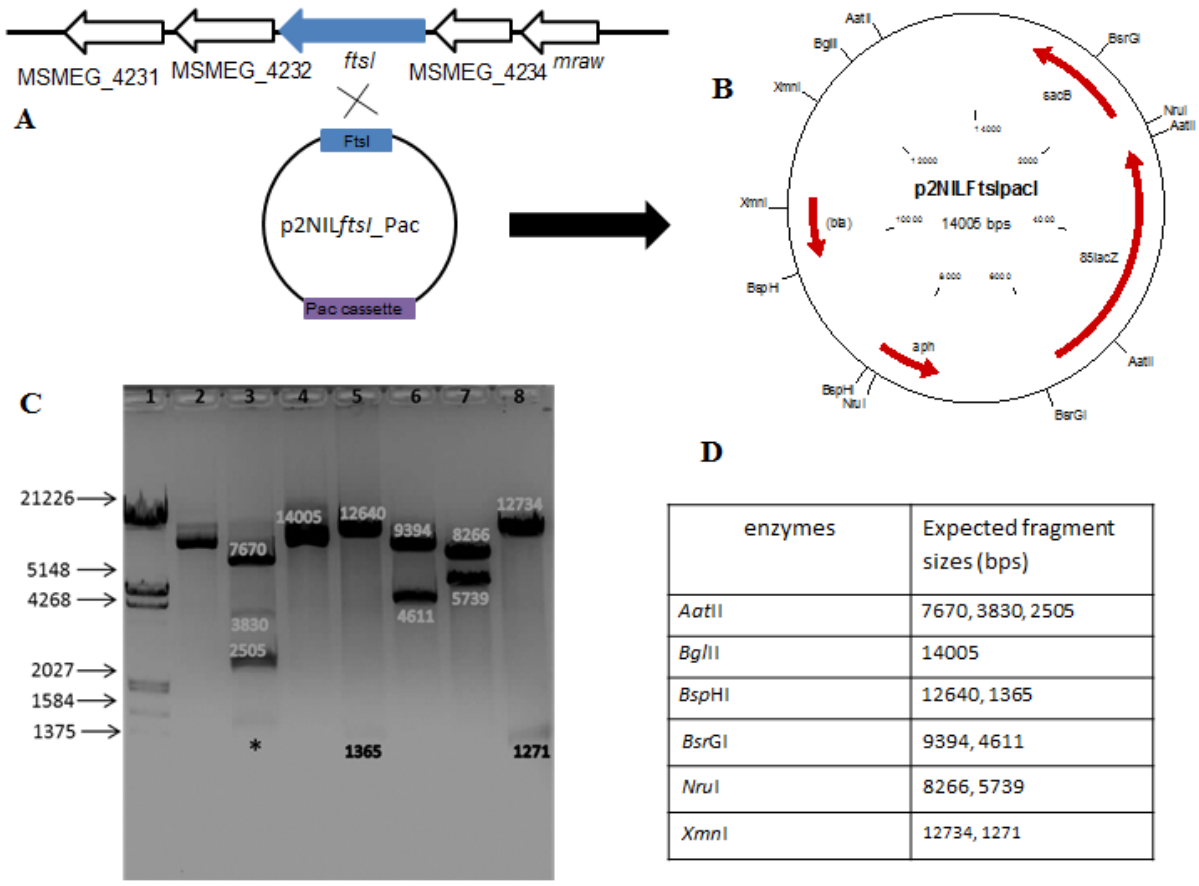
The suicide vectors were constructed as detailed in section 2.9.2. Briefly, 1500 bp upstream and 1500 bp downstream regions flanking the gene of interest along with 99 bp of both the 5'end and the 3'end of the gene were amplified by PCR. The PCR fragments were sub-cloned into p2NIL following the protocol in section 2.6.6. A selected clone for each construct was verified by restriction profiling with at least 6 restriction enzymes (Appendix C15, C16) and further confirmed by sequencing (results not shown). The linearized Pac cassette excised from pGOAL17 was cloned into the p2NIL*cdc48* and p2NIL*ftsI* constructs to generate final knockout constructs. A single positive clone per construct was selected and verified by restriction analysis as outlined in section 2.6.2. (Figure 3.13. and 3.14) and further confirmed by sequencing (results not shown). The genetic integrity of the p2NIL*cdc48*_Pac and p2NIL*ftsI*_Pac constructs was maintained as confirmed by the restriction analysis where the

digested clones yielded the expected fragment banding patterns. Figure 3.13. shows the restriction profile obtained from restriction digest of the p2NIL*cdc48*_Pac construct with different enzymes, all yielding the correct sizes. Notably, the *Pac*I restriction digest yielded a doublet band due to the presence of two fragments that were closely related in size. Figure 3.14. shows the restriction profile obtained from restriction digest of the p2NIL*ftsI*_Pac construct with different enzymes, no missing or aberrant bands were observed. Analysis of the constructs by sequencing revealed that no mutations were accumulated (data not shown) which further confirmed the integrity of the constructs for subsequent use in mutant generation.



enzymes	Expected fragment sizes (bps)
*Bsp*HI	12640, 1365
*Bsr*GI	9394,4611
*Nco*I	11590,1735,680
*Pac*I	7646,6359
*Sma*I	10831,3174
*Xmn*I	12297,1708

Figure 3.13: Restriction profile of the p2NIL*cdc48*_Pac knockout construct. (A) Genome map of mc^{2}155 indicating the position of *cdc48* gene within the genome. The strategy employed for construction of the knockout vector is also shown. (B) Plasmid map of the final p2NIL*cdc48*_Pac knockout construct used for transformation. (C) 0.8% agarose gel indicating expected DNA band sizes, lane (1) DNA marker III (Fermentas), lane (2) uncut construct control, lane (3) *Bsp*HI, lane (4) *Bsr*GI, lane(5) *Nco*I, lane (6) *Pac*I, lane (7) *Sma*I, lane (8) *Xmn*I. (D) Table showing restriction enzymes used for profiling and the expected fragment sizes. * in lane 6 indicates that the two fragments run together as indicated by the bright single band.



enzymes	Expected fragment sizes (bps)
*Aat*II	7670, 3830, 2505
*Bgl*II	14005
*Bsp*HI	12640, 1365
*Bsr*GI	9394, 4611
*Nru*I	8266, 5739
*Xmn*I	12734, 1271

Figure 3.14: Restriction profile of the p2NIL*ftsI*_Pac knockout construct. (A) Genome map of mc^{2}155 indicating the position of *ftsI* gene within the genome. The strategy employed for construction of the knockout vector is also shown. (B) Plasmid map of the final p2NIL*ftsI*_Pac knockout construct used for transformation. (C) 0.8% agarose gel indicating expected DNA band sizes, lane (1) DNA marker III (Fermentas), lane (2) uncut construct control, lane (3) *Aat*II, lane (4) *Bgl*II, lane(5) *Bsp*HI, lane (6) *Bsr*GI, lane (7) *Nru*I, lane (8) *Xmn*I. (D) Table showing restriction enzymes used for profiling and the expected fragment sizes. * in lane 3 indicates the extra band as a result of the enzyme's star activity.

3.2.2. Generation of *cdc48* and *ftsI* deletion mutant strains in *Msm*

3.2.2.1 Generation of *Msm* Δ*cdc48* strain

The two-step allelic exchange by homologous recombination method was employed for deletion of the *cdc48* gene in *Msm* following the protocol outlined in section 2.9.2. The p2NIL*cdc48*_Pac knockout construct was electroporated into the parental mc^{2}155 strain as per protocol outlined in 2.7.2. Integration of p2NIL*cdc48*_Pac construct into the genome of mc^{2}155 by homologous recombination resulted in generation of *cdc48* SCO strains. Following generation of an SCO strain, an unmarked Δ*cdc48* mutant (represented by white antibiotic-sensitive colonies) was generated as described in section 2.9.2. The putative *cdc48* deletion mutants were identified by PCR screening as per the protocol in section 2.6.1.1. and

further verified by Southern blot analysis as indicated in section 2.9.3. Ten white colonies were picked for PCR screening to identify potential clones. The PCR strategy used to screen knockout mutants involved the use of primers that amplify the full length *cdc48* gene. In the wildtype strains, a full length amplicon of 2238 bp is expected. In the knockout mutants, only a small region of the gene is amplified due to part of the gene being deleted, which would result in generation of a smaller fragment of 198 bp, indicating the presence of the mutant allele. PCR screening (Figure 3. 15B) revealed the presence of five potential *cdc48* deletion mutant strains (clones 2, 4, 6, 7 and 10) as determined by the presence of the 198 bp band, representing the mutant allele (Δ*cdc48*) in comparison to a 2338 bp band of the wildtype allele (Figure 3.15).

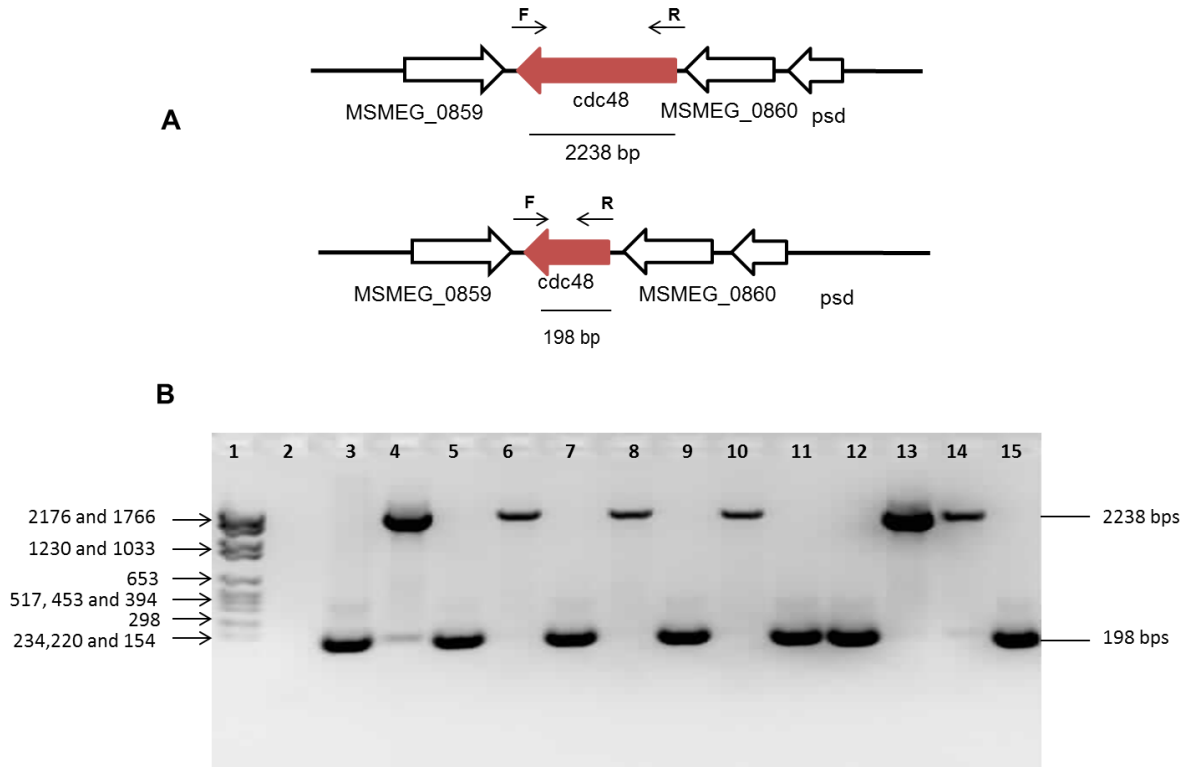


Figure 3.15: PCR screening of Δ*cdc48* deletion mutants. (A) Schematic representation of genomic maps of the wildtype and mutant *cdc48* region. Primer binding sites (arrows) and expected amplicon sizes are shown. F = forward primer. R = reverse primer. (B) PCR screen of *cdc48* deletion. Lane (1) DNA marker VI, lane (2) no DNA control, lane (3) p2NIL*cdc48*_Pac knockout construct, (4) wildtype, lane (5) SCO, lane (6-15) possible mutants 1-10.

Three of the potential Δ*cdc48* strains (clones 2, 4 and 6) were taken forward for further analysis by Southern blotting. Southern blot analysis was conducted to confirm the genotype of Δ*cdc48* strains. Genomic DNA of mc^{2}155, Δ*cdc48* and SCO strains was digested with *Bam*HI and Southern blot analysis was conducted on these strains as per protocol in section

2.9.3. Wildtype mc^{2}155 strain displayed expected fragment sizes of 3334 bp and 2495 bp, the SCO strain displayed 3913 bp, 3334 bp and 461 bp fragments and both the Δ*cdc48* strains displayed expected 3334 bp and 461 bp fragments confirming that the Δ*cdc48* strain retains the truncated copy of the *cdc48* gene (Figure 3.16).

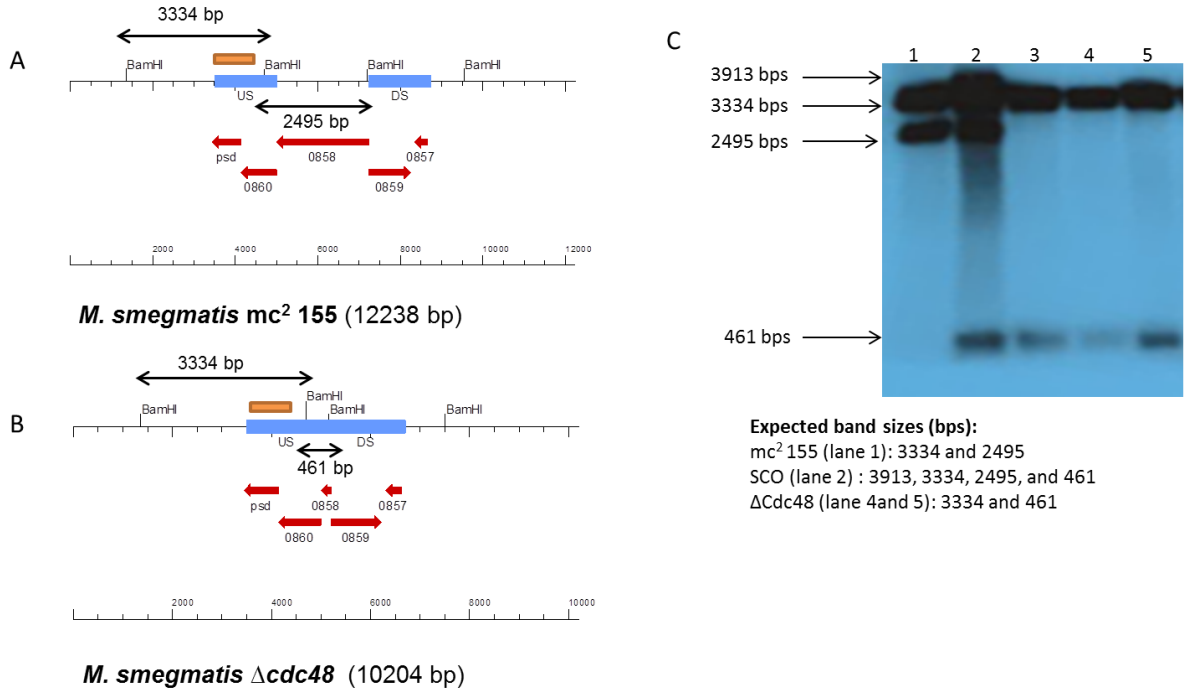


Figure 3.16: Southern blot analysis of *Msm* Δ*cdc48* strain. (A) Genomic map of mc^{2}155 strain showing expected fragment sizes for the wildtype *cdc48* allele. (B) Genomic map of Δ*cdc48* mutant strain showing expected fragment sizes for the mutant *cdc48* allele. (C) Southern blot showing *BamHI* digested DNA fragments bound by the designed *cdc48* specific probe (represented by orange rectangles in A and B). lane (1) mc^{2}155, lane (2) SCO, lane (3-5) Δcdc48 strains.

3.2.2.2. Generation of *Msm* Δ*ftsI* strain

For deletion of the *ftsI* gene in *Msm*, the two-step allelic exchange by homologous recombination procedure was conducted as per protocol outlined in section 2.9.2. The p2NIL*ftsI*_Pac knockout construct was electroporated into the parental mc^{2}155 strain as per protocol outlined in 2.7.2., which resulted in integration of the construct into the genome of mc^{2}155 by homologous recombination generating *ftsI* SCO strains. Following generation of SCO strain, attempts were made to generate an unmarked Δ*ftsI* mutant (represented by white antibiotic-sensitive colonies) as described in section 2.9.2. PCR screening was conducted to identify possible *ftsI* deletion mutants as per protocol in section 2.6.1.1. White colonies were picked for PCR screening to identify potential clones. The same PCR strategy used to screen

the above *cdc48* knockout mutants was also employed for this experiment, whereby amplification of the *ftsI* gene in the wildtype strain would result in a full length amplicon of 1947 bp as expected while in the knockout mutants, only a small region of the gene would be amplified due to part of the gene being deleted yielding a smaller fragment of 198 bp. Initially, 10 colonies were screened and all the clones in this screen appeared to be wildtype revertants as confirmed by the presence of a 1947 bp band found in lanes 6-15 (Figure 3. 17B). Additional clones (50) were screened and no potential mutants were revealed. All the remaining clones had reverted to the wildtype genotype and others retained the SCO genotype as confirmed by the presence of both the wildtype and mutant allele bands (data not shown). The observed SCO genotype post sucrose counter selection suggests that the strains had been subjected to compensatory mutation in the *lacZ* and *sacB* genes, which allowed for growth in the presence of sucrose. These observations highlighted the possibility that *ftsI* is essential and could not be targeted for gene deletion. In order to test for this, additional 45 white colonies were screened and none of them revealed the mutant genotype (results not shown), thus confirming that *ftsI* is essential for growth *in vitro*.

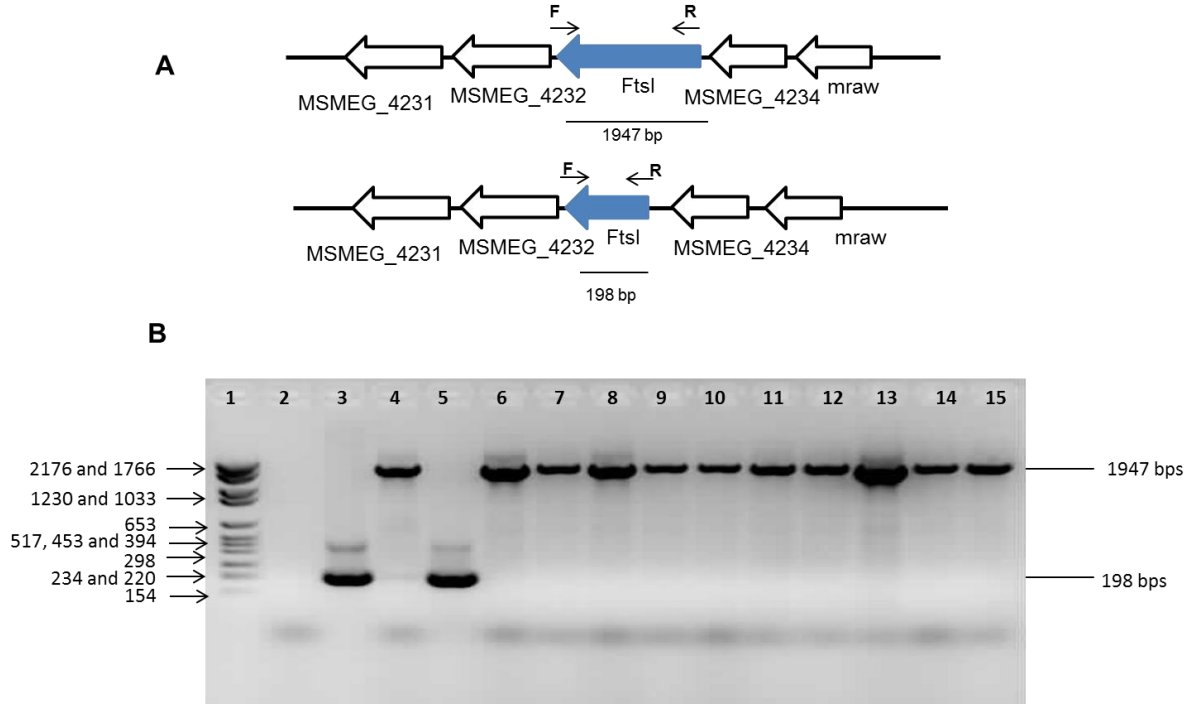


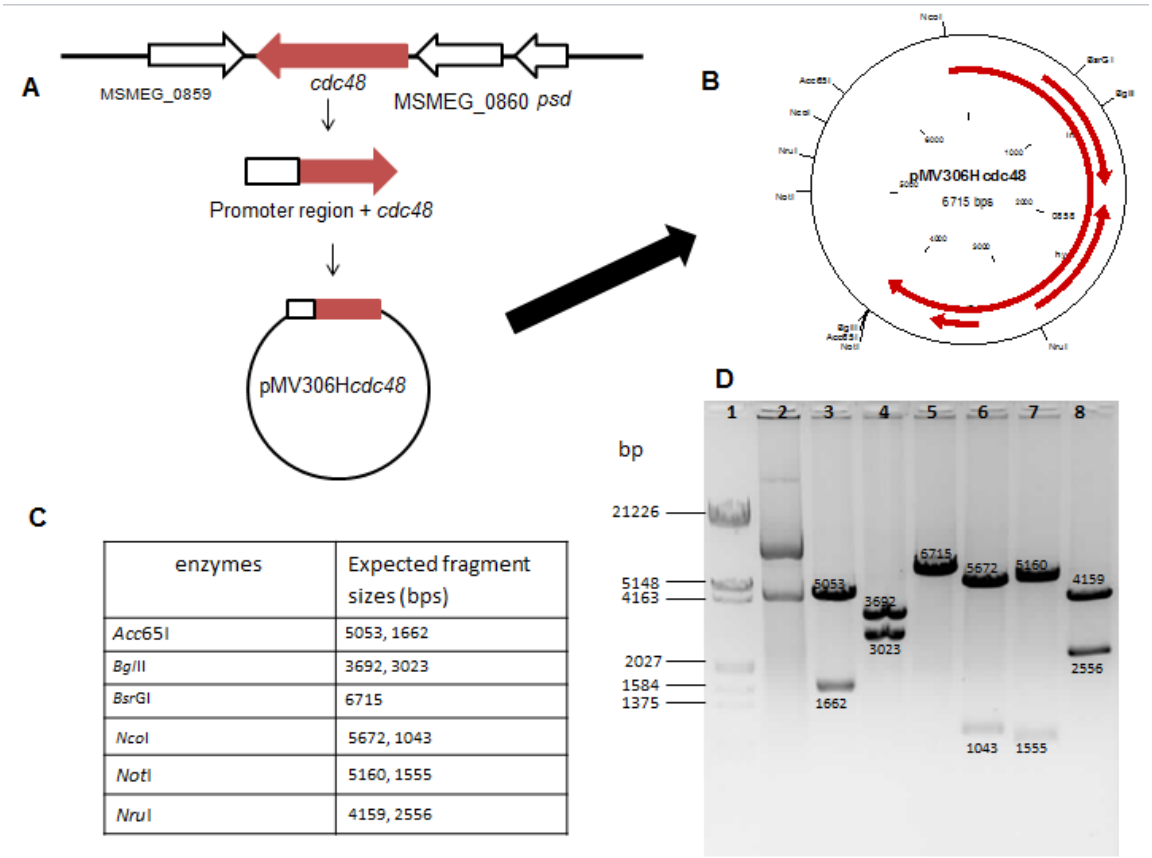
Figure 3.17: PCR screening of Δ*ftsI* deletion mutants. (A) Schematic representation of genomic maps of wildtype and mutant *ftsI* region. Primer binding sites (arrows) and expected amplicon sizes are shown. F = forward primer. R = reverse primer. (B) PCR screen of *ftsI* deletion. Lane (1) DNA marker VI, lane (2) no DNA control, lane (3) p2NIL*ftsI*_Pac knockout construct, (4) wildtype, lane (5) SCO, lane (6-15) clone 1-10.

3.2.3. Genetic complementation of Δ*cdc48* strain

Genetic complementation of the Δ*cdc48* strain was conducted to confirm that any phenotypic variation observed from the mutant strain was only due to loss of the functional copy of the gene and not due to polar effects. This was accomplished by reintroducing a functional copy of *cdc48* gene in the background of the mutant strain (see section 2.10.).

3.2.3.1. Construction of the *cdc48* complementation vector

The *cdc48* complementation vector was constructed by amplifying the wildtype *cdc48* allele and the 200 bp upstream native *cdc48* promoter region by PCR, followed by cloning of the amplicons into the pMV306H integrating vector as per protocol outlined in section 2.6.6. Subsequent clones were screened and a single positive clone was selected, verified by restriction analysis as outlined in section 2.6.2. (Figure 3.18D) and further confirmed by sequencing (results not shown). Figure 3.18. demonstrates that the restriction profile obtained from restriction digest of the pMV306H*cdc48* yielded correct sizes. Sequencing results revealed no mutations, thus confirming the integrity of the construct.



enzymes	Expected fragment sizes (bps)
Acc65I	5053, 1662
BglII	3692, 3023
BsrGI	6715
NcoI	5672, 1043
NotI	5160, 1555
NruI	4159, 2556

See figure legend on the next page.

Figure 3.18: Restriction profile of the pMV306H*cdc48* construct. (A) Genome map of mc^{2}155 indicating the location of *cdc48* gene within the genome. The strategy employed for construction of the complementation vector is also shown. (B) Plasmid map of the final pMV306H*cdc48* construct used for transformation. (C) Table showing restriction enzymes used for profiling and the expected fragment sizes. (D) 0.8% agarose gel indicating expected DNA band sizes, lane (1) DNA marker III (Fermentas), lane (2) uncut construct control, lane (3) *Acc*65I, lane (4) *Bgl*II, lane(5) *Bsr*GI, lane (6) *Nco*I, lane (7) *Not*I, lane (8) *Nru*I.

3.2.3.2. Generation of Δ*cdc48* complemented strain (Δ*cdc48*::*cdc48*)

The pMV306H*cdc48* construct was electroporated into the Δ*cdc48* strain following the protocol in section 2.7.2. to generate the Δ*cdc48*::*cdc48* complemented strain. The pMV306H vector allows for integration of the functional *cdc48* gene into the *attB* site in the genome of mycobacteria. To confirm that integration of the complementing gene was successful, PCR screening was performed to confirm site-specific integration of the construct (Figure 3.19). Primers were targeted to the *att* region where the observed PCR products of 282 bp and 320 bp confirmed that the pMV306H*cdc48* construct had integrated at the correct site (Figure 3.19).

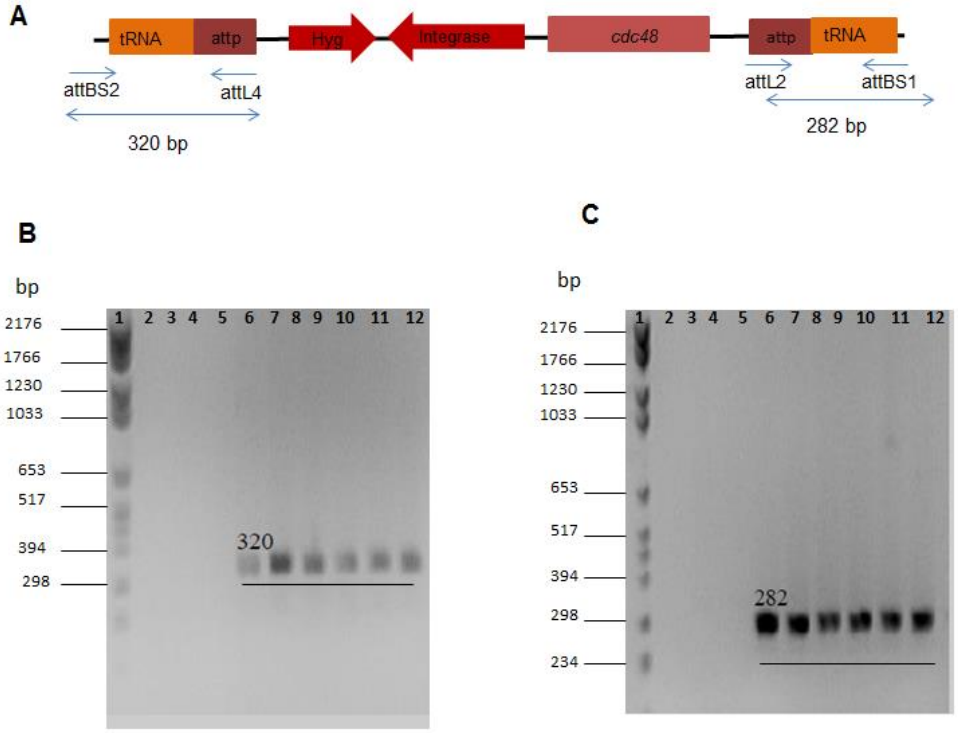


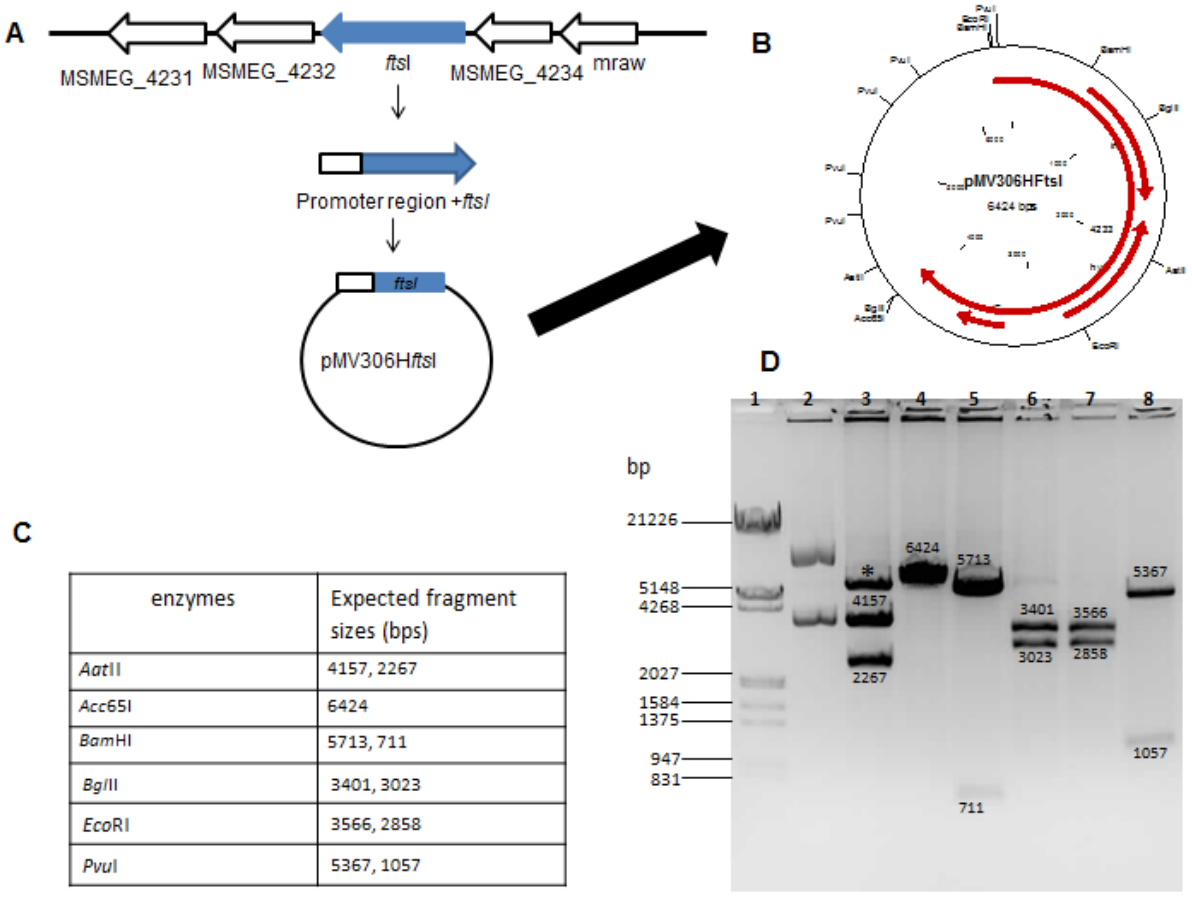
Figure 3.19: PCR confirmation of site-specific integration of pMV306H*cdc48* into Δ*cdc48* mutant. (A) Schematic representation of *Msm* chromosome showing pMV306H*cdc48* integrated into the *attB* site. Primer binding sites (arrows) and expected amplicon sizes are shown. (B) PCR reaction with *attBS2* + *attL4* primer set. (C) PCR reaction with *attL2* + *attBS1* primer set. Lane (1) Marker VI, lane (2) no DNA control, lane (3) wildtype, lane (4) Δ*cdc48*, lane (5-12) potential clones carrying pMV306H*cdc48* complementation vector.

3.2.4. Generation of *ftsI* deletion mutant in the merodiploid strain

Following unsuccessful attempts of generating a *ftsI* gene knockout mutant by allelic exchange, another method was employed to evaluate the physiological role of the *ftsI* gene product in *Msm*. This method allows for inactivation of the wildtype copy of the gene in the presence of a second copy of the gene (termed the wildtype complementing gene) located elsewhere in the genome. A strain carrying two copies of a gene in this conformation is referred to as a merodiploid strain. In this way, the wildtype complementing gene expressed from the native promoter on the integrating vector, allows for deletion of the native copy. To achieve this, a *ftsI* complementation vector was first constructed and then integrated into the genome of *ftsI* SCO strain, generating a merodiploid strain (Figure 2.6). Following this, the merodiploid strain was subjected to counter-selection for DCOs as per standard protocol.

3.2.4.1. Construction of *ftsI* complementation vector

For construction of the complementation vector, the wildtype *ftsI* allele was amplified by PCR including the 200 bp native *ftsI* promoter region, followed by cloning of the amplicons into the pMV306H integrating vector as per the protocol outlined in section 2.6.6. Subsequent clones were screened and a single positive clone was selected, verified by restriction analysis as outlined in section 2.6.2. (Figure 3.20D) and further confirmed by sequencing (results not shown). Restriction enzymes used for profiling the pMV306H*ftsI* construct yielded the expected banding patterns with the exception of *Aat*II, which had an extra band (Figure 3.20). Analysis of the construct by sequencing further confirmed the integrity of the construct for subsequent use in generation of the complement strain. This suggests that the extra *Aat*II band is the result of an unmapped site in the vector backbone.



enzymes	Expected fragment sizes (bps)
*Aat*II	4157, 2267
*Acc*65I	6424
*Bam*HI	5713, 711
*Bgl*II	3401, 3023
*Eco*RI	3566, 2858
*Pvu*I	5367, 1057

Figure 3.20: Restriction profile of the pMV306H*ftsI* construct. (A) Genome map of mc^{2}155 indicating the location of *ftsI* gene within the genome. The strategy employed for construction of the complementation vector is also shown. (B) Plasmid map of the final pMV306H*ftsI* construct used for transformation. (C) Table showing restriction enzymes used for profiling and the expected fragment sizes. (D) 0.8% agarose gel indicating expected DNA band sizes, lane (1) DNA marker III (Fermentas), lane (2) uncut construct control, lane (3) *Aat*II, lane (4) *Acc*65I, lane(5) *Bam*HI, lane (6) *Bgl*II, lane (7) *Eco*RI, lane (8) *Pvu*I.

3.2.4.2. Generation of Δ*ftsI* mutant strain in the merodiploid background

To generate *ftsI* mutant, a merodiploid strain was first generated by electroporating the pMV306H*ftsI* complementation vector into the previously generated *ftsI* SCO recombinant strain, following the protocol outlined in section 2.7.2. A schematic representation of this approach is shown in Figure 2.6. This was then followed by extraction of genomic DNA from the resultant merodiploid strain as per protocol in section 2.5.2.1, and the DNA was then used for PCR screening as indicated in section 2.6.1.1. to confirm successful integration of complementation vector into the SCO recombinant strain. PCR screening confirmed the correct interaction of the construct as indicated by observed expected bands (Figure 3.21). Five of the selected colonies for PCR screen appeared to exhibit correct integration pattern.

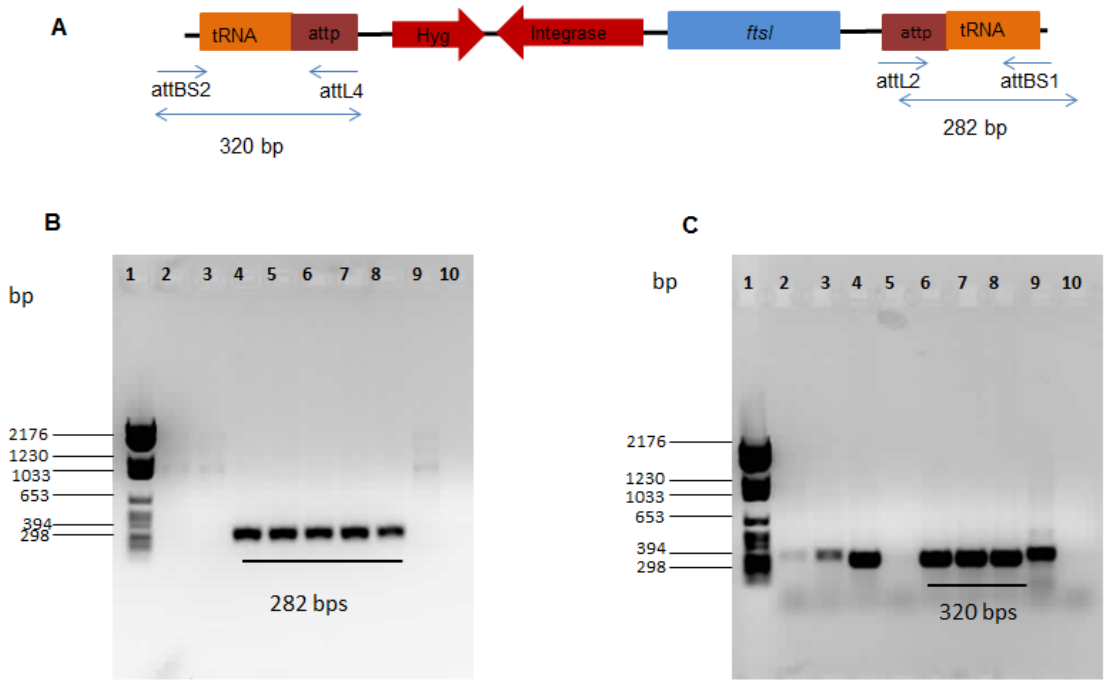


Figure 3.21: PCR confirmation of site-specific integration of pMV306H*ftsI* into *ftsI* SCO strain. (A) Schematic representation of *Msm* chromosome showing pMV306H*ftsI* integrated into the *attB* site. Primer binding sites (arrows) and expected amplicon sizes are shown (B) PCR reaction with *attL2* + *attBS1* primer set. (C) PCR reaction with *attBS2* + *attL4* primer set. Lane (1) Marker VI, lane (2-8) potential clones carrying pMV306H*ftsI* complementation vector. Lane (9) wildtype, lane (10) no DNA control. The band in lane 9 of figure C is probably due to template contamination.

Following this, the strain was subjected to counter-selection for DCO strains as per the protocol outlined in section 2.12. White colonies were picked for PCR screening to identify potential clones containing the mutant allele. One hundred and forty colonies were screened and no potential mutants were revealed (data not shown). Most of the screened clones had reverted to the wildtype genotype and others retained the SCO genotype. It was unclear why an *ftsI* mutant could not be generated in the merodiploid strain and no further attempts were made to delete this gene.

3.2.5. Phenotypic characterization of Δ*cdc48* mutant

To investigate the role of the *cdc48* gene in cell growth, division and structural maintenance of *Msm*, a number of assays were carried out on the Δ*cdc48* strain to compare against the wildtype and complemented strains. This included analyses of growth kinetics, cell permeability/ integrity, cell morphology and division by use of cell wall staining chemical probes and different forms of microscopy.

3.2.5.1. The role of Cdc48 in regulating *Msm* growth kinetics

To evaluate the role of Cdc48 in regulating *Msm* growth kinetics, growth analyses were carried out on the wildtype mc^2155, the Δ*cdc48* mutant and the complemented derivative strains. Growth kinetics were determined by the use of growth curves conducted in triplicate and growth assays were set up as described in section 2.13.1. The data revealed that Cdc48 is dispensable for growth and plays no significant role in regulating *Msm* growth kinetics as indicated by the slight, but non-significant ($p>0.05$) delay in growth kinetics of the Δ*cdc48* strain, particularly during the exponential growth phase (Figure 3.22). As observed in Figure 3.22, the complemented strain struggled to grow compared to the mutant and wildtype strains and this could be due to the effect of Hyg antibiotic present in the media, which was used to grow the strain and select for the complementing vector.

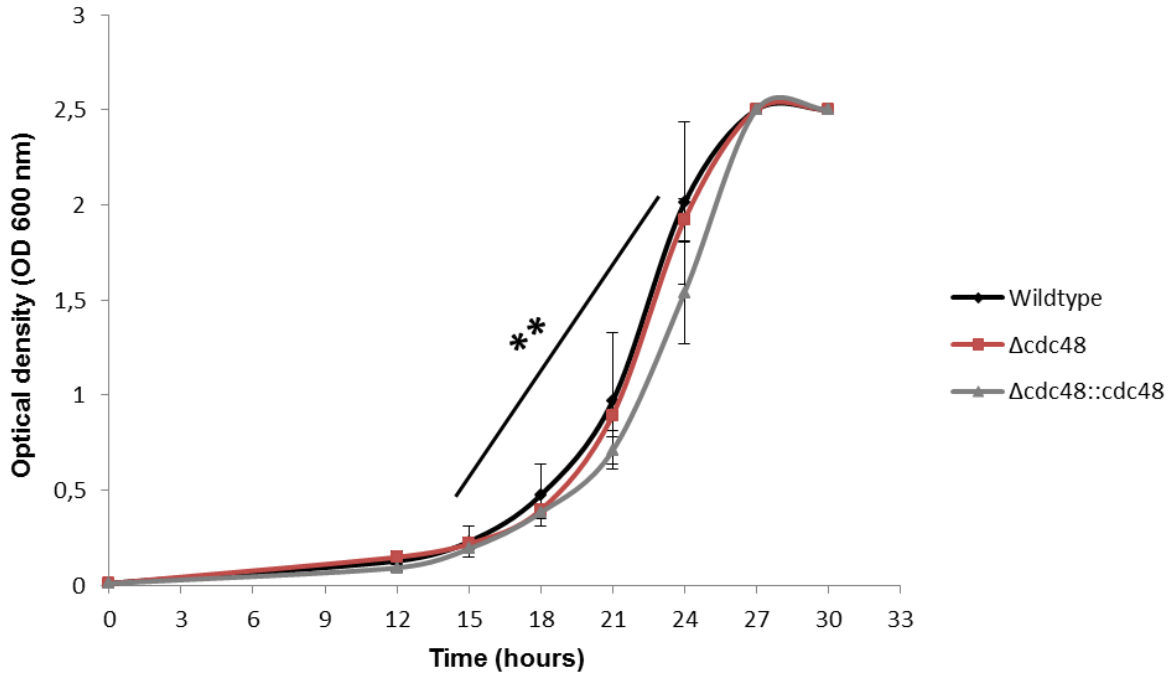


Figure 3.22: Growth kinetics of the Δ*cdc48* strain in comparison to the wildtype and complemented strains. Growth analyses were conducted by measuring the increase in optical density (OD_{600}) of the cultures at three hour intervals over 30 hours and the data was then used to generate scatter plots. The data shown represent the means of three independent replicates and the error bars represent standard error obtained from standard deviation of the triplicates. Unpaired student T-test was used with ** representing p-value > 0.05.

3.2.5.2. Cdc48 plays a role in antibiotic sensitivity and cell wall permeability

In addition to determining the role of Cdc48 in *Msm* growth kinetics, we investigated whether loss of *cdc48* gene affected the susceptibility of *Msm* to various drugs. This was done by assessing the minimum inhibitory concentrations (MICs) for selected cell wall targeting antibiotics in the Δ*cdc48* mutant in comparison to the parental mc^2155 strain and the Δ*cdc48*::*cdc48* genetically complemented strain. The MIC is described as the antibiotic concentration that gives visible growth inhibition. The assay was prepared as per the protocol in section 2.13.2. The results revealed that loss of *cdc48* resulted in a 4-fold increase in susceptibility to amoxicillin, a cell wall targeting antibiotic that inhibits cell wall biosynthesis by inhibiting transpeptidases that catalyze peptidoglycan cross-linking (Table 3.5 and Figure 3.23). A 2-fold increase in susceptibility is generally not considered significant. However, repeatedly the Δ*cdc48* strain displayed an increase in susceptibility to other cell wall targeting antibiotics such as D-cycloserine and vancomycin, suggesting that the difference might be significant (Figure 3.23).

Table 3.5: MICs (µg/ml) of the wildtype, Δ*cdc48* and Δ*cdc48*::*cdc48* strains. Shown in brackets is the fold increase in drug susceptibility of the Δ*cdc48* mutant over wildtype.

	MIC (µg/ml)*		
Drug	**Wildtype**	**Δ*cdc48***	**Δ*cdc48*::*cdc48***
Amoxycillin	32	10.67 (3)	26.67
D-cycloserine	6.25	3.13 (2)	6.25
Ethambutol	0.27	0.4 (-)	0.27
Imepenem	100	100 (0)	100
Isoniazid	100	100 (0)	100
Teicoplanin	12.5	12.5 (0)	12.5
Vancomycin	0.1	0.05 (2)	0.1

*Fold change over the MIC observed in wildtype is shown in parenthesis

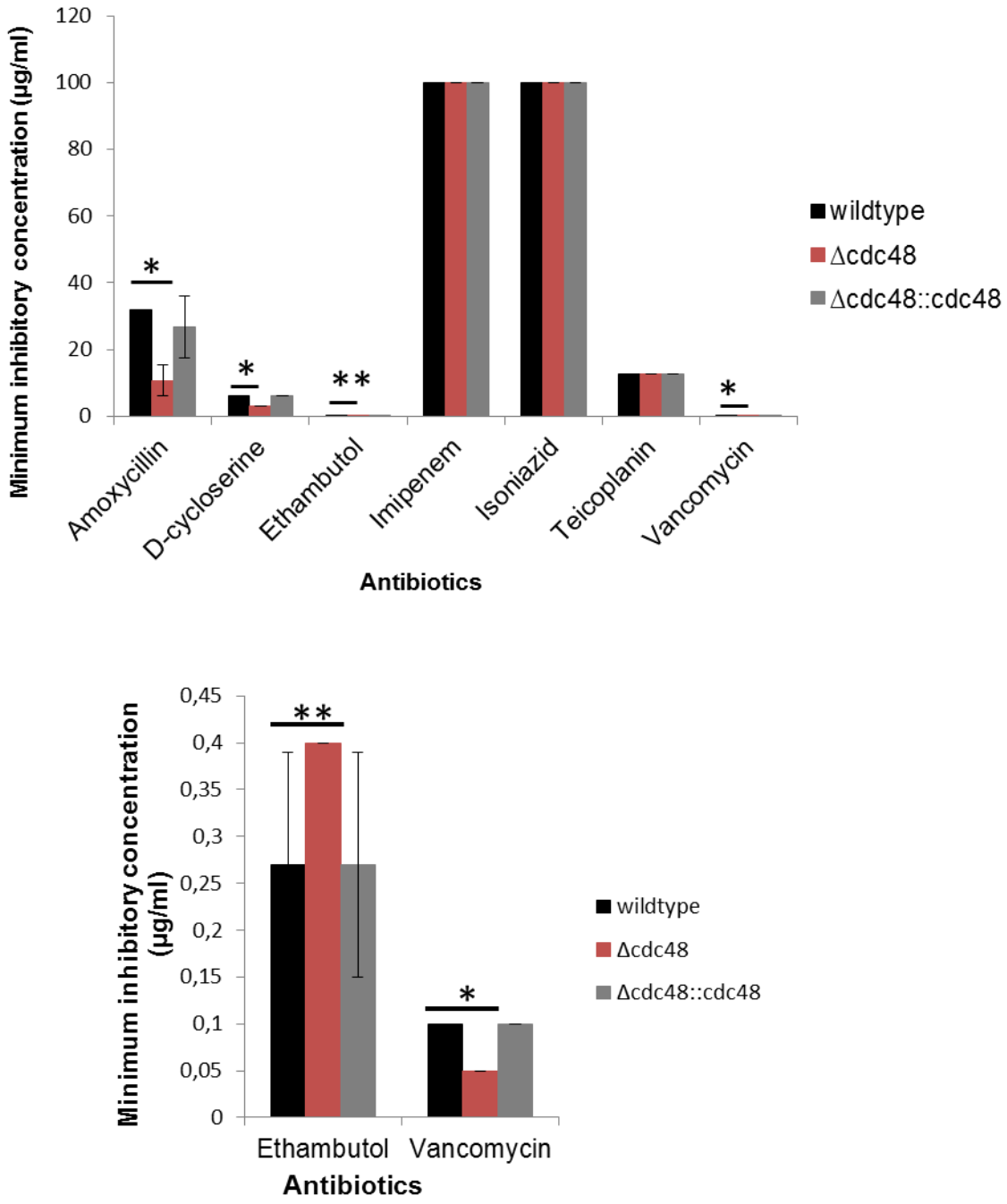


Figure 3.23: Minimum inhibitory concentrations (MICs) of the Δ*cdc48* strain in comparison to the wildtype and complemented strains. The strains were exposed to drug treatment for 7 days from which the MIC was determined for different antibiotics. The Δ*cdc48* strain showed increased susceptibility to amoxicillin, D-cycloserine and vancomycin. The data shown represent the means of three independent replicates and the error bars represent standard error obtained from standard deviation of the triplicate experiments. Unpaired student T-test was used with p-value <0.05 considered significant *, p-value > 0.05 ** non-significant.

The intrinsic resistance of mycobacteria to various antibiotics is mostly attributed to their relatively impermeable cell wall, which provides a barrier to foreign compounds and limits

drug uptake (Brennan and Nikaido, 1995). As the Δ*cdc48* mutant exhibited increased susceptibility to selected antibiotics, we hypothesized that this strain may have a weakened cell wall, which is more permeable to compounds thus facilitating drug uptake. To further evaluate this, the ethidium bromide (EtBr) uptake/ diffusion assay was performed as outlined in section 2.13.3. In this assay, accumulation of EtBr is assessed in relation to cell wall permeability. EtBr is highly fluorescent inside the cell and emits weak fluorescence outside the cell. From the results obtained, the Δ*cdc48* strain seemed to be more permeable, compared to the wildtype as indicated by the increased fluorescence observed for this strain indicating high EtBr accumulation (Figure 3.24). Overall, these results revealed that loss of *cdc48* may have led to an increase in susceptibility to cell wall targeting antibiotics and enhanced cell permeability, but the results are not yet amenable to a statistical assessment of the data.

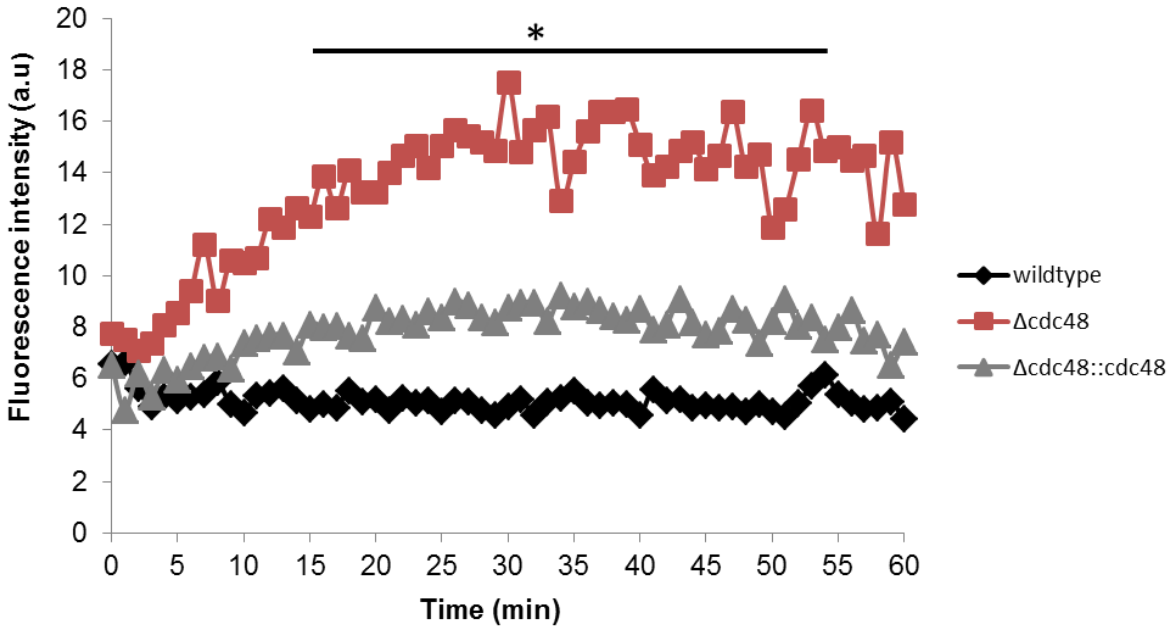


Figure 3.24: Δ*cdc48* cell wall permeability assessment. Cell wall permeability was monitored by quantifying accumulation of EtBr (5 µg/ml) into the cells of the Δ*cdc48* mutant strain, wildtype and complemented strains over an hour. The data shown represent one experiment, see appendix C19 for the other two. Unpaired student T-test was used with. *: p-value <0.05, using technical replicates from one experiment. Time limitations precluded further repetition.

3.2.5.3. Microscopic analyses

SEM and fluorescence microscopy (in conjunction with various fluorescent chemical probes) were employed as described in section 2.13.4. to evaluate the overall structure of Δ*cdc48* individual cells in comparison to wildtype and complemented strains. These analyses were

carried out to investigate the possible role of Cdc48 in maintaining a number of cellular processes. Examination of Δ*cdc48* cell surface morphology by SEM revealed distinct morphological defects in comparison to the wildtype, including formation of V-shaped cells, pole bulging cells, kinking and chaining cells as shown in Figure 3.25. The observed phenotypes that were robustly different in Δ*cdc48* and wildtype were quantified. Cells with pole bulges (indicated by blue arrows in Figure 3.25) occurred more frequently in the Δ*cdc*48 mutant strain and a significant number of cells in the mutant strain were short and V-shaped (indicated by the green arrow in Figure 3.25) compared to rod shaped cells in the wildtype mc^2155 strain, Figure 3.26. Chaining cells with multiple septal bridges (depicted by red arrows in Figure 3.25) were also observed however, there was no significant difference between the number of these cells in the wildtype and mutant strain and this could possibly be due to a limited number of cells quantified (Figure 3.26). These observed phenotypes point to a possible role of Cdc48 in maintaining cell growth, division and cell shape.

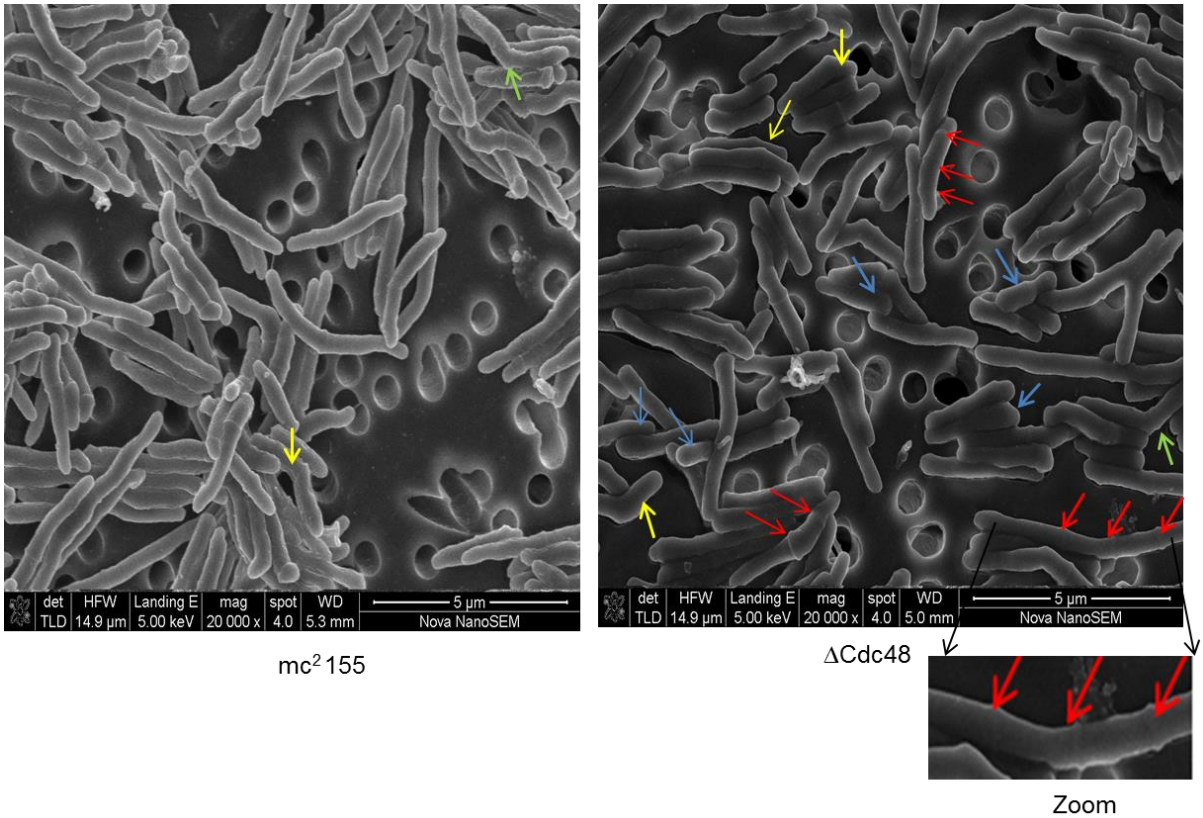


Figure 3.25: SEM micrographs of wildtype mc^2155 and Δ*cdc48* strains. Loss of *cdc48* results in cell morphological defects such as formation of short V-shaped cells (green arrows), chaining cells (red arrows), cells with pole bulges (blue arrows) and kinks (yellow arrows). 100 cells were viewed per replicates.

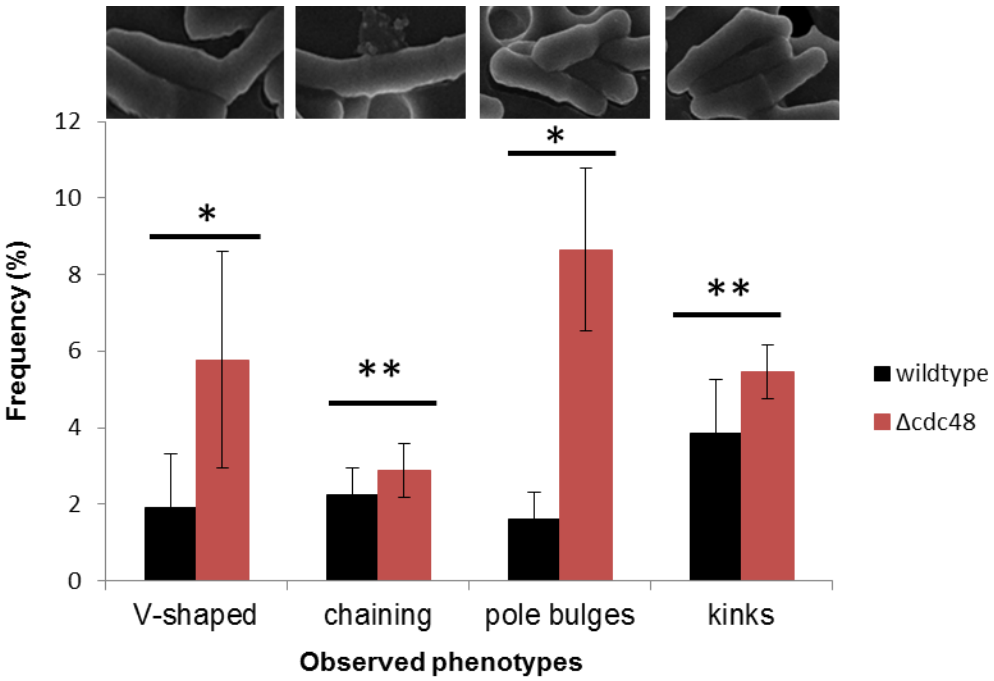


Figure 3.26: Quantification of the Δ*cdc48* morphological defects revealed by SEM in comparison to wildtype. The graph, which is representative of two experiments, shows a significant increase in the frequency of cells possessing pole bulges and V-shaped cells in the mutant strain. A notable increase in the frequency of cells with kinking phenotype was also observed. Error bars represent standard error obtained from standard deviation of the replicates. n= 156 cells were viewed per replicates, *: $p < 0.05$, **: $p > 0.05$.

In addition to SEM, fluorescent microscopy was performed to assess the role of Cdc48 in cell division by evaluating localization of new PG synthesis. This was achieved by the use of cell wall staining chemical probes as described in section 2.13.4.1 and 2.13.4.2. Staining of the cell wall *in vivo* with fluorescent D-alanine analogue that is incorporated into the PG layer by click chemistry allowed for labelling of sites of new PG synthesis. Mycobacteria grow by incorporating newly synthesized PG subunits at the cell poles and/or septum (Brown et al., 2011). Deletion of *cdc48* did not result in impaired PG synthesis as this growth pattern was retained in the Δ*cdc48* mutant and there were no differences in septal and polar staining as observed in Figure 3.27. However, the Δ*cdc48* strain seemed to have slightly reduced polar staining when compared to the wildtype and the complemented strain. These phenotypes were quantified and we observed that approximately 90 % of cells for all three strains showed polar PG localization and the remaining cells had both polar and septal localization, or had diffused staining (Figure 3.28). Notably, the Δ*cdc48* strain had some cells that were slightly shorter than those of the wildtype hence we further quantified cell length by measuring polar distance within the cells. There was no difference in cell length, with high frequency of cells falling within the range of 2.1-4 µm corresponding to the normal size of *Msm* (Figure 3.29).

In addition to PG staining, the MA layer was also stained using a DMN-Trehalose stain which is composed of trehalose attached to a solvatochromic dye. This probe fluoresces when DMN-Tre is converted to trehalose monomycolate and incorporated into the bacterial cell wall (Kamariza *et al*., 2018). DMN-Tre staining revealed formation of multiple septa in the Δ*cdc48* strain (Figure 3.30). Taken together, these phenotypes revealed that the last stages of cell division were arrested in the Δ*cdc48* mutant. Collectively, these results show that deletion of *cdc48* does not lead to PG synthesis and cell elongation impairment hence synthesis of new PG continues in the mutant strain however, the last steps of cell separation are defective.

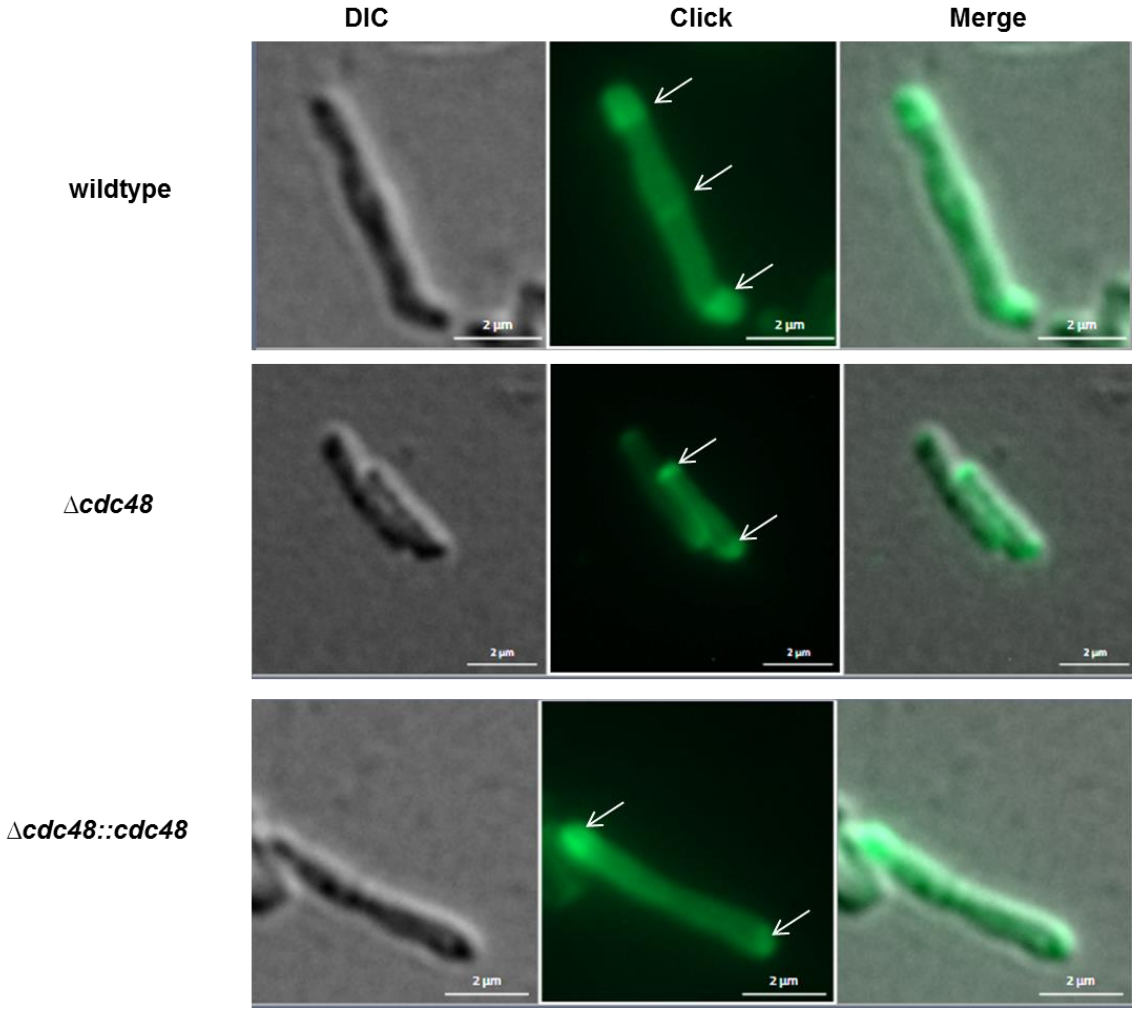


Figure 3.27: Microscopic analysis of the PG-synthesis ability of the Δ*cdc48* strain in comparison to the wildtype and Δ*cdc48::cdc48* strains. Assessment of PG synthesis was achieved by labelling of the PG with the fluorescent D-alanine analogue by click chemistry and sites of PG incorporation were visualized by fluorescent microscopy. New PG subunits localize to the poles in all three stains as shown by the fluorescent green spots at the poles. 100 cells were assessed for each experiment. The arrows indicate the sites of new PG incorporation.

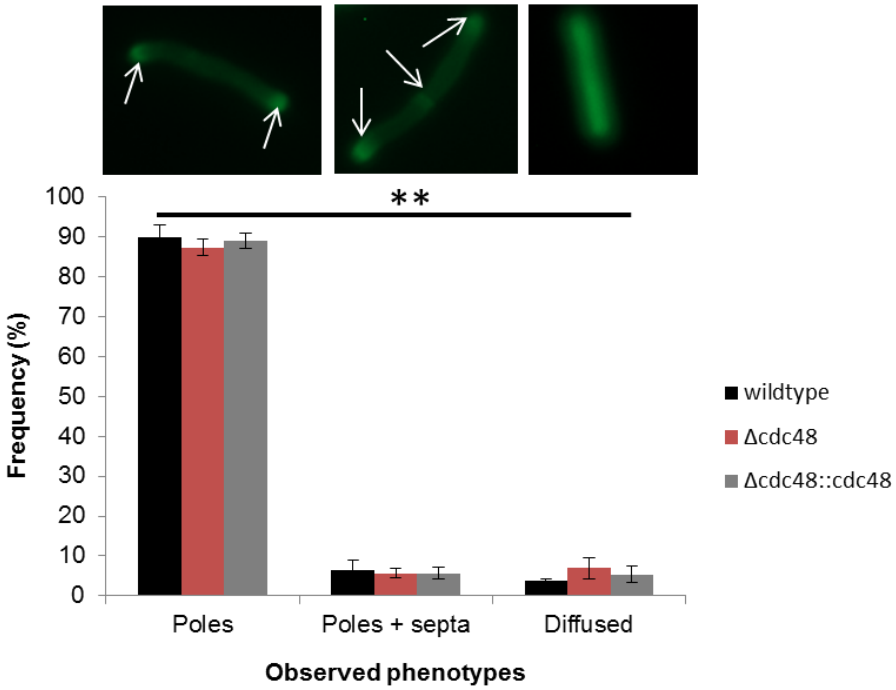


Figure 3.28: Quantification of the staining patterns revealed by microscopic analysis of the PG-synthesis ability of the Δ*cdc48* strain, the wildtype and Δ*cdc48::cdc48* strains . New PG synthesis localized to the poles in 85% of the cells. Less than 10% of the cells displayed both septal and polar PG localization, while others had a diffused staining pattern. The graph represents three independent experiments. Errors bars indicate standard error obtained from standard deviation of the triplicate experiments. n=100. **: p >0.05. The white arrows indicate the sites of new PG incorporation

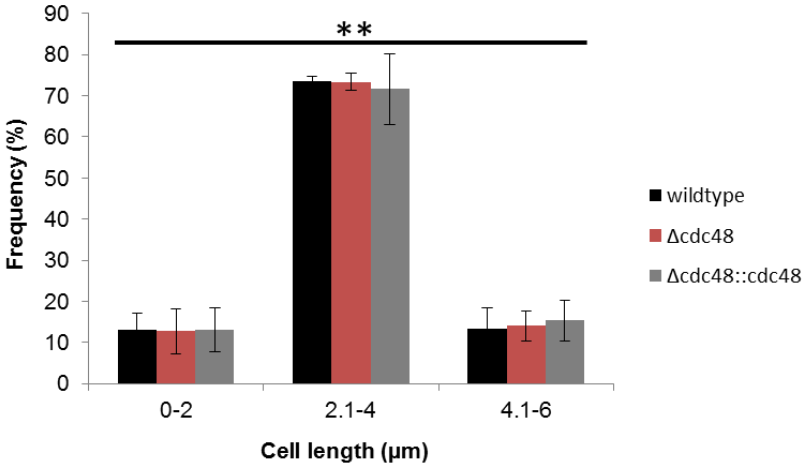


Figure 3.29: Cell length quantification in the Δ*cdc48* mutant. The size of the bacterial cells was measured from pole to pole. The graph shows change in cell length distribution observed in the wildtype, Δ*cdc48* and Δ*cdc48::cdc48* strains. In general, a large number of cells had cell sizes within the range of 2.1-4 µm. There was no significant difference in Δ*cdc48* and wildtype cells across all measured size ranges. The graph represents three independent experiments. Errors bars indicate standard error obtained from standard deviation of the triplicate experiments. n=100. **: p >0.05.

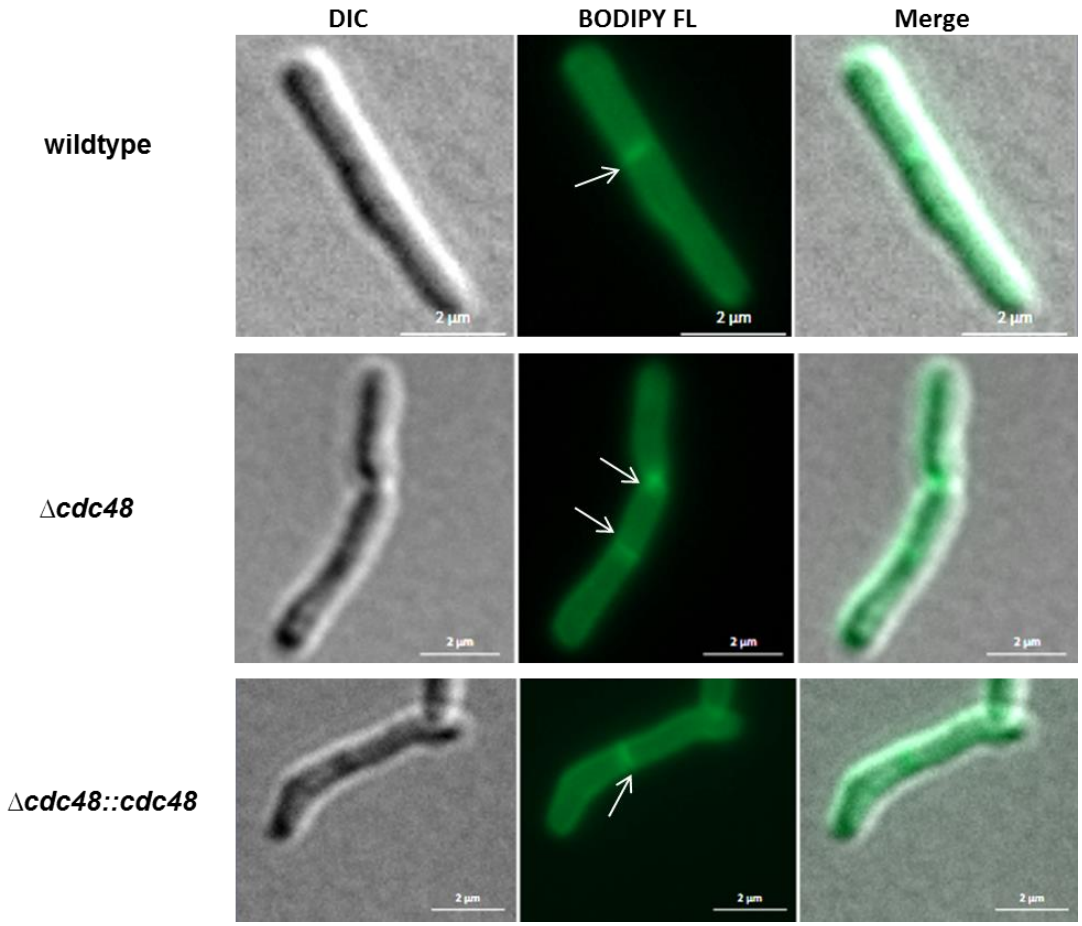


Figure 3.30: Microscopic analysis of Δ*cdc48* strain phenotypes in comparison to the wildtype and Δ*cdc48::cdc48* strains after DMN-Trehalose staining. Assessment of cell division defects was achieved by labelling of the cell wall with the DMN-trehalose stain. Fluorescent microscopy revealed formation of multiple septa in the Δ*cdc48* mutant strain compared to the single septum observed in the wildtype and Δ*cdc48::cdc48* strain. 100 cells were assessed per experiment. The arrows indicate the sites of septal formation.

3.2.5.4. Localization of FtsZ in the Δ*cdc48* mutant

Bacterial cell division is a dynamic process requiring a spatially coordinated invagination of the cell membrane and cell wall (Kumar *et al*., 2010). This process is mediated by FtsZ filaments that recruit septal PG-synthesizing enzymes to the division site (Typas *et al*., 2012). As cell wall morphology analysis in the Δ*cdc48* mutant revealed formation of cellular chains and cells with abnormal septa suggestive of cell separation arrest, we further investigated cell division using FtsZ as a division reporter. This was achieved by assessing localization of GFP-tagged derivative of FtsZ in the wildtype and mutant strains as described in section 2.14. Localization of FtsZ_GFP in the Δ*cdc48* mutant confirmed the formation of multiple septa, as indicated by the presence of multiple foci (Figure 3.31 and 3.32). This confirmed the presence of cellular chains consisting of multiple cells, separated by septal bridges. The

number of septa per bacterium was quantified and it was observed that 40 % of Δ*cdc48* cells contained at least three septa in contrast to only 2 % for wildtype as shown in Figure 3.32. The proportion of cells that had at least one septum was 99 % in the wildtype and approximately 60 % in the Δ*cdc48* mutant.

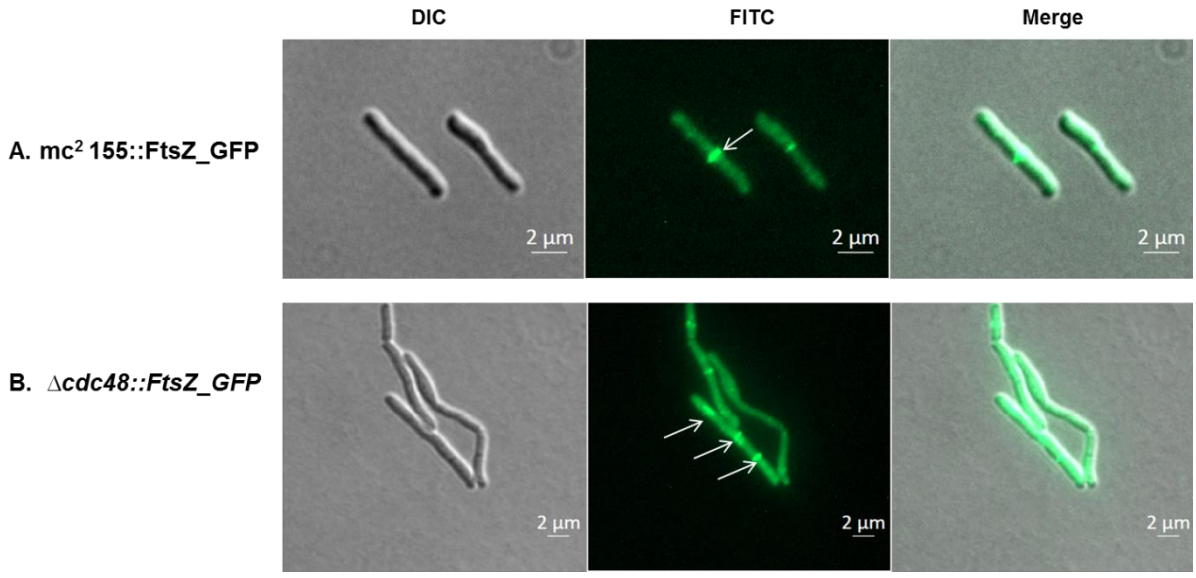


Figure 3.31: Localization of FtsZ_GFP in the Δ*cdc48* mutant in comparison to the wildtype. (A) In the wildtype mc^{2}155 strain, FtsZ_GFP localized to the division site as displayed by the formation of a single mid-cell foci (white arrow). (B) FtsZ_GFP displayed a punctate localization pattern in the mutant strain (white arrows). 100 cells were assessed per experiment.

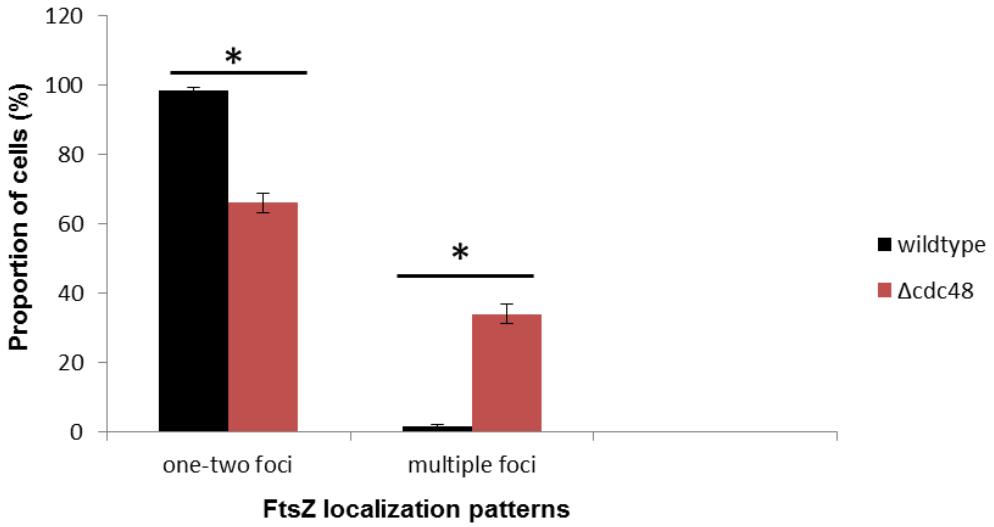


Figure 3.32: Quantification of FtsZ_GFP *in vivo* localization patterns. The graph shows that 99 % and 60% of cells displayed FtsZ_GFP mid-cell localization in the wildtype and mutant strains, respectively. In the Δ*cdc48* mutant, 40 % of cells exhibited punctate FtsZ_GFP localization pattern as shown by formation of multiple foci. n=100 Error bars represent standard error obtained from standard deviation. *: $p < 0.05$.

4. Discussion

TB continues to be a significant public health burden and the leading cause of death worldwide despite the availability of treatment (WHO, 2015). The alarming rise of drug resistance has compromised the efficacy of current anti-TB therapies. In addition, the intrinsic resistance of mycobacteria to most antimicrobial agents has further given rise to challenges in TB treatment. This intrinsic resistance is attributed to the impermeable nature of the mycobacterial cell wall, which provides a barrier to toxic substances and limits the diffusion of drugs into the cell (Brennan and Nikaido, 1995). Considering this, there is an urgent need for new and highly effective therapeutics. In this context, the mycobacterial cell wall has been identified as a potential drug target for development of anti-TB drugs, particularly the PG layer. The coordination of PG remodelling is crucial for bacterial growth and division, as well as maintenance of structural integrity, disruption of which could result in cell death. Furthermore, disturbances in PG metabolism can lead to increased cell wall permeability due to compromised cell wall integrity, eventually giving rise to antibiotic susceptibility (Kieser *et al*., 2015a). Therefore, understanding mycobacterial cell wall biosynthesis and identifying key protein complexes that underlie cell growth and division is crucial for the development of novel anti-TB drugs.

The constant growth and division of the cell requires continuous remodelling of the PG layer to allow for a range of functions, including the insertion of newly synthesized units (Peters *et al*., 2016). This process is facilitated by multiple enzymes and tight coordination of the activity of these enzymes is required to maintain bacterial cell shape, structural integrity and cell viability (Cava *et al*., 2013). This study focuses on D,D-CPases, a set of enzymes involved in regulating the amount of PG cross-links by trimming pentapeptides in the newly synthesized PG to tetrapeptides, via removal of the terminal D-alanine (Peters *et al*., 2016). D,D-CPases are present in high protein copy number per cell, when compared to their HMM counterparts and they have been implicated in maintenance of bacterial cell shape (Nelson and Young, 2001). In *E. coli* all 7 D,D-CPases are dispensable for cell survival, with the exception of PBP5, and deletion of these enzymes does not affect cell growth or morphology (Nelson and Young, 2001). Collective studies conducted in our lab demonstrated that *Msm* encodes four D,D-CPase homologues, which during growth are expressed in varying abundance, and deletion of these enzymes resulted in no growth or morphological defects, with the exception of MSMEG_6113, which could not be deleted as it is essential for mycobacterial growth (Ealand *et al*., unpublished). Several studies have revealed the

existence of protein-protein interaction complexes that are pivotal to a number of mycobacterial cellular processes. PBPs have been proposed to act in a complex to fully exert their function in cell growth and division (Sauvage et al., 2008). To further expand our knowledge on the functional roles of the essential MSMEG_6113 and the highly expressed (in terms of transcript abundance) MSMEG_2433, additional studies were conducted to establish a foundation for investigating whether these D,D-CPases exert their functions as individual proteins or whether they form part of protein complexes in mycobacteria. These studies revealed that MSMEG_6113 and MSMEG_2433 interact with key regulators of cell division and elongation (D. Ralefeta and R. Asmal, unpublished). Considering these findings, we sought to further interrogate the role of the two D,D-CPases through protein interaction and genetic knockout studies in *Msm*.

Two previous MSc studies, by D. Ralefeta and R. Asmal, identified D,D-CPase interacting partners using either bacterial or yeast 2-hybrid systems respectively. In this study, we sought to confirm the interacting partners for MSMEG_6113 and MSMEG_2433 that were previously identified by Mr. D. Ralefeta using full length clones. The roles of MSMEG_6113 and MSMEG_2433 in mycobacterial physiology were further investigated by confirming interaction between the two D,D-CPases and their identified putative partnering proteins as well as characterizing these partners. Confirmation of these interacting partners was achieved by the use of M-PFC assay. Whilst numerous partners were confirmed, only four partners (two for each) were taken forward due to time constrains. In addition, only a subset of MSMEG_6113 partners were further characterized through gene knockout studies as MSMEG_6113 is considered to be essential.

Interaction of MSMEG_6113 and MSMEG_2433 with HMM PBPs

HMM PBPs participate in PG synthesis through glycosyltransferase activities and transpeptidase activities and they have been shown to play a role in cell elongation and septation (Ghosh et al., 2008). In this study, we report that the transpeptidase domain of *Msm* D,D-CPases is responsible for mediating interaction between D,D-CPases and HMM PBPs. Our data suggest that FtsI, a class B PBP and PonA1, a class A PBP, bind to the PG hydrolase domain of MSMEG_6113 and MSMEG_2433 respectively. These individual interactions form complexes, possibly involved in PG synthesis and hydrolysis during cell growth and division. In *E. coli*, a PG synthase PBP1B has been shown to interact with a lytic transglycosylase MltA and structural protein MipA, providing evidence that PG-synthesizing

and hydrolyzing complexes assemble to facilitate PG elongation and mid-cell septation (Vollmer *et al*., 1999). Multiple interactions between PG remodelling enzymes with different functions have also been identified in mycobacteria (Hett *et al*., 2008; Hett *et al*., 2010).

FtsI, is one of the essential septasomal components for cell division in mycobacteria and related organisms (Weiss et al., 1999; Wissel *et al*., 2004; Datta *et al*., 2006). The essentiality of this gene for mycobacterial viability was demonstrated in this study where generation of *ftsI* deletion mutant by allelic exchange was not possible, confirming that the gene is essential for *in vitro* growth. Consistent with these results is the observation that *Mtb ftsI* counterpart is essential for growth as determined by transposon mutagenesis (Sassetti *et al*., 2003). In *E. coli*, localization of FtsI to the division site is seen at later stages of cell growth and throughout septation (Weiss *et al*., 1999). Moreover, its localization to the division site is dependent on FtsZ and other intervening Fts proteins suggesting that FtsI is recruited to the septal ring through a cascade of protein-protein interactions involved in divisome assembly (Buddelmeijer and Beckwith, 2002; Wissel *et al*., 2004). A multiprotein interaction complex containing FtsI-FtsW-FtsZ has been identified in mycobacteria and this complex is proposed to regulate the initiation of septation (Datta *et al*, 2006). Interaction between the C-tail of FtsW and FtsZ strengthens FtsW and FtsI interaction, providing a link between septal PG biosynthesis and cell division (Datta *et al*., 2006). FtsI has also been demonstrated to associate with Wag31 (the polar anchor protein) during transitioning of the division septum to the pole (Mukherjee *et al*., 2009). Herein we demonstrate a novel interaction between MSMGE_6113 and FtsI in *Msm*. This interaction suggests that MSMEG_6113 may be involved in regulating septal PG hydrolysis during the process of cytokinesis, considering that FtsI is involved in initiation of septation.

PonA1 is a major determinant of polar growth in mycobacteria and the rate of polar growth is modulated by phosphorylation (Kieser *et al*., 2015a). In *Msm*, PonA1 predominantly localizes to the cell poles where it promotes PG expansion and localizes occasionally at the septum during cell division (Hett *et al*., 2010; Kieser *et al*., 2015a). PonA1 is involved in regulation of a number of cellular processes in mycobacteria including spatial establishment of the new pole growth and maintenance of cell shape and length, both of which are required for normal mycobacterial growth and are critical during *Mtb* infection (Kieser *et al*., 2015a). Depletion of *ponA1* in mycobacteria results in growth defects and formation of cells with morphological abnormalities (Hett *et al*., 2010, Kieser *et al*., 2015a), suggesting that PonA1 is important for maintaining cell wall synthesis. In addition, alteration in PonA1 activity results in changes in

antibiotic susceptibility in both *Msm* and *Mtb* (Kieser *et al*., 2015a). Similar to FtsI, PonA1 has also been found to form protein interaction complexes. For instance, it interacts with the essential PG hydrolase RipA, where it modulates the activity of RipA during cytokinesis (Hett *et al*., 2010). In another study it was reported to associate with L,D-transpeptidase LdtB in *Mtb*, suggesting that PBPs work together with transpeptidases to synthesize new PG during growth (Kieser *et al*., 2015b). The identified interaction between PonA1 and MSMEG_2433 in this study indicates that MSMEG_2433 may be recruited to the poles by PonA1 following organization of a new pole, where MSMEG_2433 is involved in PG hydrolysis during elongation.

Interaction of MSMEG_6113 and MSMEG_2433 with AAA+ protein family

Members of the AAA+ protein family are commonly referred to as AAA+ proteases and are prevalent in all taxa (Alhuwaider and Dougan, 2017). This family of proteases use common structural and operational mechanisms to perform diverse biological functions in the cell, including protein quality control, proteolysis, protein and nucleic acid translocation, membrane fusion, DNA replication and recombination, transcription regulation, biogenesis of organelles and remodelling of macromolecular complexes (Neuwald *et al*., 1999; Ogura and Wilkinson, 2001; Erzberger and Berger, 2006). The molecular mechanisms of these proteins and how they function in mycobacteria are still at the early stages of discovery. Recent work has highlighted the significance of AAA proteases in the physiology of mycobacteria and several mycobacterial AAA proteases have been biochemically characterized, including the essential zinc metalloprotease FtsH (Anilkumar *et al*., 2004; Srinivasan *et al*., 2006), the proteasome ATPase Rv2115c (Darwin *et al*., 2005), the essential casein lytic protein (Clp) proteases ClpC1 and ClpX (Schmitz and Sauer, 2014) and Msm0858/Cdc48 (Unciuleac *et al*., 2016). In this study, we focus on *Msm* FtsH and Cdc48.

The role of FtsH is poorly understood in mycobacteria, nevertheless, based on *E. coli* FtsH mutant strain complementation experiments, it appears that mycobacterial FtsH shares overlapping substrate specificity with *E. coli* FtsH, as it can recognize heterologous substrates such as heat shock transcription factor σ^{32}, SecY proteins and the phage λ CII repressor protein (Anilkumar *et al*., 2004; Srinivasan *et al*., 2006). Amino acid sequence alignment demonstrated that *Msm* FtsH shares conserved regions with that of *E. coli* as the two share 48.4 % identity at the amino acid sequence level. Based on these observations, FtsH is proposed to play a role in quality control mechanisms in mycobacteria, enabling regulation of

protein complex activities by controlling the availability of specific integral and cytoplasmic proteins and/or their degradation rate (Anilkumar *et al*., 2004; Srinivasan *et al*., 2006). In *B. subtilis*, GFP tagged derivative of FtsH displays mid-cell localization in dividing vegetative cells (Wehrl *et al*., 2000) suggesting a possible role for this protease in septal biogenesis. In addition to septal localization, Anilkumar and colleagues demonstrated that in *E. coli*, the cell division protein FtsZ is subjected to degradation by FtsH *in vitro*, pointing to an additional role for FtsH as a negative regulator of FtsZ (Anilkumar *et al*. 2001). This is further substantiated by the observed reduced intracellular levels of FtsZ in *Mtb* FtsH-overexpressing strain (Kiran *et al*., 2009). In *Mtb*, expression levels of FtsH are upregulated upon exposure to reactive nitrogen and oxygen intermediates, as well as growth in macrophages (Kiran *et al*., 2009). In addition, a FtsH overexpression strain displays growth defects and reduced viability *ex vivo* and *in vitro*, pointing to the fact that FtsH plays a crucial role in stress response pathways and cell survival (Kiran *et al*., 2009). Considering that MSMEG_2433 interacts with FtsH in *Msm*, it is possible that the former is involved in septal PG hydrolysis where its activity is regulated by FtsH, which in turn interacts with FtsZ and could directly regulate the levels of FtsZ by its proteolytic activity. We propose that a MSMEG_2433-FtsH-FtsZ complex regulates initiation of septation in mycobacteria. However, our explanations in this regard are speculative and require further investigation.

The cell division protein Cdc48 is relatively uncharacterized in prokaryotic cells. It belongs to the same family of proteins as FtsH, which is involved in a number of cellular processes in mycobacteria including regulation of FtsZ. One of the key functions of Cdc48 is to maintain protein homeostasis via a network of protein quality control processes (Meyer *et al*., 2012). Cdc48 shares conserved motifs with FtsH but it is unclear whether this protein retains a proteolytic mechanism to facilitate similar cellular processes as FtsH. However, there is a possibility that Cdc48 could directly play a role in regulating FtsZ levels or indirectly influence FtsZ levels by degrading other proteins that stabilize FtsZ. Herein we demonstrate interaction between MSMEG_6113 and Cdc48 and propose that MSMEG_6113 is involved in cellular pathways that mediate the correct septal placement during cell division through interaction with Cdc48. Given that Cdc48 is not well characterized in bacteria, we investigated its role in the physiology of mycobacteria through gene knockout studies and our results support our hypothesis of a possible MSMEG_6113-Cdc48-FtsZ complex, which links PG synthesis and cell division. As with FtsI, this hypothesis requires further investigation.

Deletion of *cdc48* from the genome of *Msm* resulted in no significant defects in cell survival and bacterial growth kinetics, confirming that this gene is not essential for mycobacterial growth and survival *in vitro*. These results are supported by previous findings from a high density mutagenesis screen that demonstrated that the *Mtb* homologue of *cdc48* was non-essential for growth *in vitro* (Sassetti *et al*., 2003; Griffin *et al*., 2011). However, the enhanced sensitivity to amoxicillin, D-cycloserine and vancomycin as well as a probable increase in cell wall permeability that prevails when Cdc48 is deleted, suggests a possible role for Cdc48 in maintaining cell wall integrity. Cdc48 possibly maintains the integrity of the cell wall by regulating the amount and/or the activity of MSMEG_6113. In the absence of Cdc48, the transpeptidase activity of MSMEG_6113 may be dysregulated, resulting in a decrease in cross-links formation due to the unavailability of the tetrapeptide substrate required by HMM PBPs and/or L,D- transpeptidases. This could lead to a weakened cell wall with increased permeability to antibiotics. In mycobacteria, loss of endopeptidase activity of RipA and RipC results in increased susceptibility to lysozyme (Mavrici *et al*., 2014, Martinelli and Pavelka, 2016). In addition, deletion of RipA and RipB causes enhanced sensitivity to erythromycin, rifampicin and vancomycin (Mavrici *et al*., 2014, Martinelli and Pavelka, 2016). Kieser and colleagues (2015b) demonstrated that the inactivation of LdtMt2 and PonA2 causes enhanced sensitivity to teicoplanin and meropenem, while PonA1 deletion increases sensitivity to ethambutol. Our study and these previous findings indicate that disruption of cell wall integrity increases cell wall permeability and also results in enhanced antibiotic sensitivity. Figure 4.1 illustrates the proposed model for Cdc48 function in mycobacteria.

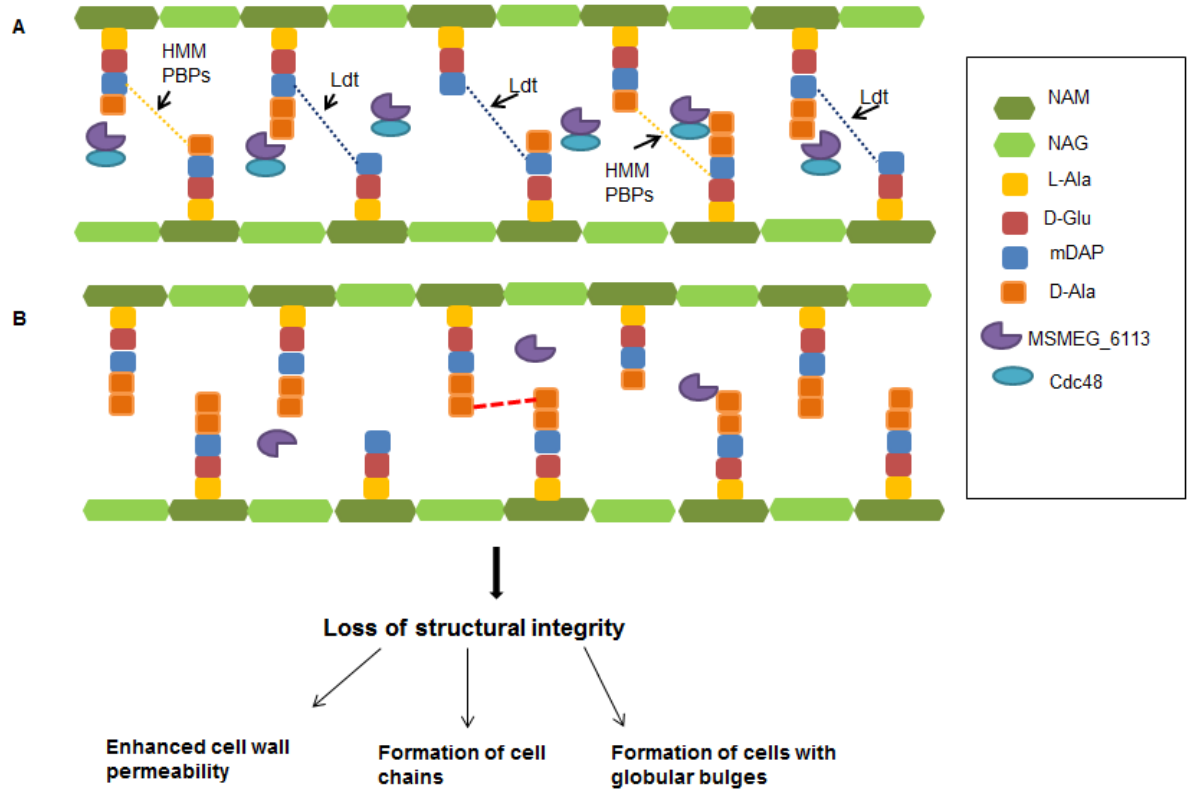


Figure 4.1: Proposed model of Cdc48 function in mycobacterial physiology: Cdc48 forms a protein complex with MSMEG_6113, a D,D-CPase involved in PG hydrolysis. (A) When Cdc48 is present, it regulates the activity and/or amount of MSMEG_6113 which functions to modulate the degree of PG cross-links by trimming pentapeptides in the newly synthesized PG to tetrapeptides. The generated tetrapeptides are then used as substrates for formation of 3-3 and 3-4 cross-links by Ldts and HMM PBPs respectively, resulting in a thick, rigid PG layer. (B) When the Cdc48-MSMEG_6113 complex is disrupted by deletion/inactivation of Cdc48, the hydrolase activity of MSMEG_6113 gets dysregulated, resulting in accumulation of pentapeptides which might form inappropriate (red line) cross-links or an overall decrease in PG cross-links due to the absence of the substrate. This then causes the PG layer to lose its structural and morphological integrity, giving rise to the defects observed. This explanation is largely speculative and requires further validation. Figure drawn by student.

Microscopic analyses of the Δ*cdc48* deletion strain revealed the presence of morphological defects such as cells with globular bulges, multiple septa and formation of chains suggesting that Cdc48 is required for proper coordination of cell separation. Localization of new PG synthesis revealed no defects in PG synthesis as the Δ*cdc48* deletion strain retained polar and/or septal PG localization patterns. However, the last stages of cell division were arrested, particularly cell separation. In the PBP5 mutant, formation of cells with chains (similar to Δ*cdc48* phenotype) was observed and this phenotype was thought to be due to an increase in pentapeptide side-chain levels, which caused formation of inappropriate inter-strand peptide cross-links (Nelson and Young, 2001). The production of cells with globular bulges in the

Δ*cdc48* deletion strain phenocopies the morphology of PonA1 depleted strain. This morphological defect is characteristic of dysregulated and/or increased PG hydrolytic activity, causing loss of structural integrity. Bulbous regions in the PonA1 depleted strain is indicative of increased cell wall hydrolysis and loss of morphological and structural integrity (Hett *et al*., 2010). Recent findings demonstrated that the absence of non-classical transpeptidases, which catalyse the predominant 3-3 cross-links in PG, LdtA and LdtB, leads to production of short bulging cells (Schoonmaker *et al*., 2014). RipA requires proteolytic cleavage for its full catalytic activity to degrade septal PG and separate daughter cells (Ruggiero *et al*., 2010; Chao *et al*., 2013). In mycobacteria, this hydrolase has been shown to be activated through interaction with RpfB (Hett et al., 2008) and more recently, Botella and colleagues demonstrated that the periplasmic protease MarP, activates RipA during acid stress (Botella *et al*., 2017). Based on our interaction work and the observed phenotypes, we propose that Cdc48 is involved in PG hydrolysis where it regulates the activity of MSMEG_6113 and possibly other hydrolases involved in septal PG degradation to facilitate cell separation. Given that the role of Cdc48 in cell division has not been elucidated, our explanations in this regard require further validations.

To further investigate division defects in our mutants, we assessed localization of GFP tagged derivative of FtsZ in *Msm*. Polymerization of FtsZ into a ring-like structure initiates septation. The FtsZ ring functions as a scaffold for downstream septal PG remodelling enzymes and it produces the energy required for constriction of the membrane during cell division (Hett *et al*., 2008). The observation of multiple FtsZ rings in the Δ*cdc48* deletion strain indicates failure to coordinate cell division. Formation of multiple FtsZ rings in this strain could results from FtsZ misplacement or dysregulated FtsZ levels due to the absence of putative FtsZ regulator proposed in this study, Cdc48. These results support the Cdc48-Ftsz protein complex proposed earlier herein, where Cdc48 regulates FtsZ levels directly or indirectly by degrading FtsZ stabilizing proteins. However, further analysis of these results is needed to validate the presence of the proposed complex in coordinating mycobacterial cell growth and division, as well as elucidating the mechanism by which Cdc48 regulates FtsZ.

5. Conclusion and future studies

5.1. Conclusion

Careful coordination of cell wall remodelling is critical for mycobacterial growth and division. Collectively, this MSc demonstrates the presence of protein-protein interaction complexes containing PG synthases and hydrolases, as well as proteases, which function together to facilitate both growth and division. Our results confirm that D,D-CPases exert their function through interaction with other proteins in the cell and are required for maintaining cell wall integrity. This is the first study to identify Cdc48 as part of the regulatory mechanism that controls mycobacterial growth and division. This was evidenced by lack of coordinated cell division and dysregulated cell wall integrity in the absence of this protein. Our study highlights that identification and disruption of key protein complexes could present a mechanism to block cell growth and thus identify possible drug targets that can be exploited for the development of new TB drugs.

5.2. Future Studies

Future work will entail interrogation of the functional roles of the remaining D,D-CPase interacting partners through gene knockout/knockdown studies. Co-localization of the identified partners would also be useful do elucidate the mechanisms by which these proteins function together to coordinate crucial cellular processes. As our results revealed the existence of MSMEG_6113 and Cdc48 protein complex, and a possible role of Cdc48 in regulating the activity of MSMEG_6113 during PG hydrolysis, assessment of the behaviour of MSMEG_6113 in the absence of Cdc48 would provide further support for the putative role of Cdc48 in division regulation.

6. Appendices

Appendix A – Media and Solutions

Table A1. Media and supplements

Media / Supplement	Components
Luria- Bertani Agar (LA)	5 g yeast extract, 10 g tryptone, 10 g NaCl and 1.5 g agar dissolved in 1L sdH_2O.
Luria- Bertani Broth (LB)	5 g yeast extract, 10 g tryptone and 10 g NaCl dissolved in 1L sdH_2O.
2xTY	10 g yeast extract, 16 g tryptone and 10 g NaCl dissolved in 1L sdH_2O.
Middlebrook 7H9	4.7 g Difco Middlebrook 7H9 powder and 2ml glycerol dissolved in 986 ml sdH_2O. Autoclave. 10 ml 100 X glucose salts and 2 ml Tween80.
Middlebrook 7H10	19 g Difco Middlebrook 7H10 powder and 5ml glycerol dissolved in 985 ml sdH_2O. Autoclave. 10 ml 100 X glucose salts.
Glucose salts (100X)	20 g glucose and 8.5 g NaCl dissolved in 100 ml sdH_2O.
Tween80 (25%)	10 ml Tween80 dissolved in 40 ml sdH_2O.
Sucrose (75%)	75 g sucrose dissolved in 100 ml sdH_2O
X-gal (2)%	1 g X- gal dissolved in 50 ml deionized DMF

Table A2. Solutions used for *E. coli* plasmid DNA extractions

Solution	Composition
Solution I	50 mM glucose, 25 mM Tris- HCl (pH 8) and 10 mM EDTA dissolved in sdH_2O. Autoclave.
Solution II	1% SDS and 0.2 M NaOH dissolved in sdH_2O.
Solution III	3 M Potassium acetate and 11.5% acetic acid dissolved in sdH_2O.

Table A3. Solutions used for *Msm* DNA extractions

Solutions	Composition
TE buffer	10 mM Tris- HCl (pH 8) and 10 mM EDTA dissolved in sdH_2O. Autoclave.
CTAB/NaCl	4.1**%** NaCl and 10% N – acetyl- N, N, N – trimethyl ammonium bromide dissolved in sdH_2O. Filter sterilize.

Table A.4 Solutions used for DNA precipitation

Solution	Composition
Chloroform: Isoamyl alcohol	24 ml chloroform and 1ml isoamyl alcohol.
Sodium Acetate	3 M sodium acetate dissolved in sdH_2O (pH5.2). Autoclave.

Table A5. Solutions used for DNA electrophoresis

Solution	Composition
TAE	50 X stock solution: 242 g Tris base 57.1 ml glacial acetic and 100 ml EDTA (pH 8) made up to 1L with sdH_2O.
Ethidium Bromide	10 mg/ml dissolved in sdH_2O.

Table A6. Agarose gel recipes

Gel percentage	Amount of agarose (g) in 50 ml TAE
0.8	0.4
1	0.5
2	1

Table A7. Solutions used for preparation of *E. coli* competent cells

Solution	Composition
TfbI	30 mM potassium acetate, 100 mM rubidium chloride, 10 mM calcium chloride, 50 mM manganese chloride and 15% v/v glycerol made up in sdH_2O. Adjusted to pH 5.8 with acetic acid.
TfbII	10 mM rubidium chloride, 75 mM calcium chloride, 10 mM MOPS and 15% v/v glycerol made up in sdH_2O. Adjusted to pH 6.5 with diluted NAOH.

Table A8. Southern blot solutions

Solution	Composition
Denaturation solution	1.5 M NaCl and 0.5 M NaOH dissolved in sdH_2O.
Depurination solution	0.25 M HCl dissolved in sdH_2O.
TBE (1X)	100 ml 10 X Tris-Borate-EDTA (Sigma) dissolved in 900 ml sdH_2O.
SSC (20X)	0.3 M Sodium citrate and 3 M NaCl dissolved in sdH_2O.
SDS (10%)	10 g SDS powder dissolved in 100 ml sdH_2O.
Solution 1	0.1% SDS and 2 X SSC dissolved in sdH_2O.
Solution 2	0.1% SDS and 0.5 X SSC dissolved in sdH_2O.
Maleic Acid Buffer	1.5 M NaCl and 1 M Maleic acid dissolved in sdH_2O. Adjusted to pH 7.5 with NaOH pellets.
Wash buffer	0.1 M Maleic Acid Buffer and 0.3% Tween20.
Blocking solution (Roche)	1 X blocking solutions dissolved in Maleic Acid Butter.
Detection buffer	0.1 M NaCl and 0.1 M Tris-HCl dissolved in sdH_2O (pH 9.5)
Antibody solution (Roche)	Dilute 1: 10000 in blocking solution.
CSPD (Roche)	Disodium 3-(4-methoxysoiro {1, 2-dioxetane-3, 2'-(5'-chloro) tricycle [$3.3.1.1^{3,7}$] decan}-4-yl)phenyl phosphate.
Stripping solution	0.2 M NaOH and 0.1% SDS dissolved in sdH_2O.

Appendix B: Primers

Table B1: Primers used for generation of full length partners for M-PFC assay

Primer pair	Primer sequence	Restriction site
MSMEG_2433_F	CGCGCGGAATTCATGTGGAGGTACGCCTTCGGG	*Eco*RI
MSMEG_2433_R	GCGCGCAAGCTTTCAGAGCGCCCCGATGCTCGC	*Hind*III
MSMEG_6900_F	CGCGCGCAGCTGATGCCGCCCGACGACCGGTTG	*Pvu*II
MSMEG_6900_R	GCGCGCAAGCTTTCACGGAGGCGGCGGGGCTCC	*Hind*III
MSMEG_4227_F	CGCGCGCTGCAGATGAACAAGGGTTCGCGGGAC	*Pst*I
MSMEG_4227_R	GCGCGCAAGCTTTCATGACGCCTTCTTCCGTGC	*Hind*III
MSMEG_0031_F	CGCGCGGGATCCATGAACACCTCACTGCGCCGG	*Bam*HI
MSMEG_0031_R	GCGCGCAAGCTTTCATGAACCCTCCCGCAGCGC	*Hind*III
MSMEG_6105_F	CGCGCGGGATCCATGAACCGGAAAAATGTTATC	*Bam*HI
MSMEG_6105_R	GCGCGCAAGCTTTCAGCCGTGCGGGTTCGACCG	*Hind*III
MSMEG_6113_F	CGCGCGGAATTCATGAGCGATAGGCTGACGCGC	*Eco*RI
MSMEG_6113_R	GCGCGCAAGCTTTCATGCGCCGCATCCGCAGCT	*Hind*III
MSMEG_4233_F	CGCGCGGGATCCATGAGCCGGCGGGGCGACCGT	*Bam*HI
MSMEG_4233_R	GCGCGCAAGCTTTCAGGTGGCCTGCAATGTCAA	*Hind*III
MSMEG_0858_F	CGCGCGCAGCTGGGAAGGTGACATGTCGCAGGG	*Pvu*II
MSMEG_0858_R	GCGCGCAAGCTTTCGTCGAGGGTCAACGCTTCT	*Hind*III
MSMEG_5637_F	CGCGCGCTGCAGATGTACAGCATGCGCAGGTCG	*Pst*I
MSMEG_5637_R	GCGCGCAAGCTTTCATCTGGTGAACGTCCCCGT	*Hind*III
MSMEG_0365_F	CGCGCGCAGCTGATGCCGGGTTCGATCTTTGAG	*Pvu*II
MSMEG_0365_R	GCGCGC AAGCTTTCATCTCACCGGCACCCGCGG	*Hind*III
MSMEG_6112_F	CGCGCGCTGCAGATGAGCCGGCCCACCATGACC	*Pst*I
MSMEG_6112_R	GCGCGCAAGCTTTCACAGCACGCGATCGATCCA	*Hind*III

*The underlined region indicates the restriction site used for cloning.

Table B2: Primers used for domain truncation

Primer pair	Primer sequence	Restriction site
MSMEG_2433SP_F	CGCGCGCAGCTGATGTGGAGGTACGCCTTCGGG	*Pvu*II

MSMEG_2433SP_R	GCGCGCAAGCTTCGCGCGGGCGACGGGCACTGC	*Hind*III
MSMEG_2433TP_F	CGCGCGCAGCTGGGTCGGATCGGTGGCCCCGCC	*Pvu*II
MSMEG_2433TP_R	GCGCGCAAGCTTGCCGTACATCATCGCGATCAC	*Hind*III
MSMEG_2433CT_F	CGCGCGCAGCTGCTGGTGAAAGAGGGCGGGCCG	*Pvu*II
MSMEG_2433CT_R	GCGCGCAAGCTTTCAGAGCGCCCCGATGCTCGC	*Hind*III
MSMEG_6113SP_F	CGCGCGCAGCTGATGAGCGATAGGCTGACGCGC	*Pvu*II
MSMEG_6113SP_R	GCGCGCAAGCTTCGCGGCGGCGACGACGGCGAC	*Hind*III
MSMEG_6113LR_F	CGCGCGCAGCTGGCCCTGTTCACCGGCAAACAC	*Pvu*II
MSMEG_6113LR_R	GCGCGCAAGCTTGTGGGCTGTGTGCGCCCACCG	*Hind*III
MSMEG_6113TP_F	CGCGCGGAATTCCACCGTGGAATCGCGGCGGTC	*Eco*RI
MSMEG_6113TP_R	GCGCGCAAGCTTTCATGCGCCGCATCCGCAGCT	*Hind*III

*The underlined region indicates the restriction site used for cloning.

Table B3: Primers used for amplification of genes for mutant generation

Primer pair	**Primer sequence**	**Restriction site**
MSMEG_0858US_F	GTGGGTACCTCCAGCATTCCCCCGATG	*Acc*65I
MSMEG_0858US_R	GTGAGATCTCAGCGCGGAGGTGTTCAG	*Bgl*II
MSMEG_0858DS_F	GTGAGATCTGTCACGGCCGCCGACGTC	*Bgl*II
MSMEG_0858DS_R	GTGAAGCTTTGGGCAGAACCGTGTTGG	*Hind*III
MSMEG_4233US_F	GTGAAGCTTGGCGCACCGGCGGCCATC	*Hind*III
MSMEG_4233US_R	GTGAGATCTCACGCGGGTACGCCGGGT	*Bgl*II
MSMEG_4233DS_F	GTGAGATCTGCGCCGTTGTTCCACGAG	*Bgl*II
MSMEG_4233DS_R	GTGGGTACC CCTTTACCCGCGATCAGC	*Acc*65I

*The underlined region indicates the restriction site used for cloning.

Table B4: Primers used for amplification of genes for mutant complementation

Primer pair	**Primer sequence**	**Restriction site**
MSMEG_0858cmp_F	GCGCGCGATATCCATCGTGATCATGGTCATCAT	*Eco*RV
MSMEG_0858cmp_R	GCGCGCGATATCCTAACGCTTCTCGGCGAACTC	*Eco*RV
MSMEG_4233cmp_F	GCGCGCGATATCCCGTTGGCGACGCCACAGGCG	*Eco*RV
MSMEG_4233cmp_R	GCGCGCGATATCTCAGGTGGCCTGCAATGTCAA	*Eco*RV

*The underlined region indicates the restriction site used for cloning.

Table B5: Primers used for confirmation of site specific integration of complementing vector

Primer pair	Primer sequence	Restriction site
*att*BS2 *att*L4	ACAGGATTTGAACCTGCGGC AATTCTTGCAGACCCCTGGA	None
*att*BS1 *att*L1	ACGTGGCGGTCCCTACCG CTTGGATCCTCCCGCTGCGC	None

Appendix C: Figures

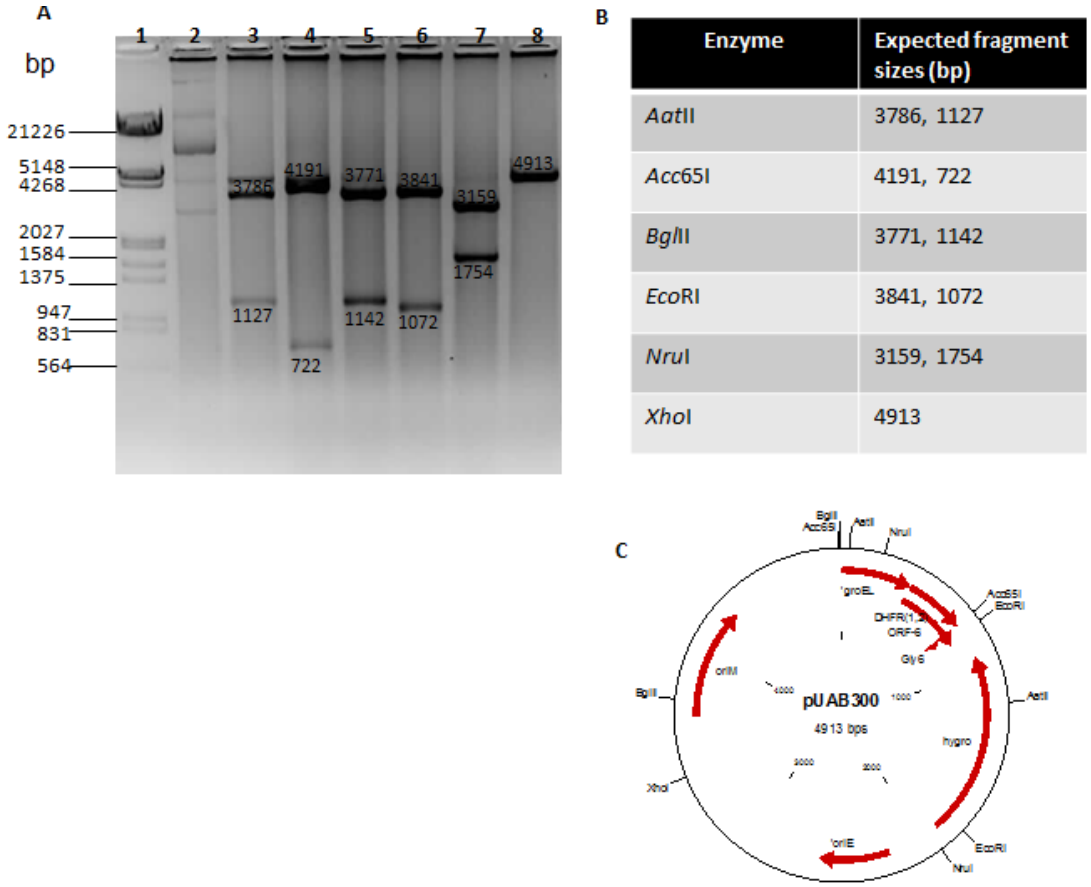
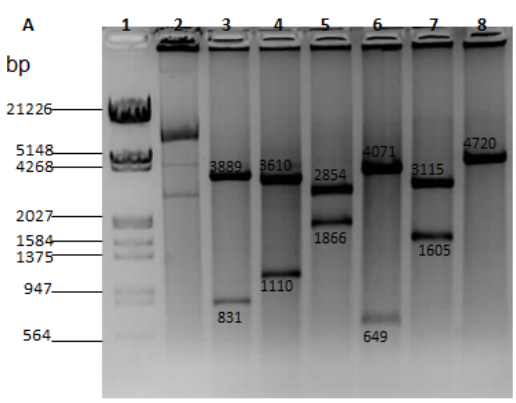


Figure C1: Restriction profile of pUAB300. (A) 0.8% agarose gel indicating expected DNA band sizes, lane (1) DNA marker III (Fermentas), lane (2) uncut vector control, lane (3) *Aat*II, lane (4) *Acc*65I, lane(5) *Bgl*II, lane (6) *Eco*RI, lane (7) *Nru*I, lane (8) *Xho*I. (B) Table showing restriction enzymes used for profiling and the expected fragment sizes. (C) Plasmid map of pUAB300 vector.



B

Enzyme	Expected fragment sizes (bp)
*Nru*I	3889, 831
*Nsp*I	3610, 1110
*Pst*I	2854, 1866
*Pvu*I	4071, 649
*Sma*I	3115, 1605
*Xho*I	4720

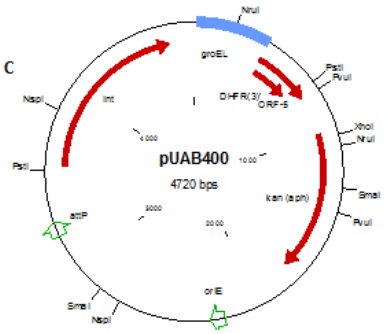
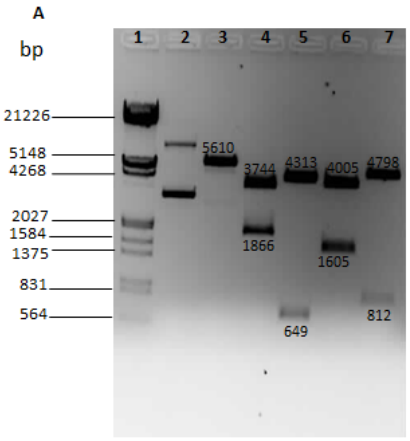


Figure C2: Restriction profile of pUAB400. (A) 0.8% agarose gel indicating expected DNA band sizes, lane (1) DNA marker III (Fermentas), lane (2) uncut vector control, lane (3) *Nru*I, lane (4) *Nsp*I, lane (5) *Pst*I, lane (6) *Pvu*I, lane (7) *Sma*I, lane (8) *Xho*I. (B) Table showing restriction enzymes used for profiling and the expected fragment sizes. (C) Plasmid map of pUAB400 vector.



B

enzyme	Expected fragment sizes (bp)
*Hind*III	5610
*Pst*I	3744,1866
*Pvu*I	4313, 649
*Sma*I	4005, 1605
*Xho*I	4798, 812

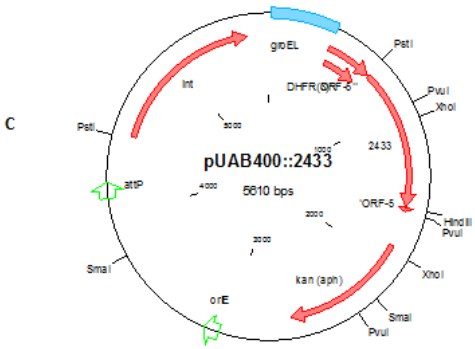


Figure C3: Restriction profile of pUAB400::2433. (A) 0.8% agarose gel indicating expected DNA band sizes, lane (1) DNA marker III (Fermentas), lane (2) uncut construct control, lane (3) *Hind*III, lane (4) *Pst*I, lane (5) *Pvu*I, lane (6) *Sma*I, lane (7) *Xho*I. (B) Table showing restriction enzymes used for profiling and the expected fragment sizes. (C) Plasmid map of the final pUAB400::2433 construct used for transformation.

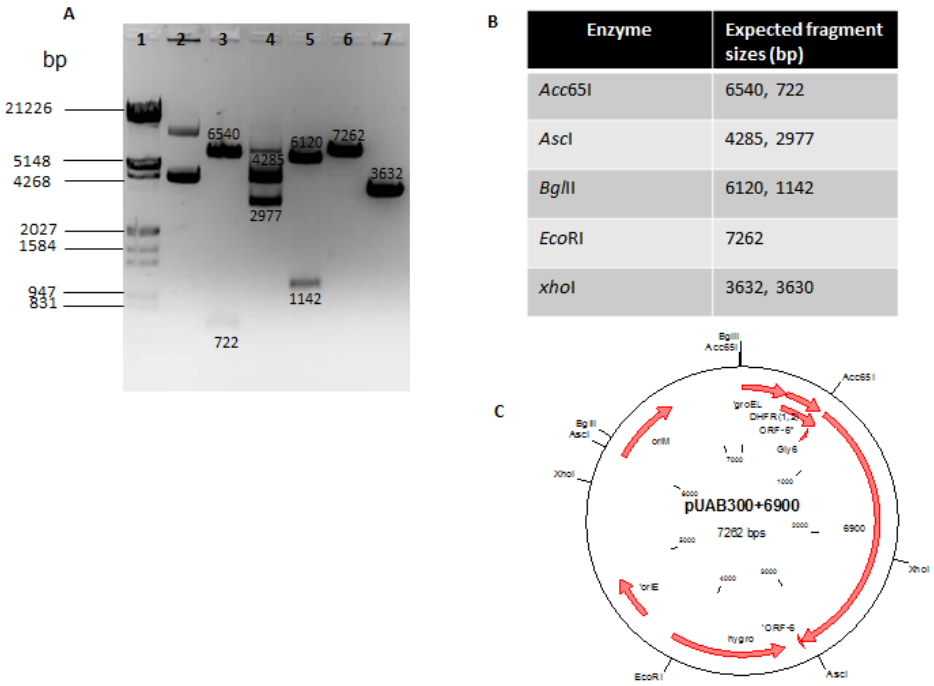


Figure C4: Restriction profile of pUAB300::6900. (A) 0.8% agarose gel indicating expected DNA band sizes, lane (1) DNA marker III (Fermentas), lane (2) uncut construct control, lane (3) *Acc*65I, lane (4) *Asc*I, lane (5) *Bgl*II, lane (6) *Eco*RI, lane (7) *Xho*I. (B) Table showing restriction enzymes used for profiling and the expected fragment sizes. (C) Plasmid map of the final pUAB300::6900 construct used for transformation.

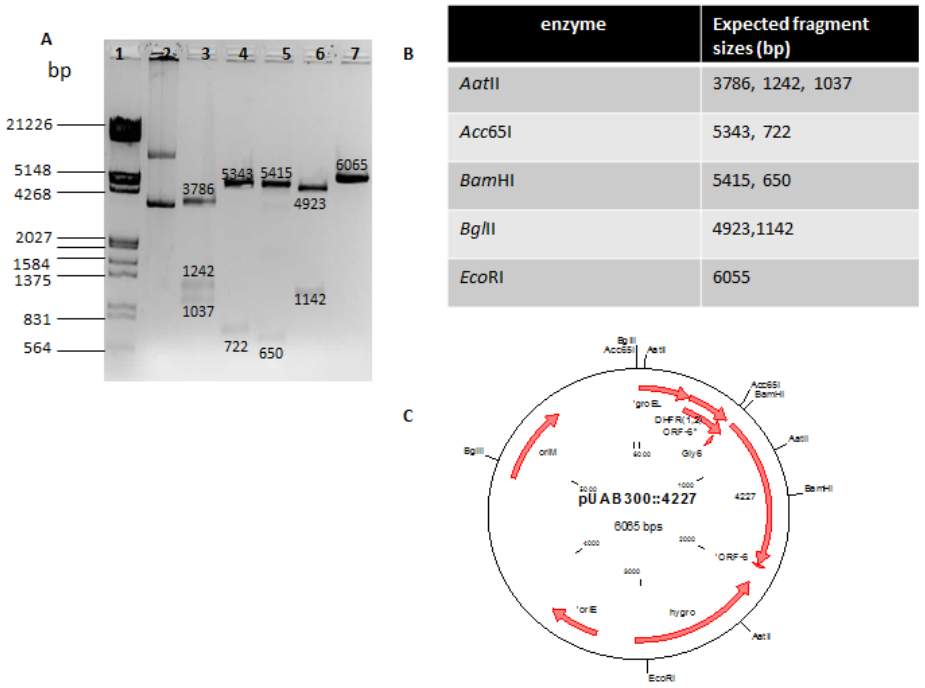
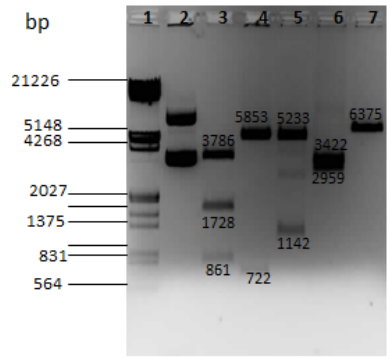


Figure C5: Restriction profile of pUAB300::4227. (A) 0.8% agarose gel indicating expected DNA band sizes, lane (1) DNA marker III (Fermentas), lane (2) uncut construct control, lane (3) *Aat*II, lane (4) *Acc*65I, lane (5) *Bam*HI, lane (6) *Bgl*II, lane (7) *Eco*RI. (B) Table showing restriction enzymes used for profiling and the expected fragment sizes. (C) Plasmid map of the final pUAB300::4227 construct used for transformation.

A



B

enzyme	Expected fragment sizes (bp)
*Aat*II	3786, 1728, 861
*Acc*65I	5853, 722
*Bgl*II	5233, 1142
*Bsp*HI	3422, 2959
*Eco*RI	6375

C

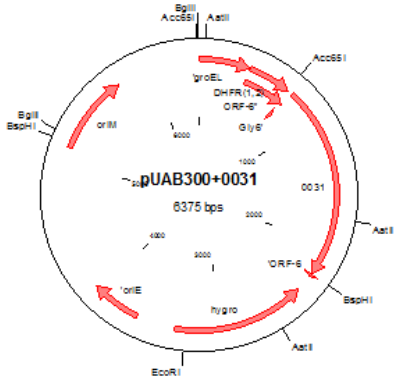
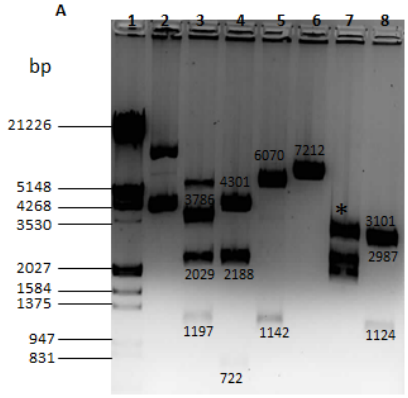


Figure C6: Restriction profile of pUAB300::0031. (A) 0.8% agarose gel indicating expected DNA band sizes, lane (1) DNA marker III (Fermentas), lane (2) uncut construct control, lane (3) *Aat*II, lane (4) *Acc*65I, lane (5) *Bgl*II, lane (6) *Bsp*HI, lane (7*) Eco*RI. (B) Table showing restriction enzymes used for profiling and the expected fragment sizes. (C) Plasmid map of the final pUAB300::0031 construct used for transformation.

A



B

enzyme	Expected fragment sizes (bps)
AatII	3786, 2029, 1197
Acc65I	4301, 2188, 722
BglII	6070, 1142
EcoRI	7212
NotI	4696, 2216
SmaI	3101, 2987, 1124

C

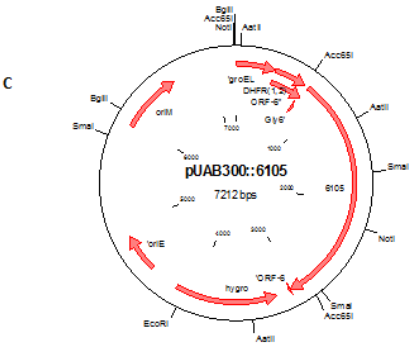


Figure C7: Restriction profile of pUAB300::6105. (A) 0.8% agarose gel indicating expected DNA band sizes, lane (1) DNA marker III (Fermentas), lane (2) uncut construct control, lane (3) *Aat*II, lane (4) *Acc*65I, lane (5) *Bgl*II, lane (6) *Eco*RI, lane (7) *Not*I, lane (8) *Sma*I. (B) Table showing restriction enzymes used for profiling and the expected fragment sizes. (C) Plasmid map of the final pUAB300::6105 construct used for transformation. *Not*I digest yielded aberrant bands shown by * in figure A lane 7.

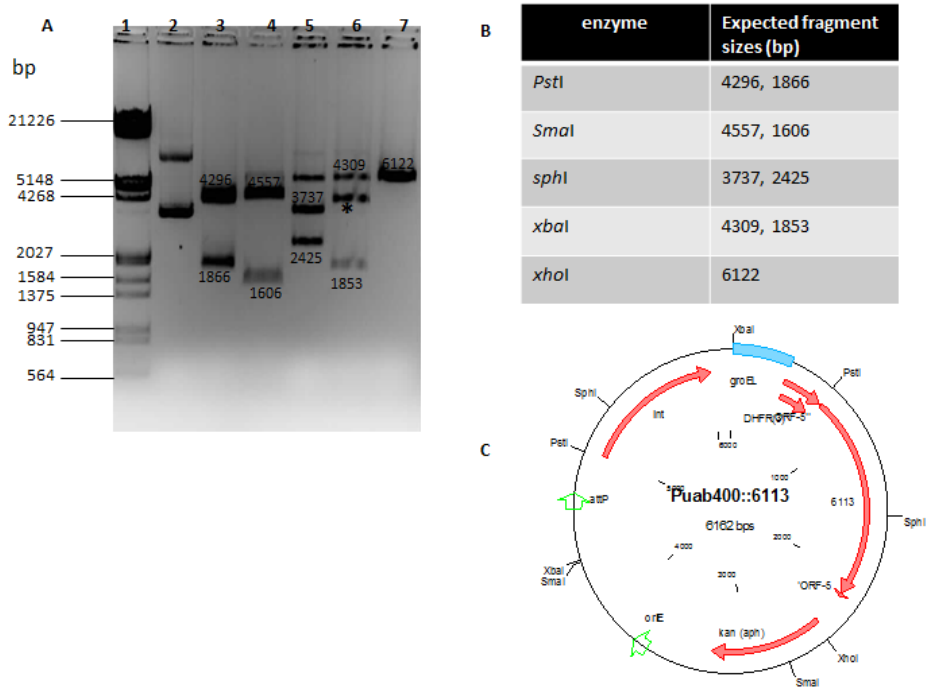


Figure C8: Restriction profile of pUAB400::6113. (A) 0.8% agarose gel indicating expected DNA band sizes, lane (1) DNA marker III (Fermentas), lane (2) uncut construct control, lane (3) *Pst*I, lane (4) *Sma*I, lane (5) *Sph*I, lane (6) *Xba*I, lane (7) *Xho*I. (B) Table showing restriction enzymes used for profiling and the expected fragment sizes. (C) Plasmid map of the final pUAB400::6113 construct used for transformation. *Sph*I digest yielded an extra band due to the enzyme star activity.

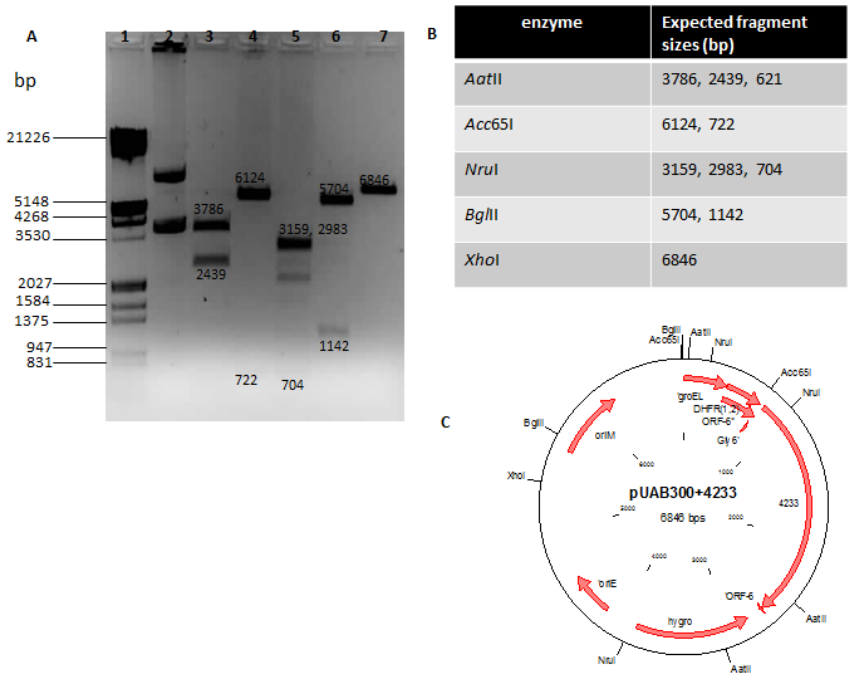
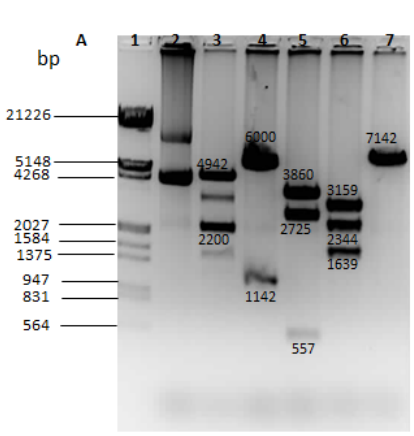


Figure C9: Restriction profile of pUAB300::4233. (A) 0.8% agarose gel indicating expected DNA band sizes, lane (1) DNA marker III (Fermentas), lane (2) uncut construct control, lane (3) *Aat*II, lane (4) *Acc*65I, lane(5) *Nru*I, lane (6) *Bgl*II, lane (7) *Xho*I. (B) Table showing restriction enzymes used for profiling and the expectedfragment sizes. (C) Plasmid map of the final pUAB300::4233 construct used for transformation. A partial digest by *Nru*I was observed in lane 5 as indicated by additional light bands.



B

Enzyme	Expected fragment sizes (bp)
*Bam*HI	4942, 2200
*Bgl*II	6000, 1142
*Eco*RI	3860, 2725, 557
*Nru*I	3159, 2344, 1639
*Xba*I	7142

C

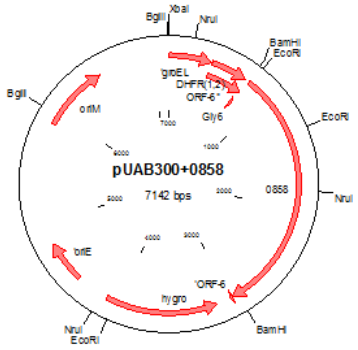
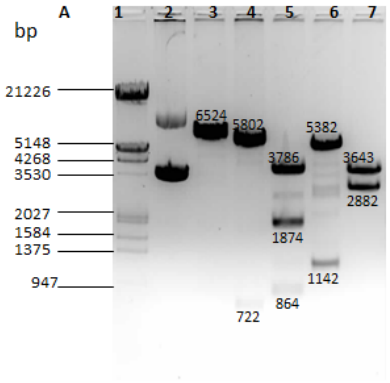


Figure C10: Restriction profile of pUAB300::0858. (A) 0.8% agarose gel indicating expected DNA band sizes, lane (1) DNA marker III (Fermentas), lane (2) uncut construct control, lane (3) *Bam*HI, lane (4) *Bgl*II, lane (5) *Eco*RI, lane (6) NruI, lane (7) *Xba*I. (B) Table showing restriction enzymes used for profiling and the expected fragment sizes. (C) Plasmid map of the final pUAB300::0858 construct used for transformation.



B

enzyme	Expected fragment sizes (bps)
EcoRI	6524
Acc65I	5802, 722
AatII	3786, 1874, 864
BglII	5382, 1142
xhoI	3643, 2882

C

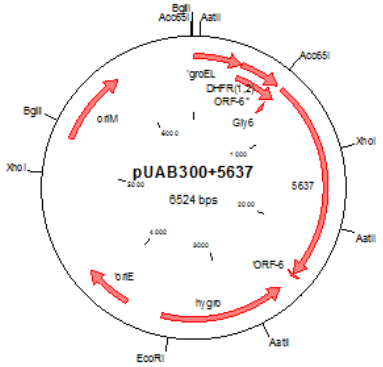
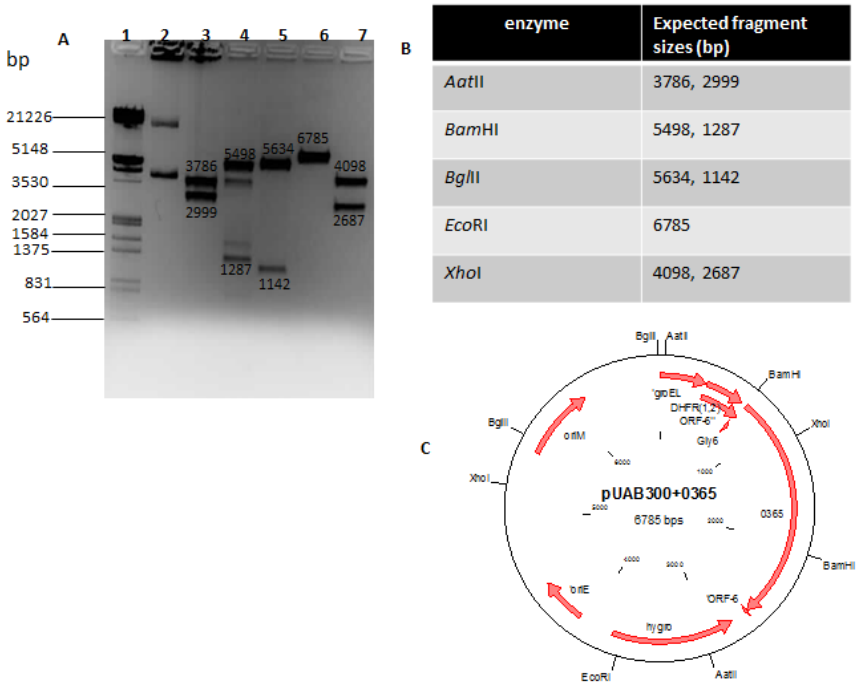
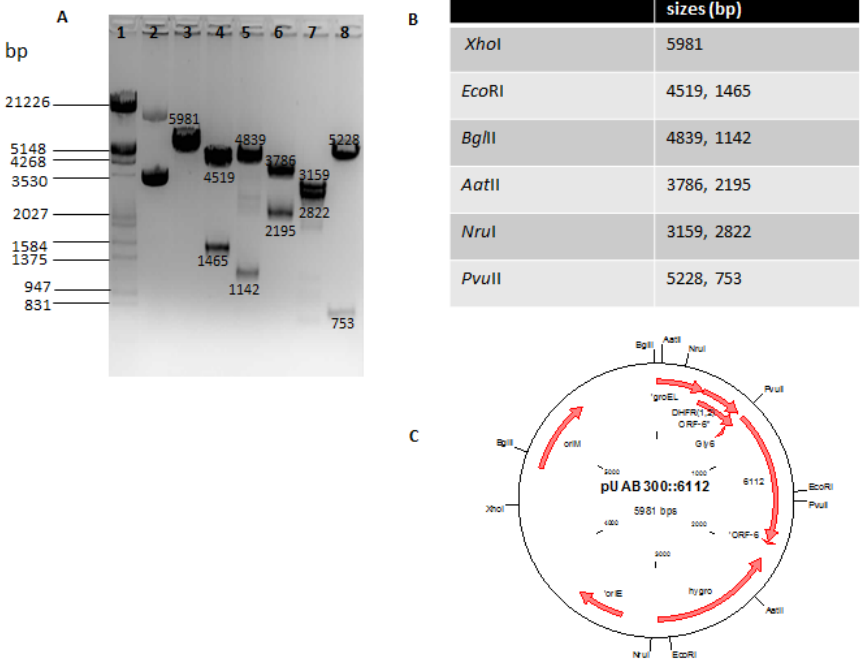


Figure C11: Restriction profile of pUAB300::5637. (A) 0.8% agarose gel indicating expected DNA band sizes, lane (1) DNA marker III (Fermentas), lane (2) uncut construct control, lane (3) *Eco*RI, lane (4) *Acc*65I, lane(5) *Aat*II, lane (6) *Bgl*II, lane (7*) Xho*I. (B) Table showing restriction enzymes used for profiling and the expected fragment sizes. (C) Plasmid map of the final pUAB300::5637 construct used for transformation. Additional light bands in lanes 5 and 6 are most likely the result of partial digests.



enzyme	Expected fragment sizes (bp)
*Aat*II	3786, 2999
*Bam*HI	5498, 1287
*Bgl*II	5634, 1142
*Eco*RI	6785
*Xho*I	4098, 2687

Figure C12: Restriction profile of pUAB300::0365. (A) 0.8% agarose gel indicating expected DNA band sizes, lane (1) DNA marker III (Fermentas), lane (2) uncut construct control, lane (3) *Aat*II, lane (4) *Bam*HI, lane(5) *Bgl*II, lane (6) *Eco*RI, lane (7) *Xho*I. (B) Table showing restriction enzymes used for profiling and the expected fragment sizes. (C) Plasmid map of the final pUAB300::0365 construct used for transformation. Additional light bands in lane 4 are most likely the result of partial digests.



enzyme	Expected fragment sizes (bp)
*Xho*I	5981
*Eco*RI	4519, 1465
*Bgl*II	4839, 1142
*Aat*II	3786, 2195
*Nru*I	3159, 2822
*Pvu*II	5228, 753

Figure C13: Restriction profile of pUAB300::6112. (A) 0.8% agarose gel indicating expected DNA band sizes, lane (1) DNA marker III (Fermentas), lane (2) uncut construct control, lane (3) *Xho*I, lane (4) *Eco*RI, lane(5) *Bgl*II, lane (6) *Aat*II, lane (7) *Nru*I, lane (8) *Pvu*II. (B) Table showing restriction enzymes used for profiling and the expected fragment sizes. (C) Plasmid map of the final pUAB300::6112 construct used for transformation. Additional light bands in lanes 5 and 7 are most likely the result of partial digests.

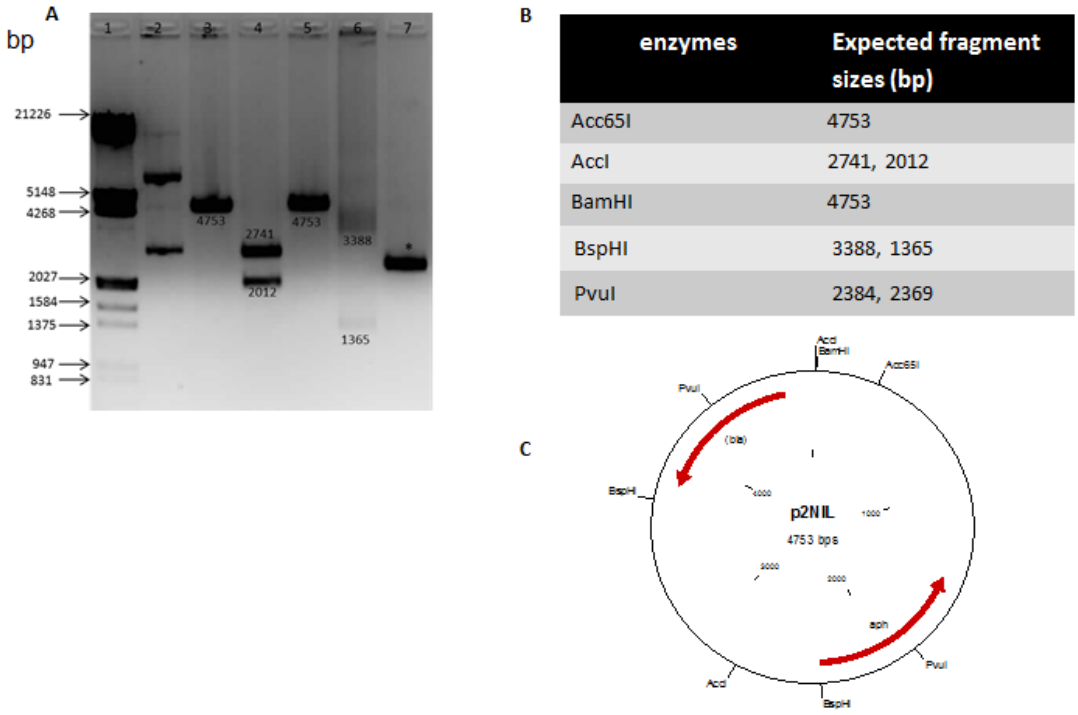


Figure C14: Restriction profile of p2NIL. (A) 0.8% agarose gel indicating expected DNA band sizes, lane (1) DNA marker III (Fermentas), lane (2) uncut vector control, lane (3) *Acc*65I, lane (4) *Acc*I, lane(5) *Bam*HI, lane (6) *Bsp*HI, lane (7) *Pvu*I. (B) Table showing restriction enzymes used for profiling and the expected fragment sizes. (C) Plasmid map of the p2NIL vector.

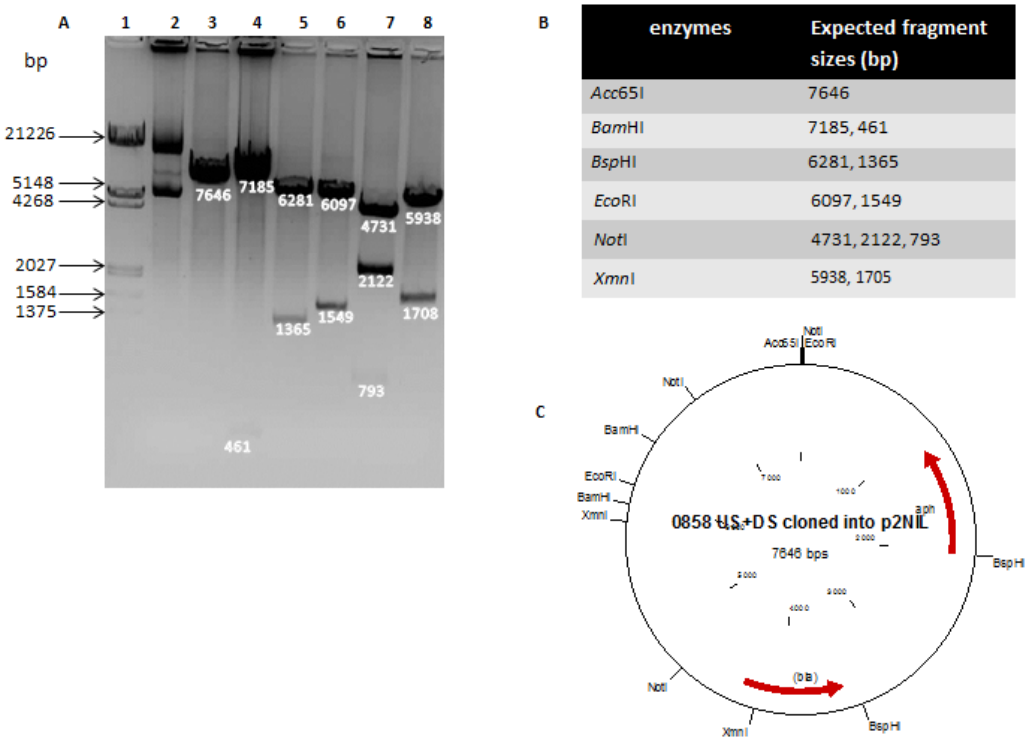
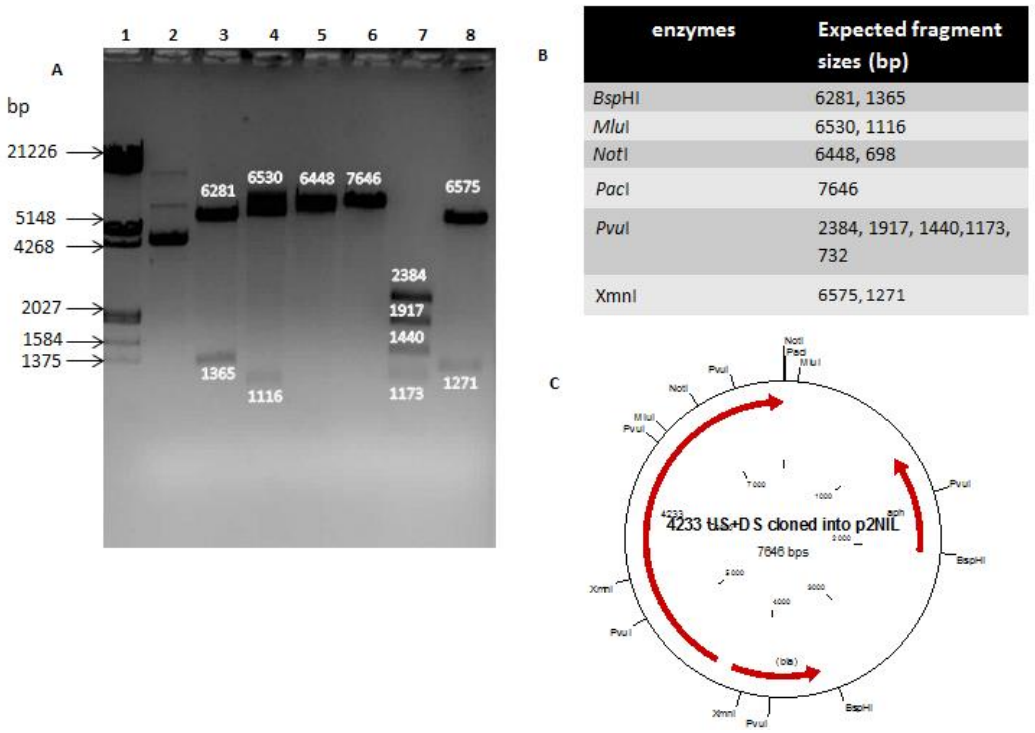
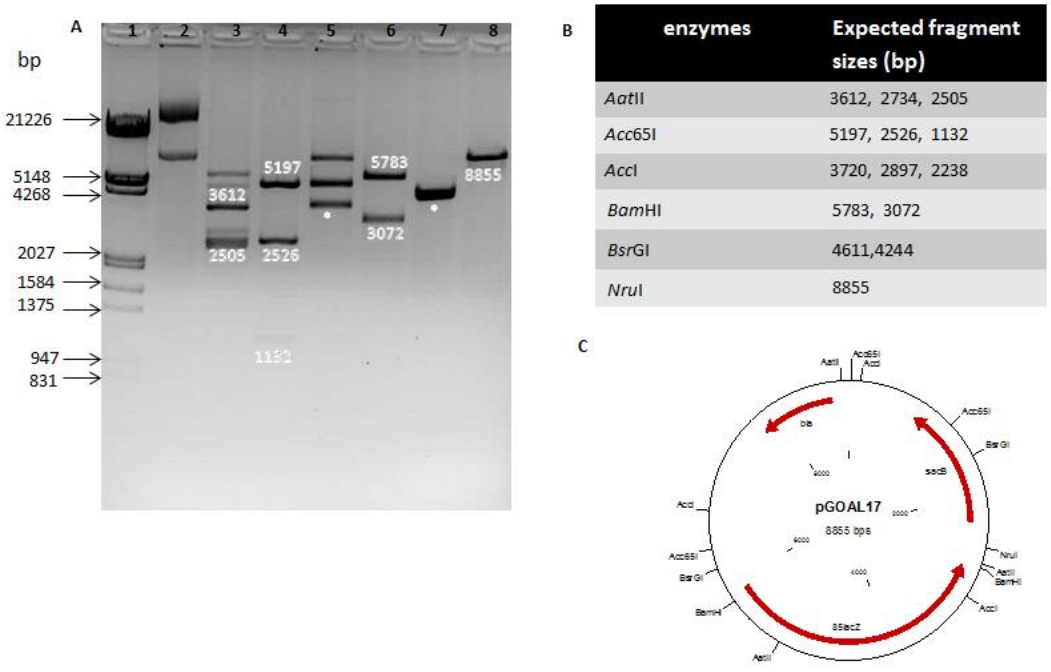


Figure C15: Restriction profile of p2NIL*cdc48*. (A) 0.8% agarose gel indicating expected DNA band sizes, lane (1) DNA marker III (Fermentas), lane (2) uncut vector control, lane (3) *Acc*65I, lane (4) *Bam*HI, lane(5) *Bsp*HI, lane (6) *Eco*RI, lane (7) *Not*I, lane (8) *Xmn*I. (B) Table showing restriction enzymes used for profiling and the expected fragment sizes. (C) Plasmid map of the final p2NIL*cdc48* construct used for transformation.



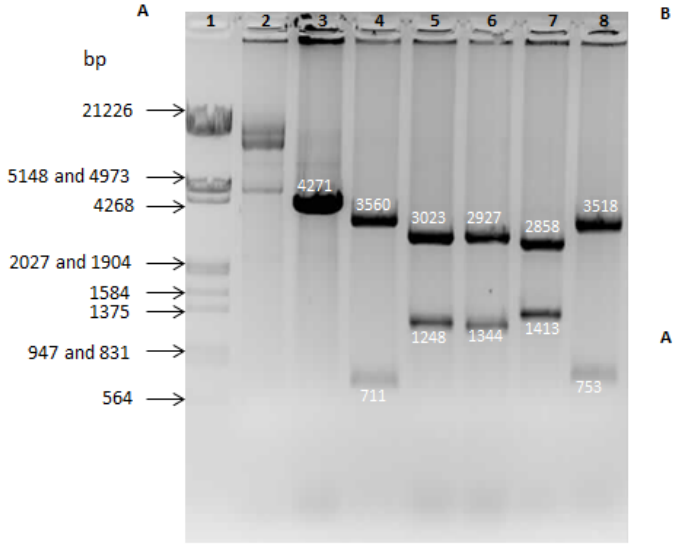
enzymes	Expected fragment sizes (bp)
*Bsp*HI	6281, 1365
*Mlu*I	6530, 1116
*Not*I	6448, 698
*Pac*I	7646
*Pvu*I	2384, 1917, 1440,1173, 732
XmnI	6575, 1271

Figure C16: Restriction profile of p2NIL*ftsI*. (A) 0.8% agarose gel indicating expected DNA band sizes, lane (1) DNA marker III (Fermentas), lane (2) uncut vector control, lane (3) *Bsp*HI, lane (4) *Mlu*I, lane(5) *Not*I, lane (6) *Pac*I, lane (7) *Pvu*I, lane (8) *Xmn*I. (B) Table showing restriction enzymes used for profiling and the expected fragment sizes. (C) Plasmid map of the final p2NIL*ftsI* construct used for transformation.



enzymes	Expected fragment sizes (bp)
*Aat*II	3612, 2734, 2505
*Acc*65I	5197, 2526, 1132
*Acc*I	3720, 2897, 2238
*Bam*HI	5783, 3072
*Bsr*GI	4611,4244
*Nru*I	8855

Figure C17: Restriction profile of pGOAL17. (A) 0.8% agarose gel indicating expected DNA band sizes, lane (1) DNA marker III (Fermentas), lane (2) uncut vector control, lane (3) *Aat*II, lane (4) *Acc*65II, lane(5) *Acc*I, lane (6) *Bam*HI, lane (7) *Bsr*GI, lane (8) *Nru*I. (B) Table showing restriction enzymes used for profiling and the expected fragment sizes. (C) Plasmid map of pGOAL17 vector. * in lane 5 shows that *Acc*I digest yielded aberrant bands most likely the results of the enzyme mapping to the vector backbone and not the region of interest. * in lane 7 indicates that the two fragments run together as indicated by the bright single band.



B

enzymes	Expected fragment sizes (bp)
*Acc*65I	4271
*Bam*HI	3560, 711
*Bgl*II	3023, 1248
*Msc*I	2927, 1344
*Eco*RI	2858, 1413
*Pst*I	3518, 753

A

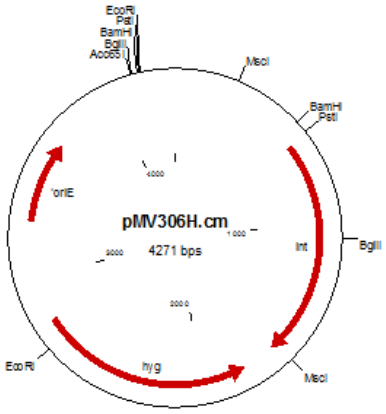


Figure C18: Restriction profile of pMV306H. (A) 0.8% agarose gel indicating expected DNA band sizes, lane (1) DNA marker III (Fermentas), lane (2) uncut vector control, lane (3) *Acc*65I, lane (4) *Bam*HI, lane(5) *Bgl*II, lane (6) *Msc*I, lane (7) *Eco*RI, lane (8) *Pst*I. (B) Table showing restriction enzymes used for profiling and the expected fragment sizes. (C) Plasmid map of pMV306H vector.

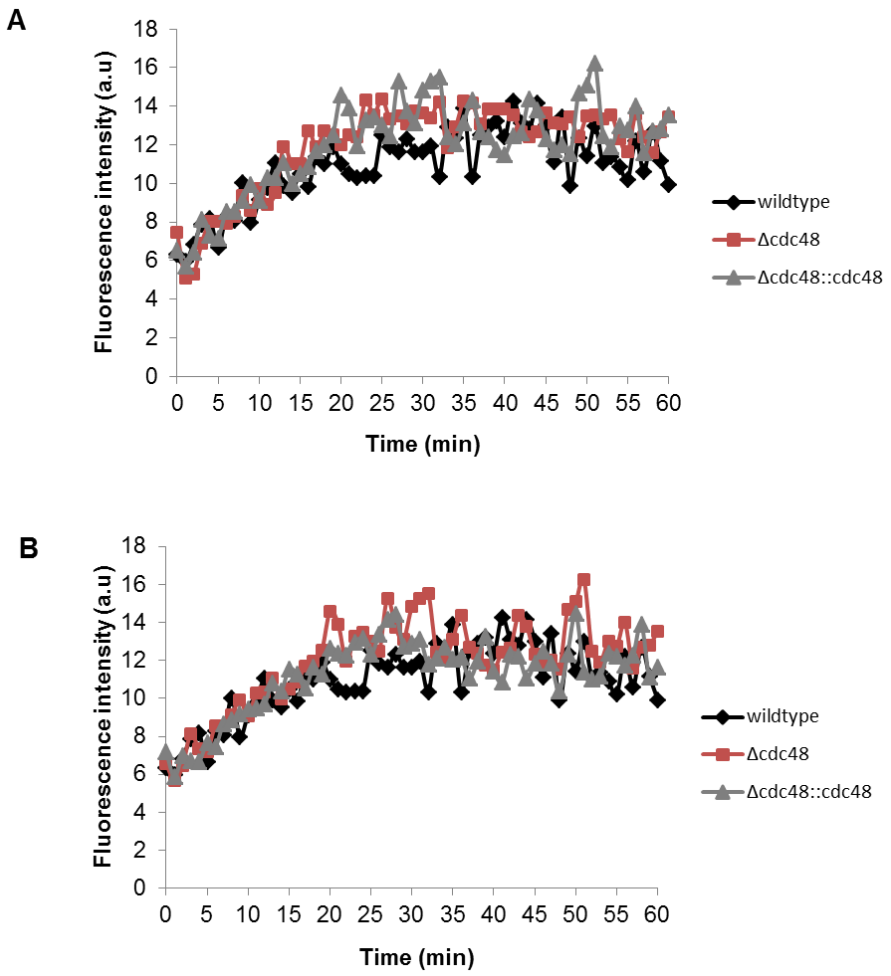


Figure C19: Δ*cdc48* cell wall permeability assessment. Cell wall permeability was monitored by quantifying accumulation of EtBr (5 µg/ml) into the cells of the Δ*cdc48* mutant strain, wildtype and complemented strains over an hour. (A) The data obtained from experiment 2. (B) The data obtained from experiment 3.

Appendix D: DNA molecular weight markers

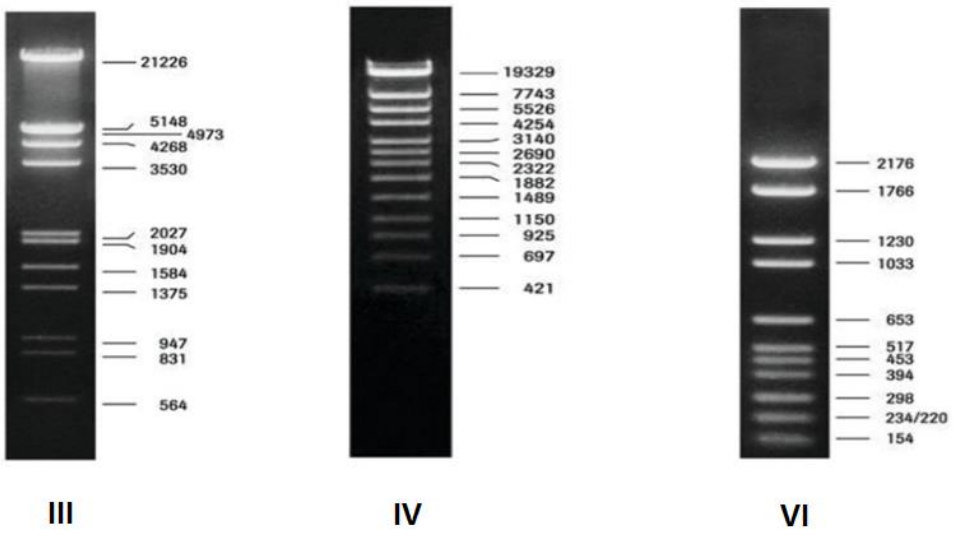


Figure D1: DNA molecular weight markers used in this study.

References

Aldridge, B.B., Fernandez-Suarez, M., Heller, D., Ambravaneswaran, V., Irimia, D., Toner, M. and Fortune, S.M. (2012) Asymmetry and aging of mycobacterial cells lead to variable growth and antibiotic susceptibility. *Science*, **335**, 100-104.

Alhuwaider, A.A.H and Dougan, D.A. (2017) AAA+ Machines of Protein Destruction in Mycobacteria. *Frontiers in Molecular Biosciences*, **4**, 49.

Andrews, J.R., Noubary, F., Walensky, R.P., Cerda, R., Losina, E. and Horsburgh, C.R. (2012) Risk of progression to active tuberculosis following reinfection with *Mycobacterium tuberculosis*. *Clinical Infectious Diseases,* **54**, 784-91.

Anilkumar, G., Srinivasan, R, Anand, S.P. and Ajitkumar, P. (2001) Bacterial cell division protein FtsZ is a specific substrate for the AAA family protease FtsH. *Microbiology*, **147**, 516-17.

Anilkumar, G., Srinivasan, R. and Ajitkumar, P. (2004) Genomic organization and in vivo characterization of proteolytic activity of FtsH of *Mycobacterium smegmatis* SN2. *Microbiology*, **150**, 2629-39.

Bansal-Mutalik, R. and Nikaido, H. (2014) Mycobacterial outer membrane is a lipid bilayer and the inner membrane is unusually rich in diacyl phosphatidylinositol dimannosides. Proceedings of the *National Academy of Science of the United States of America*, **111**, 4958-63.

Birnboim, H. C. and Doly, J. (1979) A rapid alkaline extraction procedure for screening recombinant pasmid DNA. *Nucleic Acids Research*, **17**, 1513-1523.

Boshoff, H. I. and Barry, C. E., 3RD (2006) Is the mycobacterial cell wall a hopeless drug target for latent tuberculosis? *Drug Discovery Today :Disease Mechanisms,* **3**, 237-245.

Bottela, H., Vaubourgeix, J., Lee, M.H., Song, N., Xu, W., Makinoshima, H., Glickman, M. and Ehrt, S. (2017) *Mycobacterium tuberculosis* protease MarP activates a peptidoglycan hydrolase during acid stress. *EMBO Journal*, **36** (4), 536-48.

Bouhss, A., Trunkfield, A.E., Bugg, T.D. and Mengin-Lecreulx, D. (2008) The biosynthesis of peptidoglycan lipid-linked intermediates. *FEMS Microbiology Reviews,* **32**, 208-233.

Brennan, P.J. and Nakaido, H. (1995) The envelope of mycobacteria. *Annual Review in Biochemistry*, **64**, 29-63.

Brown, P.J., Kysela, D.T. and Brun, Y.V. (2011) Polarity and diversity of growth mechanisms in bacteria. *Seminars in Cell and Developmental Biology*, **22**, 790-8.

Buddelmeijier, N. and Beckwith, J. (2002) Assembly of cell division proteins at the *E. coli* cell center. *Current Opinion in Microbiology*, **5**, 553-57.

Cava, F., Kuru, E., Brun, Y.V. and De Petro, M.A. (2013) Models of cell wall growth differentiation in rod-shaped bacteria. *Current Opinion in Microbiology*, **16**, 731-37.

Chao, M.C, Kieser, K.J., Mimani, S., Mavrici, D., Aldridge, B.B., Fortune, S.M., Alber, T. and Rubin, E.J. (2013) Protein complexes and proteolytic activation of the cell wall hydrolase RipA regulate septal resolution in mycobacteria. *PLos Pathogens*, **9**, e1003197.

Chowdhury, C. and Ghosh, A.S. (2011) Differences in active-site microarchitecture explain the dissimilar behaviours of PBP5 and 6 in *Escherichia coli*. *Journal of Molecular Graphics and Modelling*, **29**, 650-56.

Daniel, R.A., Harry, E.J. and Errington, J. (2000) Role of penicillin-binding protein PBP 2B in assembly and functioning of the division machinery of *Bacillus subtilis*. *Molecular Microbiology*, **35**, 299-311.

Datta, P., Dasgupta, A., Singh, A.K., Mukherjee, P., Kundu, M. and Basu, J. (2006) Interaction between FtsW and penicillin-binding protein 3 (PBP3) directs PBP3 to mid-cell, controls cell septation and mediates the formation of a trimeric complex involving FtsZ, FtsW and PBP3 in mycobacteria. *Molecular Microbiology*, **62**, 1655-73.

Darwin, K.H., Lin, G., Chen, Z., Li, H. and Nathan, C.F. (2005) Characterization of *Mycobacterium tuberculosis* proteasomal ATPase homologue. *Molecular Microbiology*, **55**, 561-571.

De Backer, A.I., Mortele, K.J., De Keulenaer, B.L. and Parizel, P.M. (2006) Tuberculosis: epidemiology, manifestations, and the value of medical imaging in diagnosis. *Journal of the Belgian Society of Radiology*, **89**, 243-50.

Derouaux, A., Sauvage, E. and Terrak, M. (2013) Peptidoglycan glycosyltransferase substrate mimics as templates for the design of new antibacterial drug. *Frontiers in Immunology*, **4**, 78.

Denome, S.A., Elf, P.K., Henderson, T.A., Nelson, D.E. and Young, K.D. (1999) *Escherichia coli* mutants lacking all possible combinations of eight penicillin-binding proteins: viability, characteristics, and implications for peptidoglycan synthesis. *Journal of Bacteriology*, **181**, 3981-93.

Dörr, T., Lam, H, Alwvarez, L., Cava, F., Davis, B.M. and Waldor, M.K. (2014) A novel peptidoglycan binding protein crucial for PBP1A-mediated cell wall biogenesis in *Vibrio cholerae*. *PLos Genetics*, **10**, e1004433.

Dye, C. (2006) Global epidemiology of tuberculosis. *Lancet*, **367**, 938-940.

Egan, A.J. and Vollmer, W. (2013) The physiology of bacterial cell division. *Annals of the New York Academy of Sciences*, **1277**, 8-28.

Ealand, C.S., Asmal, R. and Kana, B.D. (unpublished) An essential DD-carboxypeptidase determines localization of peptidoglycan synthesis in mycobacteria.

Erzberger, J.P. and Berger, J.M. (2006) Evolutionary relationships and structural mechanisms of AAA+ proteins. *Annual Review of Biophysics and Biomolecular Structure*, **35**, 93-114.

Esmail, H., Barry, C.E. 3rd, Young, D.B. and Wilkinson, R.J. (2014) The ongoing challenge of latent tuberculosis. *Philosophical Transactions of the Royal Society B*, **369**, 20130437.

Getahun, H. *et al*. (2015) Management of latent *Mycobacterium tuberculosis* infection: WHO guidelines for low tuberculosis burden countries. *European Respiratory Journal*, **46**, 1563-1576.

Ghosh, A. S.,Chowdhury, C. and Nelson, D. E. (2008) Physiological functions of D-alanine carboxypeptidases in *Escherichia coli*. *Trends in Microbiology*, **16**(7), 309-317.

Goffin, C. and Ghuysen, J.M. (2002) Biochemistry and comparative genomics of SxxK superfamily acyltransferases offer a clue to the mycobacterial paradox: presence of penicillin-susceptible target proteins versus lack of efficiency of penicillin as a therapeutic agent. *Microbiology and Molecular Biology Reviews*, **66**, 702-38.

Gonzalo-Asensio, J., Aguilo, N., Marinova, D. and Martin, C. (2017) Breaking transmission with vaccines: the case of Tuberculosis. *Microbiology Spectrum*, **5**(4), MBTB-0001-2016.

Gordhan, B. G. and Parish, T. (2001) Gene Replacement using Pretreated DNA. *Methods in Molecular Medicine,* **54**, 77-92.

Griffin, J.E., Gawronski, J.D., Dejesus, M.A., Ioerger, T.R., Akerley, B.J. and Sasseti, C.M. (2011) High-resolution phenotypic profiling defines genes essential for mycobacterial growth and cholesterol catabolism. *PLoS Pathogens,* **7** (9), e1002251.

Heidrich, C., Ursinus, A., Berger, J., Schwarz, H. and Höltje, J.V. (2002) Effects of multiple deletion of murein hydrolases on viability, septum cleavage and sensitivity to large toxic molecules in *Escherichia coli*. *Journal of Bacteriology*, **184** (22), 6093- 99.

Henry, X. Amoroso, A., Coyette, J. and Joris, B. (2010) Interaction of ceftobiprobe with the low-affinity PBP5 of *Enterococcus faecium*. *Antimicrobial Agents and Chemotherapy*, **54**, 953-55.

Hett, E.C., Chao, M.C., Steyn, A.J., Fortune, S.M., Deng, L.L. and Rubin, E.J. (2007) A partner for resuscitation-promoting factors of *Mycobacterium tuberculosis*. *Molecular Microbiology*, **66**, 658-68.

Hett, E. C. and Rubin, E. J. (2008) Bacterial growth and cell division: a mycobacterial perspective. *Microbiology and Molecular Biology* Reviews, **72**(1), 126-156.

Hett, E.C., Chao, M.C. and Rubin, E.J. (2010) Interaction and Modulation of Two Antagonostic Cell Wall Enzymes of Mycobacteria. *PLos Pathogens*, **6** (7), e1001020.

Jankute, M., Cox, J.A., Harrison, J. and Besra, G.S. (2015) Assembly of the Mycobacterial cell wall. *Annual Review of Microbiology*, **69**, 405-423.

Kana, B.D., Gordhan, B.G., Downing, K.J., Sung, N., Vostroktunova, G., Machowski, E.E., Tsenova, L., Young, M., Kaprelyants, A., Kaplan, G. and Mizrahi, V. (2008) The resuscitation-promoting factors of *Mycobacterium tuberculosis* are required for virulence and resuscitation from dormancy but are collectively dispensable for growth *in vitro*. *Molecular Microbiology*, **67**, 672-84.

Kaur, D., Guerin, M. E., Skovierova, H., Brennan, P. J. & Jackson, M. (2009) Chapter 2: Biogenesis of the cell wall and other glycoconjugates of *Mycobacterium tuberculosis*. *Advances in Applied Microbiology,* **69**, 23-78.

Kamariza, M., Sheih, P., Ealand, C.S., Peters, J.S., Chu, B., Rodriguez-Rivera, F.P, Babu Saint, M.R., Treuren, W.V., Martinson, N., Kalscheuer, R., Kana, B.D. and Bertozzi, C.R. (2018) Rapid detection of *Mycobacterium tuberculosis* in sputum with a solvatochromic trehalose probe. *Science Translational Medicine*, **10** (143), e6310.

Kieser, K. J. and Rubin, E. J. (2014). How sisters grow apart: mycobacterial growth and division. *Nature Reviews Microbiology*, **12**(8), 550-62.

Kieser, K.J., Boutte, C.C., Kester, J.C., Baer, C.E., Barczak, A.K., Meniche, X., Chao, M.C., Rego, E.H., Sassetti, C.M., Fortune, S.M. and Rubin, E.J. (2015a) Phosphorylation of the Peptidoglycan Synthase PonA1 Governs the Rate of Polar Elongation in Mycobacteria. *PLoS Pathogens*, **11** (6), e1005010.

Kieser, K.J., Baranowski, C., Chao, M.C., Long, J.E., Sassetti, C.M., Waldor, M.K., Sacchettini, J.C., Ioerger, T.R. and Rubin, E.J. (2015b) Peptidoglycan synthesis in Mycobacterium tuberculosis is organized into networks with varying drug susceptibility. *Proceedings of the National Academy of Sciences*, **112**, 13087-092.

Kiran, M., Chauhan, A., Dziedzic, R., Maloney, E., Mukherji, S.K., Madiraju, M. and Rajagopalan, M. (2009) *Mycobacterium tuberculosis ftsH* expression in response to stress and viability. *Tuberculosis* (Edinb), **89**, 70-73.

Koul, A., Arnoult, E., Lounis, N., Guillemont, J. and Andries, K. (2011) The challenge of new drug discovery for tuberculosis. *Nature*, **469**, 483-90.

Korsak, A., Vollmer, W. and Markiewics, Z. (2005) *Listeria monocytogenes* EGD lacking penicillin-binding protein 5 (PBP5) produces a thicker cell wall. *FEMS Microbiology Letters*, **251**, 281-8.

Kumar, K., Awasthi, D., Berger, W.T., Tonge, P.J., Slayden, R.A. and Ojima, L. (2010) Discovery of anti-TB agents that target the cell-division protein FtsZ. *Future Medical Chemistry*, **2** (8), 1305-23.

Kumar, A., Kumar, S., Kumar, D., Mishra, A., Dewangan, R. P., Shrivastava, P., Ramachandran, S. and Taneja, B. (2013) The structure of Rv3717 reveals a novel amidase from *Mycobacterium tuberculosis*. *Acta Crystallographica Section D Biological Crystallography*, **69**, 2543-2554.

Laddomada, F., Miyachiro, M.M. and Dessen, A. (2016) Structural Insights into protein-protein interactions involved in bacterial cell wall biogenesis. *Antibiotics*, **5**, 14.

Larsen, M. H. (2000) Appendix 1. IN HATFUL, G. F., JACOBS, W. R., JR. (Ed.) *Molecular genetics of mycobacteria*. Washington, D.C., ASM Press.

Lee, T.K. and Huang, K.C. (2013) The role of hydrolases in bacterial cell-wall growth. *Current Opinion in Microbiology*, **16** (6), 760-6.

Lee, W. B., Kang, J. S., Yan, J. J., Lee, M. S., Jeon, B. Y., Cho, S. N., and Kim, Y. J. (2012) Neutrophils Promote Mycobacterial Trehalose Dimycolate-Induced Lung Inflammation via the Mincle Pathway. *PLoS Pathogens*, **8,** e1002614.

Lin, P.L., Ford, C.B., Coleman, M,T., Myers, A.J., Gawande, R., Loerger, T., Sacchettin, J., Fortune, S.N. and Flynn, J.L. (2014) Sterilization of granulomas is common in active and latent tuberculosis despite within-host variability in bacterial killing. *Nature Medicine*, **20**, 75-9.

Lonnroth, K., Castro, K.G., Chakaya, J.M., Chauhan, L.S., Floyd, K., Glaziou, P. and Raviglione, M.C. (2010) Tuberculosis control and elimination 2010-50: cure, care, and social development. *Lancet*, **375**, 1814-1829.

Macheboeuf, P, Contreras-Martel, C., JOB, V., Dideberg, O. and Dessen, A. (2006) Penicillin binding proteins: key players in bacterial cell cycle and drug resistance processes. *FEMS Microbiology Reviews*, **30**, 673-91.

Machowski, E. E., Senzani, S., Ealand, C. and Kana, B. D. (2014) Comparative genomics for mycobacterial peptidoglycan remodeling enzymes reveals extensive genetic multiplicity. *BMC Microbiology*, **14**(1): 1.

Mainardi, J.L., Villet, R., Bugg, T.D., Mayer, C. and Arthur, M. (2008) Evolution of peptidoglycan biosynthesis under the selective pressure of antibiotics in Gram-positive bacteria. *FEMS Microbiology Reviews*, **32**, 386- 408.

Magnet, S., Arbeloa, A., Mainardi, J.L., Hugonnet, J.E., Fourgeaud, M., Dubost, L., Marie, A., Delfose, V., Mayer, C., Rice, L.B. and Arthur, M. (2007) Specificity f L,D-transpeptidases from gram-positive bacteria producing different peptidoglycan chemotypes. *Journal of Biological Chemistry*, **282**, 13151-59.

Marakalala, M.J., Raju, R.M, Sharma, K., Zhang, Y.J., Eugenin, E.A., Prideaux, B., Daudelin, I.B., Chen, P.Y., Booty, M.G., Kim, J.H., Eum, S.Y., Via, L.E., Behar, S.M., Barry, C.E., 3rd, Mann, M., Dartios, V. and Rubin, E.J. (2016) Inflammatory signal in human tuberculosis granulomas is spatially organized. *Nature Medicine*, **20**, 531-8.

Martinelli, D.J. and Pavelka, M.S. (2016) The RipA and RipB peptidoglycan endopeptidases are individually nonessential to *Mycobacterium smegmatis*. *Journal of Bacteriology*, **198**, 1464-75.

Mavrici, D., Marakalala, M.J., Holton, J.M., Prigozhin, D.M., Gee, C.L., Zhang, Y.J., Rubin, E.J., and Alber, T. (2014) *Mycobacterium tuberculosis* FtsX extracellular domain activates the peptidoglycan hydrolase, RipC. *Proceeding of the National Academy of Sciences of the United State of America*, **111**, 8037-42.

Meyer, H., Bug, M. and Bremer, S. (2012) Emerging functions of the VCP/p97 AA-ATPase in ubiquitin system. *Nature Cell Biology*, **14**, 117-123.

Meberg, B.M., Paulson, A.L., Priyadarshini, R. and Young, K.D. (2004) Endopeptidase penicillin-binding proteins 4 and 7 play auxiliary roles in determining uniform morphology of *Escherichia coli*. *Journal of Bacteriology*, **186**, 8326-36.

Miranda, M.S., Breiman, A., Allain, S., Deknuydt, F. and Altare, F. (2012) The Tuberculosis Granulomar: An Unsuccessful Host Defence Mechanism Providing a Safety Shelter for the Bacteria? *Clinical and Developmental Immunology*, **2012**, 137-141.

Mishra, A. K., Driessen, N. N., Appelmelk, B. J. and Besra, G. S. (2011) Lipoarabinomannan and related glycoconjugates: structure, biogenesis and role in *Mycobacterium tuberculosis* physiology and host-pathogen interaction. *FEMS Microbiology Review*, **35**, 1126-57.

Möll, A, Dörr, T., Alverez, L., Davis, B., Cava, F. and Waldor, M.K. (2015) A D,D-caborxypeptidase is required for *Vibrio cholerae* halotolerance. *Environmental Microbiology*, **17** (2), 527-40.

Morlot, C., Noirclerc-Savoye, M., Zapun, A., Dideberg, O. and Vernet, T. (2004) The DD-carboxypeptidase PBP3 organizes the division process of *Streptococcus pneumoniae*. *Molecular Microbiology*, **51**, 1641-8.

Mukamolova, G.V., Kaprelyants, A.S., Young, D.I., Young, M. and Kell, D.B. (1998) A bacterial cytokine. *Proceedings of the National Academy of Sciences*, **95** (15), 8916-21.

Mukherjee, P., Sureka, K., Datta, P., Hossain, T., Barik, S., Das, K.P., Kundu, M. and Basu, J. (2009) Novel role of Wag31 in protection of mycobacteria under oxidative stress. *Molecular Microbiology*, **73**, 103-19.

Nahid, P. *et al*. (2016) Official American Thoracic Society/Centers for Disease Control and Prevention/Infectious Diseases Society of American clinical practice guideline: treatment and drug-susceptible tuberculosis. *Clinical Infectious Diseases*, **63**, 147-195.

Nelson, D.E. and Young, K.D. (2000) Penicillin-binding protein 5 affects cell diameter, contour, and morphology of *Escherichia coli*. *Journal of Bacteriology*, **182**, 1714-21.

Nelson, D.E. and Young, K.D. (2001) Contributions of PBP5 and DD-Carboxypeptidase Penicillin-Binding Proteins to maintenance of cell shape in *Escherichia coli*. *Journal of Bacteriology*, **183**, 3055-64.

Neuwald, A.F., Aravind, L., Spouge, J.L. and Koonin, E.V. (1999) AAA+: A class of chaperon-like ATPases associated with assembly, operation, and disassembly of protein complexes. *Genome Research*, **9**, 27-43.

Nikitushkin, V.D., Demina, G.R., Shleeva, M.O., Guryanova, S.V., Ruggiero, A., Berisio, R. and Kaprelyants, A.S. (2015) A product of RpfB and RipA joint enzymatic action promotes the resuscitation of dormant mycobacteria. *FEBS Journal*, **282**, 2500-11.

Ogura, T. and Wilkinson, A.J. (2001) AAA+ superfamily ATPase: common structure-diverse function. *Genes Cells*, **6**, 575-97.

Onozaki, I., Law, I., Sismanidis, C., Zignol, M., Glaziou, P. and Floyd, K. (2015) National tuberculosis prevalence surveys in Asia, 1990-2012: an overview of results and lessons learned. *Tropical Medicine and International Health*, **20**, 1128-45.

Pai, M., Behr, M.A., Dowdy, D., Dheda, K., Divangahi, M., Boehme, C.C., Ginsberg, A., Swaminathan, S., Spigelman, M., Getahun, H., Menzies, D. and Raviglione, M. (2016) Tuberculosis. *Nature Reviews Disease Primers*, **2**, e16076.

Parish, T. and Stoker, N.G. (2000) Use of a flexible cassette method to generate a double unmarked *Mycobacterium tuberculosis* tlyA plcABC mutant by gene replacement. *Microbiology*, **146**, 1969-75.

Peters, K., Kannan, S., Rao, V.A., Biboy, J., Vollmer., D., Erickson, S.W., Lewis, R.J., Young, K.D. and Vollmer, W. (2016) The redundancy of Peptidoglycan Carboxypeptidases Ensures Robust Cell Shape Maintenance in *Escherichia coli*. *MBio*, **7**, e00819-16.

Popham, D.L., Gilmoree, M.E. and Setlow, P. (1999) Roles of low-molecular-weight penicillin-binding proteins in *Bacillus subtilis* spore peptidoglycan synthesis and spore properties. *Journal of Bacteriology*, **181**, 126-32.

Potluri, L., Karczmarek, A., Verheul, J., Pitte, A., Wilkin, J.M., Werth, N., Banzhaf, M., Vollmer, W., Young, K.D., Nguyen-Disteche, M., and Blaauwen, T. (2010) Septal and lateral wall localization of PBP5, the major D,D-carboxypeptidase of *Escherichia coli*, requires substrate recognition and membrane attachment. *Molecular Microbiology*, **77**(2), 300-23.

Rossi, C.G.A., Gomez-Puertas, P. and Serrano, J.A.A. (2016) In vivo function of and molecular characterization of the penicillin-binding protein 4 (DacB) of *Pseudomonas aeruginosa*. *BMC Microbiology*, **16**, 234.

Ruggiero, A., Marasco, D., Squeglia, F., Soldini, S., Pedone, E., Pedone, C. and Berisio, R. (2010) Structure and functional regulation of RipA, a mycobacterial enzyme essential for daughter cell separation. *Structure*, **18**, 1184-90.

Sambrook, J., Fritsch, E. F., Maniatis, T. (1989) Molecular Cloning. A laboratory manual. . Second ed. Cold Spring Harbour, New York. Cold Spring Harbour Laboratory Press.

Santi, I., Dhar, N., Bousbaine, D., Wakamoto, Y. and McKinney, J.L. (2013) Single-cell dynamics of chromosome replication and cell division cycles in mycobacteria. *Nature Communications*, **4**, 1-10.

Santos, J.M., Lobo, M., Matos, A.P., De Petro, M.A. and Arraiano, C.M. (2002) The gene *bolA* regulates *dacA* (PBP5), *dacC* (PBP6) and *ampC* (AmpC), promoting normal morphology in *Escherichia coli*. *Molecular Microbiology*, **45**, 1729-40.

Sassetti, C.M, Boyd, D.H. and Rubin, E.J. (2003) Genes required for mycobacterial growth defined by high density mutagenesis. *Molecular Microbiology*, **48** (1), 77-84.

Sauvage, E., Kerff, F., Terrak, M., Ayala, A. and Charlier, P. (2008) The penicillin-binding proteins: structure and role in peptidoglycan biosynthesis. *FEMS Microbiology Reviews*, **32**, 234-58.

Scheffers, D.J. and Errington, J. (2004) PBP1 is a component of the *Bacillus subtilis* cell division machinery. *Journal of Microbiology*, **186**, 5153-56.

Scheffers, D.J., and Pinho, M.G. (2005) Bacterial cell wall synthesis: new insights from localization studies. *Microbiology and Molecular Biology Reviews*, **69**(4), 585-607.

Schmitz, K.R. and Sauer, R.T. (2014) Substrate delivery by the AAA+ ClpX and ClpC1 unfoldases activates the mycobacterial ClpP1P2 peptidases. *Molecular Microbiology*, **93**, 617-628.

Schoonmaker, M.K., Bishai, W.R. and Lamichhane, G. (2014) Nonclassical transpeptidases of *Mycobacterium tuberculosis* alter cell size, morphology, cytosolic matrix, protein localization, virulence and resistance to β-lactams. *Journal of Bacteriology*, **196**, 1394-1402.

Sham, L.T., Tsui, H.L., Land, A.D., Barendt, S.M. and Winkler, M.E. (2012) Recent advances in pneumococcal peptidoglycan biosynthesis suggest new vaccine and antimicrobial targets. *Current Opinion in Microbiology*, **15**, 194-203.

Singh, A., Mai, D., Kumar, A. and Steyn, A. J. (2006) Dissecting virulence pathways of *Mycobacterium tuberculosis* through protein–protein association. *Proceedings of the National Academy of Sciences*, **103**(30), 11346-11351.

Singh, B., Nitharwal. R.G., Ramesh, M., Pettersson, B.M., Kirsebom, L.A. and Dasgupta, S.(2013) Asymmetric growth and division in *Mycobacterium* spp: compensatory mechanisms for non-medial septa. *Molecular Microbiology*, **88**, 64-76.

Snapper, S.B., Melton, R.E., Mustafa, S., Kieser, T. and Jacobs, W.R., JR (1990) Isolation and characterization of efficient plasmid transformation mutants of *Mycobacterium smegmatis*. *Molecular Microbiology*, **4**, 1911-9.

Srinivassan, R., Anilkumar, G., Rajeswari, H. and AjitKumar, P. (2006) Functional characterization of AAA family FtsH protease of *Mycobacterium tuberculosis*. *FEMS Microbiology Letters*, **259**, 97-105.

Stefanova, M.E., Tomberg, J., Olesky, M., Höltje, V.C., Gutheil, W.G. and Nicholas, R.A. (2003) *Neisseria gonorrhoeae* penicillin-binding protein 3 exhibits exceptionally high carboxypeptidase and beta-lactam binding activities. *Biochemistry*, **42** (49), 14614-25.

Steidl, R., Pearson, S., Stephenson, R.E., Ledala, N., Sitthisak, S., Wilkinson, B.J. and Jayaswal, R.K. (2008) *Staphylococcus aereus* cell wall stress stimulon gene-lacZ fusion strains: potential for use in screening for cell wall-active antimicrobials. *Antimicrobial Agents and Chemotherapy*, **52**, 2923-25.

Swaminathan, S. and Rekha, B. (2010) Pediatric tuberculosis: global overview and challenges. *Clinical Infectious Diseases*, **50**, 184-194.

Tayler, A.E., Ayala, J.A., Niumsup, P., Westphal., K., Baker, J.A., Zhang, L., Walsh, T.R., Weidemann, B., Bennett, P.M. and Avison, M.B. (2010). Induction of β-lactamase production in *Aeromonas hydrophila* is responsive to β-lactam-mediated changes in peptidoglycan composition. *Microbiology*, **156** (8), 2327-35.

Thunnissen, M.M., Fusetti, F., de Boer, B. and Dijkstra, B.W. (1995) Purification, crystallisation and preliminary X-ray analysis of penicillin binding protein 4 from *Escherichia coli*, a protein related to class A β-lactamases. *Journal of Molecular Biology*, **247**, 149-153.

Tiemersma, E.W., van der Werf, M.J., Borgdorff, M.W., Williams, B.C. and Nagelkerkr, N.J. (2011) Natural history of tuberculosis: duration and fatality of untreated pulmonary tuberculosis in HIV negative patients: a systemic review. *PLoS ONE*, **6**. e17601.

Tipper, D.J. and Strominger, J.L. (1965) Mechanism of action of penicillins: a proposal based on their structural similarity to acyl-D-alanyl-D-alanine. *Proceedings of the National Academy of Sciences of the United States of America*, **54**, 1138-41.

Tortoli, E., Nanetti, A., Piersimoni, C., Cichero, P., Farina, C., Mucignat, G., Scarparo, C., Bartolini, L., Valentini, R., Nista, R., Gesu, G., Tosi, C.P., Crovatto M. and Brusarosco, G. (2001) Performance assessment of new multi-plex probe assay for identification of mycobacteria. *Journal of Clinical Microbiology*, **39**, 1079-1084.

Typas, A., Banzhaf, M., Gross, C.A. and Vollmer, W. (2012) From the regulation of peptidoglycan synthesis to bacterial growth and morphology. *Nature Reviews Microbiology*, **10**, 123-36.

Uehara, T. and Park, J.T. (2007) An anhydro-*N*-acetylmuramyl-*L*-alanine amidase with broad specificity tethered to the outer membrane of *Escherichia coli*. *Journal of Bacteriology*, **189**, 5634-41.

Unciuleac, M.C, Smith, P.C. and Shuman, S. (2016) Crystal structure and biochemical characterization of a *Mycobacterium smegmatis* AA-type nucleoside triphosphatase phosphohydrolase (Msm0858). *Journal of Bacteriology*, **10**, 1521-33.

van Heijenoort, J. (2011) Peptidoglycan hydrolases of *Escherichia coli*. *Microbiology and Molecular Biology Reviews*, **75** (4), 636-63.

van Leth, F., van der Werf, M.J. and Borgdorff, M.W. (2008) Prevalence of tuberculosis infection and incidence of tuberculosis: a re-assessment of the Styblo rule. Bull. *World Health Organization*, **86**, 20-26.

Vollmer, W., Joris, B., Charlier, P., and Foster, S. (2008) Bacterial peptidoglycan (murein) hydrolases. *FEMS Microbiology Reviews*, **32**(2), 259-286.

Vollmer., W, von Rechenberg, M. and Holje, J.V. (1999) Demonstration of molecular interactions between the murein polymerase PBP1B, the lytic transglycosylase MltA, and the scaffolding protein MipA of *Escherichia coli*. *Journal of Biological Chemistry*, **274**, 6726-34.

Wehrl, W., Niederwes, M. and Schumann, W. (2000) The FtsH protein accumulates at the septum of *Bacillus subtilis* during cell division and sporulation. *Journal of Bacteriology*, **182**, 3870-73.

Weiss, D.S., Chen, J.C., Ghigo, J., Boyd, D. and Beckwith, J. (1999) Localization of FtsI (PBP3) to the Septal Ring Requires Its Membrane Anchor, the Z Ring, FtsA, FtsQ and FtsL. *Journal of Bacteriology*, **181** (2), 508-20.

Wilson, K. (1997) Preparation of genomic DNA from bacteria. *Current Protocols in Molecular Biology*, **2**, 41-45.

Wissel, M.C. and Weiss, D.S. (2004) Genetic analysis of the cell division protein FtsI (PBP3): amino acid substitutions that impair septal localization of FtsI and recruitment of FtsN. *Journal of Bacteriology*, **186**, 490-502.

White, C.L., Kitich, A. and Gober, J.W. (2010) Positioning cell wall synthetic complexes by the bacterial morphogenetic proteins MreB and MreD. *Molecular Microbiology*, **76**, 616-633.

World Health Organization (2010) Guidelines for Treatment of Tuberculosis 4th edn.

World Health Organization (2014) Guidelines on the Management of Latent Tuberculosis Infection.

World Health Organization (2015). Global tuberculosis report 2015.

World Health Organization (2017). Global tuberculosis report 2017.

Wyke, A.W., Ward, J.B., Hayes, M.V. and Curtis, N.A. (1981) A role in vivo for penicillin-binding protein 4 of *Staphylococcus aureus*. *European Journal of Biochemistry*, **119**, 389-93.

Zapun, A., Contreras-Martel,C. and Vernet, T. (2008) Penicillin-binding proteins and β-lactam resistance. *FEMS Microbiology Reviews*, **32**, 361-385.

Zumla, A., Raviglione, M., Hafner, R. and von Reyn, C.F. (2013a) Tuberculosis. *New England Journal of Medicine*, **368**, 745-55.

Zumla, A., Nahid, P. and Cole, S.T. (2013b) Advances in the development of new tuberculosis drugs and treatment regimens. *Nature Reviews Drug Discovery*, **12**, 388-404.